WIND TUNNEL INVESTIGATION OF THE STATIC STABILITY AND CONTROL EFFECTIVENESS OF A ROTARY TAIL IN A PORTABLE UAV

THESIS

José R. Rivera Parga, Lieutenant, Mexican Navy
AFIT/GAE/ENY/04-D02

DEPARTMENT OF THE AIR FORCE
AIR UNIVERSITY

AIR FORCE INSTITUTE OF TECHNOLOGY

Wright-Patterson Air Force Base, Ohio

AFIT/GAE/ENY/04-D02

WIND TUNNEL INVESTIGATION OF THE STATIC STABILITY AND CONTROL EFFECTIVENESS OF A ROTARY TAIL IN A PORTABLE UAV

THESIS

Presented to the Faculty

Department of Aeronautics and Astronautics

Graduate School of Engineering and Management

Air Force Institute of Technology

Air University

Air Education and Training Command

In Partial Fulfillment of the Requirements for the

Degree of Master of Science in Aeronautical Engineering

Jose Ramon Rivera Parga

Lieutenant, Mexican Navy

December 2004

AFIT/GAE/ENY/04-D02

WIND TUNNEL INVESTIGATION OF THE STATIC STABILITY AND CONTROL EFFECTIVENESS OF A ROTARY TAIL IN A PORTABLE UAV

José R. Rivera Parga

Lieutenant, Mexican Navy

Approved:

//SIGNED//	9th December 2004
Prof. Mark F. Reeder (Chairman)	date
//SIGNED//	9th December 2004
Lt Col Raymond Maple (Member)	date
//SIGNED//	9th December 2004
Prof. Richard Cobb (Member)	date

Abstract

The Air Force Research Lab, Munitions Directorate, Flight Vehicles Integration Branch (AFRL/MNAV) developed a man-portable, carbon-fiber matrix UAV with a flexible rectangular wing of 24” span and 6” chord, 18.2" length. For practical benefits, there is a rising need for the development of smaller and lighter UAV’s to perform similar missions to that of their full-size counterparts.

The objective of this experimental study was to determine the general behavior and the aerodynamic characteristics of rotary tails. The rotary tail mechanism studied enabled control of two degrees of freedom and was configured to provide elevator deflection and rotation. Its effects on the static stability and control effectiveness were measured using the Air Force Institute of Technology (AFIT) low speed wind tunnel. The yaw moment provided by each rotary tail was found to be on the same order of magnitude as a typical rudder, and in that respect it offers promise as an effective flight control scheme. However, it was also found that the side force, and consequently the yaw moment, generated by the tail controls were strongly coupled, which could lead to challenging aircraft control issues. The configurations used in this thesis would reduce the storage length by 48%.

The contribution to the longitudinal stability by each tail was found to be small, and by maintaining the original wing characteristics of the UAV the vehicle was stable in roll. Pitch stability was obtained by locating the center of gravity ahead of the neutral point. Using a rotary tail consisting of a tapered, swept flat plate, yaw stability was not

obtained. On the other hand, pitch and yaw control was obtained and even a small amount of roll control was attained. Yaw stability was gained by placing two vertical stabilizers on the tail.

Acknowledgements

I wish to express my gratitude to my Lord God from whom I have received all that I have in my life and who has allowed me to finish this thesis.

There are not words to describe my thankfulness to my advisor, Dr Mark Reeder, who had the idea of using a rotary tail for a UAV and who helped me as well as guided me not only during the development of this thesis, but also since I arrived to AFIT. His support and teaching were indispensable for performing this experiment and the subsequent writing.

My wife, who supported me during this time with her love and friendship, gave me the energy to defeat the obstacles that were present during my studies in AFIT. My two children inspired me to not give up when the problems were nearby.

It is impossible to name all of the people that in one way or another influenced me to obtain a positive attitude to reach the goal of finishing this thesis. The faculty members from whom I received classes, as well my classmates, all left me with the impression that America is a great country.

Jose R. Rivera Parga

Table of Contents

Page

Page

List of Figures

Figure Page

Page

Page

Page

Page

Page

List of Tables

Table Page

Page

Page

List of Symbols

A	Axial Force (Body Axis)
Y	Side Force (Body Axes)
N	Normal Force (Body Axes)
D	Drag Force (Wind Axis)
S	Side Force (Wind Axes)
L	Lift Force (Wind Axes)
NF	Balance Normal Force Sensor
AF	Balance Axial Force Sensor
SF	Balance Side Force Sensor
PM	Balance Pitch Moment Sensor
RM	Balance Roll Moment Sensor
YM	Balance Yaw Moment Sensor
AR	Aspect Ratio
S	Wing Area
C	Wing Root Chord
$\bar{c}$	Wing Mean Chord
Re	Reynolds Number at the Chord
M	Mach Number
R	Ideal Gas Constant
CG	Center of Gravity
M.A.C.	Mean Aerodynamic Chord
UAV	Unmanned Air Vehicle
2b	Wing Span
q_∞	Far Field Dynamic Pressure
U_∞	Far Field Velocity
a	Speed of Sound
L	Roll Moment
M	Pitch Moment
N	Yaw Moment
ρ	Air Density
μ	Air Viscosity
α	Angle of attack
β	Sideslip Angle
ψ	Yaw angle ($\psi = -\beta$)
Γ	Wing Dihedral Angle
Φ	Wing Roll Angle
δe	Elevator Deflection
δr	Rudder Deflection Angle
δrn	Rotation Angle of the Tail
C_X	Axial Force Coefficient (Body Axes)
C_Y	Side Force Coefficient (Body Axes)

C_Z	Normal Force Coefficient (Body Axes)
C_L	Lift Coefficient
C_S	Side Force Coefficient
C_D	Drag Force Coefficient
C_l	Roll Moment Coefficient
Cm	Pitch Moment Coefficient
Cn	Yaw Moment Coefficient
Cm_α	Longitudinal Stability Derivative
Cn_β	Directional Stability Derivative
$C_{l\beta}$	Roll Stability Derivative
lb_f	Pounds Force
lb_m	Pound Mass
“	Inches
‘	Feet
°	Degrees (360º = 2Π radians)

WIND TUNNEL INVESTIGATION OF THE STATIC STABILITY AND CONTROL EFFECTIVENESS OF A ROTARY TAIL IN A PORTABLE UAV

I. Introduction

1.1. Background

1.1.1. Historical Antecedents

Even before the success of the Wright brothers in December 1903, there were some other aircraft that achieved unmanned flight; however, perhaps the most significant advance brought about by the Wright brothers' aircraft was in the area of flight control. These days, due to the advances in understanding and technology it is possible to have a controlled flight of an aircraft that is not habited by a human being (Raymer, 1999: 679).Through history, unmanned aircrafts have received different names, such as drone, pilot-less and remote-piloted vehicle; however today the most common label is unmanned aerial vehicle (UAV). It is a testimony to the Wright brothers that even today, most aircraft, manned and unmanned utilizes the similar control surfaces to apply moments in each of the three axes of the aircraft.

The use of these vehicles includes both military and civil areas. For the military, there are tactical uses such as battlefield reconnaissance, damage assessment, and visual surveillance and as a platform for transportation of chemical, biological or radiation sensors. On the other hand, these unmanned air vehicles can be used in civilian applications such as search and rescue, border patrol, air sampling, and police surveillance (Huayi, Dong and Zhoaying, 2004: 1).

Presently there exists a great variety of UAV's, and as a consequence, it is not clear from the literature if the aerospace, military or scientific community has adopted a standard categorization for UAV concepts. However, Richard M. Wood developed a classification that is a function of Reynolds number and either span or weight as shown in Figure 1. It can be seen that Wood set four classes of UAV: Micro UAV, Meso UAV, Macro UAV and Mega UAV. (Wood, 2002: 2).

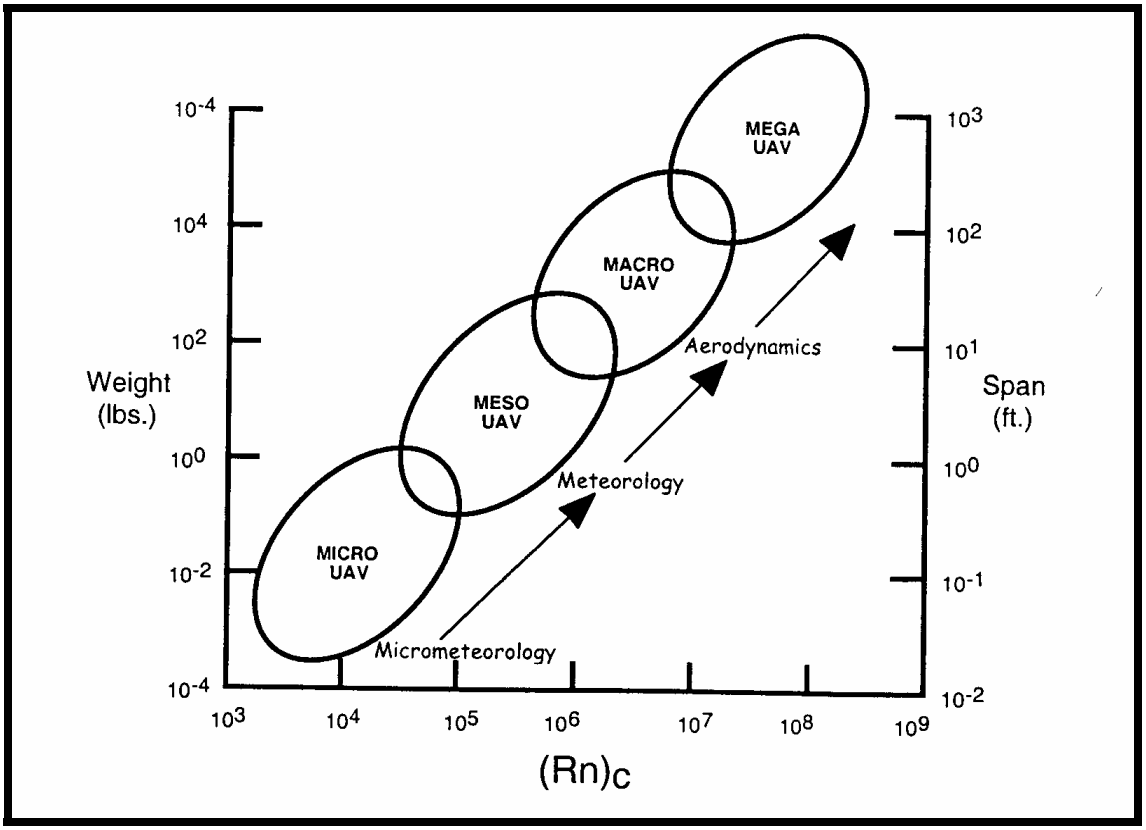

Figure 1. Classification of UAV's

Two of the most widely known United States Arm Forces UAV's that today are in operation are the General Atomics *Predator* and the Teledyne-Ryan *Global Hawk*. The Predator is a pusher-prop powered low-speed aircraft which is equipped with visual light and infrared (IR) cameras and can also carry a ground-looking radar. The Global Hawk is

a much larger, jet powered aircraft. It is equipped with electro-optical and IR sensors, as well as synthetic aperture radar with moving target indicator.

For tactical reasons and due to the advances in technology, there is a rising need for the development of smaller and cheaper UAVs to perform similar missions to that of their full-sized counterparts, especially at the platoon level. Some of the most known portable UAVs currently in use in the United States Armed Forces are: the Lockheed Martin *Desert Hawk,* the Army's *Shadow*, the Marine Corps' *Dragon Eye,* and the Navy's *Silver Fox* (See Figure 2). Moreover, due to the fact that in 1993 RAND corporation suggested that the development of very small flying vehicles could give the U.S. military services an important advantage in the upcoming decades (Kennon and Grasmeyer,2003:1), several institutions and companies have developed some of the prototypes. Some published examples include AeroVironment Inc. that developed the Black Widow MAV (Micro Air Vehicle) which are electrically propelled, remotely controlled and carries a video camera and the MAV called WASP. Porsin-Sirirak developed a battery-powered Microbat MAV with a weight of 11 g which could fly for 5-18 sec. Yan, Koo, Sastry and Shim developed a micromechanical flying insect with a wing span of less than 25mm and a mass of 100 mg using a novel thorax fabrication method (Huayi, Dong and Zhoaying, 2004: 1). The company ONERA developed a 201 gram. MAV called Mirador. Some of these MAV's are shown in Figure 3.

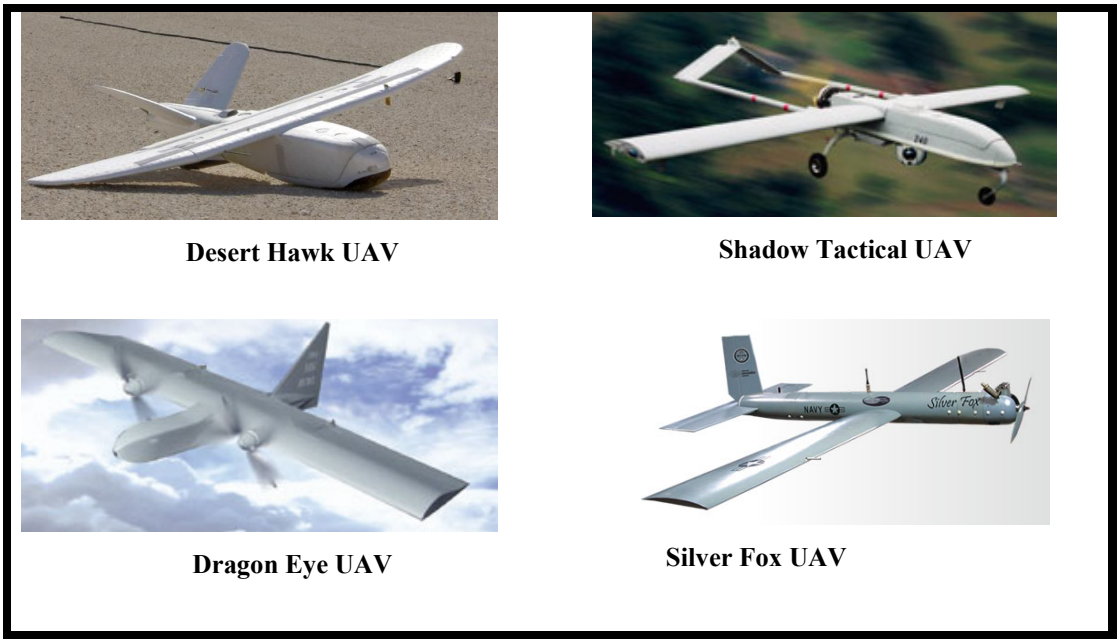

Figure 2. Some of The Current Portable UAV's of The United States Armed Forces (Silver Fox, 2004. AAI Corp, 2004. Sparta, 2004. Military.Com, 2004)

The United Sates Air Force has led the development of technology in many cases through its history, and in like manner the Air Force Research Lab, Munitions Directorate, Flight Vehicles Integration Branch (AFRL/MNAV) developed a man-portable, carbon-fiber matrix MAV with a flexible rectangular wing of 24" span and 6" chord called Combat-Camera (BATCAM), for the Air Force Special Tactics in the global war on terror (GWOT). The goal of this UAV is to provide the soldier the capability of knowing, in real time, the conditions of the battlefield that is ahead or "over the next hill" (Deluca, 2004:3).

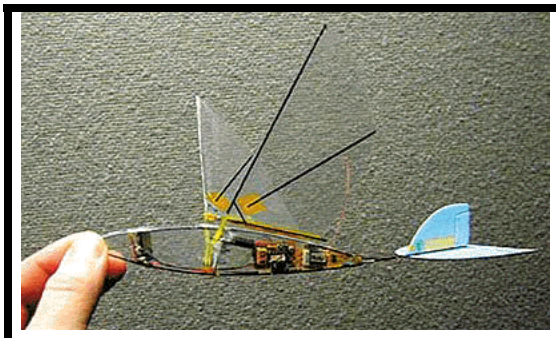

Microbat

Onera Mirador

Aerovironment Black Widow

Aerovironment WASP

Figure 3. Some Examples of MAV's (Aeroviroment, 2004. Ribaud & Dessones, 2004)

AFRL/MNAV developed several variations of this UAV design that have been flight, tested and subsequently improved their performance. Captain Antony M. DeLuca (USAF) performed and documented an experimental wind tunnel investigation into the aerodynamic performance of both rigid and flexible wings of these MAV's. One advantage of the flexible wing is that, when it is transported, its wing can be folded and as a consequence, it obtains a compact storage space in the span direction. A second advantage was that the wing flexure was found to delay stall and increase the breadth of

the peak L/D for a given angle of attack. The practical benefit of this is presumably to reduce the aircraft fluctuations due to gusts.

The development of techniques for building a UAV have been focused in different areas such as structures, materials, control, aerodynamics, propulsion, and avionics. In all these areas, great advances have been reached. However, in the area of aerodynamics most portable UAVs still use the conventional flight control surfaces that the rest of aviation uses. The focus of the present study is on an innovative variation on the traditional means of controlling the MAV studied in the experimental investigation made by Captain DeLuca (DeLuca; 2004). The possible logistical advantages to this control approach are described below.

1.2. Motivation

One goal inherent to portable UAV design is to reduce the space required for storage in order to save room in the transportation of this device, whether stored in munitions compartments or carrier by soldiers.

The idea was born from the fact that the shorter the UAV length the better. One possible solution was to modify the UAV into a tailless aircraft; however, the main characteristic of the UAV is the flexibility and foldability of its wing (See Figure 4). Since all tailless aircraft rely on multiple ailerons to control pitch, yaw and roll, this was not viewed as a realistic possibility. Another solution was to keep the tail but at the same time reduce the length of the UAV without modifying the stability or affecting controllability. In order to reduce the length of the airplane it is necessary to compensate for the reduced moment arm of the flight control of the tail.

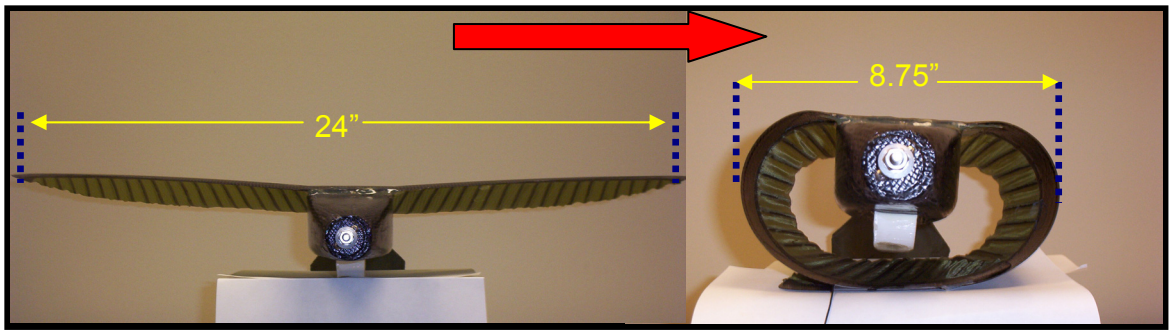

Figure 4. Wing Flexibility of the UAV

As in the early years of aviation, an idea was formed by observing the flight of birds. From an empirical observation, most airplanes have a long horizontal moment arm, compared with birds (Figure 5). A cursory further quantitative analysis helped to confirm that such observation was right, because some of these animals have a horizontal tail volume coefficient which is smaller compared to the man-made flying machines. In other words, if it is considered that the horizontal tail volume coefficient is given by the formula (Raymer; 1999:123):

$$C_{HT} = \frac{L_{HT} * S_{HT}}{\overline{C}_W * S_W} \qquad (1)$$

Where:

$L_{HT=}$ Horizontal moment arm

$\overline{C}_W$ = Wing mean chord

S_W= Wing area

S_{HT}= Tail area

Figure 5. Empirical Comparison of the Horizontal Moment Arm Between an Airplane (Airbus, 2004) and a Bird (Johnson, 2004)

It is easy to see that this value it is a good indication of the relationship between areas of the wing and horizontal stabilizer, moreover, its value it is directly proportional to the tail moment arm.

Taking approximates values of some birds acquired by analyzing the data presented by Jeremy M.V. Rayner (Rayner; 1988: 27) and compared with average values for airplanes given by Daniel P. Raymer (Raymer; 1999:125), a comparison of tail volume coefficient between some birds and some types of airplanes was made and is presented in Table 19 and Table 20 as well as in Figure 6.

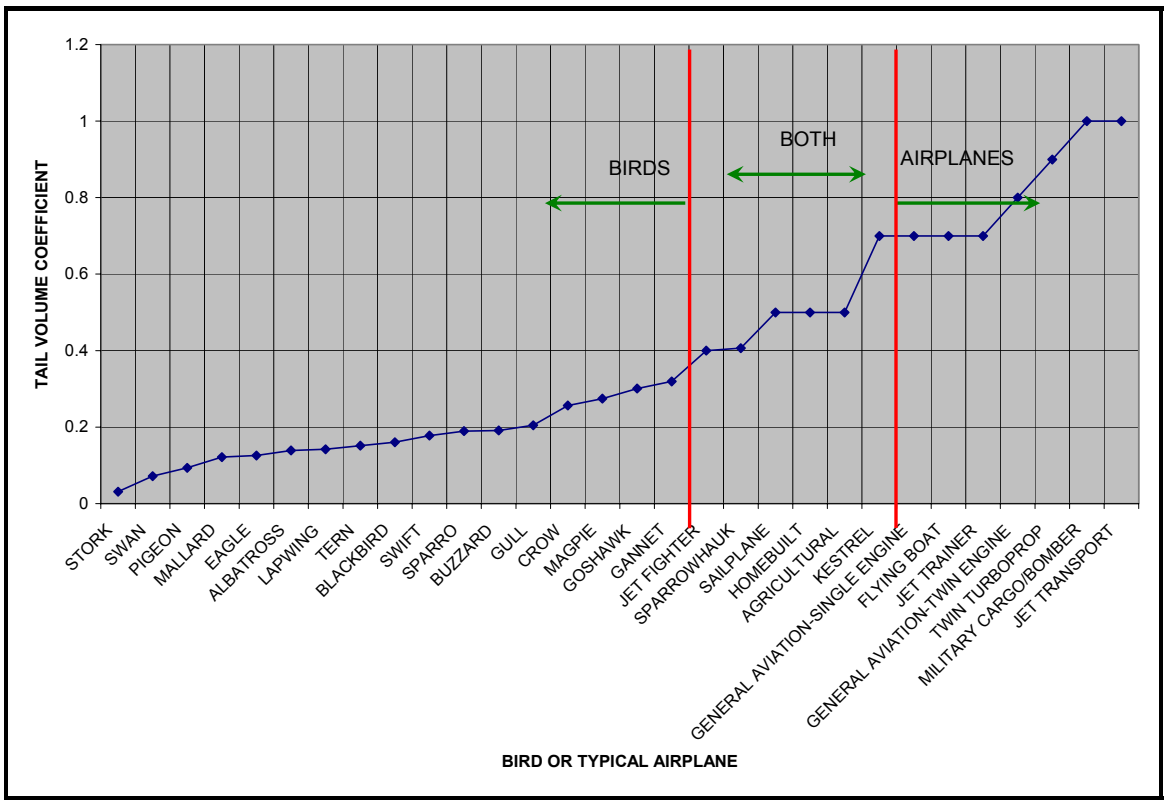

Figure 6. Comparison of Tail Volume Coefficient Between Some Birds and Type of Airplanes

As can be seen in the data presented, some birds can develop a totally controllable flight with a lower control volume coefficient than that used for airplanes. However, it is important to consider the fact that birds perform control of their flight by using their wings too (Horton-Smith; 1938:38).

In a few words, the motivation for this thesis was born from the idea of adapting to the design of the tail of the UAV to the flight control technique that the tail of some birds uses. In order to do this, a new tail configuration for the UAV was designed and called “Rotary tail”, this tail differs from the conventional tail in that it is possible to move it in elevator deflection for pitch control as in a conventional tail and at the same

time it can be moved around the X body axis in a circular movement to provide yaw and roll control (Please refer to Figure 39 and Figure 40).

1.3. Research Objective

The objective of this experimental study is to determine the general behavior and the aerodynamic characteristics that a rotary tail provides to a portable UAV and its effect on the static stability and control effectiveness. Experiments were conducted by employing the Air Force Institute of Technology (AFIT) low speed, open circuit wind tunnel. This goal was reached by obtaining the following data:

a. Measure and comparison of the aerodynamic forces and moments on a UAV with two different tail configurations.

b. Calculate the lift, drag, and side force coefficients, C_L,C_D, C_S, for two tail configurations at tunnel speeds of U_∞ = 30 mph.

c. Calculate the pitch, roll and yaw moment coefficients, C_l, C_m, C_n on two tail configurations at 30 mph.

d. Calculate the stability derivatives $C_{m\alpha}$, $C_{l\beta}$, $C_{n\beta}$ for two tail configurations

e. Calculate the aerodynamic force and moment coefficients for two tail configurations at 30 mph with various combinations of control surface deflection settings.

1.4. Chapter Summary

Chapter I of this thesis described the historical antecedents, motivation, and the research objective. Chapter II reviews the literature related to the thesis: aerodynamic

forces and moments on an airplane, static stability and control, Function of the tail in airplanes, function of the tail in birds, description of the original UAV and tail configuration descriptions. Chapter III describes the methodology used for the experiments: description of the equipment, experimental procedure and data processing. Chapter IV presents the results and analysis of the data obtained. Finally Chapter V sets the conclusions and recommendations.

II. Literature Review

2.1. Introduction

How well an aircraft flies and how easily it can be controlled are subjects studied in aircraft stability and control (Nelson; 1998:39). This chapter explains the definitions as well as basic principles of aerodynamics and static stability and control that are related to the analysis of the tails that were tested.

2.2. Coordinate Systems and Aerodynamic Definitions

In order to define the different forces and moments that act on an aircraft, the customary definitions of the body and wind axis systems for aircraft analysis were used. It is important to notice that these coordinate or references systems are a set of three orthogonal axes and by international convention, they are always labeled in a right-hand sequence.

a. Body Axes.

As can be seen in Figure 7, the body axes are always fixed to the airplane and move with it; with the X axis aligned with the fuselage, the Y axis pointing to the right wing of the airplane and the Z axis downward. Each of the axes of this system is designated with a subscript “b”. These axes are fixed to the center of gravity of the airplane. The aerodynamic force components in these axes are called axial, side and normal forces. Some authors give the notation of X, Y and Z to these forces (Nelson; 1998:20) but others gave them the notation of A, Y and N, respectively (Barlow, Rae and Pope; 1999:237). For this thesis the first notation was used.

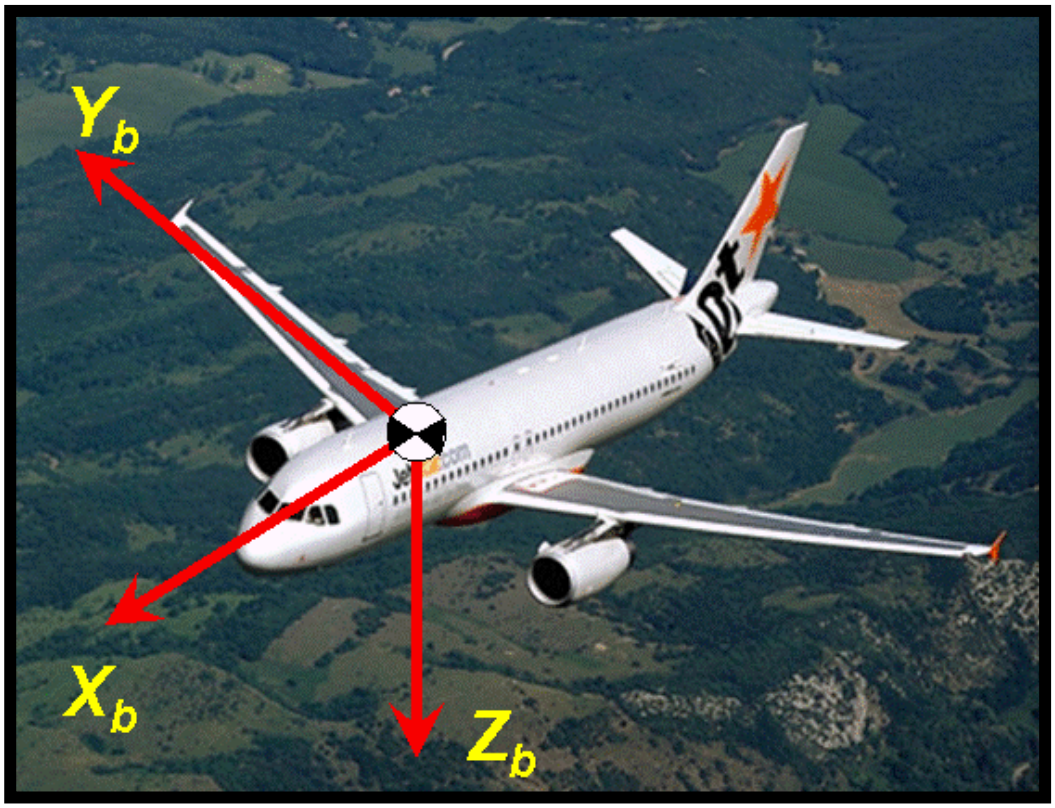

Figure 7. Body Axis Coordinate System (Photo: Airbus, 2004)

The aerodynamic forces are described in terms of dimensionless coefficients by dividing such forces by flight dynamic pressure and a reference area (S). For airplanes is the wing platform area. As a result, the body forces coefficients are defined by the following formulas:

$$C_x = \frac{X}{\frac{1}{2}\rho v^2 S}$$ **(Axial force coefficient, Body axes)** **(2)**

$$C_y = \frac{Y}{\frac{1}{2}\rho v^2 S}$$ **(Side force coefficient Body axes)** **(3)**

$$C_z = \frac{Z}{\frac{1}{2}\rho v^2 S} \quad \textbf{(Normal force coefficient, Body axes)} \quad (4)$$

In this body-axes reference, the moments produced about the center of gravity of the airplane are defined as: Rolling moment (L), which is about the X axis; Pitch moment (M), which is about the Y axis; and Yaw moment (N), which is about the Z axis. In the same fashion as the forces, these moments are defined as dimensionless coefficients by using flight dynamic pressure, a reference area (S), that is the wing platform area, and a characteristic length (L) that is wing span for the rolling and yaw moment and the mean chord for the pitching moment (Nelson; 1998:21). As a consequence, the following formulas define these moment coefficients:

$$C_l = \frac{L}{\frac{1}{2}\rho v^2 Sb} \quad \textbf{(Rolling moment coefficient, Body axes)} \quad (5)$$

$$C_m = \frac{M}{\frac{1}{2}\rho v^2 S\bar{c}} \quad \textbf{(Pitching moment coefficient, Body axes)} \quad (6)$$

$$C_n = \frac{N}{\frac{1}{2}\rho v^2 Sb} \quad \textbf{(Yawing moment coefficient, Body axes)} \quad (7)$$

Figure 8 and Table 1 show the forces, moments and coefficients in the body axes reference system.

Table 1. Forces, Moments and Coefficients in the Body Axes Reference System.

	Roll Axis Xb	***Pitch Axis Yb***	***Yaw Axis Zb***
Aerodynamic Forces	X (Axial)	Y(Side)	Z(Normal)
Aerodynamic Forces Coefficients	C_X	C_Y	C_Z
Aerodynamic Moments	L	M	N
Aerodynamic Moment Coefficients	C_l	C_m	C_n

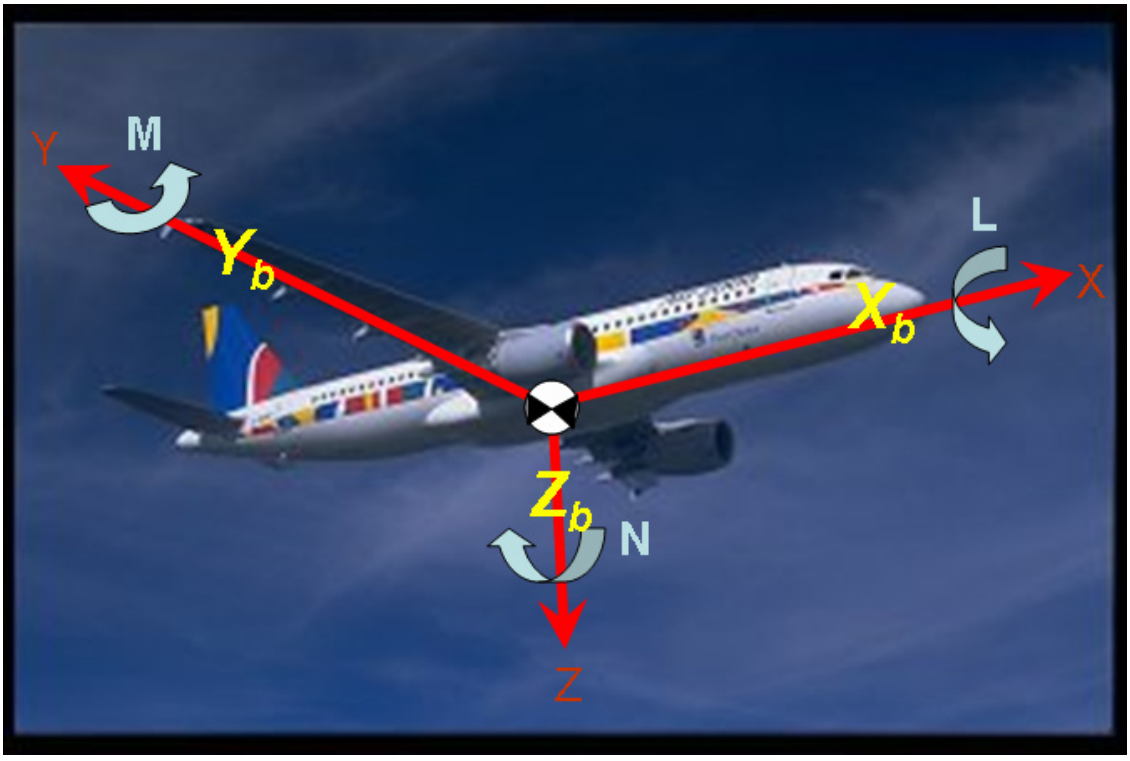

Figure 8. Forces and Moments in the Body Coordinate System (Photo: Airbus, 2004)

b. Wind Axes

In this axis system the X-axis is oriented into the relative wind, independently of the angle of attack or side slip angle of the aircraft.

Each of the axes of this system is designated with a subscript "w". As can be seen in Figure 9, X_w is pointing into the wind, Z_w is pointing down and Y_w is pointing to the right. The force component of this axes are drag (D), lift (L) and side (S) forces, respectively. Notice that the convenience of these axes is based in the fact that lift, by definition is always perpendicular to the wind.

As in the body axes, the force components in the wind axes are defined as coefficients by using the flight dynamic pressure and a reference area (wing platform area) as is shown in the following formulas:

$$C_L = \frac{L}{\frac{1}{2}\rho v^2 S} \quad \textbf{(lift coefficient, wind axes)} \qquad \textbf{(8)}$$

$$C_D = \frac{D}{\frac{1}{2}\rho v^2 S} \quad \textbf{(Drag coefficient, wind axes)} \qquad \textbf{(9)}$$

$$C_S = \frac{SideForce}{\frac{1}{2}\rho v^2 S} \quad \textbf{(Side force coefficient, wind axes)} \qquad \textbf{(10)}$$

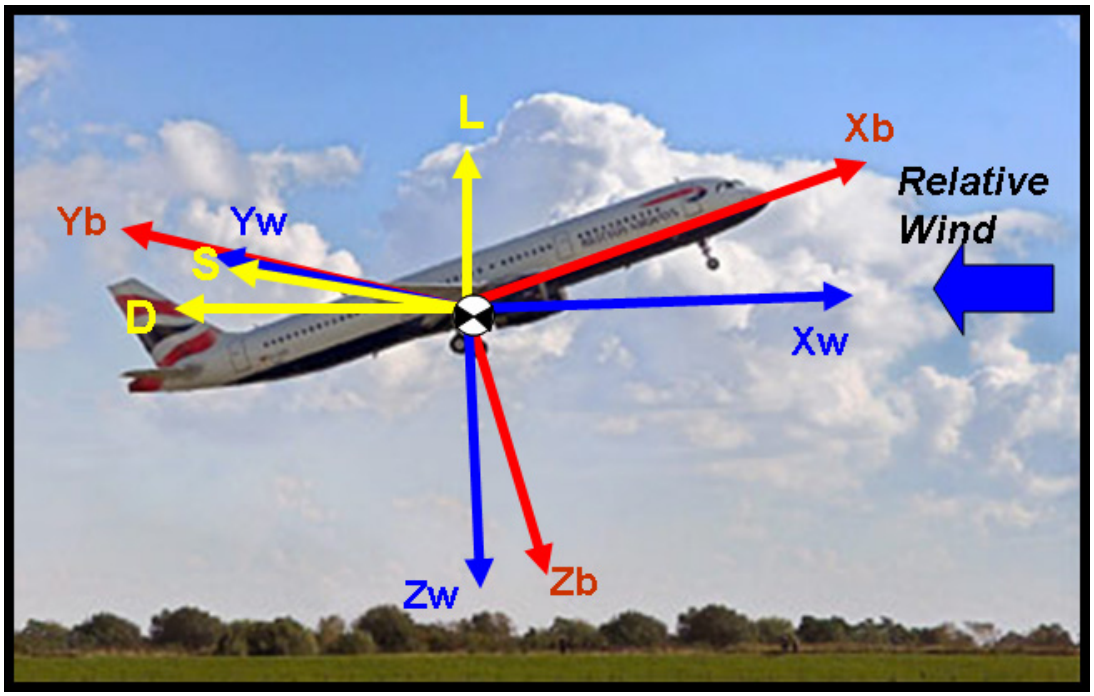

Figure 9. Wind Axis and its Force Components (Photo: Airbus, 2004)

Two orientation angles (with respect to the relative wind) are needed to delineate the forces and moments already defined. These angles are the angle of attack (α) and side slip angle (β). The angle of attack (α) is the angular difference between the relative wind and the X axes of the body in the body X-Z plane. It is positive when the relative wind is on the underside of the aircraft. The sideslip angle (β) is the angular difference between the relative wind and the X axes of the body in the body X-Y plane. It is positive when the relative wind is on the right side of the airplane. (Stevens and Lewis; 2003:72). Figure 10 and Figure 11 show these angles.

One of the most important aspects of stability analysis is related to the response to changes in angular orientation and as a consequence, the derivatives of moment and force coefficients with respect to α or β play an important roll in this analysis. In order to

indicate the derivatives of these coefficients, subscripts are used. For instance, Cm_{α} represents the derivative of the longitudinal moment coefficient with respect to the angle of attack.

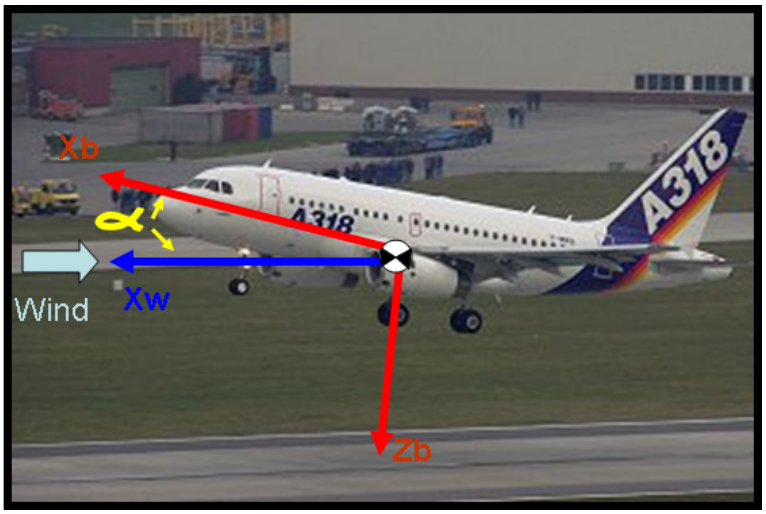

Figure 10. Definition of Angle of Attack (Photo: Airbus, 2004)

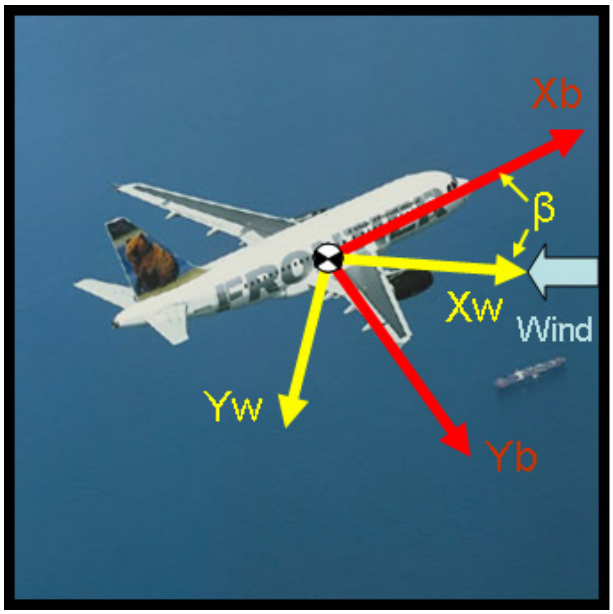

Figure 11. Definition of Sideslip Angle (Photo: Airbus, 2004)

2.3. Static Stability and Control

When an aircraft is flying it is subject not only to the aerodynamic forces already mentioned, but also to disturbances that move the aircraft from its equilibrium position. These disturbances can be due to the pilot or due to atmospheric phenomena such as winds or turbulence. The characteristic of the aircraft that make it return to the original equilibrium condition is called stability.

It is desirable that an airplane has stability in order to increase the safety of the flight; however some aircraft have little or no stability, therefore they are flown by using artificial stability provided by an electromechanical device called a stability augmentation system. (Nelson; 1998:39)

It is important to note that due to the definition of stability, any change in the design of the UAV can be done without consideration of stability if the aircraft uses artificial stability; nevertheless, the lack of stability will require more actuation of the flight controls, and as a consequence the range and simplicity of the UAV will decrease due to the increase of the electric power consumption. Moreover, no stability will adds complexity to the UAV due to the necessity of such as flight control system.

Stability is related to an equilibrium state, and thus it is necessary to define this term. Equilibrium state is the condition of the airplane when the resultants of all the forces that act over the airplane as well of the moments about its center of gravity are zero. If these forces and moment do not sum to zero then the airplane has translational or rotational accelerations. (Nelson; 1998:39)

Depending on the way that the airplane returns to its original equilibrium state, there exist two kinds of stability: static and dynamic stability.

Static stability is present if the forces created by the disturbed state act in the correct direction to return the airplane to its original equilibrium condition (Raymer; 1999:481). An aircraft is statically unstable if these forces act in the opposite direction and as a consequence the result will increase the non-equilibrium condition. For instance, if the airplane pitch moment is disturbed due to an increase in angle of attack, and this airplane is statically unstable; then the airplane will increase the angle of attack instead of decreasing it. Lastly, an aircraft is neutrally stable if once it is disturbed it will keep in the new non-equilibrium state with no action of forces that try to correct it or make it worst.

Dynamic stability is related to the time history of the motion of the aircraft after it was disturbed from its equilibrium state (Nelson; 1998:41). When a disturbance is present energy is added to the system. It can be said that energy is dissipated if this disturbance reduces its magnitude as time goes on. This dissipation of energy is called positive damping, and as a consequence the aircraft returns to its equilibrium position smoothly because it has dynamic stability. On the other hand, if once the aircraft is disturbed more energy is added to the system instead of dissipating the energy; the system is said to have negative damping. An aircraft with negative damping is dynamically unstable. Figure 12 shows a representation of static and dynamic stability. The focus of this thesis is in the static stability of a UAV with a rotary tail.

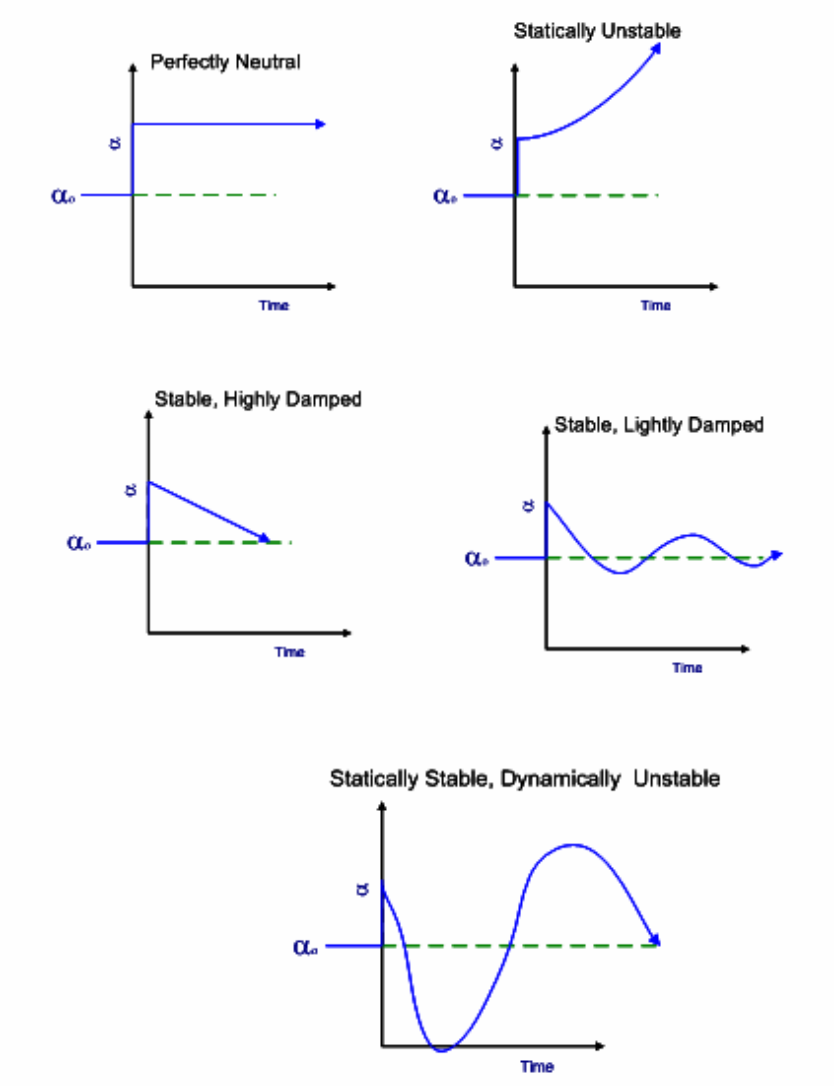

Figure 12. Static and Dynamic Stability

2.3.1. Longitudinal Static Stability.

Longitudinal static stability is evaluated by using a plot of C_m versus α. This plot shows the behavior of the airplane once it is disturbed from its equilibrium point in the longitudinal axes. Figure 13 illustrates two examples of pitching moment curves. The point at which the airplanes are flying at trim condition (C_{mcg}=0) is represented by the

point where the curves intersect the α axes and it is denoted by point "2". It can be seen that if a disturbance increases the angle of attack of both airplanes to point 3, airplane A will develop a negative pitch moment that will reduce the mentioned angle of attack, on the other hand, airplane B will develop a positive pitch moment that will help to increase the angle of attack; Moreover, if the disturbance decrease the angle of attack to point 1, once again the only airplane that will produce the correct pitch moment to correct the disturbance will be airplane A. For this reason airplane A is said to have static longitudinal stability and airplane B is longitudinally static unstable. In conclusion, in order for an airplane to have longitudinal static stability, the slope of the plot Cm versus α must be negative:

$$\frac{\partial C_m}{\partial \alpha} < 0$$

In addition of this condition, in order to have the capability of trim the airplane at positive angle of attack, it is necessary that the curve intercepts the angle of attack axes in the positive region ($C_{m0}>0$) (Nelson; 1998:43).

The main components of the airplane that contribute to the longitudinal static stability are the wing, tail, fuselage and engine (Raymer; 1999: 484).

The wing contribution can be analyzed by using Figure 14. The summation of all the moments about the center of gravity of the aircraft is represented by the following equation (Nelson; 1998:45):

$$M_{cgw} = L_w * Cos(\alpha_w - i_w)[X_{cg} - X_{ac}] + D_w * Sin(\alpha_w - i_w)[X_{cg} - X_{ac}] +$$

$$L_w * Sin(\alpha_w - i_w)[Z_{cg}] - D_w * \cos(\alpha_w - i_w)[Z_{cg}] + M_{acw} \qquad \textbf{(11)}$$

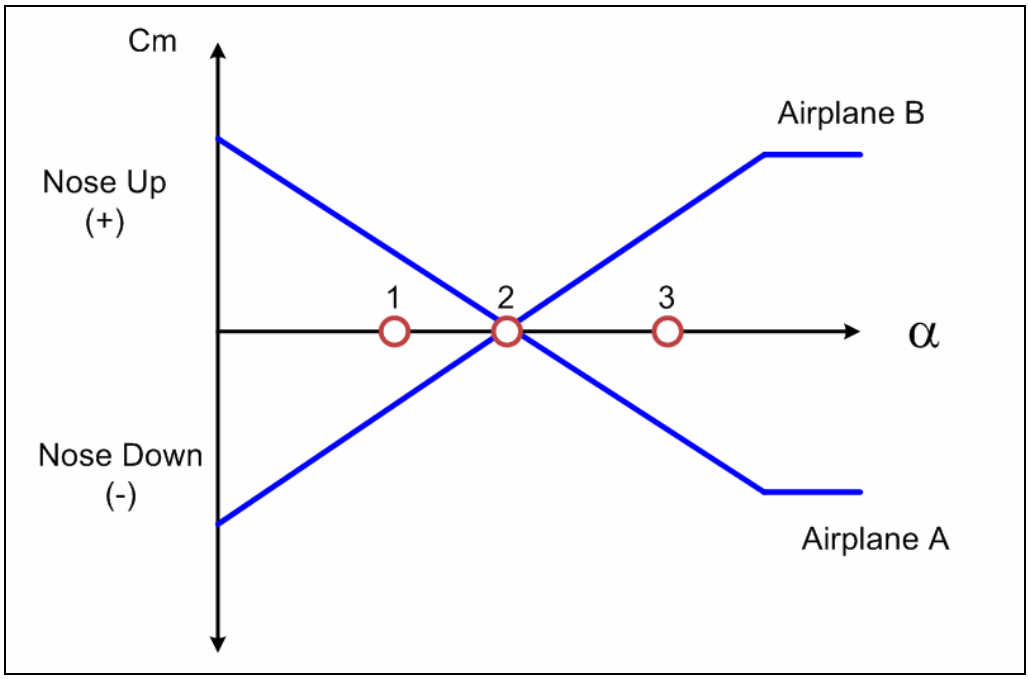

Figure 13. Longitudinal Static Stability

If this equation is divided by $\frac{1}{2} * \rho * v^2 * \bar{c} * S$, and is simplified by assuming small angles of attack and neglecting the vertical contribution and by applying the condition for static stability, the following equation that reflects the wing contribution of the wing alone to the static stability of the whole airplane is obtained (Nelson; 1998:46):

$$C_{m_\alpha} = C_{L_\alpha}\left(\frac{Xcg}{\bar{c}} - \frac{Xac}{\bar{c}}\right) \qquad \textbf{(12)}$$

The tail contribution can be analyzed by using Figure 15. The pitching moment due to the tail can be obtained by the following procedure: First, the sum of moments produced by the tail about the center of gravity of the airplane is written as:

$$M = -l[L * Cos(\alpha_{FRL} - \varepsilon) + D * Sin(\alpha_{FRL} - \varepsilon)] - Zcg[D * DCos(\alpha_{FRL} - \varepsilon) - LSin(\alpha_{FRL} - \varepsilon)] + Mac \qquad \textbf{(13)}$$

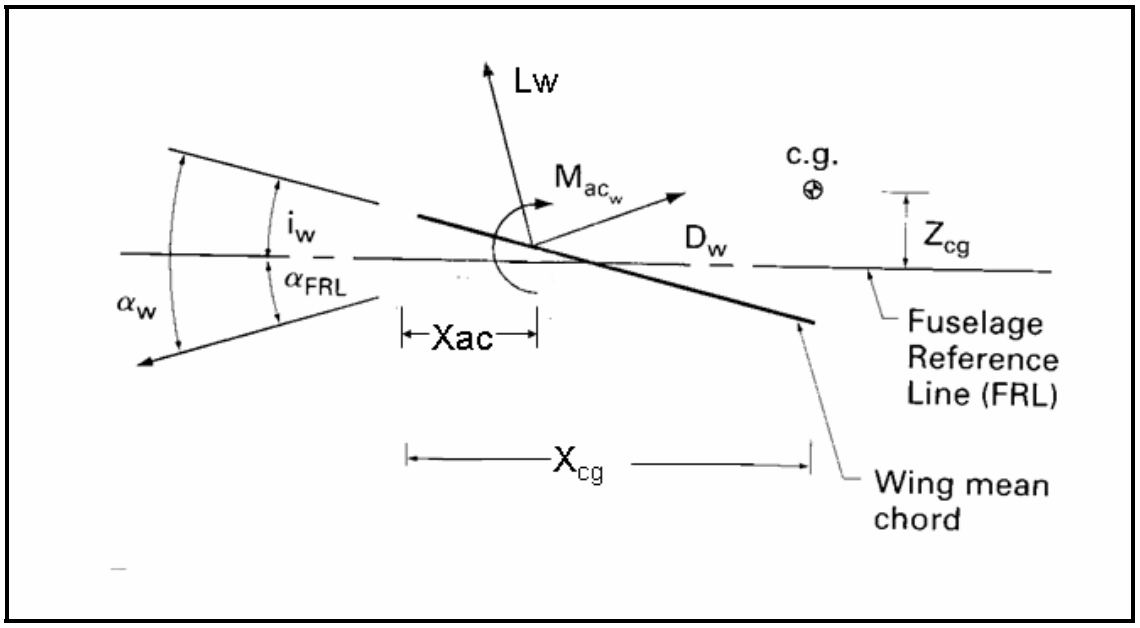

Figure 14. Wing Contribution to the Longitudinal Static Stability (Nelson; 1998:45)

If the second and third terms are neglected because their contribution is relatively small, a small-angle assumption is made, and the condition for static stability is used, then the prior equation becomes the following one that states the contribution of the tail to the longitudinal static stability of the whole airplane (Nelson; 1998:49):

$$C_{m_\alpha} = -\eta * V_H * C_{L\alpha}(1 - \frac{d\varepsilon}{d\alpha}) \qquad \textbf{(14)}$$

Where:

$$\eta = \text{Tail efficiency} = \frac{\frac{1}{2} * \rho * V_t^2}{\frac{1}{2} * \rho * V_w^2}$$

$$V_H = \text{Horizontal tail volume ratio} = \frac{l_t * S_t}{(S\ \bar{c})}$$

$C_{L\alpha}$=Slope of the tail lift curve

$\frac{d\varepsilon}{d\alpha}$ = The rate of change of downwash angle with angle of attack= $\frac{2 * C_{L\alpha_w}}{\pi * AR_W}$

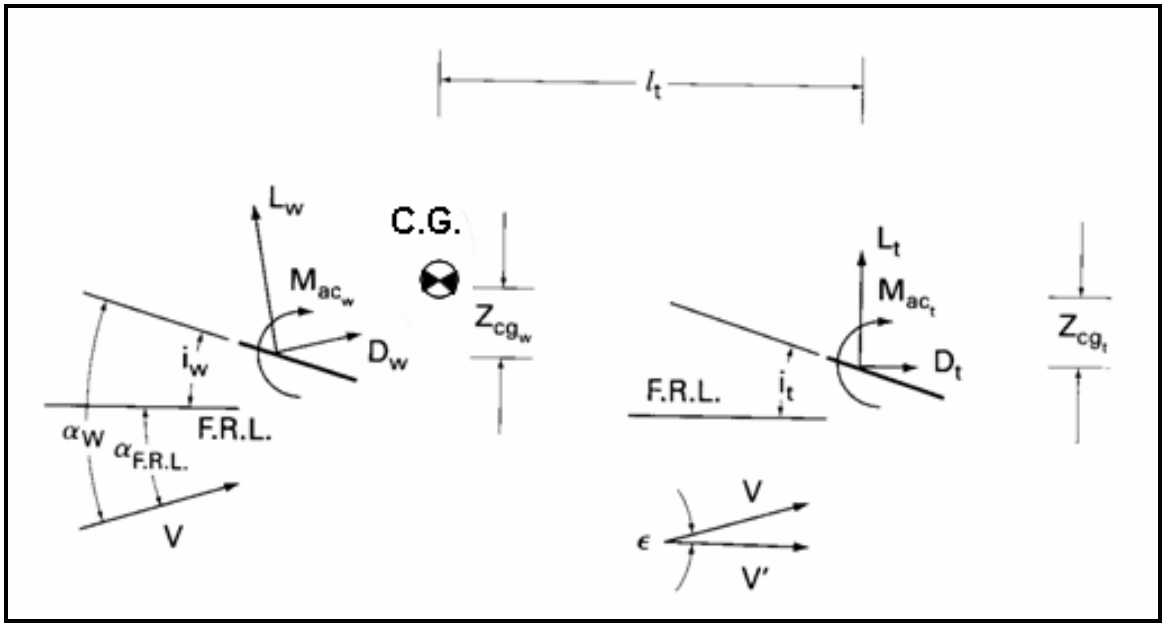

Figure 15. Tail Contribution to the Longitudinal Static Stability (Nelson; 1998:47)

The fuselage contribution to the longitudinal static stability of the airplane is expressed by using the following formulation which derives from the aerodynamic characteristic analysis of long, slender bodies studied by Munk in 1920 and its extension to fuselages made by Multopp in 1942. In order to apply it, it is necessary to divide the fuselage into segments. (Nelson; 1998:53):

$$Cm_\alpha = \frac{1}{36.5 * S * \bar{c}} \sum_{x=0}^{x=l_f} w_f^2 \frac{\partial \varepsilon_u}{\partial \alpha} \Delta X \qquad \textbf{(15)}$$

Where: W_f=The average width of the fuselage section

ΔX=The length of the fuselage increments.

S=The wing reference area

$\frac{\partial \varepsilon_u}{\partial \alpha}$=The change in local flow angle with angle of attack.

The propulsion unit can have a huge influence in the stability of the airplane; however, even if it is possible to derive an expression for its contribution to the longitudinal static stability, the actual contribution is difficult to estimate and it is commonly obtained from powered –wind tunnel models (Nelson; 1998:56).

Finally, in order to obtain an equation that expresses all the factors that influence the static stability of an airplane, it is necessary to do a summation of the components, and the final expression is:

$$Cm_\alpha = C_{L_{\alpha_W}}(\frac{Xcg}{\bar{c}} - \frac{Xac}{\bar{c}}) + Cm_{\alpha_F} - \eta V_H C_{L_{\alpha_T}}(1 - \frac{d\varepsilon}{d\alpha}) \quad \textbf{(16)}$$

It can be perceived in the preceding formula that the pitching–moment derivative changes with the location of the center of gravity. There exists a position of the center of gravity where a change in angle of attack does not provide change in pitching moment. This point is called the neutral point and is labeled Xnp. This point represents the aerodynamic center of the complete airplane; therefore, when the center of gravity is located in this position, the aircraft is neutrally stable. If the center of gravity is ahead of the neutral point the pitching moment derivative is negative and as consequence the

airplane is stable. On the other hand, when the center of gravity is aft of the neutral point the pitching-moment derivative is positive and the aircraft is unstable.(Raymer;1999:487).

The influence of this neutral point in the longitudinal static stability of the whole aircraft is shown in Figure 16 and its formulation is obtained by setting $C_{m\alpha} = 0$ in Equation 16 and solving for the center of gravity position, obtaining the following equation:

$$\frac{X_{NP}}{\bar{c}} = \frac{Xac}{\bar{c}} - \frac{Cm_{\alpha_F}}{C_{L\alpha_W}} + \eta * V_H * \frac{C_{L\alpha_T}}{C_{L\alpha_W}}\left(1 - \frac{d\varepsilon}{d\alpha}\right) \qquad \textbf{(17)}$$

It is important to notice that the formulas for longitudinal static stability mentioned are used for conventional airplanes. However, these are not applied directly to rotary tails, because the moments produced in this kind of tail are function of both elevator deflection and rotation. To address this need, wind tunnel experiments were performed. In Chapter III the procedure used for the experiments is provided and in Chapter IV the results are shown.

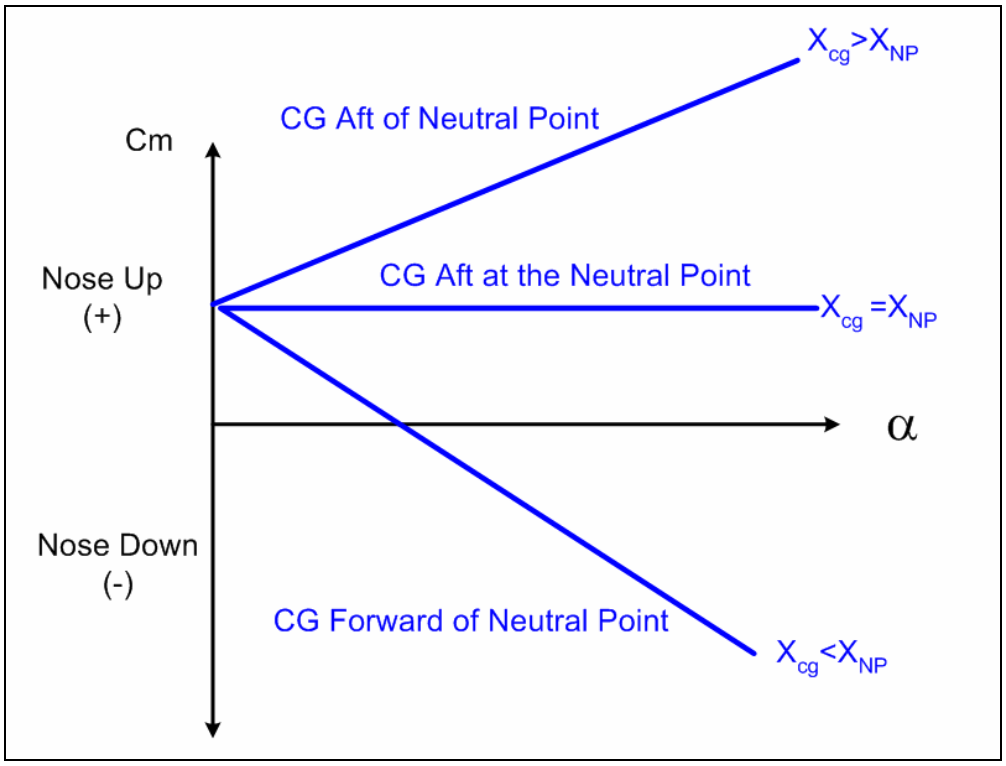

Figure 16. Influence of the Center of Gravity on the Longitudinal Static Stability

2.3.2. Longitudinal Control.

For conventional subsonic airplanes, the longitudinal control is made by using an aerodynamic control surface called an elevator. This is a movable surface at the trailing edge of the horizontal tail. The symbol used to designate deflection angles of the elevator is δe. In accordance with the sign convention as can be seen in Figure 17, from the side view of an airplane, elevator deflection is positive when the elevator deflects down and it is negative when its deflection is upward. Similar to the notation used for defining the change in force or moment coefficient with respect to angle of attack or sideslip angle, control deflection subscripts are used to indicate the response to the control deflection. For instance, Cm_{δ_e} indicates the pitch moment coefficient to the elevator deflection. In

supersonic airplanes the complete horizontal stabilizer surfaces moves, this control surfaces is called stabilator (Stevens and Lewis; 2003:95).

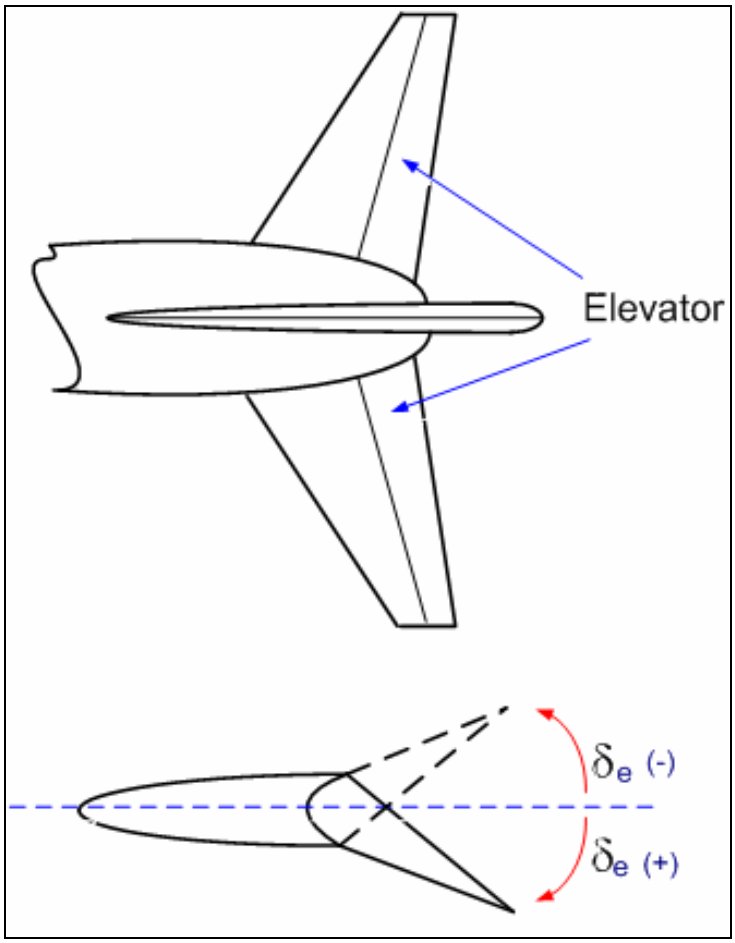

Figure 17. Conventional Elevator Deflection

The factors that influence the design of a control surface are control effectiveness, hinge moments and aerodynamics and mass balancing. Control effectiveness is a measure of the efficiency of the control surface in producing the desired moment in the airplane. The hinge moment is related to the magnitude of the force required to move the surface control and aerodynamic and mass balancing is associated with techniques to control the

hinge moments in order to keep the control stick forces within a desirable range (Nelson; 1998:63). This thesis is focused on the control effectiveness of the rotary tails.

When the elevator is deflected, the pitch moment and the total lift of the airplane change. This change can be represented in a plot of Cm versus Alpha or Cm versus C_L. In these kinds of plots, the slope of the curve does not change; the only difference between the curves that represent different elevator deflections is the position in the plot due to the different trim angles. This situation is shown in Figure 18.

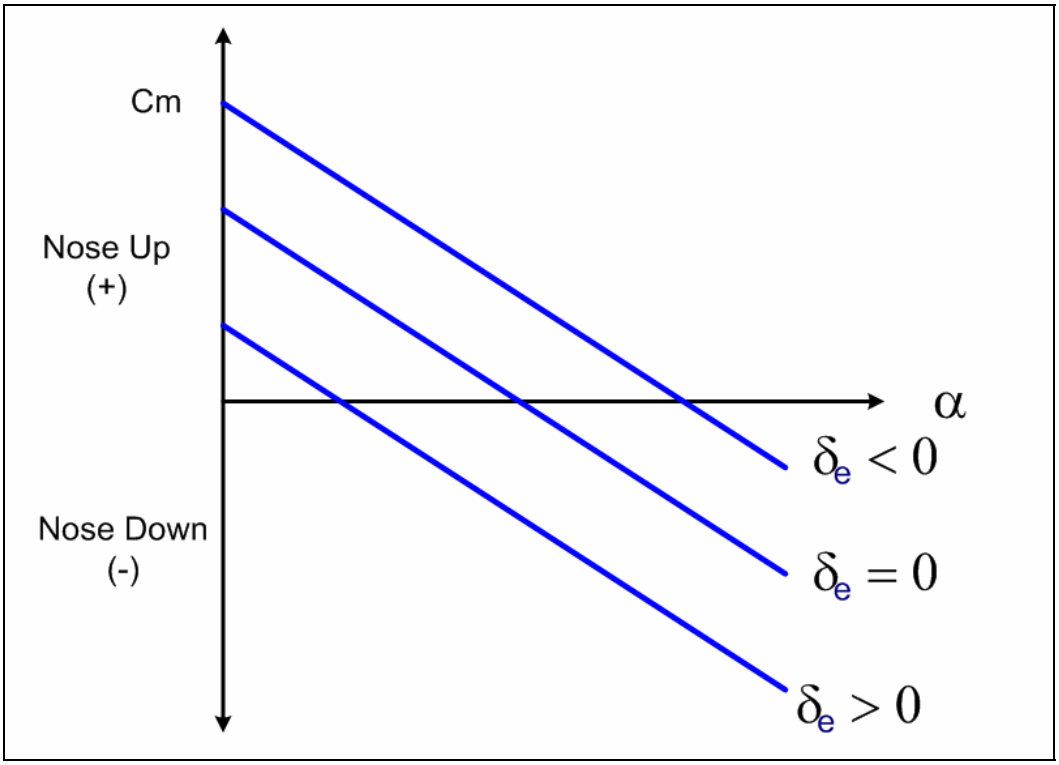

Figure 18. Influence of the Elevator on the Longitudinal Static Stability

The change in lift due to the deflection of the elevator is represented by the following equation (Nelson; 1998:63):

$$\Delta C_L = C_{L_{\delta_e}} * \delta_e \qquad \textbf{(18)}$$

where: $$C_{L_{\delta_e}} = \frac{dC_L}{d\delta e} \qquad (19)$$

Moreover, the change in the lift due to the elevator deflection can be expressed as a change in the lift force acting on the tail:

$$\Delta C_L = \frac{S_T}{S} * \eta \frac{d\ C_{Lt}}{d\delta e} \delta e \qquad (20)$$

where $\frac{d\ C_{Lt}}{d\delta e}$ is called the elevator effectiveness and is a function of the size of the elevator (Nelson; 1998:64).

On the other hand, the change in pitch moment is represented by the following equation (Nelson; 1998:64):

$$\Delta Cm = Cm_{\delta_e} * \delta e \qquad (21)$$

where: $$Cm_{\delta_e} = \frac{dCm}{d\delta e} = -V_H * \eta * \frac{d\ C_{Lt}}{d\delta e} \qquad (22)$$

The term Cm_{δ_e} is called the elevator control power and its value directly affects the elevator effectiveness.

Recall that the formulas for longitudinal control mentioned are used for conventional airplanes. On the other hand, these are not applied directly to rotary tails because the moments produced in this kind of tail are function of both elevator deflection and rotation. To address this need, wind tunnel experiments were performed. In Chapter

III the procedure used for the experiments is provided and in Chapter IV the results are shown.

2.3.3. Static Roll Stability.

An airplane has roll stability if a restoring moment is produced when it is disturbed from the attitude of wings-level.

A plot of C_l versus Beta is used to evaluate this stability in an airplane. Figure 19 shows two different curves as example of stability conditions. It can be seen that the condition for static roll stability is $C_{l_\beta} < 0$.

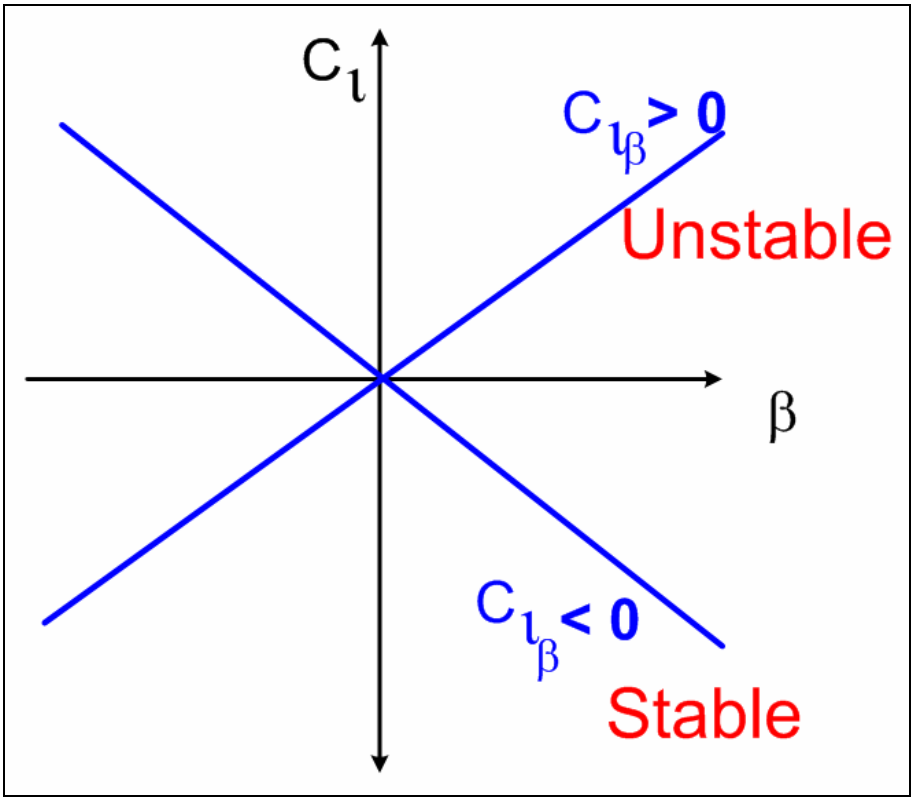

Figure 19. Static Roll Stability

The main factors that affect this stability are wing dihedral, wing sweep, position of the wing on the fuselage and the vertical tail. (Dittrich; 1966: VIII-30)

The major contributor to static roll stability is wing dihedral angle, which is represented by the by the Greek capital letter gamma Γ. Wing dihedral is the angle of the wing with respect to the horizontal; it is positive if the tips of the wing are higher than its root, and it is negative if they are below the root of the wing.

Figure 20 shows the effect of the wing dihedral in the static roll stability. When an airplane that has positive dihedral is disturbed from the wings level attitude by a relative wind represented in figure 20 from a positive slide slip; the wing toward which the aircraft is sideslipping increases its angle of attack and as a consequence increases the lift; moreover, the other wing has the opposite effect: decreasing the angle of attack and therefore the lift produced. This change on the lift produced in the wings generates a roll moment that is the opposite of that produced by the disturbance.

The change in the angle of attack produced can be expressed as (Nelson; 1998:79):

$$\Delta\alpha = \frac{Vn}{u} \quad \textbf{(23)}$$

where Vn=V Sin Γ

If the sideslip angle is approximated by $\beta = \frac{v}{u}$, and assuming that that the dihedral is small, this change in the angle of attack can be expressed as:

$$\Delta\alpha \cong \beta * \Gamma \quad \textbf{(24)}$$

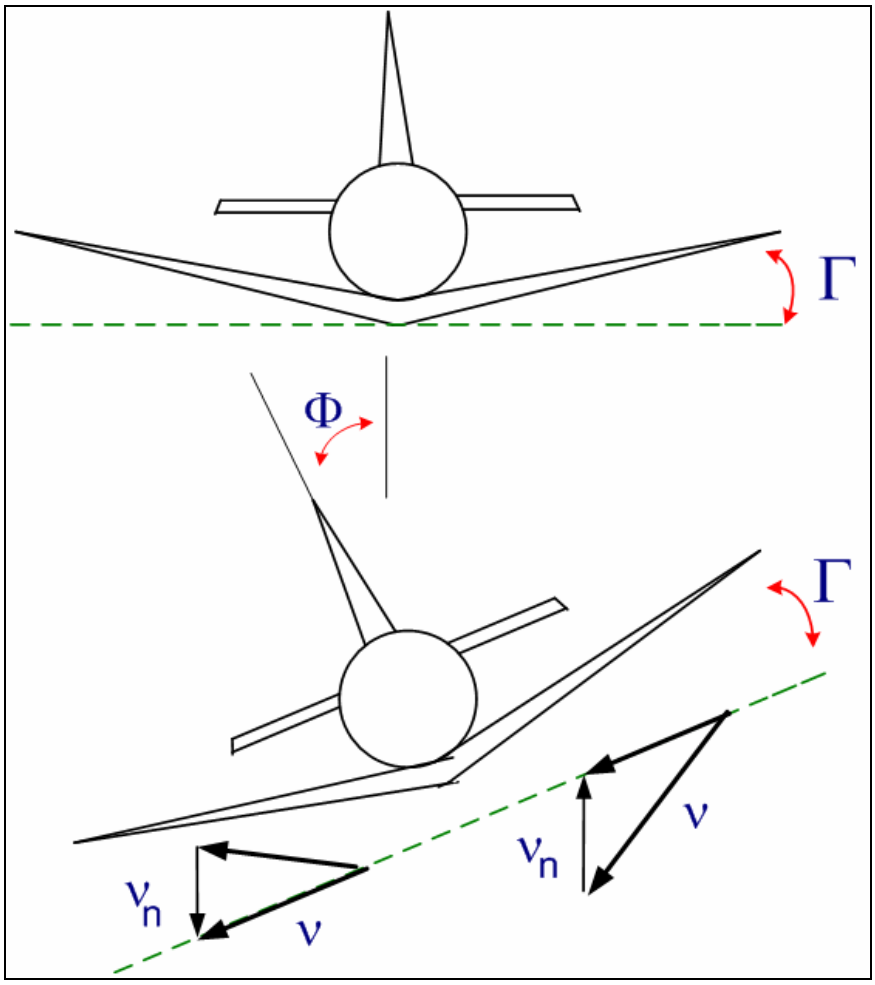

Figure 20. Dihedral Contribution to the Roll Stability

The effect of a wing sweep angle is shown in Figure 21. This contribution is based in the fact that in a swept back wing the wing that is in the same side where the wind comes from is subject to a increase in the sweep angle and the other wind decreases its sweep angle; as a consequence, the wing that is toward the wind increases its lift and the other wing decreases it, producing a roll moment that is opposite to the one created by the wind. This phenomena is based on the fact that the characteristics of a swept wing are functions of the value of the velocity normal to the quarter chord for subsonic flight, then,

the dynamic pressure for the right wing is based in the velocity defined by (Dittrich; 1966: VIII-30):

$$V * Cos(\Lambda - \beta) \quad \textbf{(25)}$$

On the other hand, the dynamic pressure for the right wing is based on the velocity defined by:

$$V * Cos(\Lambda + \beta) \quad \textbf{(26)}$$

It can be seen that the dynamic pressure and as a consequence the lift created in each wing will produce the roll moment already mentioned that is opposite to the one produced by the disturbance.

The effect on the roll stability of the position of the wing with respect to the fuselage can be visualized in Figure 22. In airplanes with a high wing there is an increase in the angle of attack in the wing that is on the side of the wind and of course a decrease of this angle in the opposite wing. As a consequence, the dihedral effect is increased in these high-wing airplanes. On the other hand, in airplanes with low wing this phenomena is opposite and it can be said that the fuselage produces a destabilizing dihedral effect; therefore the low-wing airplanes will require a greater value of wing dihedral angle in order to keep an acceptable value of $C_{l\beta}$, compared with the angles required by a high wing airplane (Dittrich; 1966: VIII-35).

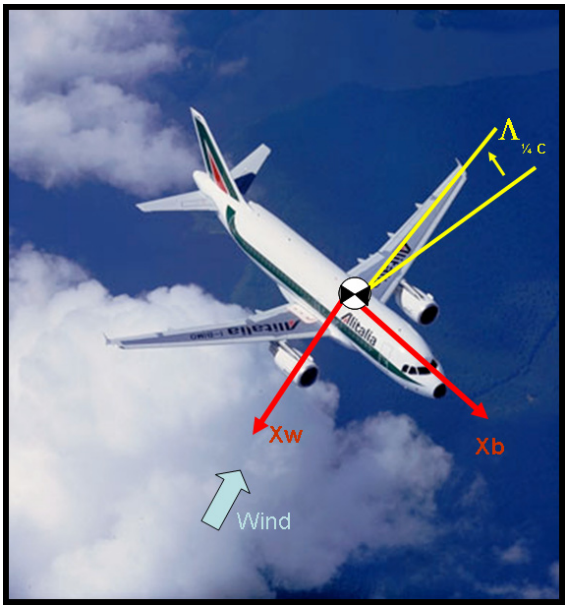

Figure 21. Effect of the Wing Sweep on Roll Stability (Photo: Airbus, 2004)

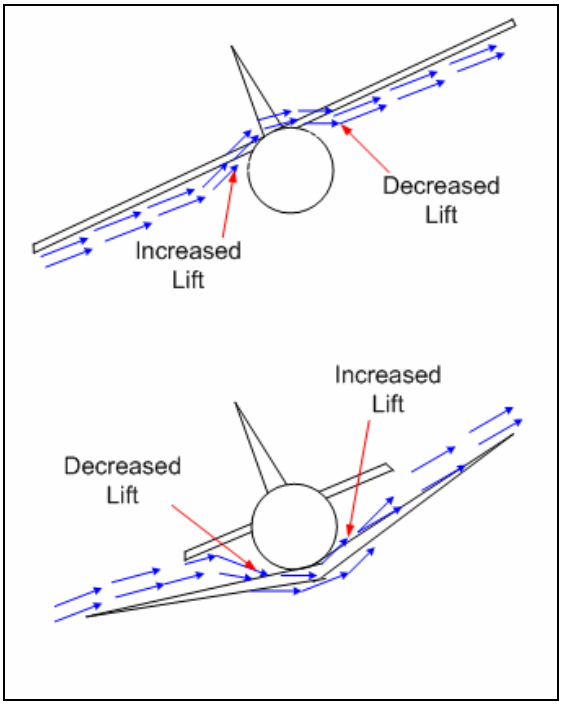

Figure 22. Fuselage Contribution to the Roll Stability

The contribution to the static roll stability due to the vertical stabilizer can be visualized in Figure 23. This contribution is produced by the lift force created in the tail by the sideslip angle. This lift produces a stabilizing roll moment because the center of pressure of the vertical tail is located above the center of gravity. The rolling moment produced by a positive sideslip, in accordance with the notation used in Figure 23 is given by $L = -Z * L_F$ (Dittrich; 1966: VIII-38).

The formulas for roll stability mentioned are used for conventional airplanes. Nevertheless, the contribution of the vertical stabilizer is not applied directly to rotary tails, because the moments produced in this kind of tail are function of both elevator deflection and rotation. To understand this contribution, wind tunnel experiments were performed by using a rotary tail with vertical stabilizers. In Chapter IV the results are shown.

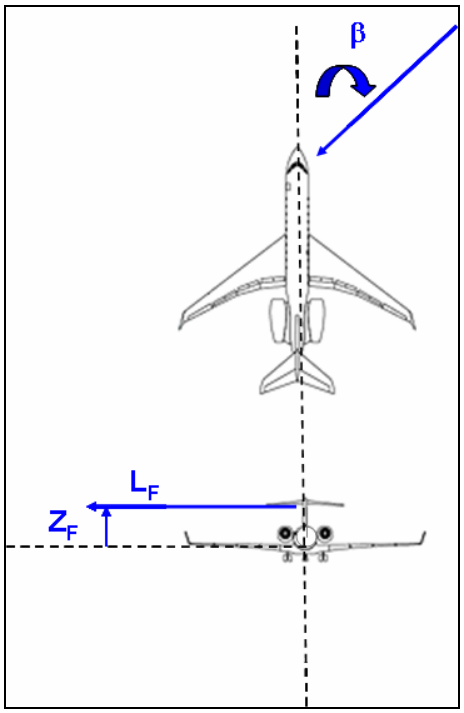

Figure 23. Effect of the Vertical Stabilizer to the Roll Stability

2.3.4. Roll Control.

In a conventional airplane, roll control is accomplished by using a differential deflection of small flaps called ailerons which are located on the outboard of the wings. The symbol used for define aileron deflection is δa. In accordance with the sign convention and as can be seen in Figure 24, a positive value of aileron deflection is one that causes a positive (right wing down) roll. Another method to develop roll control is by using spoilers on the upper surfaces of the wing. Theses spoilers work as a lift destroyer device when they are deflected. Therefore, in order to produce a roll moment, only the spoiler of one side is deflected. Both techniques work using the same basis: produce a difference between the lift in the wings in order to create a moment about the longitudinal axes. (Stevens and Lewis; 2003:91). These two methods are shown in Figure 24.

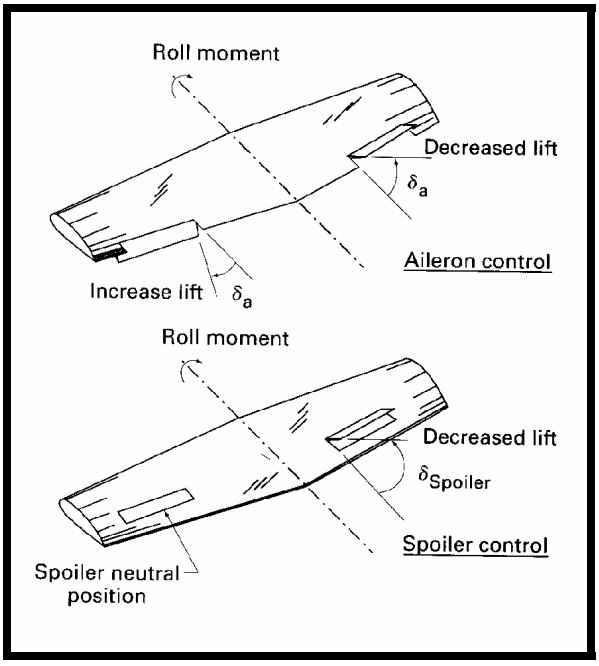

Figure 24. Roll Control (Nelson; 1998:82)

The analysis to estimating the roll control power of an aileron is made using the technique called “strip integration method”. This method is illustrated in Figure 25, and consists in the following analysis (Nelson; 1998:81):

The increment in roll moment produced by the deflection of an aileron is expressed by:

$$\Delta L = (\Delta Lift) * y \qquad \textbf{(27)}$$

In coefficient form this increment can be represented by:

$$\Delta C_l = \frac{\Delta L}{QSb} = \frac{C_l QCydy}{QSb} = \frac{C_l cydy}{Sb} \qquad \textbf{(28)}$$

The section lift coefficient C_L on the station of the ailerons is expressed as:

$$C_l = C_{l\alpha} * \frac{d\alpha}{d\delta a} = C_{l\alpha}\tau\delta a \qquad \textbf{(29)}$$

If this equation is substituted in Equation 28 and integrated over the area of the aileron the following equation is obtained:

$$C_l = \frac{2C_{L\alpha_w}\tau\delta a}{Sb}\int_{y1}^{y2} cydy \qquad \textbf{(30)}$$

Finally, the aileron control power is obtained from Equation 30 by taking the derivative with respect to the deflection of the aileron (δa):

$$C_{l_{\delta_a}} = \frac{2C_{L\alpha_w}\tau}{Sb}\int_{y1}^{y2} cydy \qquad \textbf{(31)}$$

Notice that the formulas for roll control mentioned are used for conventional airplanes. On the other hand, these are not applied directly to rotary tails because the roll moment produced in this kind of tail is function of both elevator deflection and rotation. To address this need, wind tunnel experiments were performed. In the following chapters the procedure used for the experiments as well the results are shown.

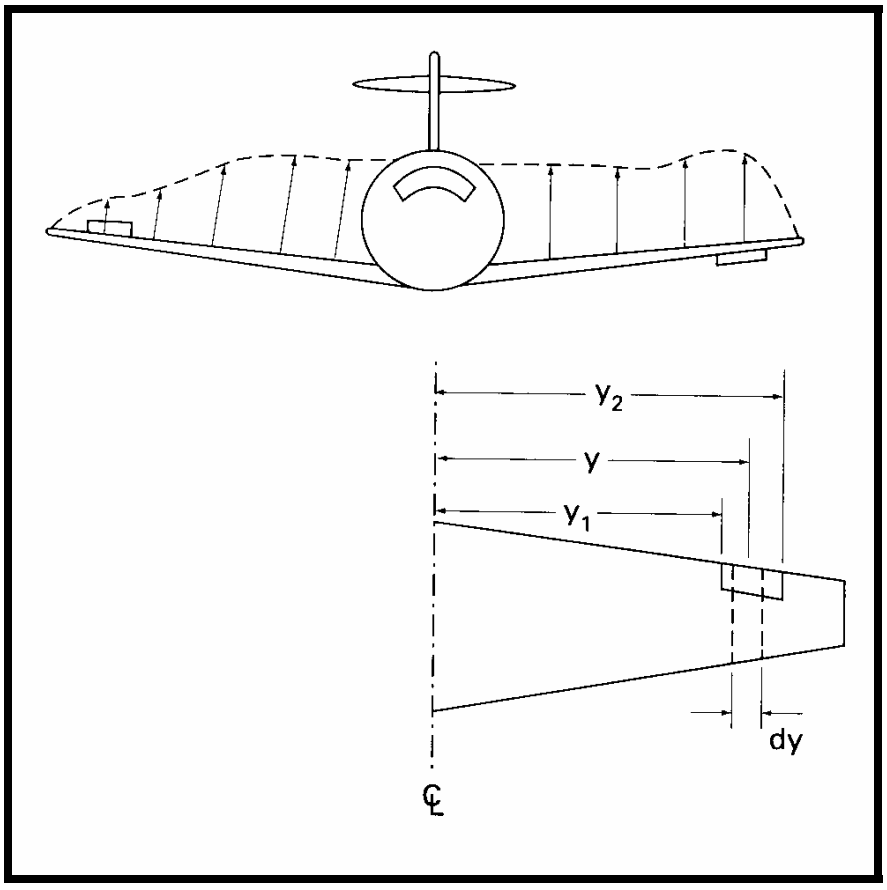

Figure 25. Strip Integration Method (Nelson; 1998:82).

2.3.5. Static Yaw Stability.

The static yaw stability, also known as weathercock stability, is related to the capability of the airplane of return to its equilibrium state when is subjected to a yaw disturbance.

This stability is analyzed by using a plot of Cn versus sideslip angle. Figure 26 shows two curves from different airplanes. Since the static yaw stability means that the airplane must develop a yaw moment that will return to its equilibrium state, it can be seen that if both airplanes are subject to a disturbance that increases their sideslip angle, only the airplane A will have this moment because it is necessary that as β becomes more positive, the Cn produced must becomes more positive, too. The condition for static yaw stability is:

$$Cn_{\beta} > 0 \qquad \textbf{(32)}$$

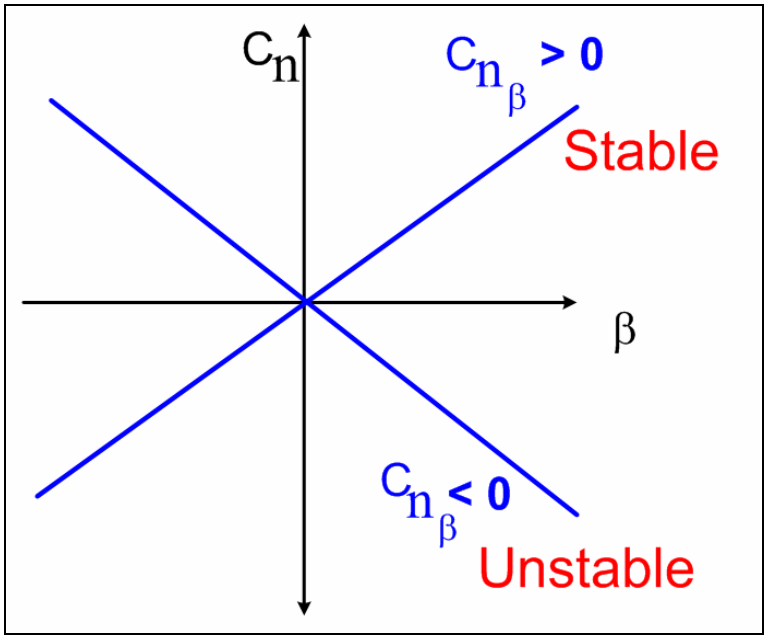

Figure 26. Static Directional Stability

Figure 27 shows an airplane in which the velocity vector does not lie in its longitudinal axes. There are two primary forces generated by a sideslip: the one produced by the fuselage and the one produced by the vertical tail (Dittrich; 1966: VIII-26). Because both forces are usually in opposite sides of the center of gravity and they are pointing in the same direction, they produce moments of different sign.

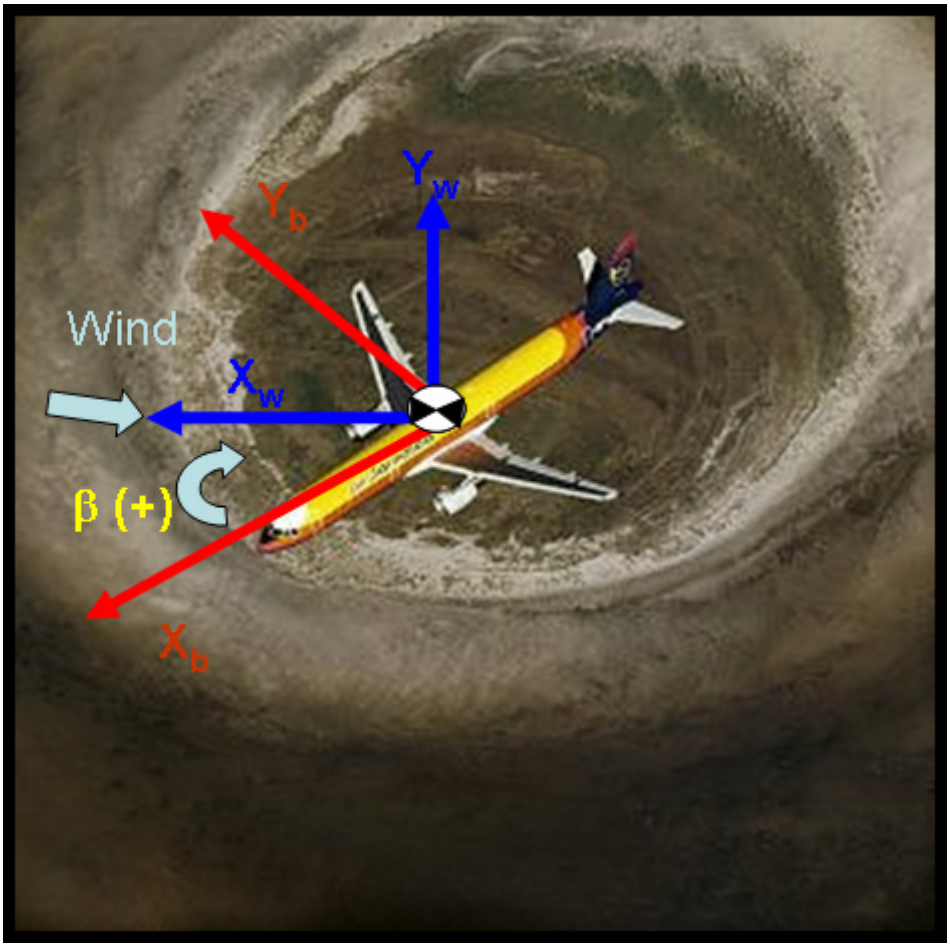

Figure 27. Directional or Yaw Static Stability (Photo: Airbus, 2004)

The fuselage, in general, creates a destabilizing contribution to the directional stability. This contribution is usually measured directly by a wind tunnel test of a model

with no vertical fin; however, there are several formulas for estimating this contribution. One of them is in the NACA report 1098 that suggest (Dittrich; 1966: VIII-27):

$$Cn_{\beta_{FUS}} = -1.3 * \frac{Volume.of.Fuselage}{b * S} * \frac{h}{w} \quad \textbf{(33)}$$

where: h= Mean fuselage depth
w= Mean fuselage with.

Because the fuselage contribution is destabilizing, it is necessary to have enough stabilizing effect made by the vertical tail. The mechanism by which the vertical tail creates its contribution is explained as following, (please refer to Figure 28) (Nelson; 1998:74-76):

The restoring side force produced by the vertical tailcan be expressed as:

$$Y_v = -C_{L\alpha_v} * \alpha_v * Q_v * S_v \quad \textbf{(34)}$$

where: v is the subscript used for the vertical tail properties.

α_V=Is the angle of attack of the vertical tail and is defined as:

$\alpha_V=\beta+\sigma$

where: σ is the sidewash angle that is caused by the flow field torsion due to the wings and fuselage.

The moment produced by the vertical tail is:

$$N_v = l_v * Y_v = l_v * C_{l\alpha\beta}(\beta + \sigma)Q_v * S_v \quad \textbf{(35)}$$

Expressed in coefficient form, this moment is:

$$Cn = \frac{N_v}{QwSb} = \frac{l_v S_v}{Sb} * \frac{Q_v}{Q_w} C_{L\alpha_v} (\beta + \sigma) = V_v \eta_v C_{L\alpha_v} (\beta + \sigma) \qquad \textbf{(36)}$$

The contribution of the vertical tail can be obtained by taking the derivative of Equation 36 with respect to β:

$$Cn_\beta = V_v * \eta_v C_{L\alpha_v} (1 + \frac{d\sigma}{d\beta}) \qquad \textbf{(37)}$$

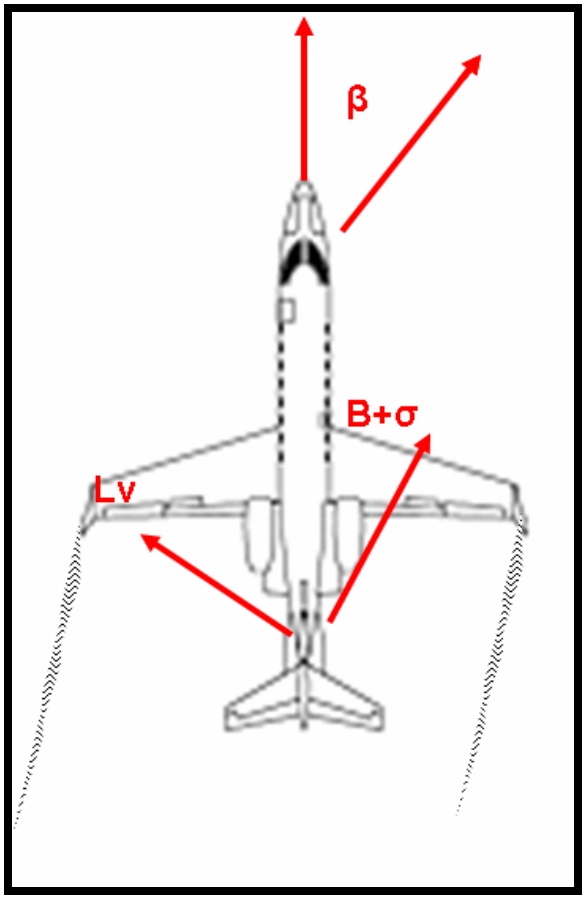

Figure 28. Vertical Tail Contribution to Yaw Stability

Since the formulas for yaw stability mentioned are used for conventional airplanes, these are not applied directly to rotary tails for the reason that the yaw moment produced in this kind of tail are function of both elevator deflection and rotation. To understand this phenomenon, wind tunnel experiments were performed. In the following chapters the procedure used for the experiments as well the results are shown.

2.3.6. Yaw Control.

The directional control is generally made by using a flap in the vertical tail that produces a moment about the Z axis. This flap is called a rudder. The symbol for defining rudder deflection is δr and as can be seen in Figure 29, the sign convention is positive when from a upper view of the airplane, the rudder is deflected to the left and is negative when is deflected to the right. A positive rudder deflection produces a positive side force and that resulting positive side force applied to the tail produces a negative yaw moment. The side force produced by the rudder can be expressed as (Nelson; 1998:77):

$$Y_v = C_{L_v} Q_v S_v \qquad \textbf{(38)}$$

As a consequence, the negative moment produced by a positive force can be expressed as:

$$N = -l_v Y_v \qquad \textbf{(39)}$$

This moment can be expressed in coefficient terms as:

$$Cn = \frac{N}{Qw * Sb} = -\frac{Q_v}{Qw}\frac{l_v S_v}{Sb}\frac{d C_{L_v}}{d\delta r}\delta r = -\eta_v V_v \frac{d C_{L_v}}{d\delta r}\delta r \qquad \textbf{(40)}$$

From this equation, the rudder control effectiveness can be expressed as the rate of change of yaw moment with rudder deflection angle as following:

$$Cn = C_{n\delta_r} * \delta r = -\eta_v V_v \frac{d\, C_{L_v}}{d\, \delta_r} \delta r \quad \textbf{(41)}$$

Solving $Cn_{\delta r:}$

$$Cn_{\delta_r} = -\eta_v V_v \frac{d\, C_{L_v}}{d\delta r} \quad \textbf{(42)}$$

The formulas for directional control mentioned are used for conventional airplanes but they are not applied directly to rotary tails because the yaw moment produced in this kind of tail is function of both elevator deflection and rotation. To understand this directional control concept, wind tunnel experiments were performed. In the following chapters the procedure used for the experiments as well the results are shown.

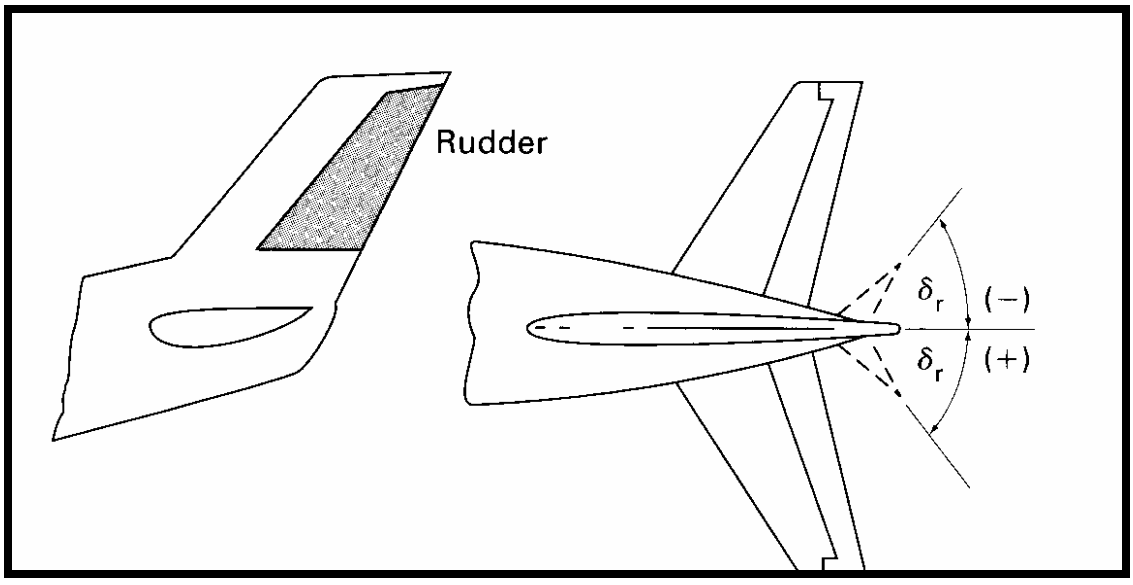

Figure 29. Sign Convention for Rudder Deflection (Nelson; 1998:77)

2.3.7. Typical Values for Derivatives of Static Stability and Control.

In order to have a reference for comparison with the values that in the following sections will be presented for the UAV using a rotary tail, Table 2 shows generic values for the derivatives of the static stability and control effectiveness. These values were obtained from the general aviation NAVION (Nelson; 1998:400).

Table 2. Typical Values for Derivatives of Static Stability and Control.

Derivative	Generic Value
$\frac{\partial Cm}{\partial \alpha}$	-0.0119
$\frac{\partial Cn}{\partial \beta}$	0.00123
$\frac{\partial C_l}{\partial \beta}$	-0.00129
$\frac{\partial Cm}{\partial \delta e}$	-0.0161
$\frac{\partial C_l}{\partial \delta_a}$	-0.00233
$\frac{\partial Cn}{\partial \delta r}$	-0.00126

2.4. Function of the Tail in Airplanes and in Birds

Because the idea of implementing a rotary tail in the UAV was born from observing the tail in birds; it is interesting to review the literature that describes the function of the tail in both, airplane and birds.

In the literature, there are different opinions on the function of the tail in birds. For instance, Horton-Smith in his book “The Flight of Birds”, page 38 says:

"A bird, like an airplane, uses rotation of wing and tail. There is no vertical fin in the bird's tail so it has to relay on banking. It is possible that a long tail, when bent to one side, may function as a rudder".

This information seems to indicate that a tail in birds plays an important role in flying and his opinion matches with John H. Storer who in his book "The Flight of Birds Analyzed Through Slow-Motion Photography", page 38 says:

"The tail of a bird, indeed, has many uses. It can steer in any direction, act as a brake, form a slot behind the wings, or become a part of the bird's lifting surface, supplementing the wings. The Swallow-tailed Kite twists its tail to steer. It may turn its tail so that either the upper or the lower surfaces will strike the air stream in steering. The tail sides of the tail maybe controlled separately."

Figure 30 shows the images presented by John H. Storer when he describes the flying of a Swallow-tailed Kite. It can be seen that this bird really uses its tail for steering and this was one of the most important phenomena to apply this control approach to a UAV.

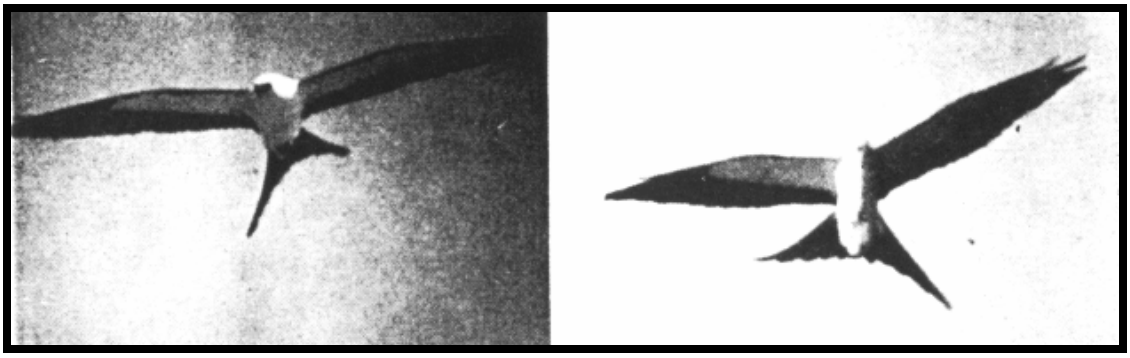

Figure 30. The Swallow-Tailed Kite Twists its Tail to Steer (Storer; 1948:39)

On the other hand, some authors think that the tails in birds does not play an important roll in flying. For example, Karl Nickel and Michael Wohlfahrt in their book "Tailless Aircraft in theory and practice", page 25 say:

"The tail of birds virtually has no stabilizing effect. It is, hence not a stabilizing instrument. Only to a limited extent is it used as a steering device. Mostly it is used at low speed as a landing flap"

As it was explained in the prior sections, the tail in airplanes provides stability and control. However, through the history of aviation there have been some airplanes that do not have a tail because the aerodynamic properties that it provides are obtained by other means: Longitudinal stability is obtained provided the wing aerodynamic center is behind the center of gravity; then, as can be seen in Equation 16, this technique will supply a negative value of Cm_{α}. Static roll stability can be achieved by wing dihedral and wing sweep and yaw stability can be achieved by using vertical fins like end-plates, winglets, central fin, etc. or by using sweepback (Nickel and Wohlfahrt;1994:110). Moreover, control of these tailless aircraft can be achieved by using only elevons (Nickel and Wohlfahrt; 1994:121). Figure 31 shows some examples of tailless aircraft.

Referring back to Figure 6 it can be seen that, in general, the tail volume coefficient of birds is smaller than that required for aircraft. By itself that would indicate that the effectiveness of the tail is less important for birds than for airplanes. Considering the comparatively enormous control authority birds can exert via their wings, this is conceivable.

A counterpoint to this argument is that birds also exert substantial control over their tails. Thus, it is conceivable that this added level of tail control enables birds to use it more effectively for steering.

In conclusion, since in accordance with the theory, a long tail is not indispensable for an airplane to fly, it is feasible to implement a rotary tail in the UAV and obtain a level of stability and controllability; This rotary tail differs from the conventional tail in

that it is possible to move it in elevator for pitch control as in a conventional tail, while at the same time it can be rotated around the X body axis in a circular movement to provide yaw and roll control (Figure 39 and Figure 40). It is important to mention that the idea of using this type of tail is not new, since in accordance with the U.S. patent num. 5,096,143 of Mar 17, 1992 William Nash invented a tail unit rotatable tailplane.

Figure 31. Examples of Tailless Aircraft (Desktop Aeronautics, 2004)

2.5. Original UAV Description

The model tested was a portable UAV develop by the Air Force Research Lab, Munitions Directorate, Flight Vehicles Integration Branch (AFRL/MNAV), for the Air Force Special Tactics Teams. It is made of carbon fiber matrix with a tapered flexible

wing, 24” span, 6”root chord and a V tail configuration. The main geometric properties are presented in Table 3 and Table 4 and Figure 32 and Figure 33. Details of the stability coefficients for the original UAV are given in the thesis developed by DeLuca (DeLuca; 2002). The most important characteristics are the following (DeLuca; 2004:15-17):

a. Mass: 320 gr. (0.705 lb_m)

b. The fuselage is a carbon fiber matrix body, with tapered rectangular shape.

c. Thin, hollow boxed tail boom.

d. High mounted, tapered flexible wing.

e. The wing is made of approximately ¼ chord length of carbon fiber leading edge with carbon fiber ribs spaced evenly from root to tip covered with military parachute material.

f. The tail has V type configuration and the control surfaces are elevons.

g. The total length is 18.2 inches.

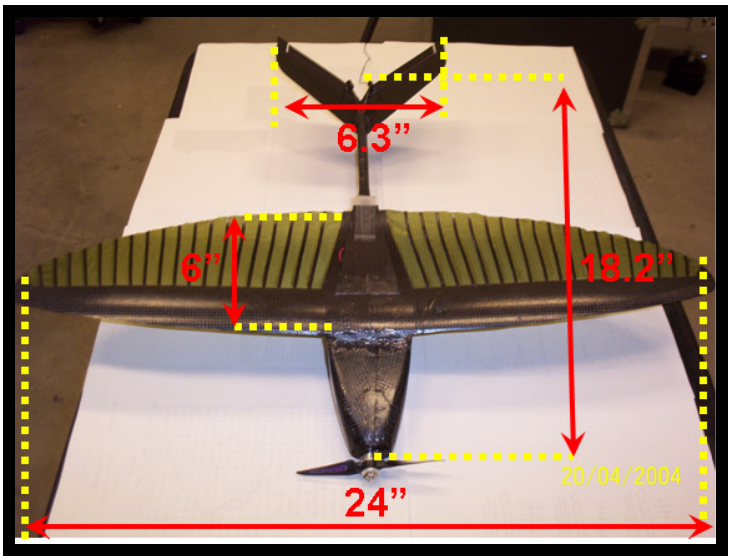

Figure 32. Original UAV

Table 3. Wing Properties of the Original UAV Configuration

Area	93.5 in^2
Root Chord	6”
Mean Aerodynamic Chord	4.2”
Span	24”
Carbon fiber Leading Edge Thickness	0.025”
Parachute Platform Thickness	0.005”
Aspect Ratio	6.16

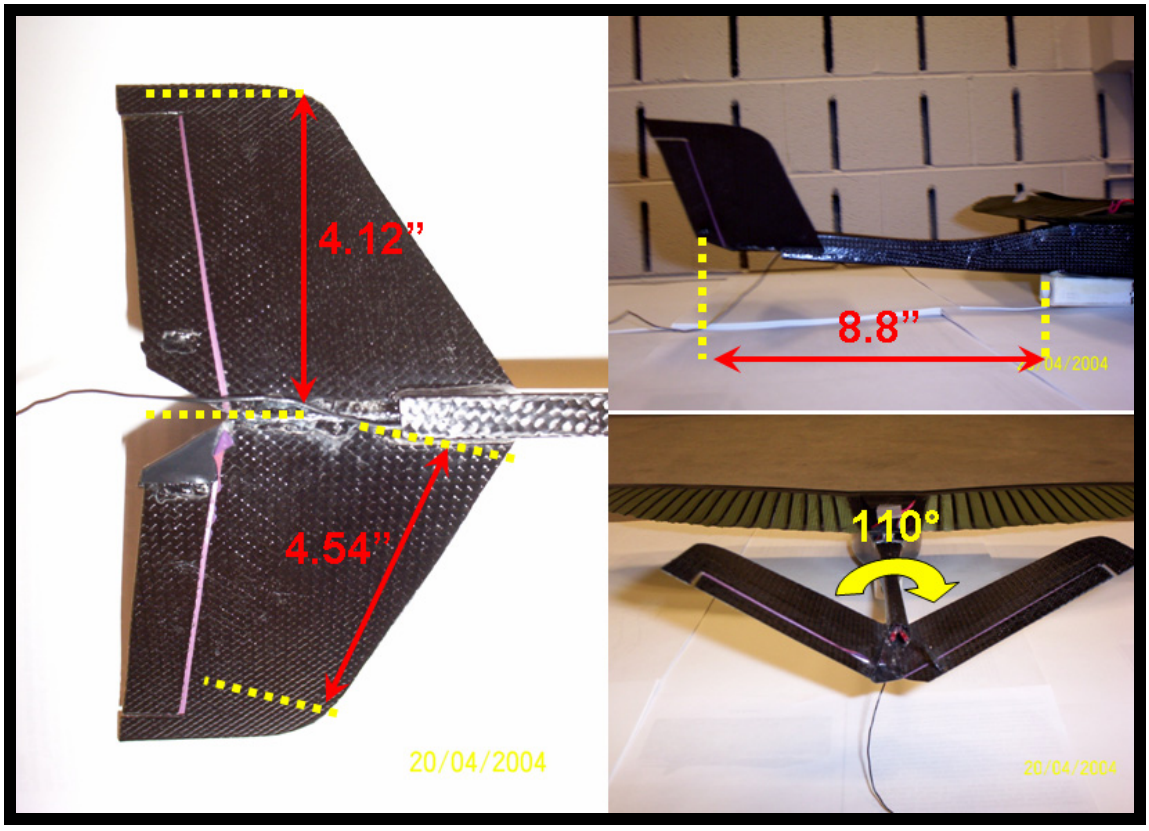

Figure 33. Original Tail of the UAV

Table 4. Tail Geometric Properties of the Original UAV Configuration

Area	14.8 in^2
Chord	2.35”
Span:	6.3”
Thickness	0.03”
Aspect Ratio	2.7
Horizontal Tail Volume Coefficient	0.54

2.6. Descriptions of the New Tails.

The original tail of the UAV was changed to a rotary tail by cutting the original fuselage in the root where the boom tail began. Because the mechanism to move the new tail was different from the old control system, a new mechanism was designed that allowed the tail to move in rotation and elevator deflection at the same time. The components of this new system were designed in SolidWorks® and installed in the fuselage of the UAV as it is shown in Figure 35. This new control mechanism uses the same actuators that the original UAV uses. The system is designed in such as way that it is possible to change the tail in a fast and easy manner by changing only two screws and a pin, as is shown in Figure 34.

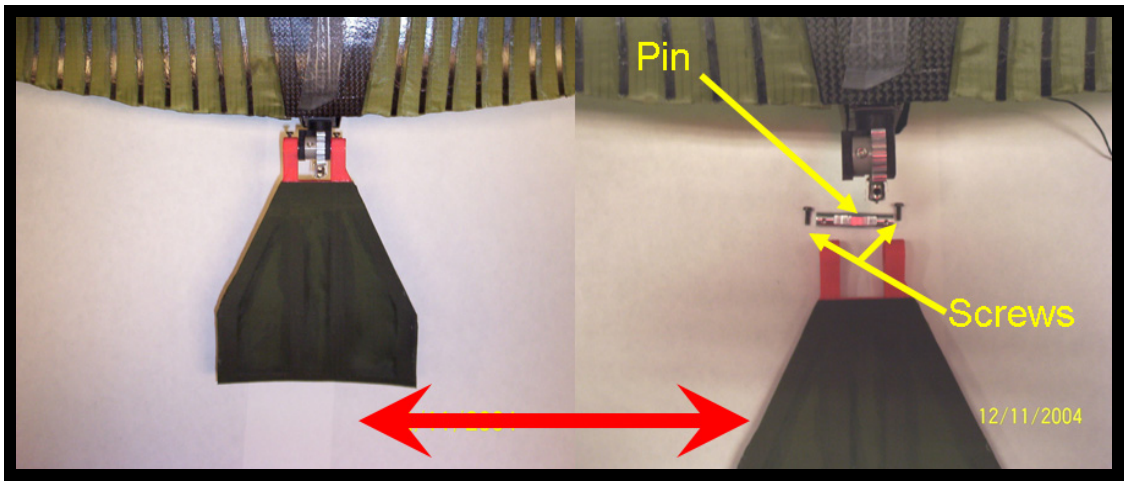

Figure 34. Mechanism to Change the Tail

Since one goal of this thesis is to characterize the static stability and control effectiveness of the UAV using a rotary tail, two tails were created from a plastic material using a rapid prototyping process and were covered with a polyester fabric. The time used for drawing it in Solid Works ™, fabrication and installation of each new tail was approximately 9 hrs. as is shown in Table 5.

Table 5. Time Used for Manufacturing a New Rotary Tail

Process	***Time***
Drawing	1 hrs.
Fabrication	6.5 hrs
Cover with fabric and installation	1.5 hrs.
Total time	9 hrs.

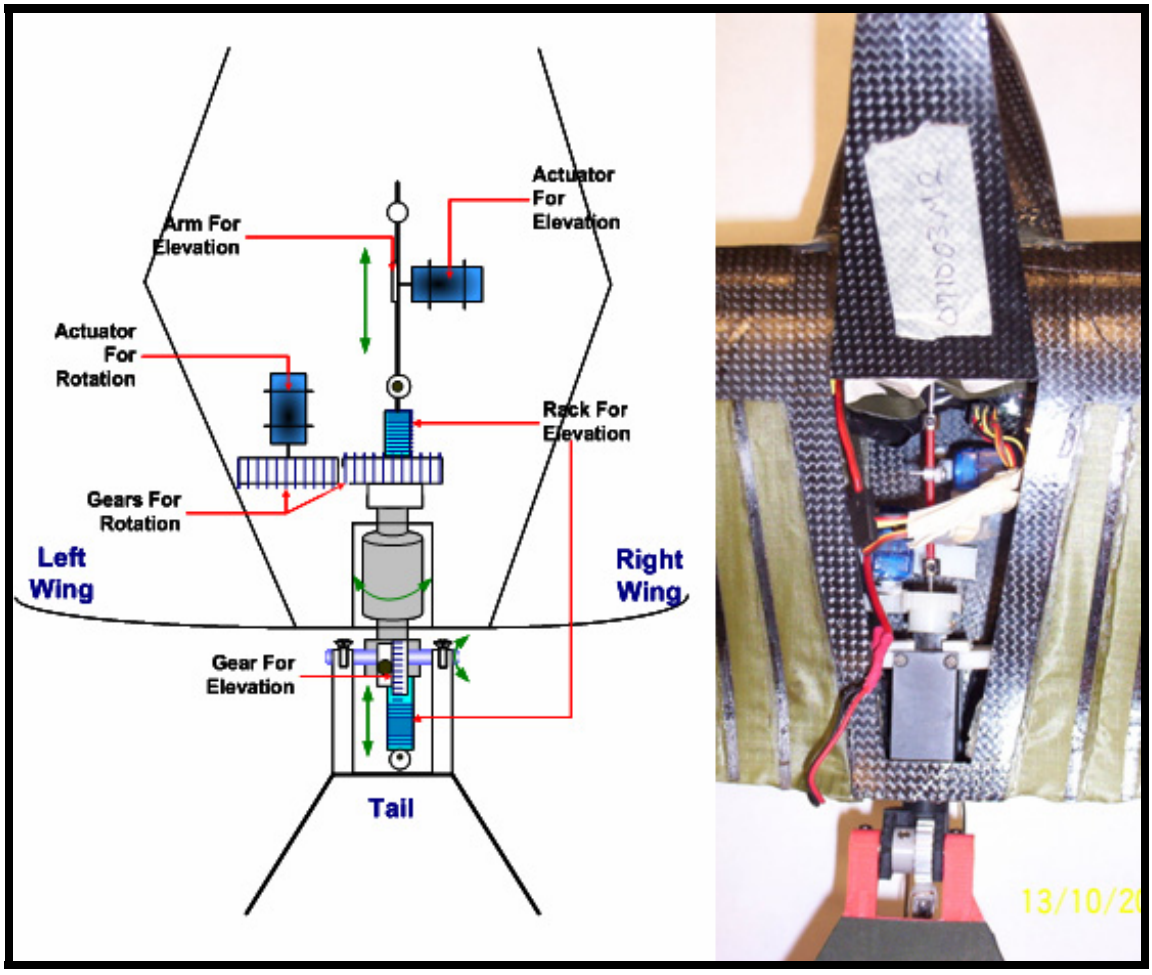

Figure 35. Diagram of the Mechanism for the Rotary Tail

The first step in the experiment was to answer the questions: How does a rotary tail work? Does it provide stability to the UAV? Can the UAV be controlled by a rotary tail? In order to answer these questions, two different tails were built. Tail 1 was built as a slightly rounded flat plate tapered, of 10 grams weight, which geometric characteristics are presented in Table 6 and Figure 36. Because this tail can be folded up over the fuselage, it reduces the total storage length of the UAV by 48 %, compared to the V-Tail design as shown in Figure 37. Its dimensions were selected to provide a tail volume

coefficient similar to a buzzard; which flight for doing visual surveillance that is the mission of the UAV.

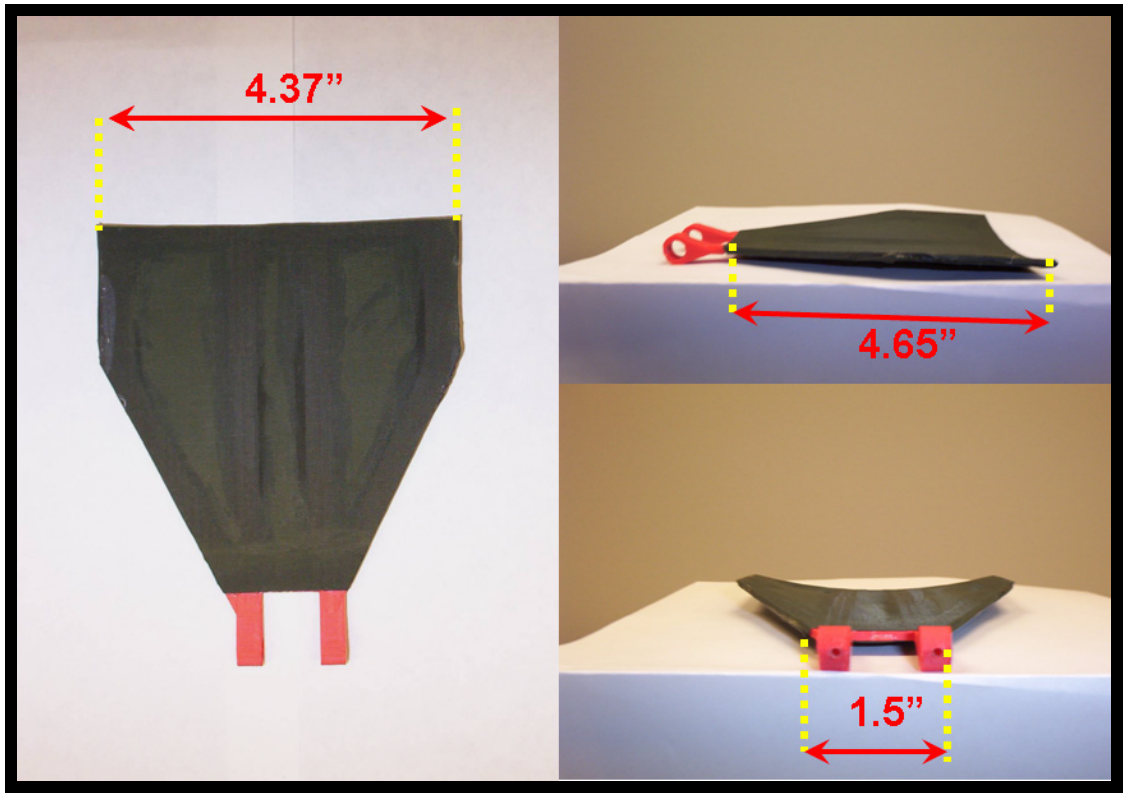

Figure 36. Characteristics Tail 1

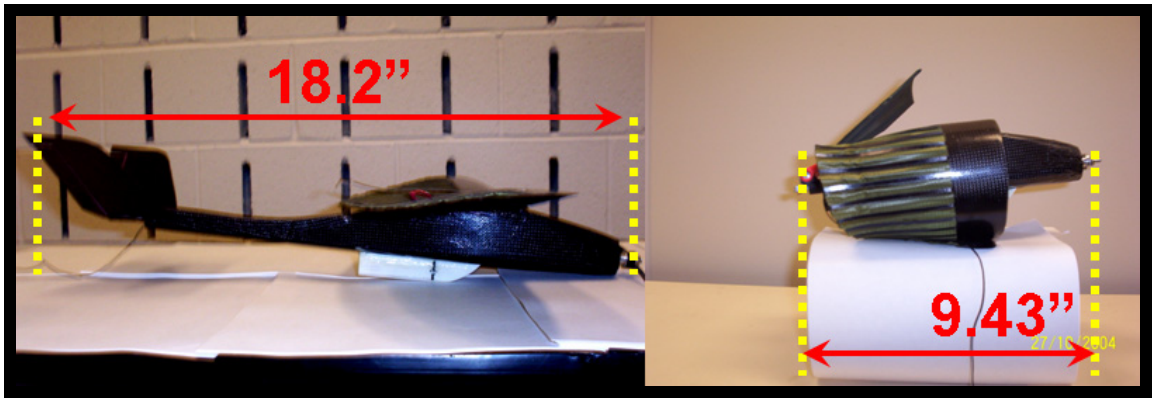

Figure 37. Length Comparison

Tail 2 was manufactured by the same procedure used for tail 1. However, this new tail includes two vertical fins that were expected to increase the weathercock stability.

In order to keep most of the variables used for the experiment with tail 1 constant, tail 2 was built maintaining the same geometric characteristics of tail 1, with the exception of the vertical tail already mentioned that increases the weight of the tail to 20 grams and proportion a total vertical fin area of 6.3434 in^2. Figure 38 shows the characteristics of tail 2; a table with geometric characteristics of tail 2 is not given because with exception of the vertical fins they are the same as the ones of tail 1.

Table 6. Geometric Characteristics of Tail 1

Area	9.42 in^2
Chord	4.66”
Span:	4.375”
Thickness	0.07”
Aspect Ratio	2.02
Taper Ratio	0.3755
Tail Volume Coefficient	0.2

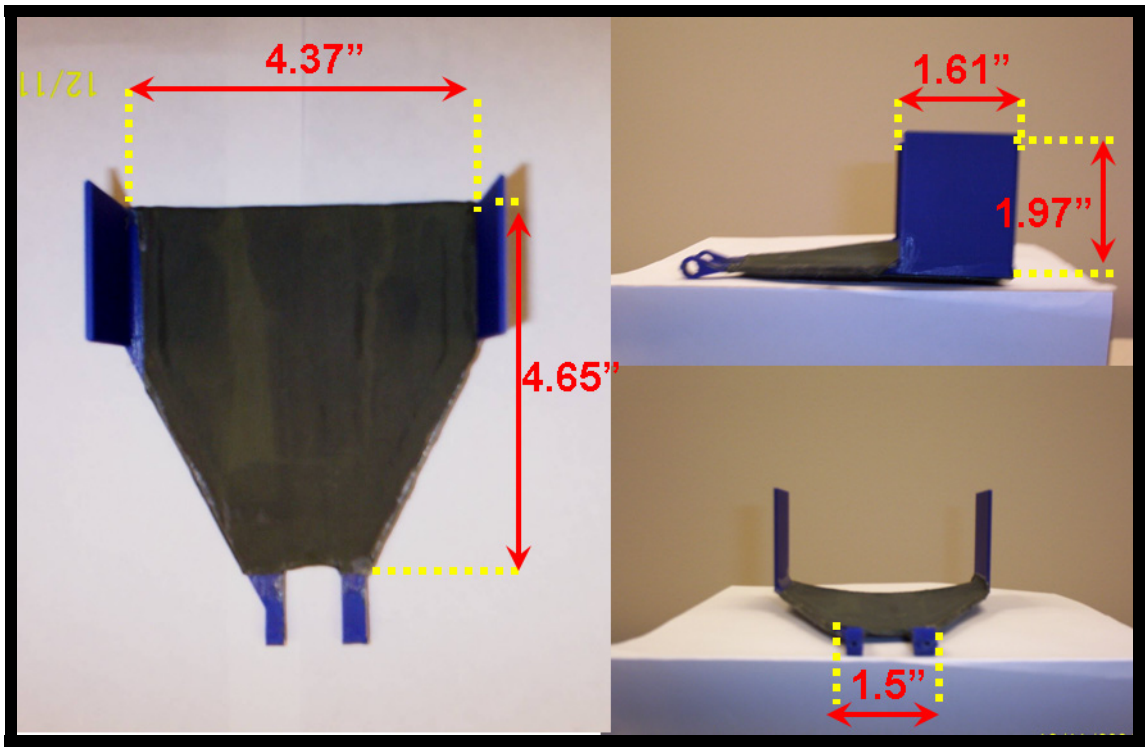

Figure 38. Characteristics Tail 2

2.6.1. Sign Conventions

The sign convention for angle deflection of common control surfaces was already mentioned in prior points; nevertheless, for rotary tails like the one that birds used and this thesis tested, no literature for the sign convention from tail deflection was found. Therefore, the convention for the deflection is shown in Figure 39. As can be seen in these figures, for elevator deflection the same notation and sign convention was used: δe is its symbol and from a side view down deflection is positive and up deflection is negative. On the other hand, since rotation in rotary tail has a similar function as a rudder in a conventional aircraft the symbol δrn was used instead of δr that is used in a common rudder and because the tail rotates around the X axis, the sign convection was taken from the right hand rule as Figure 40 shows.

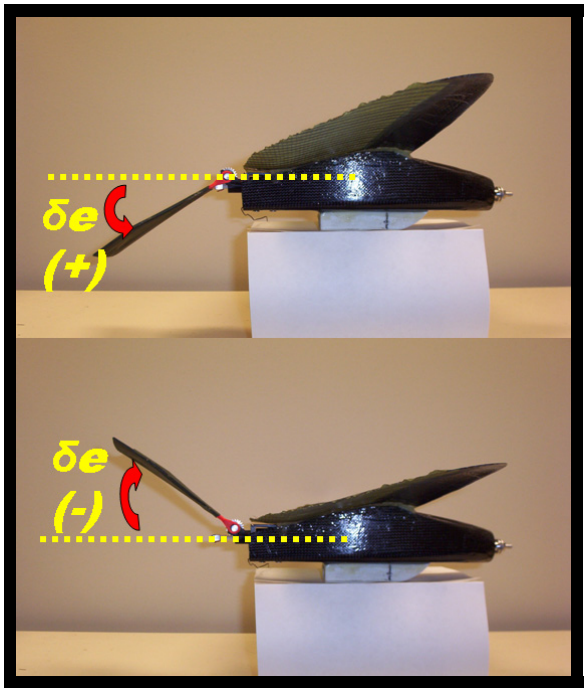

Figure 39. Elevator Deflection Convention

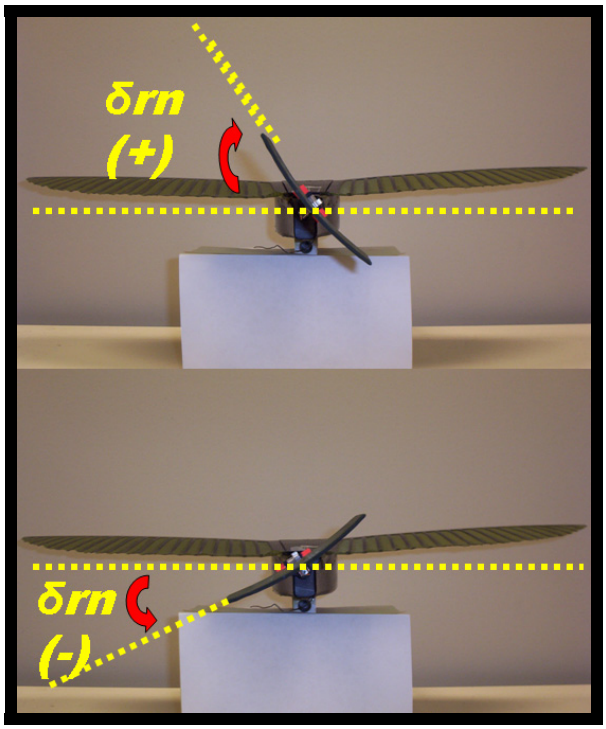

Figure 40. Sign Rotation Convention

In summary, in this chapter it was shown that the static stability is the capability of the aircraft of return to its equilibrium position when it is subject to a disturbance. This stability is divided in longitudinal, directional and roll. The equations used to evaluate stability in conventional airplanes were shown. However, these are not applied directly to rotary tails, because the moments produced in this kind of tail are function of both elevator deflection and rotation. Likewise, there is no reason to expect that the equations governing the controls for conventional airplanes will apply directly to the situation present for rotary tails. To address this need, wind tunnel experiments were performed. In the following chapter the procedure used for the experiments is provided.

III. Methodology

This chapter describes the equipment as well the procedure used for obtaining and processing the wind tunnel data obtained in the evaluation of the two rotary tails installed in the UAV.

3.1. Description of the Equipment

For this thesis, the primary equipment used was: The UAV supplied by the Air Force Research Lab, Munitions Directorate, Flight Vehicles Integration Branch (AFRL/MNAV); two rotary tails created from a plastic material using a rapid prototyping process, the low speed wind tunnel of the Air Force Institute of Technology and the balance AFIT-1 manufactured by Modern Machine & Tool Co.

Since the description of the UAV as well the tails were made in Chapter II, in the following two sections a description of the wind tunnel and the balance are presented.

3.1.1. Description of the Wind Tunnel

The wind tunnel used for this thesis was the low speed open wind tunnel manufactured by New York Blower Company .

A schematic of this tunnel is presented in Figure 41. Its main components are: inlet, contraction or nozzle, test section, diffuser, fan and exhaust.

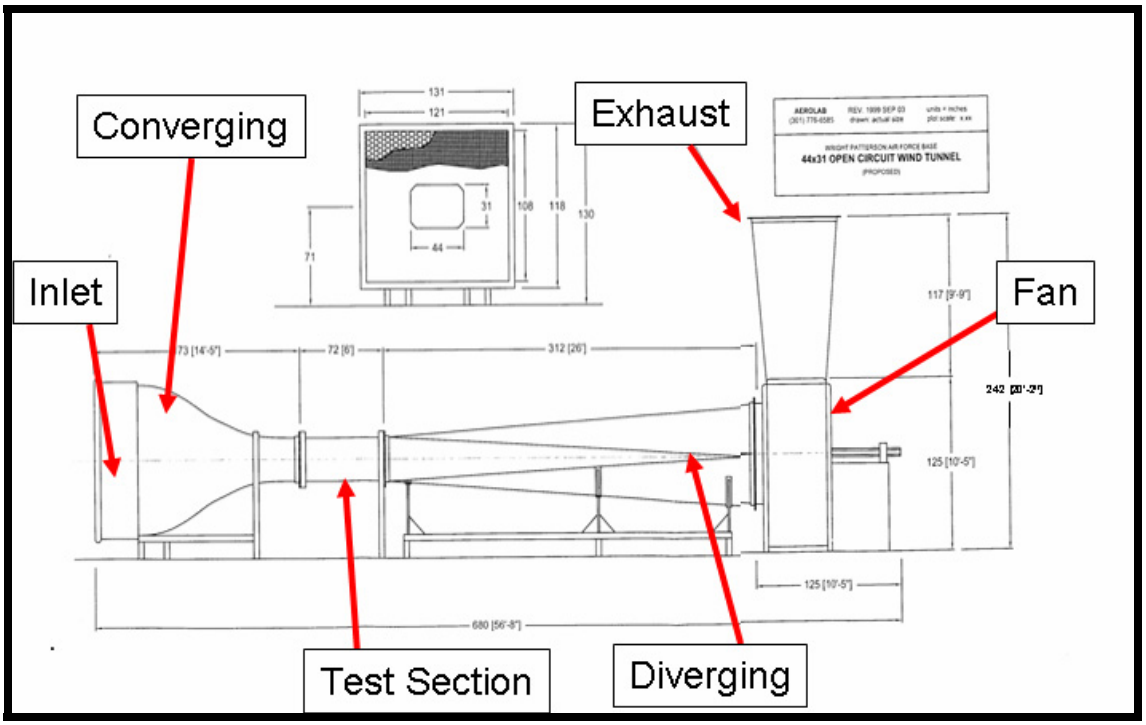

Figure 41. Wind Tunnel Schematic

The inlet section is shown in Figure 42. Since this is an open circuit tunnel this section is the place where atmospheric air is introduced to the wind tunnel. Its dimensions are 122”w * 111”h * 70”d. In order to provide a good quality of air with the minimum turbulence possible, the air is conditioned by the use of ¼ “aluminum honeycomb of an aspect ratio of 15 and four 20x20 steel mesh anti-turbulence screens.

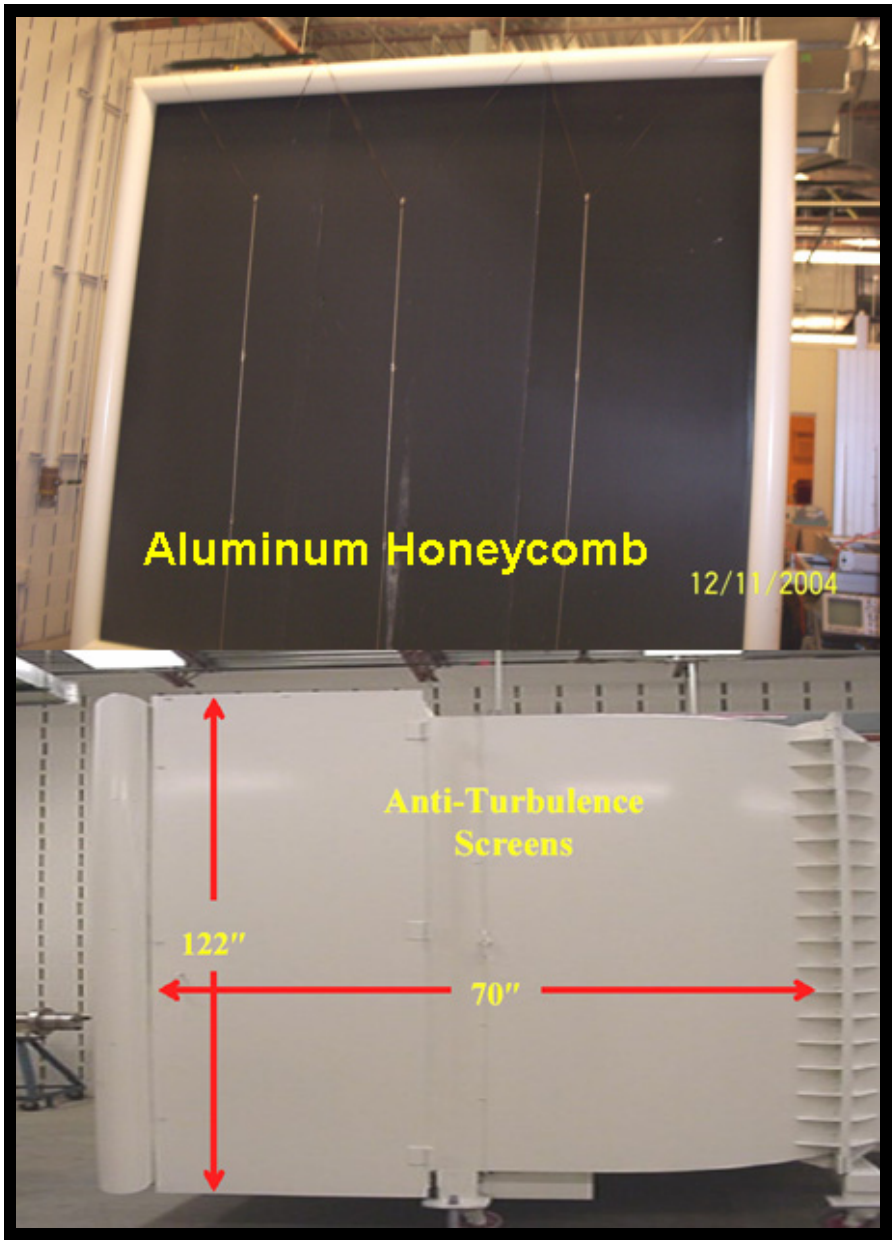

Figure 42. Wind Tunnel Inlet Section (Deluca; 2004:24)

The contraction section is presented in Figure 43. This section takes the flow from the inlet section to the test section by increasing the speed of the air. It has a contraction ratio of 9.5:1. Its dimensions are: length 95.5", initial height 111" and final height 31.5"; the initial width is 122" and the final 44".

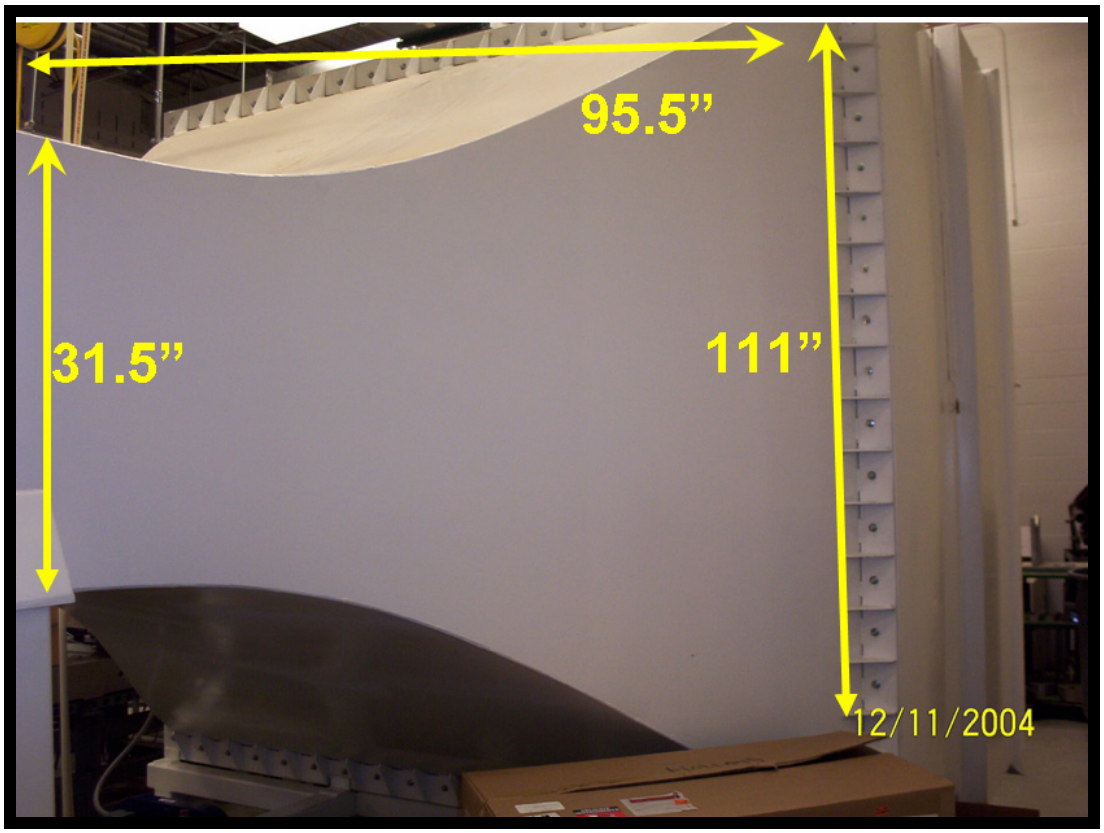

Figure 43. Wind Tunnel Contraction Section

The test section is shown in Figure 44. This section is used to place the equipment where the model is supported and tested. It is a closed type test section and has an octagonal shape. It has on both sides, gas-actuated Plexiglas doors that are used to provide access to the model; in the top of this section there is a removable plexiglas panel that can accommodate a hot-wire anemometry traversing system. The dimensions of the section are: Height: 31”, Width: 44” and Length: 72”. The maximum theoretical speed of the air through this section is 150 mph and the maximum tested speed is 148 mph. The average turbulence intensity is of 2.25% (DeLuca; 2004:97). Inside this section the support of the model consists in a remotely controlled automatic sting that enters to the tunnel through a gap that is at the bottom of the section. This sting can be moved from -

20º to +20º of angle of attack and from -15º to +15º sideslip angles. The forces and moments acting on the model are sensed in a balance that is installed as an extension of the mentioned sting. Data is sent and stored in the control computer located in the wind tunnel control room as shown in Figure 45.

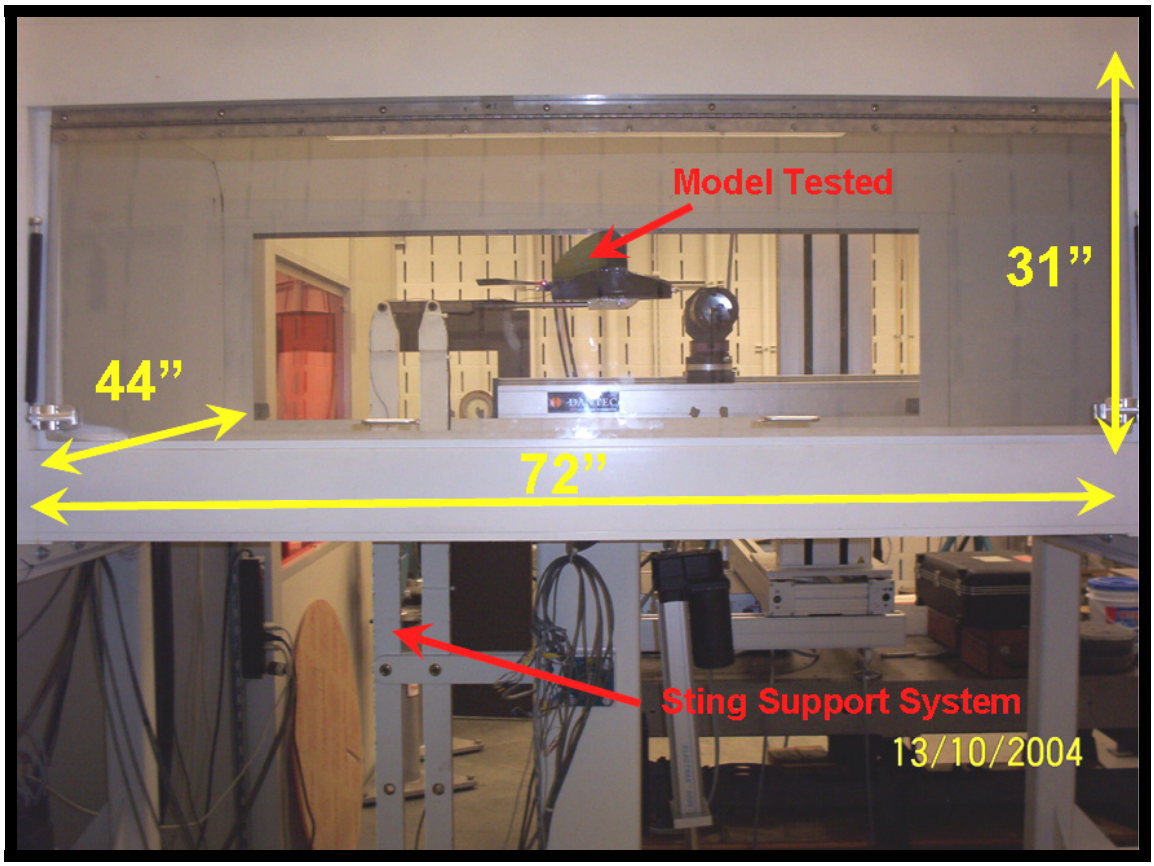

Figure 44. Wind Tunnel Test Section

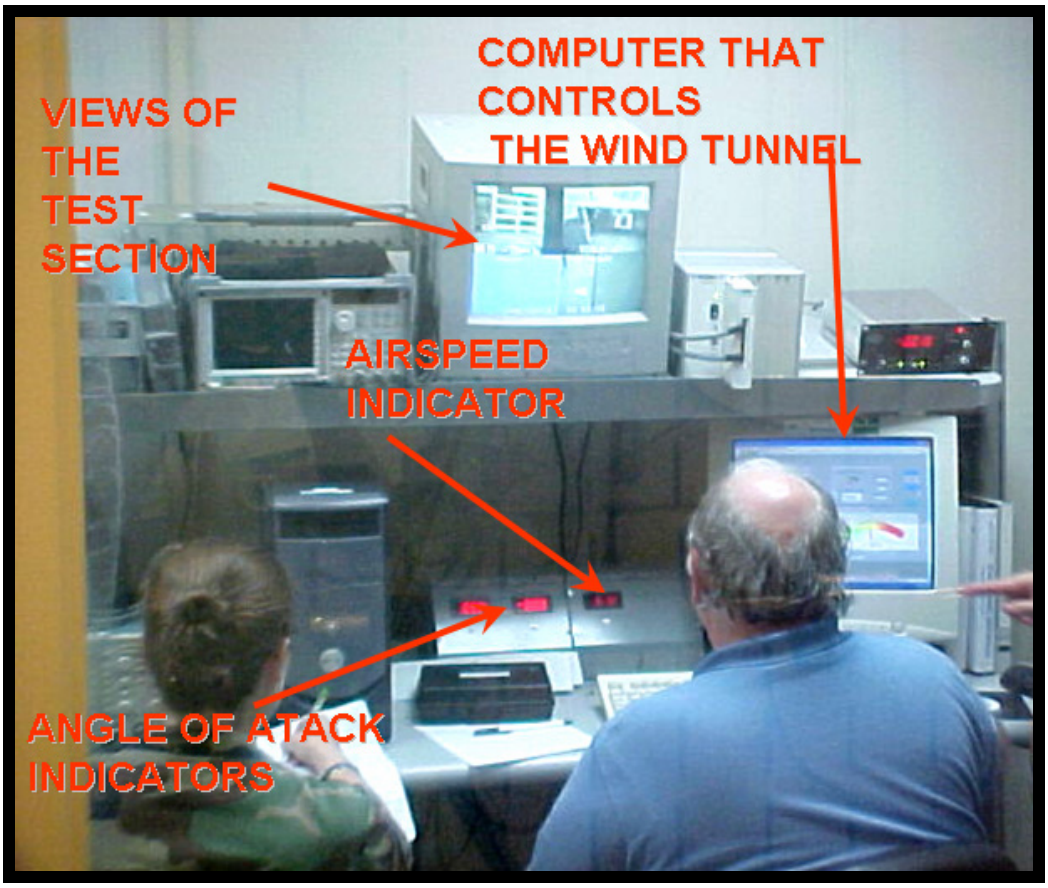

Figure 45. Wind Tunnel Control Room

The diffuser section of the wind tunnel is shown in Figure 46. The goal of this section is to reduce the speed of the air in the shortest possible distance without incurring flow separations (Barlow, Rae and Pope; 1999:80). The length of this section is 312" and connects the test section with the fan.

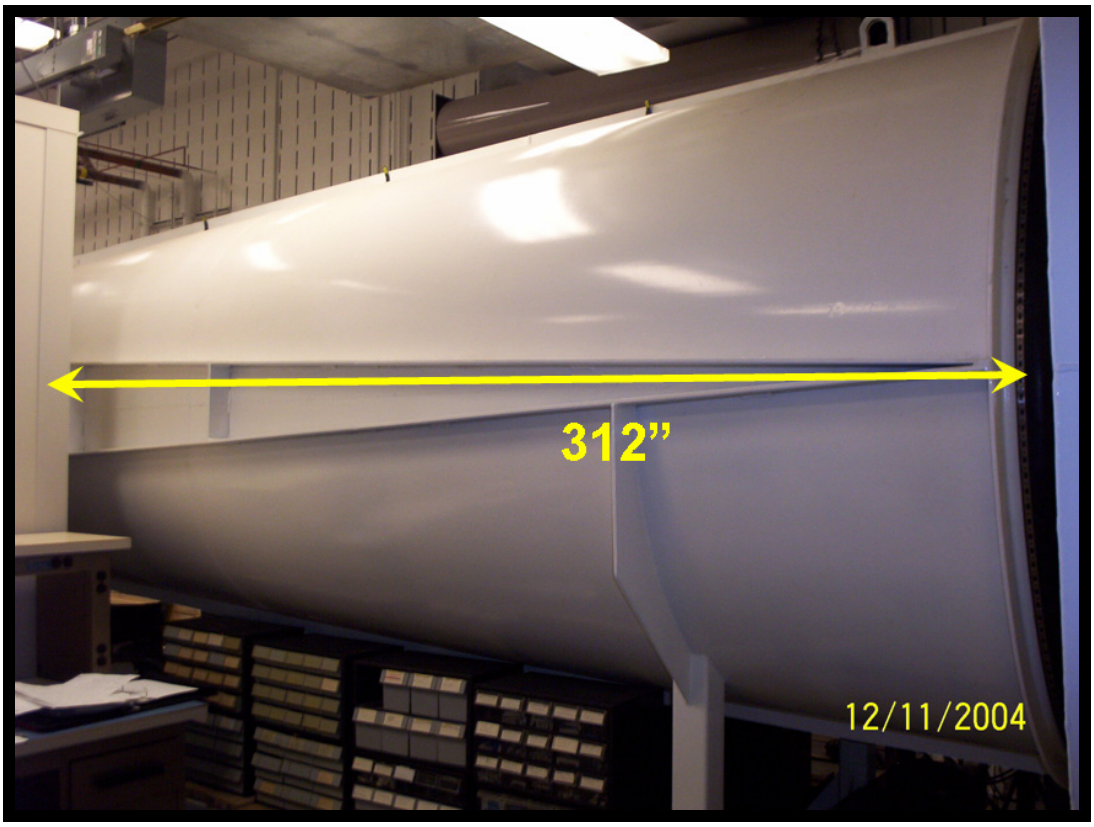

Figure 46. Diffuser Section

The fan and the exhaust section are shown in Figure 47. The purpose of the fan is to produce the circulation of air through the wind tunnel. Since this fan is located at the end of the wind tunnel, the atmospheric air that is sucked in the fan flows in a straight line from the inlet section through the convergence section, the test section, the diffuser section, the fan and finally, by a 90º of change in the direction the air is expelled to the atmosphere through the exhaust section that is located in the upper part of the fan and connects the wind tunnel to the exterior of the building by a slot in the ceiling. This fan is an ACFL/PLR Class IV type and was manufactured by New York Blower Co. It is actuated by a Premium Efficiency (EQP III) electrical motor manufactured by Toshiba,

whose characteristics are shown in Table 7. It is controlled by an adjustable frequency tunnel controller of 450 Volts, 315 Amp, manufactured by Siemens.

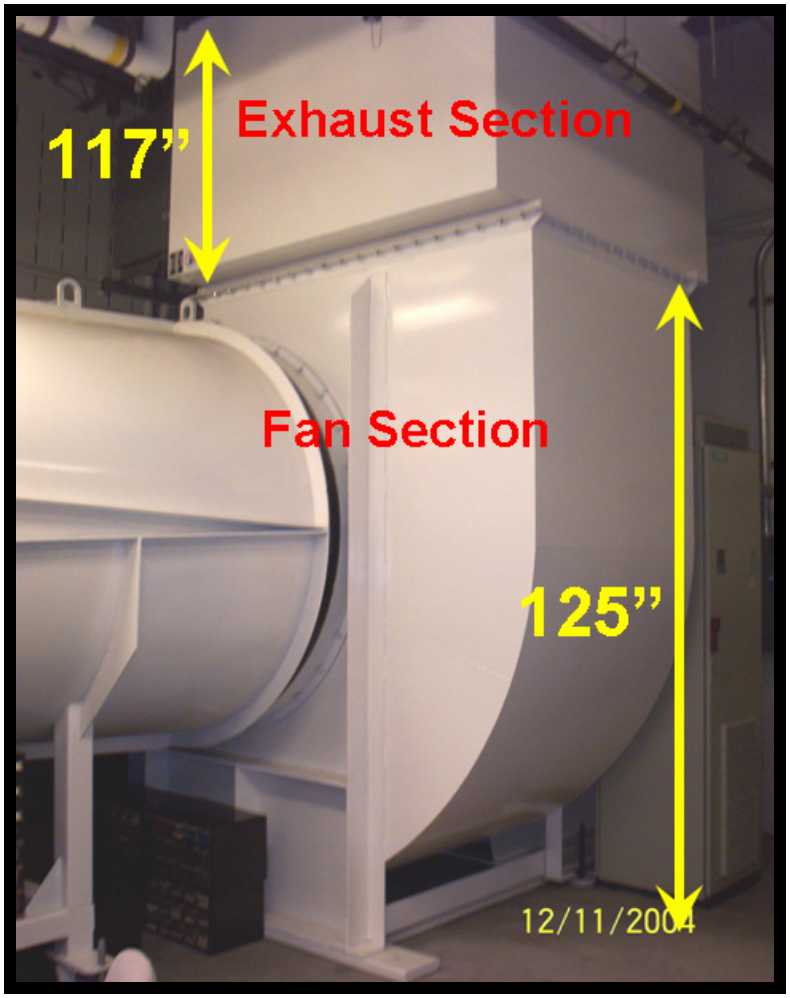

Figure 47. Fan and Exhaust Sections

Table 7. Main Characteristics of the Electric Motor

Type	EQP III, 3face induction
Power	200 BHP
Poles	4
Max. operating speed	1785 RPM
Voltage	230/460 Volts
Frequency	60 Hz Max
Amperage	444/222amp.

3.1.2. Description of the Balance

The balance used for this thesis was an internal six-component balance manufactured by Modern Machine &Tool Co, Inc and it is called AFIT-1 Balance. This balance is shown in Figure 48 and Figure 49. The balance is the device that will sense the forces and moments acting in the model. There exist two kinds of balances: internal and externals. This nomenclature depends on the locations of this device with respect on the model. For this thesis, an internal balance was used, which means that it was inserted inside the body of the UAV as is explained in the following section. The measurement is achieved due to the fact that inside an internal balance there are sensor elements called strain gage rosettes. These elements are a series of thin wire filaments (≈0.008" long) wounded in a serpentine way and attached to an epoxy bonded material. One strain gage is shown in Figure 50. The resistance of the wires is calculated using the following formula (DeLuca; 2004:149-152):

$$R = \rho * \frac{L}{A} \qquad (43)$$

Where: ρ = Resistively of the wire

L = Length of the wire

A = Cross section area of the wire

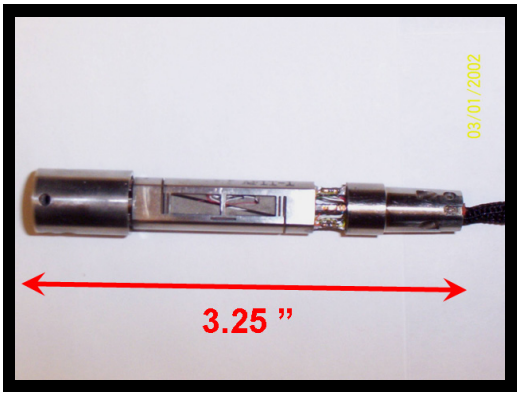

Figure 48. AFIT-1 Balance

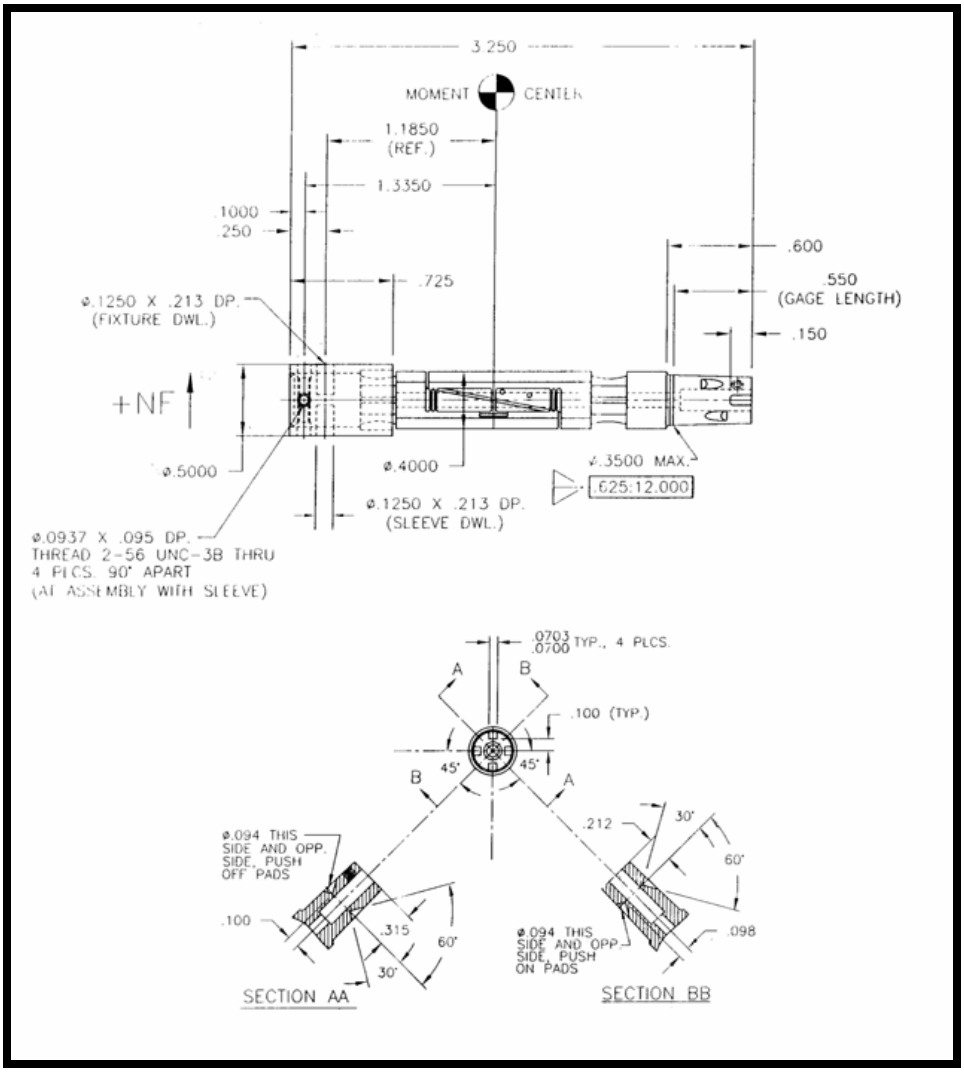

Figure 49. Geometric Characteristics of the AFIT-1 Balance (Modern Machine & Tool, Co, 2004)

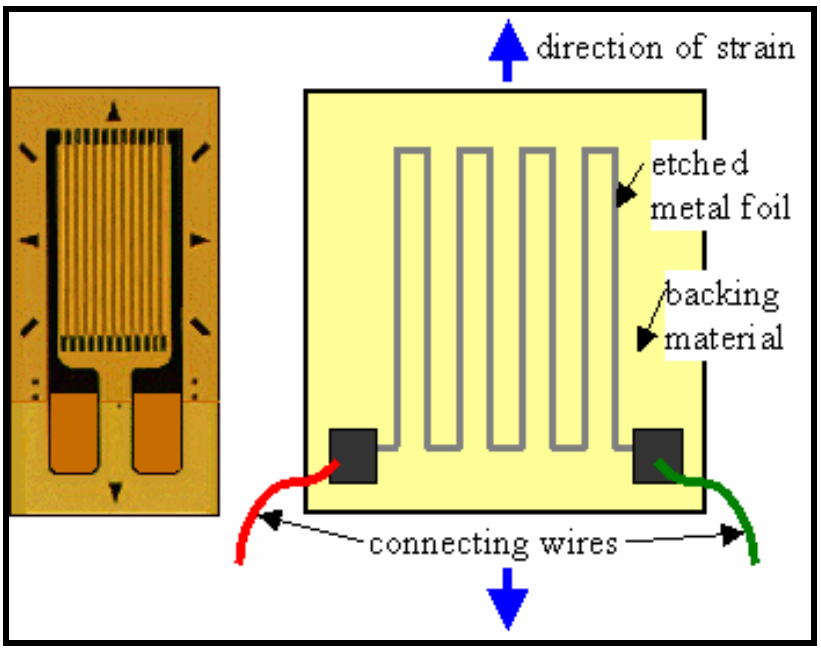

Figure 50. Typical Strain Gauge (Penn State, 2004)

In order to calculate the force acting in the strain gauge, they are placed in a Wheatstone bridge and voltage is supplied continuously across this bridge. When a load is applied to the model, the wire filaments elongate, causing a decrease in the cross sectional area and an increase in the resistance of the wires. Therefore, there will be difference between the voltage applied to the bridge and the output voltage. Having this information, the strain of the wire is calculated by using:

$$\varepsilon = 4 * \frac{Vo}{Vs} * \frac{1}{SF} \qquad \textbf{(44)}$$

where: Vo = Output voltage of the bridge

Vs = Voltage applied to the bridge

SF = Strain gauge factor

Once this strain is known the stress is calculated by using the Hooke's law:

$$\sigma = E * \varepsilon \qquad \textbf{(45)}$$

where: E = Material Modulus of Elasticity

Finally the force is calculated by using the formula F=σ*A, and the moments are calculated by using the formula M=F*L. These forces and moments are the values storage in the output data file.

The AFIT-1 balance provides an output that is composed of six variables that are named in accordance with the standard notation as shown in Table 8, where the maximum forces and moments for this balance are presented. The data related to moments are taken about the center of gravity of the balance.

The input voltage for this balance is 5 Volt's D.C. The position of the strain gages for this balance can be visualized are presented in Figure 51.

Table 8. Maximum Loads for AFIT-1 Balance

Component	***Maximum Load***
Normal Force (NF)	10 Lbs
Axial Force (AF)	5 Lbs
Side Force (SF)	5 Lbs
Pitch Moment (PM)	10 In. Lbs.
Roll Moment (RM)	4 In. Lbs.
Yaw Moment (YM)	5 In. Lbs.

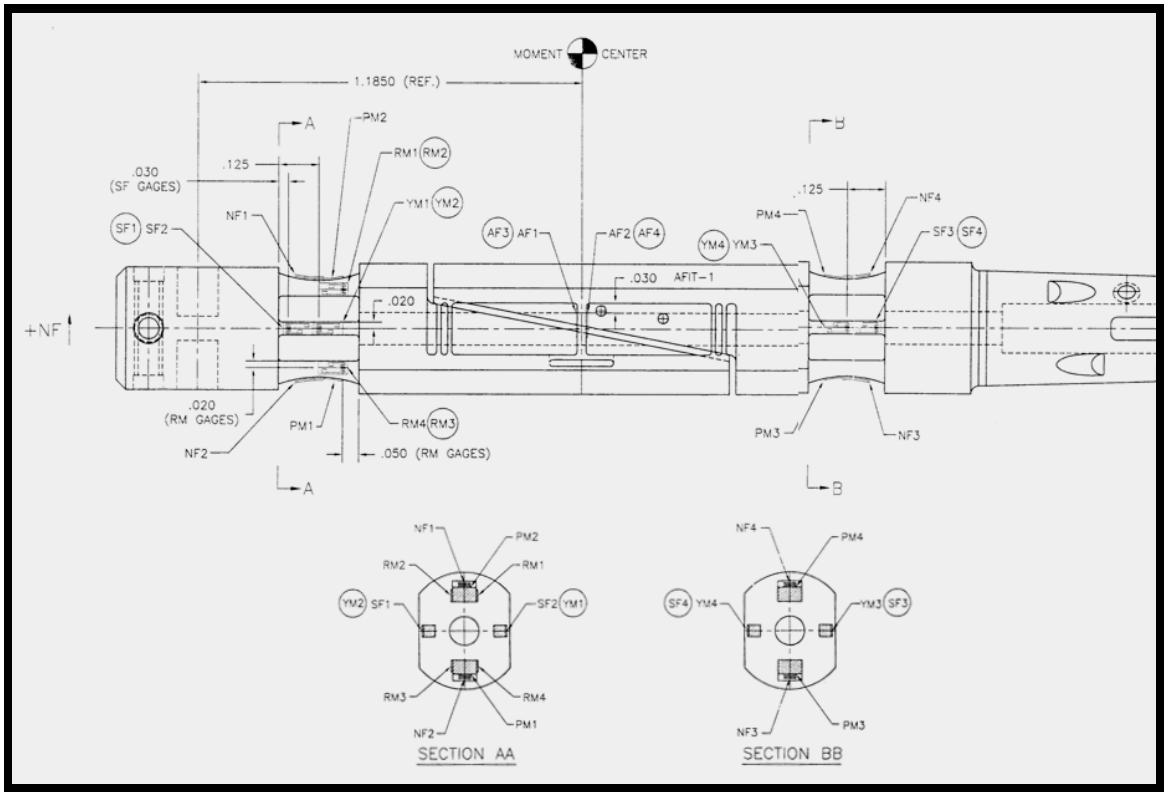

Figure 51. Position of the Strain Gauges in the AFIT-1 Balance (Modern Machine & Tool, Co, 2004).

3.2. Experimental Procedure

The first experiment using tail 1 was made with the goal of understanding the general behavior and the aerodynamic characteristics that rotary tails provide to the UAV. Once the data was analyzed, it was found that the UAV did not have directional stability; therefore, in order to provide this stability, tail 2 was built and tested. The list of the entire tests made for this experiment is presented in Chapter IV.

As a preparation for the experiment, the wind tunnel technician, Mr. Dwight Gehring, carried out a calibration of the balance using static weights, adjusting the calibration constants in the software in order to be sure that the loads applied to the

balance correspond to the ones registered by the software. Once this calibration was done, the balance was installed in the sting of the wind tunnel.

In each experiment, the following general procedure was used.

First, the UAV was installed in the sting of the wind tunnel, located in the test section. Because the balance is internal, the installation was made by using a plastic mounting block already installed on the bottom the UAV during the experimental setup made by Captain Tony DeLuca (DeLuca;2004). This plastic block is shown in Figure 52.

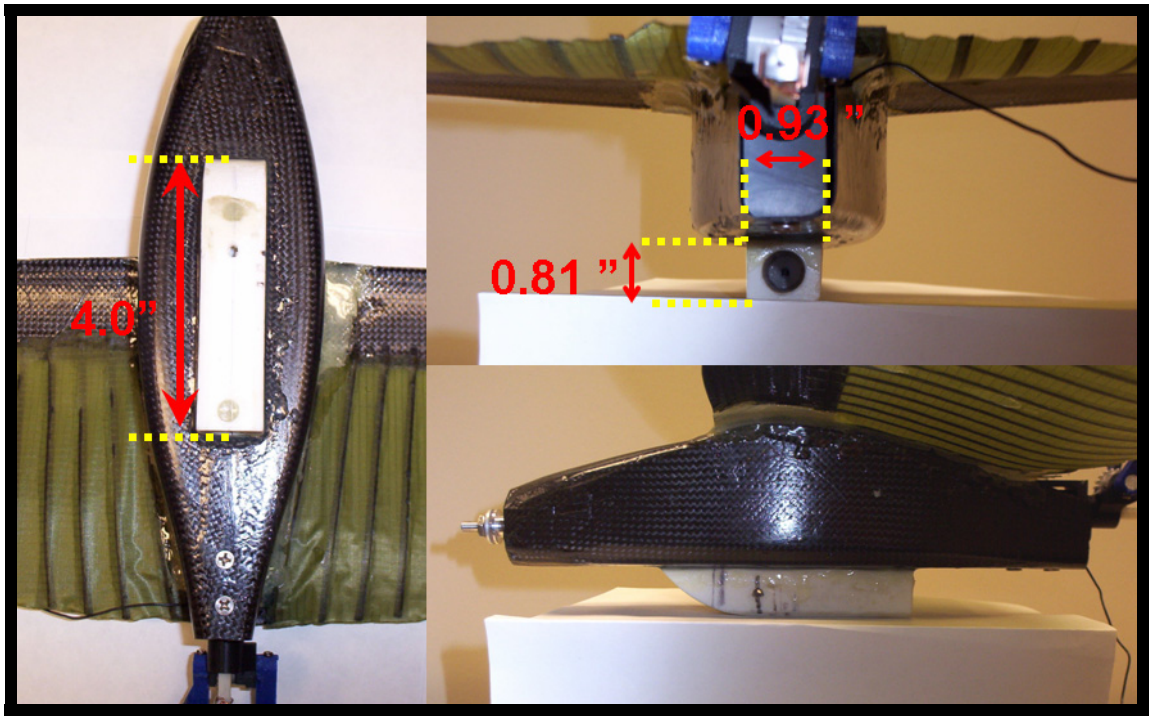

Figure 52. Mounting Block

The position of the model as well the wind tunnel velocity was controlled by a computer loaded Lab View Virtual Instrument® interface and checked with analog feedback boxes. This computer is located in the control room that is shown in Figure 53.

On the other hand, the deflection and rotation angles in the tail were measured by using a digital inclinometer and moving the controls using a RC controller.

All the wind tunnel tests were made with a 30 miles per hour of wind velocity and under the conditions mentioned in Tables 9, 10, 11, 13 and 14. This speed was selected based on the results and error analysis of Captain DeLuca (DeLuca; 2004).

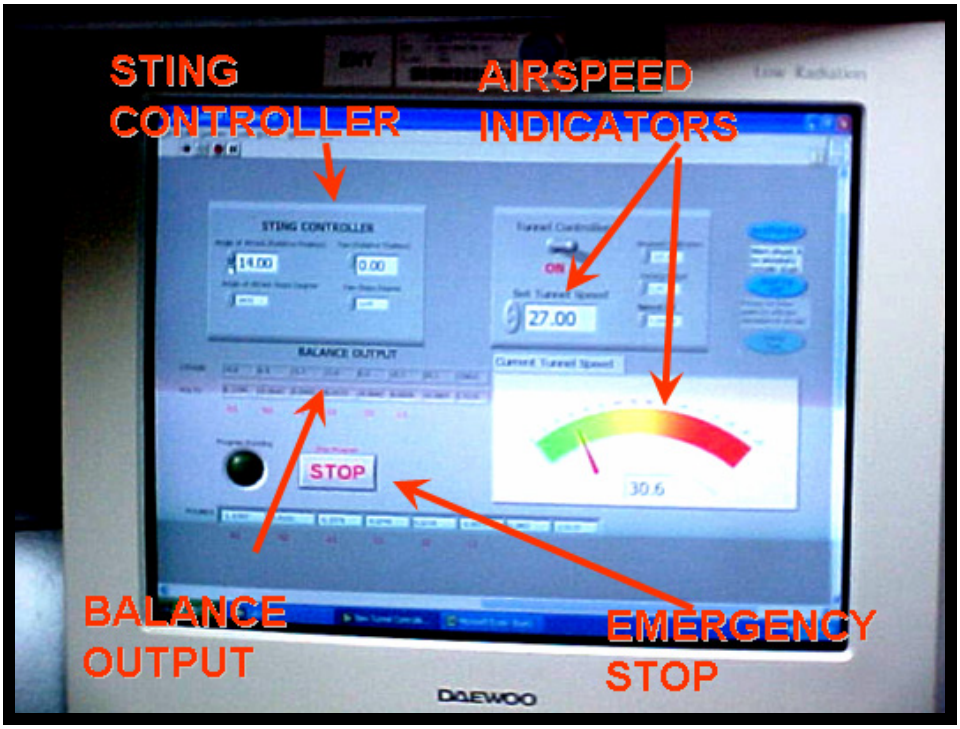

Figure 53. Wind Tunnel Control Computer

Before the fan of the wind tunnel produced any amount of wind, a measure of the tare load was taken and saved in a file for data processing. Once the relative wind is produced, the three forces (X, Y and Z) as well the three moment (L, M and N) acting on the model were sensed by the each of the six strain gauges located inside the balance. During each experiment, a 16 bit electronic data acquisition card and controller collected

the data of the forces and moment sensed by the strain gauges and transformed the analog outputs to digital signals. After that, the signals were amplified and conditioned by a low pass filter. Finally the data is stored on a Pentium computer.

Throughout each experiment, data was taken for approximately 30 seconds per point, producing an average of 40 lines of storage data in a tab-delimited text file. For each alpha run the model was moved from α=-8º to α=+8º. For the β runs the model was moved from β=-10º to β=+10º. For the parametric analysis run, the model was fixed at α=4º and β=0º and the data was taken for each different combination of elevator deflection and rotation of the tail. The alpha range was limited in order to prevent any damage to the balance.

3.3. Data Processing

The file produced with the storage data of each test was visualized by using Microsoft Excel® and transition data produced when the wind tunnel was initialized as well when the model was moved to one point to another was erased. This new "clean" file was saved and applied the following procedure by using a MATLAB® program developed by Capt. DeLuca and Lt. Gebbie and adapted by Lt. Rivera Parga to the AFIT-1 balance and for use with rotary tail models. This program, shown in Appendix C, provides a new file with all the aerodynamic properties that were plotted using Microsoft Excel® during the analysis of the results.

The file of the runs as well the file of the tare were loaded to the MATLAB® program and a single line of data representative for each point was calculated by averaging the approximately 40 lines.

The air density was calculated using the ideal gas law as well as the temperature and ambient pressure:

$$\rho = \frac{P}{R * T} \qquad \textbf{(46)}$$

The Reynolds number was calculated by using as length reference the root chord:

$$\mathrm{Re} = \frac{\rho * U\infty * C}{\mu} \qquad \textbf{(47)}$$

where:

ρ= Air Density
U∞=Tunnel velocity
C=Root chord length
μ=Air viscosity

The dynamic pressure was calculated using:

$$q\infty = \frac{1}{2} * \rho * U\infty^{2} \qquad \textbf{(48)}$$

The Mach number pressure was calculated as:

$$M = \frac{U\infty}{a} \qquad \textbf{(49)}$$

where "a" is the speed of sound and was calculated as:

$$a = \sqrt{\gamma * R * T} \qquad \textbf{(50)}$$

where γ and R are constants for air and their value are:

γ=1.4
R=1716

The effect that the static weight of the model produces as well the drag produced by the support of the model is called "tare". Since this static tare effect was evaluated before each test and since this file was already cleaned for transition points and averages

of the point were made, the following step was to fit this data in a 4^{th} order polynomial of the form:

$$y = a x^4 + b x^3 + c x^2 + dx + e \qquad \textbf{(51)}$$

where: x = Tare alpha (Independent variable)
y = Individual sensor force (Dependent variable)

For each sensor of the balance (NF, AF, SF, YM, PM, RM) a polynomial was fitted and a matrix of six polynomials was created in order to calculate the unbiased sensor forces and moments by using the following expression:

Forces & Moments unbiased=
Forces & Moment tested – Forces & Moments from tare effects **(52)**

After the tare effects were subtracted from the forces and moments sensed by the balance, the next step was to subtract the interactions that exist between sensors inside the balance. The necessity of doing this correction is based in the fact that in any balance there are errors due to the proximity between the rosettes and the fact that these sensors are non-perfect perpendicular, therefore, even if a load is applied in one perfect direction (for example axial force) there will be a value sensed by the other components (There will be a small sensed value in the load of normal and side force and the three moment). In order to correct this interaction between sensors a calibration must be done. The general scheme of this calibration consists of first loading the balance with known loads and then related its response to the known loads by using a set of calibration constants. These constants are then used to determine an unknown load applied to the balance by

using the inverse process (Patel; 2004). A matrix with all these constants is provided by the manufacturer of the balance.

The notation used for each of the forces and moments sensed by an internal balance like the one used for this thesis is the following and is illustrated in Figure 54.

NF	=	Normal Force
AF	=	Axial Force
PM	=	Pitching Moment
RM	=	Rolling Moment
YM	=	Yaw Moment
SF	=	Side Force

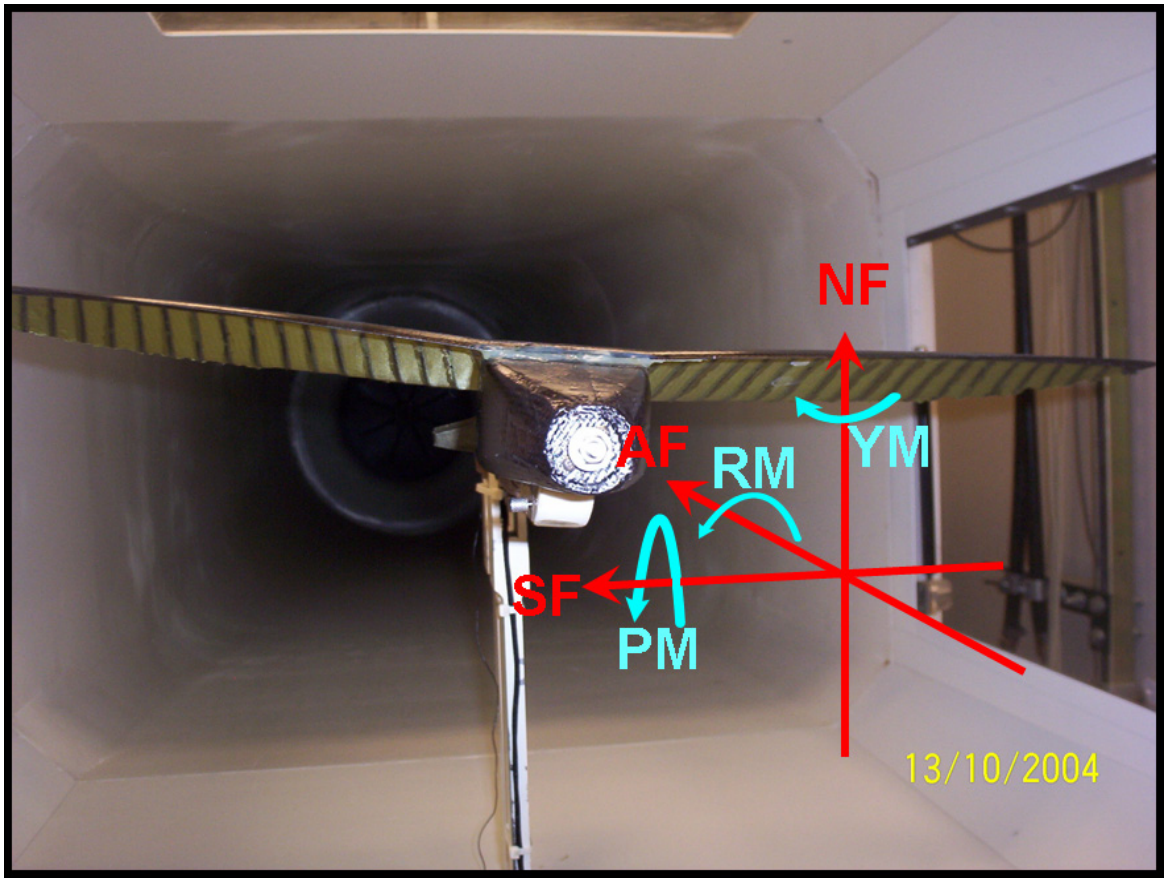

Figure 54. Nomenclature of Forces and Moments in a Internal Balance

In a six-component balance there are 26 first and second order interactions, plus one sensitivity constant per component that needs to be evaluated. This produces 162

terms for a six-component balance. The notation for these terms, the data reduction equations, as well the values for the constants used for the AFIT-1 balance utilized in this thesis are presented in Appendix D. The iterative process used for obtaining the forces and moments acting in the balance is the following:

Since the output of the balance is actually given in volts, the first step is to convert this output in Lb or in-Lb by using the constants given by the manufacturer as following (Patel; 2004):

$$\begin{aligned} NF_1 &= K_1 * MNF \\ AF_1 &= K_{29} * MAF \\ PM_1 &= K_{57} * MPM \\ RM_1 &= K_{85} * MRM \\ YM_1 &= K_{113} * MYM \\ SF_1 &= K_{141} * MSF \end{aligned} \quad \textbf{(53)}$$

where: The constants K1,K29,K57,K85,K113,K141 are given by the manufacturer, the values of MNF,MAF,MPM,MRM,MYM,MSF are the raw data from the balance in volts.

It is important to know that for the data used for this thesis, the prior step was made in the wind tunnel PC; therefore, once the data was corrected by tare effects, the iterative process was made beginning from the next step:

The values obtained in the prior point are now substituted into the interaction equation to give:

$$
\begin{aligned}
NF_2 &= NF_1 - \left[\sum (Interactions.on.NF)\right]_1 \\
AF_2 &= AF_1 - \left[\sum (Interactions.on.AF)\right]_1 \\
PM_2 &= PM_1 - \left[\sum (Interactions.on.PM)\right]_1 \\
RM_2 &= RM_1 - \left[\sum (Interactions.on.RM)\right]_1 \\
YM_2 &= YM_1 - \left[\sum (Interactions.on.YM)\right]_1 \\
SF_2 &= SF_1 - \left[\sum (Interactions.on.SF)\right]_1
\end{aligned}
\qquad \textbf{(54)}
$$

where the quantities NF2, AF2, PM2, RM2, YM2, SF2, are the partially corrected forces and moments. The substitution of these partial corrected values back into the general relation gives:

$$
\begin{aligned}
NF_3 &= NF_1 - \left[\sum (Interactions.on.NF)\right]_2 \\
AF_3 &= AF_1 - \left[\sum (Interactions.on.AF)\right]_2 \\
PM_3 &= PM_1 - \left[\sum (Interactions.on.PM)\right]_2 \\
RM_3 &= RM_1 - \left[\sum (Interactions.on.RM)\right]_2 \\
YM_3 &= YM_1 - \left[\sum (Interactions.on.YM)\right]_2 \\
SF_3 &= SF_1 - \left[\sum (Interactions.on.SF)\right]_2
\end{aligned}
\qquad \textbf{(55)}
$$

By continuing the interaction process, the nth. values of the corrected forces and moments were defined as:

$$
\begin{aligned}
NF_n &= NF_1 - \left[\sum (Interactions.on.NF)\right]_{n-1} \\
AF_n &= AF_1 - \left[\sum (Interactions.on.AF)\right]_{n-1} \\
PM_n &= PM_1 - \left[\sum (Interactions.on.PM)\right]_{n-1} \\
RM_n\, RM_1 &- \left[\sum (Interactions.on.RM)\right]_{n-1} \\
YM_n &= YM_1 - \left[\sum (Interactions.on.YM)\right]_{n-1} \\
SF_n &= SF_1 - \left[\sum (Interactions.on.SF)\right]_{n-1}
\end{aligned}
\qquad \textbf{(56)}
$$

This procedure was continued until the value of the difference between the successive iterations was less than 10^{-14}.

Due to the presence of the walls of the tunnel in the test section where the model is installed, the area through which the air flows is reduced compared with the conditions

in the real word; there is an increase in the velocity of the air that flows in the vicinity of the model. This phenomenon is called solid blockage and its correction is done by using the following equations (Barlow, Rae and Pope; 1999:368-370):

$$\varepsilon_{sb} = \varepsilon_{sb.wing} + \varepsilon_{sb,\,body}$$

$$\varepsilon_{sb,\,wing} = \frac{k_1\,\tau_1 * Wing.volume}{C^{3/2}} \qquad \textbf{(57)}$$

$$\varepsilon_{sb,\,body} = \frac{k_3\,\tau_1 * Body.volume}{C^{3/2}}$$

Where: k_1=It is the body shape factor=0.9

k_3=It is the body shape factor=0.93

τ_1=Factor of the shape of the wind tunnel test=0.83125

C=Wind tunnel test section area

After the blockage correction was calculated, it was used to correct the wind tunnel velocity and dynamic pressure by using the following equations (Barlow, Rae and Pope; 1999:141):

$$qc = q_A\left(1+\varepsilon_T\right)^2 \qquad \textbf{(58)}$$
$$Vc = V_A\left(1+\varepsilon_T\right)$$

where $\varepsilon_T = \varepsilon_{sb} + \varepsilon_{wb}$

ε_{wb} is the Wake blockage and is considered negligible.

Since the forces calculated until this point are referred to the body axis of the model and by considering that the forces in the output data were calculated by using the

sign convection in wind tunnel testing, the subsequent step is used to change the forces to wind axis forces that will provide an output of drag (from the axial force of the balance output), lift (from the normal force) and side force (from the side force); that are the standard force term used in aeronautical engineering. The wind and body reference frames are shown in Figure 55. This change of the forces from body to wind axes is made by using the following equation (Barlow, Rae and Pope; 1999:237):

$$\begin{bmatrix} D \\ S \\ L \end{bmatrix} = \begin{bmatrix} A * Cos\theta * Cos\psi + Y * Sin\psi + N * Sin\theta * Cos\psi \\ -A * Cos\theta * Sin\psi + Y * Cos\psi - N * Sin\theta * Sin\psi \\ -A * Sin\theta + N * Cos\theta \end{bmatrix} \quad \textbf{(59)}$$

where: A=Axial force

Y=Side Force

N= Normal force

θ = The pitch angle of the model

ψ = The yaw angle of the model

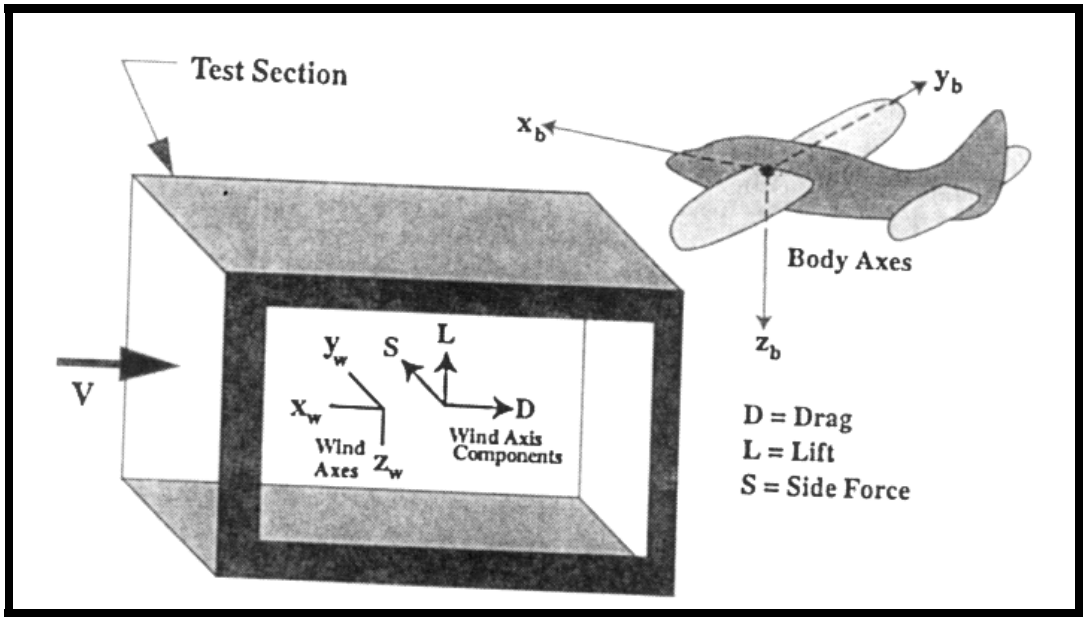

Figure 55. Wind and Body Reference Frames (Barlow, Rae and Pope; 1999:235)

In the same manner the moments are transfered from the body axes to the wind axes by using the following equations (Barlow, Rae and Pope; 1999:238):

$$\begin{bmatrix} l_w \\ m_w \\ n_w \end{bmatrix} = \begin{bmatrix} l * Cos\theta * Cos\psi - m * Sin\psi + n * Sin\theta * Cos\psi \\ l * Sin\psi * Cos\theta + m * Cos\psi + n * Sin\theta * Sin\psi \\ -l * Sin\theta + n * Cos\theta \end{bmatrix} \quad \textbf{(60)}$$

Because for stability analysis it is necessary to obtain the moments about the center of mass, the next step is to transfer the moments from the balance center to the center of mass of the model, by using the following equations (Barlow, Rae and Pope; 1999:238):

$$\begin{bmatrix} l_{wcm} \\ m_{wcm} \\ n_{wcm} \end{bmatrix} = \begin{bmatrix} l_{wbc} + S * Z_{cm} + L * y_{cm} \\ m_{wbc} - L * X_{cm} + D * Z_{cm} \\ n_{wbc} - D * y_{cm} - S * X_{cm} \end{bmatrix} \quad \textbf{(61)}$$

where $\lfloor X_{cm}\ y_{cm}\ Z_{cm} \rfloor$ are the coordinates of the center of mass of the model in the wind axes frame, with origin at the balance center. These coordinates are calculated by using the following formulas which notation is illustrated in Figure 56:

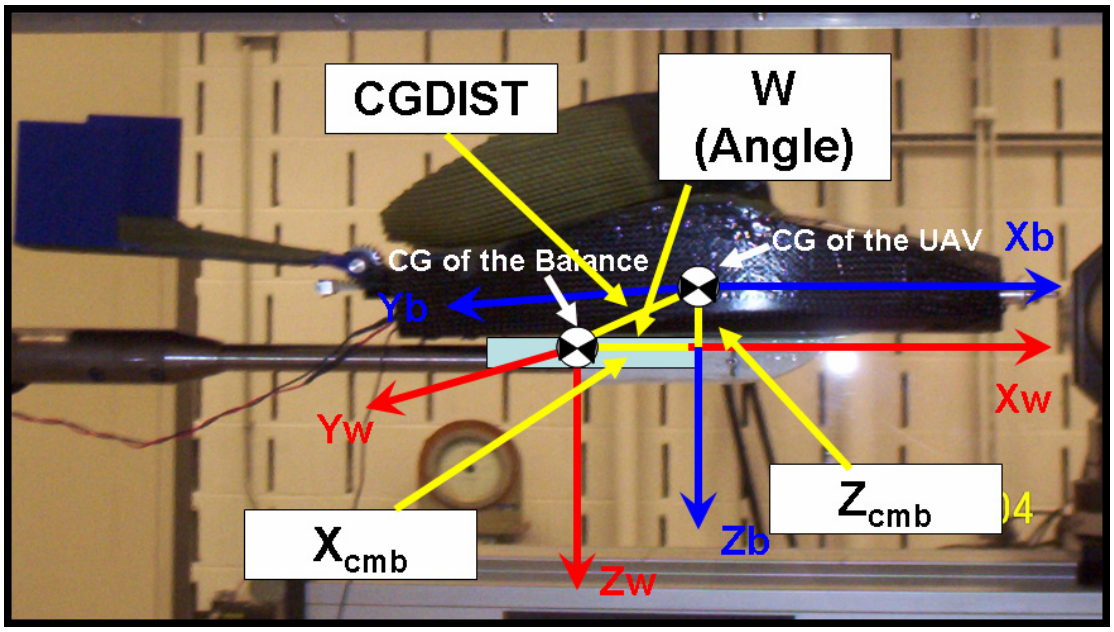

Figure 56. Notation for Position of Centers of Gravity

Since the mounting was centered laterally on the fuselage, Ycm ≈ 0, except where noted, and the direct distance between the center of mass of the model and the center of the model at zero angle of attack is defined by:

$$CGDIST = \sqrt{X_{cmb}^{\ 2} + Z_{cmb}^{\ 2}} \quad \textbf{(62)}$$

The angle between the X axes and the direct distance calculated in the prior equation, at zero angle of attack is calculated by:

$$w = \tan^{-1}\left(\frac{Z_{cmb}}{X_{cmb}}\right) \quad \textbf{(63)}$$

Finally the coordinates of the center of mass of the model in the wind axes frame with origin at the balance center for each angle of attack are calculated by:

$$\begin{aligned} X_{cm} &= Cos(\theta + w) * Cos(\psi) * CGDIST \\ y_{cm} &= Y_{cmb} + X_{cm} * \tan(\psi) \\ Z_{cm} &= -Sin(\theta + w) * CGDIST \end{aligned} \quad \textbf{(64)}$$

Once the forces and moments acting in the model were calculated, they were transformed into aerodynamic coefficients by using the following equations:

$$\begin{bmatrix} C_D \\ C_Y \\ C_L \end{bmatrix} = \begin{bmatrix} D \\ S \\ L \end{bmatrix} * \frac{1}{\frac{1}{2} \rho * u_\infty^{\,2} * Wing.area}$$

$$\begin{bmatrix} C_l \\ C_m \\ C_n \end{bmatrix} = \begin{bmatrix} \frac{l}{\frac{1}{2} \rho * u_\infty^{\,2} * Wing.area * Wing.Span} \\ \frac{m}{\frac{1}{2} \rho * u_\infty^{\,2} * Wing.area * Mean.chord} \\ \frac{n}{\frac{1}{2} \rho * u_\infty^{\,2} * Wing.area * Wing.Span} \end{bmatrix} \quad \textbf{(65)}$$

Finally, small corrections were applied to the drag coefficient, angle of attack and pitch moment due to the fact that the walls of the wind tunnel produce some interference in the air that flows around the wing; in other words, the free-air streamlines caused by a pair of trailing vortices such as are made by a uniformly loaded wing extent to infinite in free air. However, when the wing is enclosed in a duct, they become contained and the wall itself behaves as a barrier where no fluid can pass through it (Barlow, Rae and Pope;

1999:377), the corrections to the drag are done by using the following formulations (Barlow, Rae and Pope; 1999:416):

$$C_{DCorrected} = C_{DUncorrected} + \Delta C_{Dup} + \Delta C_{Dw} \qquad \textbf{(66)}$$

where: $\Delta C_{D_w} = \frac{\delta * S}{C}(C_{Lw})^2$

C = Tunnel cross section area=9.47 ft^2

$\delta = \frac{Model.span}{Tunnel.Width} = 0.1125$

ΔC_{Dup} = Zero

The correction to the angle of attack was made by using the following equations (Barlow, Rae and Pope; 1999:416):

$$\alpha_{Corrected} = \alpha_{Geometric} + \Delta \alpha_{UP} + \Delta \alpha_{w} \qquad \textbf{(67)}$$

where: $\Delta\alpha_{UP} = Zero$

$\alpha_{Geometric}$ = Uncorrected Angle of attack.

$$\Delta\alpha_W = \frac{\delta * S}{C}(57.3)C_{LW}$$

The correction made to the pitching moment was made by using the following equations (Barlow, Rae and Pope; 1999:399-417, Nelson; 1998:48 and DeLuca; 2004:44):

$$C_{m,\ CG_C} = C_{m,\ CG_u} - \Delta C_{m,\ CG_t} \qquad \textbf{(68)}$$

where: $$\Delta C_{m,\,CG_t} = \left(\frac{\partial C_{m,CG}}{\partial \delta s}\right) * \delta * \tau_2\left(\frac{S}{C}\right) * C_{LW} * (57.3)$$

$$\frac{\partial C_{m,CG}}{\partial \delta s} = -\bar{V} * \eta * C_{L\alpha_t}$$

$$C_{L\alpha_t} = \frac{\partial C_{Lt}}{\partial \alpha} \approx \left(\frac{0.1 * ARw}{ARt + 2.0}\right) * (0.8)$$

δ = Boundary correction factor = 0.1125

τ_2 = Downwash correction factor = 0.65

η = Ratio of tail to wing dynamic pressure = $\frac{q_t}{q_w}$

$\bar{V}$ = Horizontal tail volume ratio

These corrections are rather mild since b/c (model span/wide of the test section) was approximately 0.52.

IV. Results and Analysis

This chapter presents the results of the wind tunnel experimentation made with the UAV, using the two tail configurations already mentioned in Chapter II.

To control the UAV, the tails have an elevator deflection and rotation deflections; therefore, during the development of the experimentation, as well as during the results and analysis, it was given to the tail the notation and sign convention mentioned in Chapter II.

Given that it was necessary to study the stability as well the response to the different deflections of the tail configurations used in the UAV, this chapter was divided in the following four main parts:

a. Results for tail 1

b. Results for tail 2

c. Movement of the center of gravity

d. Limitations of experimental effort

An important point that must be considered in all the results presented in this chapter is that the center of gravity position is controllable in accordance with the position of the battery, as well as a consequence of the weight of each tail. These C.G. locations are mentioned in the tables where the conditions for each run are described at the beginning of each section. The notation used to described it was the subscript “cm” that indicates the position of the center of gravity of the MAV with respect to the center of the balance; if for any reason it is necessary to know the position of the center of gravity with respect to another reference such as the position from the wing leading edge it will be necessary to consider the relationship and measures that are shown on Figure 57.

Moreover, a deeper analysis that the center of gravity has in the UAV is presented in the section of “Movement of the Center of gravity”.

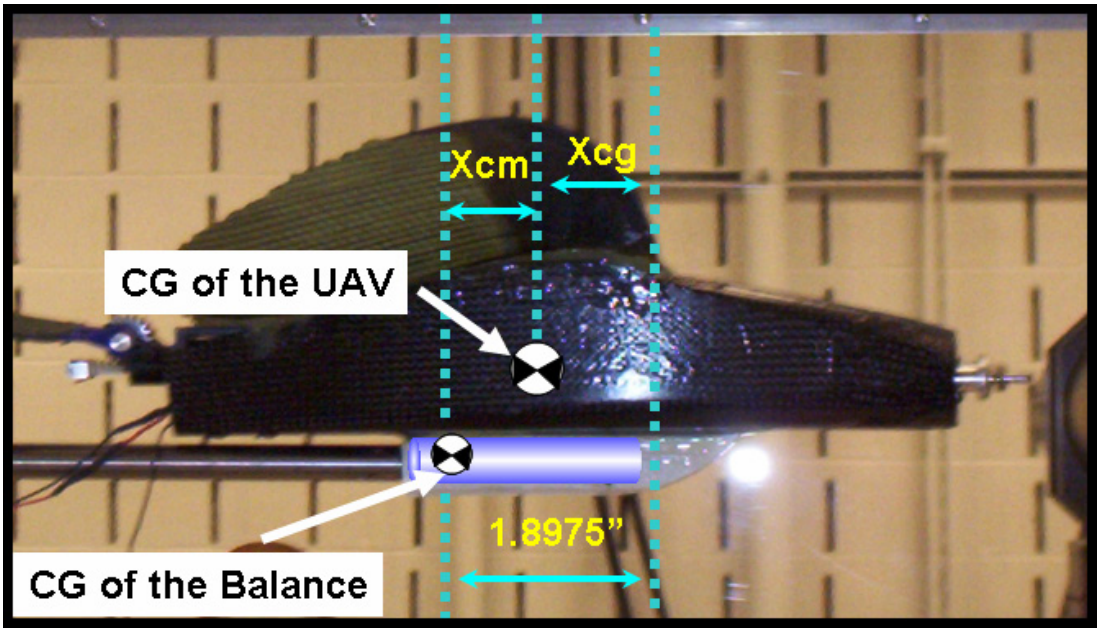

Figure 57. CG Notation

4.1. Results for Tail 1

The experiments made with this tail had as a goal to answer the questions: How are the aerodynamic forces and moments produces by a rotary tail? Is it possible to have a controllable and stable airplane with a rotary tail? In order to obtain this information, the following analyses were made by using tail 1:

a. Longitudinal static stability.

b. Longitudinal control.

c. Directional stability

d. Directional control

e. Roll stability

f. Roll control

g. Parametric analysis of the tail control using two degree of freedom.

For the analysis of longitudinal static stability as well longitudinal, directional and roll control, the alpha wind tunnel tests mentioned in Table 9 were executed. For the directional and roll stability as well as directional and roll control the beta wind tunnel tests mentioned in Table 11 were executed. Finally, for the parametric analysis of the tail control using two degrees of freedom, the wind tunnel runs mentioned in Table 10 were executed.

Table 9. Alpha Runs Completed with Tail 1

ALPHA RUNS CONDITIONS: ***α= -8º to 10º*** ***β=0º*** ***SPEED= 30 MPH***							
DATE	***DESCRIPTION***	***WEIGHT (Grams)***	***TEMP. (ºF)***	***PRES. (mm Hg)***	X_{CM}	Y_{CM}	Z_{CM}
8/3/2004	TAIL 1 δe=0º, δrn=0º	400	73.5	28.89	1.0225"	0	-1.31
8/3/2004	TAIL 1 δe=-9º, δrn=0º	400	73.5	28.89	1.0225"	0	-1.31
8/4/2004	NO TAIL	390	73.4	28.82	1.46"	0	-1.31
8/4/2004	TAIL 1 δe=8º, δrn=0º	400	73.4	28.82	1.0225"	0	-1.31
8/4/2004	TAIL 1 δe=0º, δrn=20º	400	73.4	28.82	1.0225"	0	-1.31
8/4/2004	TAIL 1 δe=-9º, δrn=20º	400	73.5	28.85	1.0225"	0	-1.31
8/4/2004	TAIL 1 δe=-9º, δrn=-20º	400	73.5	28.87	1.0225"	0	-1.31
8/4/2004	TAIL 1 δe=0º, δrn=-20º	400	73.5	28.87	1.0225"	0	-1.31
9/23/2004	TAIL 1 δe=8º, δrn=-20º	405	74.5	29.24	0.96"	0	-1.31
9/23/2004	TAIL 1 δe=8º, δrn=20º	405	73.5	29.25	0.96"	0	-1.31

Table 10. Matrix Runs Completed with Tail 1

MATRIX RUNS CONDITIONS: α= 4º β=0º SPEED= 30 MPH							
DATE	***DESCRIPTION***	***WEIGHT (Grams)***	***TEMP. (ºF)***	***PRES. (mm Hg)***	X_{CM}	Y_{CM}	Z_{CM}
9/23/2004	TAIL 1 δe=11º, δrn=32º	405	72.3	29.24	0.96"	0	-1.31
9/23/2004	TAIL 1 δe=7º, δrn=32º	405	72.3	29.24	0.96"	0	-1.31
9/23/2004	TAIL 1 δe=0º, δrn=32º	405	72.3	29.24	0.96"	0	-1.31
9/23/2004	TAIL 1 δe=-12º, δrn=32º	405	72.3	29.24	0.96"	0	-1.31
9/23/2004	TAIL 1 δe=-15º, δrn=32º	405	72.3	29.24	0.96"	0	-1.31
9/23/2004	TAIL 1 δe=11º, δrn=17º	405	72.3	29.24	0.96"	0	-1.31
9/23/2004	TAIL 1 δe=7º, δrn=17º	405	72.3	29.24	0.96"	0	-1.31
9/23/2004	TAIL 1 δe=0º, δrn=17º	405	72.3	29.24	0.96"	0	-1.31
9/23/2004	TAIL 1 δe=-12º, δrn=17º	405	72.3	29.24	0.96"	0	-1.31
9/23/2004	TAIL 1 δe=-15º, δrn=17º	405	72.3	29.24	0.96"	0	-1.31
9/23/2004	TAIL 1 δe=11º, δrn=8º	405	72.3	29.24	0.96"	0	-1.31
9/23/2004	TAIL 1 δe=7º, δrn=8º	405	72.3	29.24	0.96"	0	-1.31
9/23/2004	TAIL 1 δe=0º, δrn=8º	405	72.3	29.24	0.96"	0	-1.31
9/23/2004	TAIL 1 δe=-12º, δrn=8º	405	72.3	29.24	0.96"	0	-1.31
9/23/2004	TAIL 1 δe=-15º, δrn=8º	405	72.3	29.24	0.96"	0	-1.31
9/23/2004	TAIL 1 δe=11º, δrn=0º	405	72.3	29.24	0.96"	0	-1.31
9/23/2004	TAIL 1 δe=7º, δrn=0º	405	72.3	29.24	0.96"	0	-1.31
9/23/2004	TAIL 1 δe=0º, δrn=0º	405	72.3	29.24	0.96"	0	-1.31
9/23/2004	TAIL 1 δe=-12º, δrn=0º	405	72.3	29.24	0.96"	0	-1.31
9/23/2004	TAIL 1 δe=-15º, δrn=0º	405	72.3	29.24	0.96"	0	-1.31
9/23/2004	TAIL 1 δe=11º, δrn=-8º	405	72.3	29.24	0.96"	0	-1.31
9/23/2004	TAIL 1 δe=7º, δrn=-8º	405	72.3	29.24	0.96"	0	-1.31
9/23/2004	TAIL 1 δe=0º, δrn=-8º	405	72.3	29.24	0.96"	0	-1.31
9/23/2004	TAIL 1 δe=-12º, δrn=-8º	405	72.3	29.24	0.96"	0	-1.31
9/23/2004	TAIL 1 δe=-15º, δrn=-8º	405	72.3	29.24	0.96"	0	-1.31
9/23/2004	TAIL 1 δe=11º, δrn=-18º	405	72.3	29.24	0.96"	0	-1.31
9/23/2004	TAIL 1 δe=7º, δrn=-18º	405	72.3	29.24	0.96"	0	-1.31
9/23/2004	TAIL 1 δe=0º, δrn=-18º	405	72.3	29.24	0.96"	0	-1.31
9/23/2004	TAIL 1 δe=-12º, δrn=-18º	405	72.3	29.24	0.96"	0	-1.31
9/23/2004	TAIL 1 δe=-15º, δrn=-18º	405	72.3	29.24	0.96"	0	-1.31
9/23/2004	TAIL 1 δe=11º, δrn=-30º	405	72.3	29.24	0.96"	0	-1.31
9/23/2004	TAIL 1 δe=7º, δrn=-30º	405	72.3	29.24	0.96"	0	-1.31
9/23/2004	TAIL 1 δe=0º, δrn=-30º	405	72.3	29.24	0.96"	0	-1.31
9/23/2004	TAIL 1 δe=-12º, δrn=-30º	405	72.3	29.24	0.96"	0	-1.31
9/23/2004	TAIL 1 δe=-15º, δrn=-30º	405	72.3	29.24	0.96"	0	-1.31

Table 11. Beta Runs Completed with Tail 1

BETA RUNS CONDITIONS: α= 4º β=-10º to 10º SPEED= 30 MPH							
DATE	***DESCRIPTION***	***WEIGHT (Grams)***	***TEMP. (ºF)***	***PRES. (mm Hg)***	X_{CM}	Y_{CM}	Z_{CM}
9/23/2004	TAIL 1 δe=0º, δrn=0º	405	74	29.24	0.96"	0	-1.31
9/23/2004	TAIL 1 δe=0º, δrn=32º	405	73.8	29.242	0.96"	0	-1.31
9/23/2004	TAIL 1 δe=0º, δrn=-30º	405	74.5	29.23	0.96"	0	-1.31

4.1.1. Longitudinal Static Stability Using Tail 1

This static stability will give to the UAV the ability of return to its original angle of attack when it is perturbed from a previous longitudinal trim attitude.

Figure 60 reveals characteristics of the longitudinal static stability for tail 1 with δe =0 and δrn =0, representing the baseline case, and its comparison with the UAV with no tail. As described in Chapter II, two conditions are necessary in the graph of Cm vs. α in order for an airplane to be stable: first, $\frac{\partial Cm}{\partial \alpha}$ must be negative and Cm_0 must be positive. As seen in Figure 60, the UAV with no tail is longitudinally stable since the curve has a negative slope, in other words its average value is $\frac{\partial Cm}{\partial \alpha}$ = -0.0197. In the same figure it can be seen that the UAV using tail 1 is stable, too, since the average $\frac{\partial Cm}{\partial \alpha}$ = -0.0166; however, this stability is smaller than the one that the UAV had before tail 1 was installed.

Interestingly, the tail 1 data indicates a slight decrease in Cm_α, compared to the no tail run. An important factor test is necessary to consider: both curves represent the UAV with different position of the center of gravity. The UAV with no tail is stable in part because for that experiment the position of the center of gravity is ahead of the Neutral Point and once the tail is installed, the center of gravity is moved more backwards and as a consequence the slope of the curve is reduced.

From the prior analysis it can be said that the contribution of the tail 1 to the stability is almost negligible and the effect that is presented as a change in the slope is only the contribution of the weight rather than the contribution of the presence of a stability device as in a regular tail. This information can be confirmed by the data presented in Figure 58 and Figure 59 where the lifts of both cases are shown. Since the total lift that an aircraft has is defined as:

Total Lift = Lift due to the wing + Lift due to the tail **(69)**

it can be perceived in these figures that it is almost insignificant. For instance, the maximum difference in lift is obtained at 8 degrees of angle of attack, and at this point, the UAV with no tail had a lift coefficient of 1.3552 and with the tail it had a value of 1.3843.That represents only an increment of 2.147 %. Moreover, the lower the angle of attack, the smaller contribution of the tail to the total lift of the aircraft. In fact at negative angles of attack both curves overlap.

On the other hand, it is known that for steady level flight the lift must be equal to the weight of the airplane. Since the UAV with tail 1 weights 400 grams (0.8821 lbf); in

accordance with Figure 58 and Figure 59 the angle of attack necessary to keep steady state at 30 MPH is -1.915864º. Note that this angle is relative to the bottom of the UAV.

Another important point to notice in Figure 60 is the pitch moment produced by the UAV with no tail: For most of the angles of attack it provides a negative pitch moment and as a consequence, one would not be able to trim at positive angles of attack, in a few words, even if the condition of having a negative slope is accomplished the condition of being able to trim at positive angles of attack is not. On the other hand, the production of negative pitch moment by the MAV with no tail indicates that the moment produced by the tail should be positive, in other words the lift produced by the tail must be as a consequence of a high pressure in the upper face of the tail and a lower pressure in the lower face of it.

Since, in accordance with the prior discussion, the contribution of tail 1 to the longitudinal static stability is negligible. In order to obtain a more longitudinally static stable UAV using tail 1 one may change the center of gravity more forward, by changing some of the internal components of the UAV. However, even if the slope of the curvature is more negative the same situation of no having the capability of trim to positive angles of attack will be present, but if once this increment on the slope is achieved a deflection in the tail to negative δe values will provide a shift of this same curve to a position that will allow trim the UAV at positive angles of attack (Nelson; 1998:63)

All the analyses of changing the center of gravity of the UAV are presented in the section of “Movement of the Center of Gravity” and the effect of the deflection of the tail is presented in the section “Longitudinal control”.

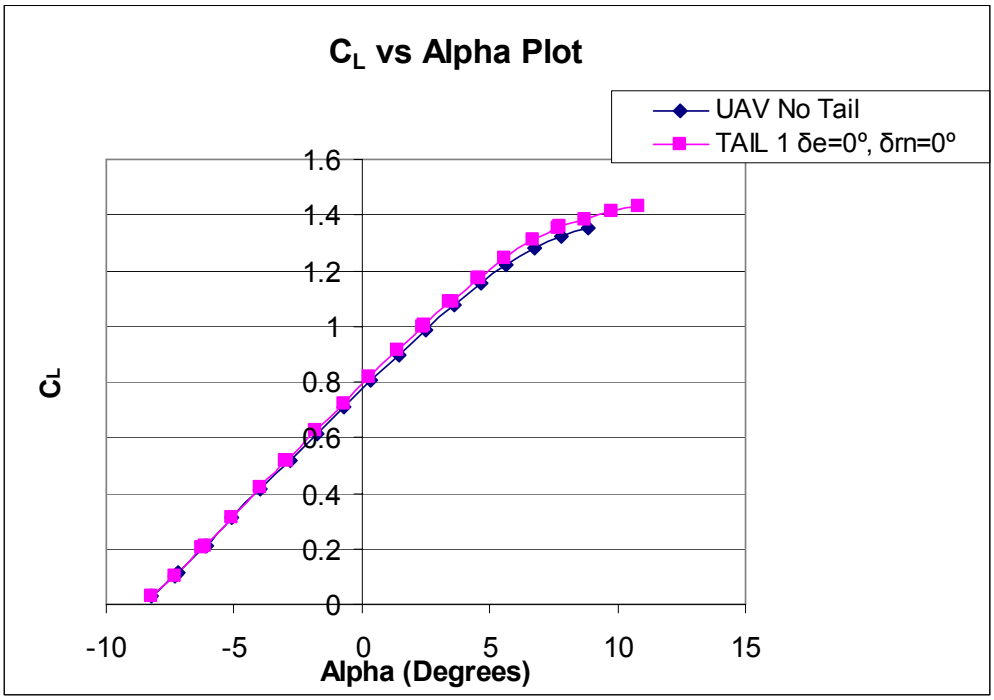

Figure 58. C_L Versus Angle of Attack

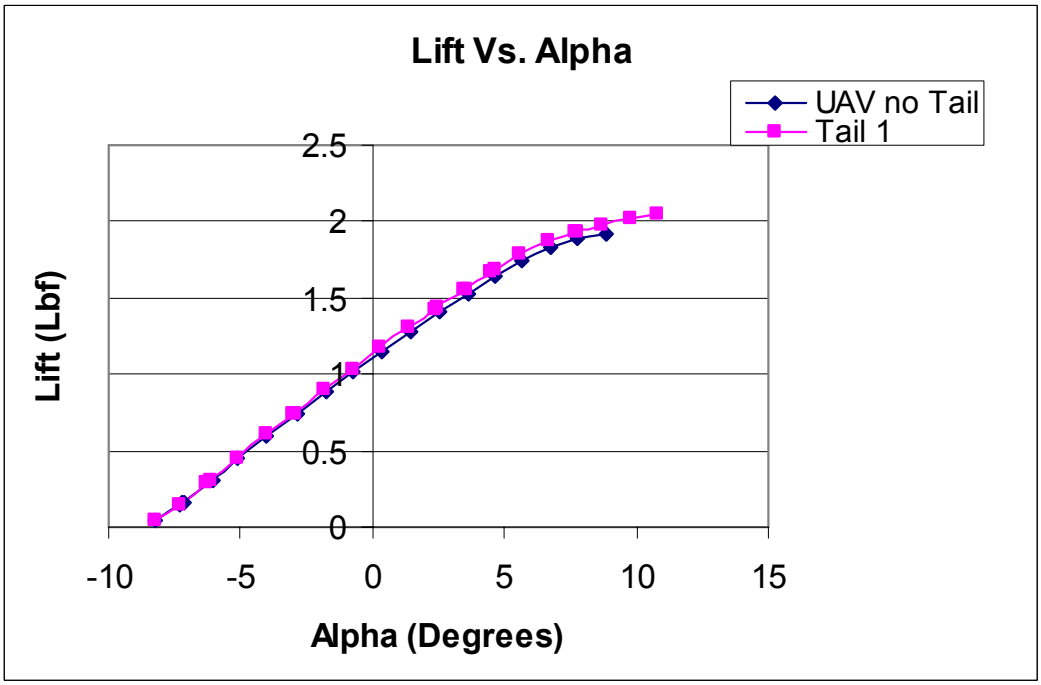

Figure 59. Lift Versus Angle of Attack

Another way to check the longitudinal static stability can be made by setting the relationship between C_m and C_L. This plot is presented in Figure 61 that reconfirms the data obtained in Figure 60.

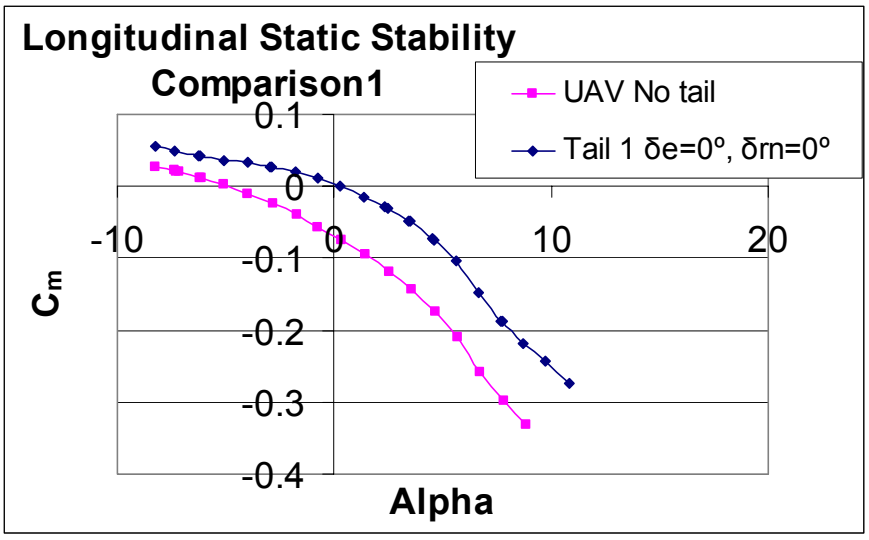

Figure 60. Longitudinal Static Stability Comparison 1

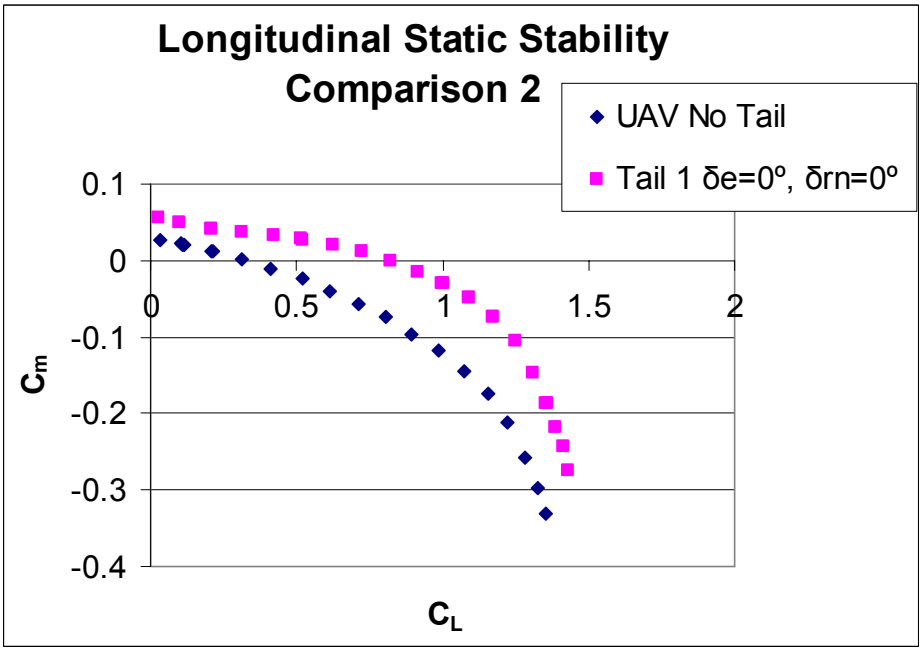

Figure 61. Static Stability Comparison 2

4.1.2. Longitudinal Control for Tail 1

In order to test the effectiveness of the different tails in the longitudinal control, the following analyses were made by considering " pure longitudinal control", in other words, using only elevator deflection (δe) with zero tail rotation (δrn = 0º):

a. Production of the pitch moment at different elevator deflections

b. Change in coefficient of lift at different elevator deflections

c. Analysis of the drag produced at different elevator deflections

a. Production of the Pitch Moment at Different Elevator Deflections

In order to analyze the production of pitch moment, a plot of C_m versus α is presented for different elevator deflections in Figure 62.

Figure 62 shows that tail 1 increases C_m at a rate of 0.0057 per degree when it is deflected in the negative direction; moreover it decreased C_m in a rate of.0082 per degree when it is deflected in the positive direction. These results are as they were expected. The reason for the difference between the control effectiveness of the positive and negative deflection can be due to the fact that the UAV with no tail has a tendency by itself of produce negative pitch moment, as a consequence, this factor is favorable in case of positive elevator deflection and is opposite to the negative deflection of the tail

Figure 64 again illustrates that the pitch moment that the UAV has with δe =0º changes as a function of angle of attack; in other words, when the UAV is with δe=0º and δrn=0º at 0.3º angle of attack Cm is 0.00033, when is at α= 4.6º Cm is -0.074 and when is at α= -4.0 º Cm is 0.033. It can be seen that at more positive angle of attack Cm becomes

more negative. This change in the pitch moment is in accord with the data presented in Figure 60 and it is consequence of the fact that the lift produced by the wing change as a consequence of the angle of attack. One important point to gain from Figure 64 is that elevator may be used to trim the airplane. Overall, it can be seen in the slope of the three curves presented in Figure 64 that the control effectiveness of the tail as a control-pitch device is virtually constant at the three different angles of attack presented.

b. Change in Coefficient of Lift at Different Elevator Deflections

Figure 63 shows the comparison of the longitudinal control by using C_m vs C_L. The data presented in this plot matches the results presented in the previous analysis.

Figure 65 presents the change in coefficient of lift due to the change in elevator deflection. This plot shows that the lift produced at positive elevator deflections are bigger that those produced at negative elevator deflections; however the principal factor that influence the lift generation is the value of alpha.

c. Analysis of the Drag Produced at Different Elevator Deflections

In order to visualize the effectiveness of a control flight is necessary to consider the force produced by this control and compared to the drag produced by itself. For this reason, Figure 66 presents this relationship for different elevator deflections. The results were as expected. In the sense that as the lift increases the drag increases, too; the rate of this relationship is the same at different elevator deflections.

The effects due to a pure elevator deflection were consistent with the expectations. There appears to be a slight loss of efficiency (~5%) with δe=-9º, but otherwise the results are very close.

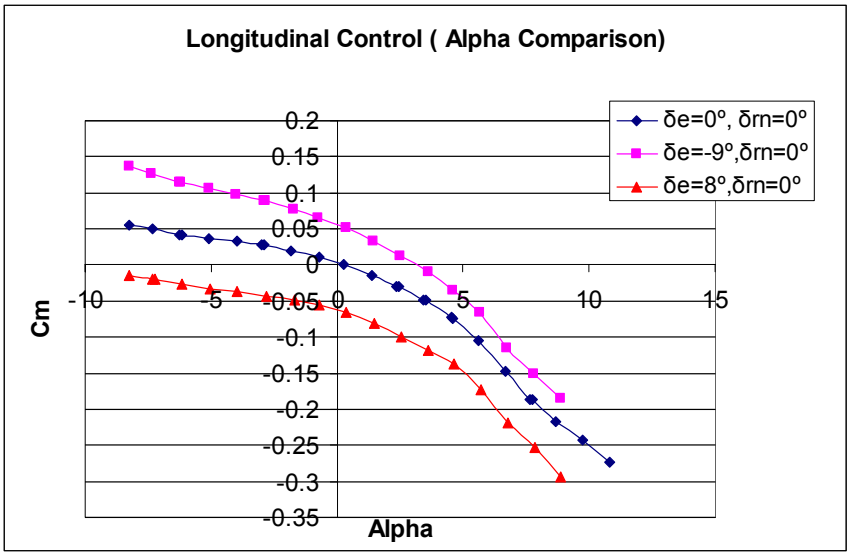

Figure 62. Longitudinal Control Comparison Using C_m Vs. Alpha

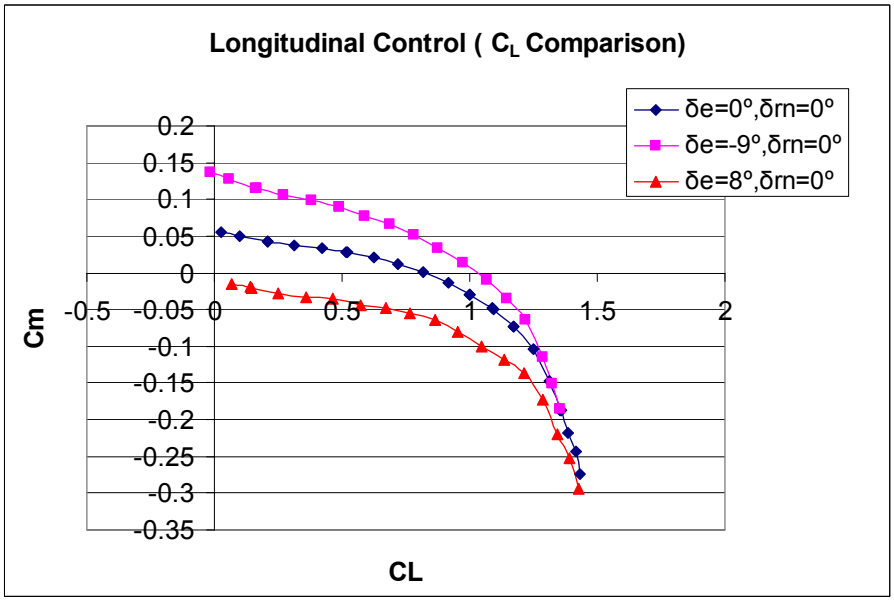

Figure 63. Longitudinal Control Comparison by Using C_m Vs. C_L

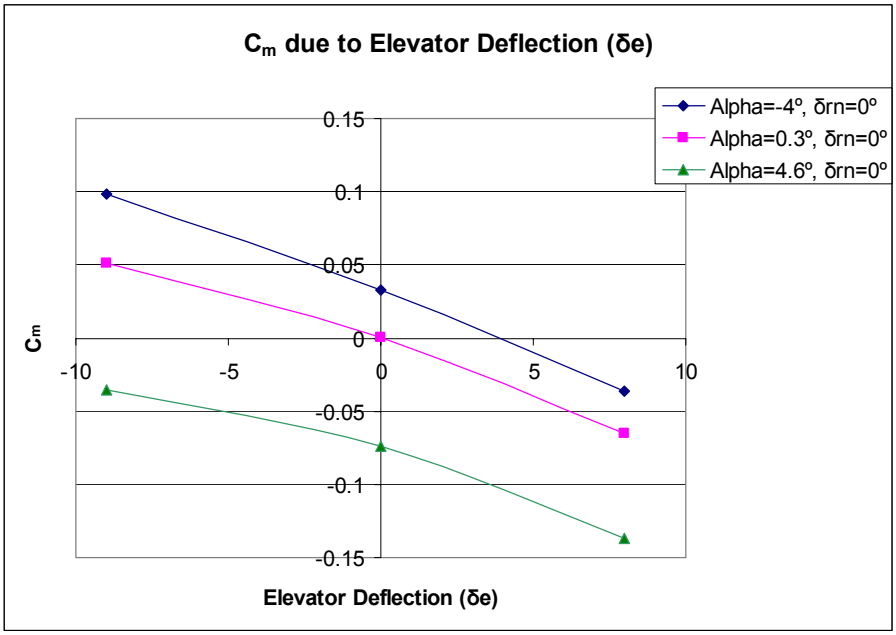

Figure 64. C_m due to Elevator Deflection (δe)

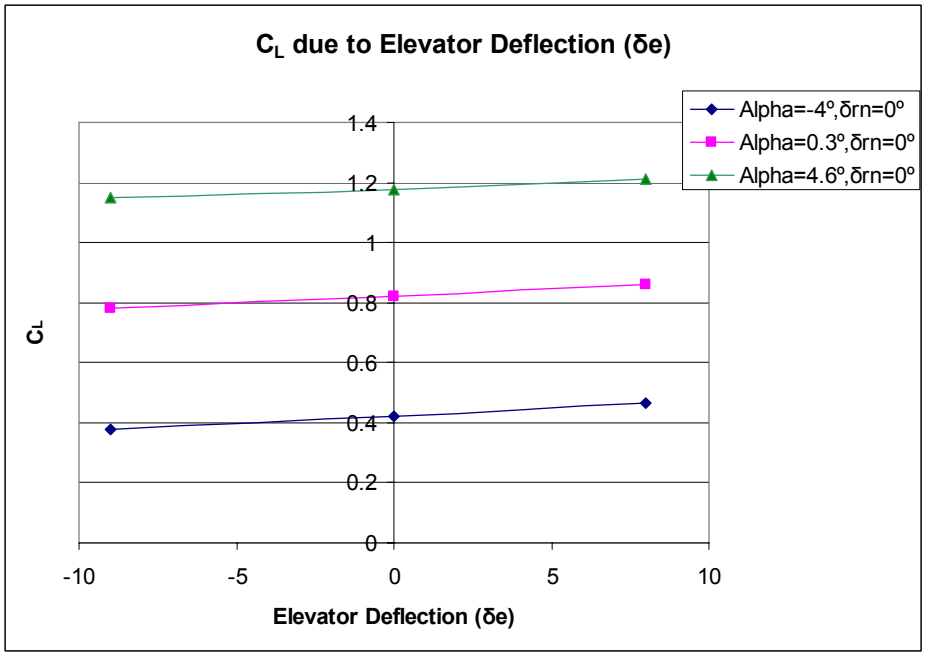

Figure 65. C_L due to Elevator Deflection (δe)

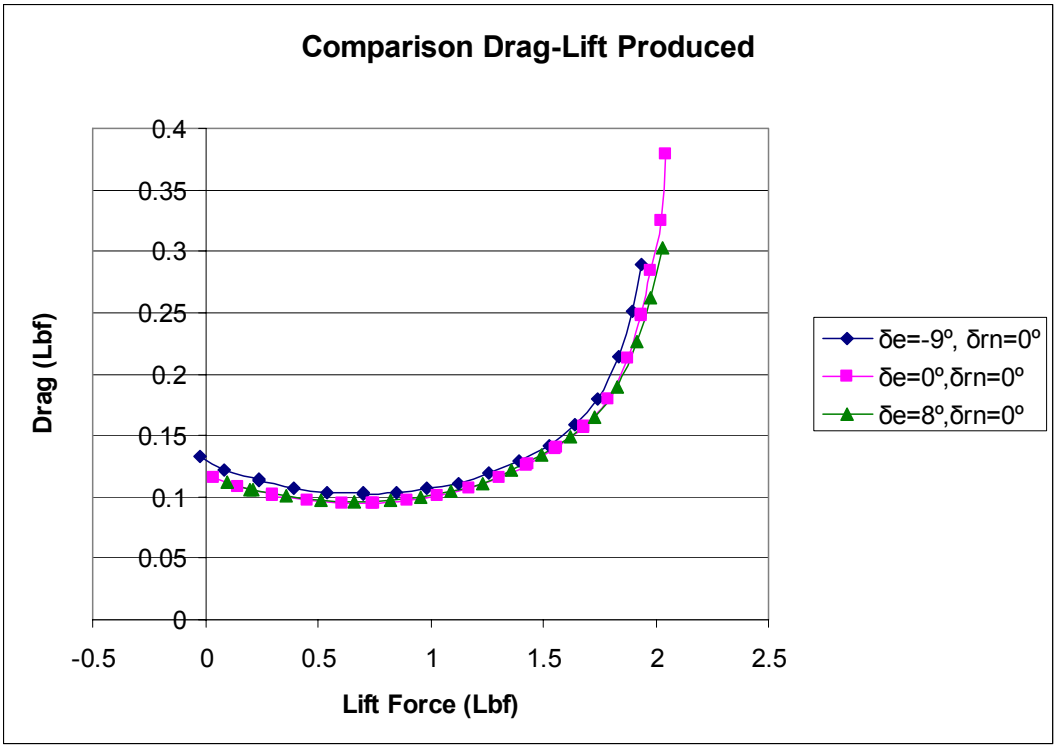

Figure 66. Relationship Between Drag-Lift Produced at Different Elevator Deflections

4.1.3. Directional Stability for Tail 1

As it was described in Chapter II, this stability will allow the UAV to return to its equilibrium condition when it is subjected to a yawing disturbance.

In order to check the directional stability of the UAV, Figure 67 was made by the wind tunnel tests given in Table 11. Notably, angle of attack was 4º for each case.

Since in order to have static directional stability, it is necessary that the condition of $C_{n\beta} > 0$ be present, it can be seen in Figure 67 that the UAV with tail 1 does not have directional static stability since $\frac{\partial Cn}{\partial \beta}$ =-0.000443. This result was not unexpected because tail 1 does not have vertical stabilizer that is the main contributor to this stability.

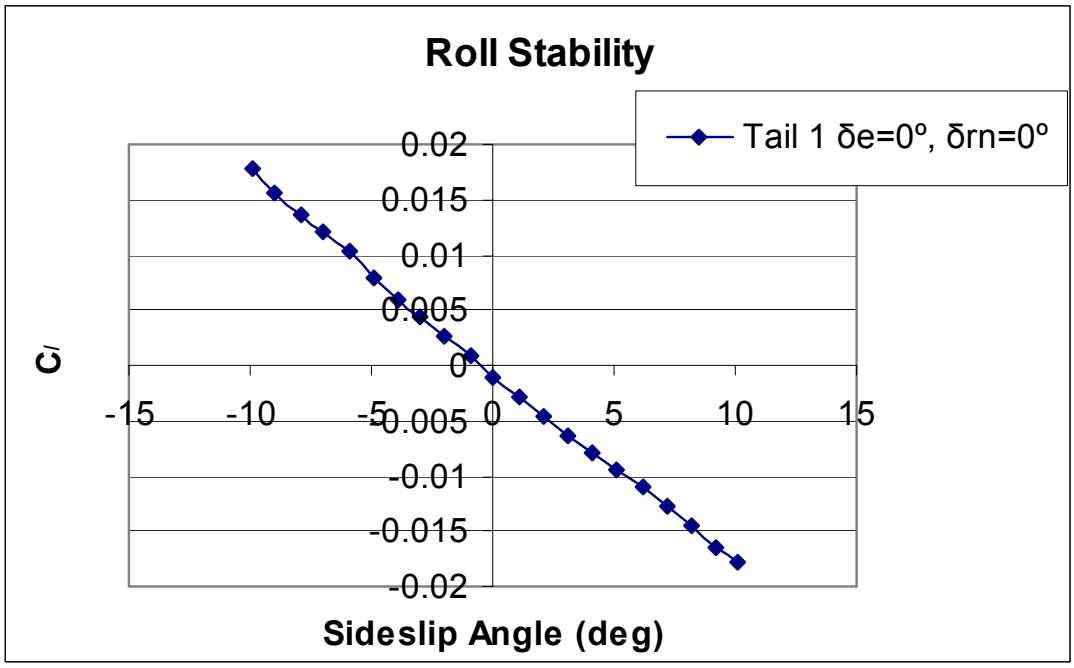

Figure 67. Directional Stability

4.1.4. Directional Control for Tail 1

Figure 68 shows that the UAV using tail 1 can be directionally controlled by using rotation of the tail. In this figure it can be seen that the change in Cn can be obtained by rotating the tail. This rotation shift the sign of the curve in the following way: Positive rotation of the tail produces a shift of the curve to the side of negative values of Cn negatives and negative rotation of the tail shift it to the positive values of Cn. It is important to consider that this data is for δe=0º because the value of the moment produced is a function of the elevator deflection, as seen in the data presented in Figure 72 and Figure 73.

The data in Figure 68 also suggests that, with an active flight control system, one would be able to correct for a directional instability. For example, an applied rotation of -30º would increase Cn to approximately +0.003, which would act to stabilize the vehicle.

In order to test the effectiveness of the different tails in directional control, in the next three sections, analysis were made first considering " pure directional control", in other words, using only rotation (δrn) with zero elevator deflection tail (δe = 0º). After that, analysis was made considering the effect of elevator in the directional control by using a comparison for δe=-9º, δe=0º and δe=8º in combination with δrn from -20º to 20º:

a. Production of the yaw moment at different tail rotations

b. Change in coefficient of side force at different tail rotations

c. Analysis of the drag produced at different tail rotations.

d. Analysis of the effects on the pitch moment coefficient due to the activation of simultaneous elevator deflection and rotation of the tail.

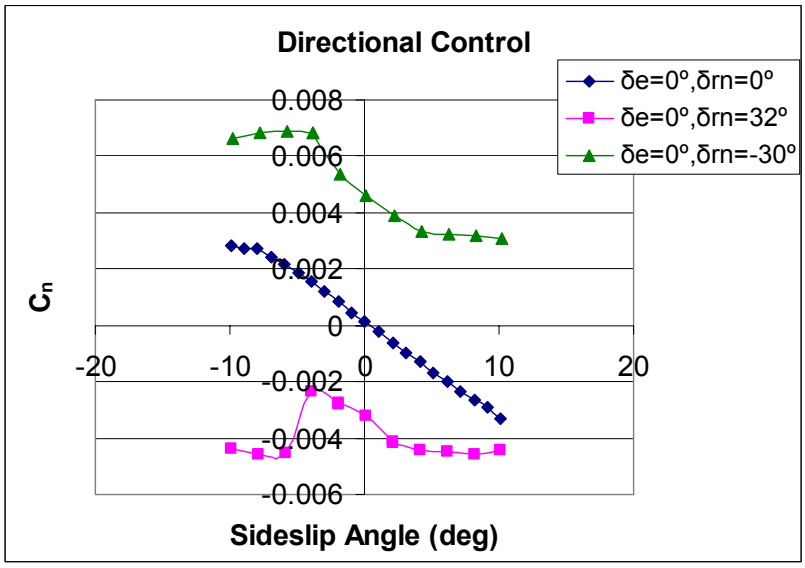

Figure 68. Directional Control

a. Production of the Yaw Moment (C_n) at Different Tail Rotations

Figure 69 shows the production of C_n using different tail rotations and compares with different alphas, keeping $\delta e=0^o$. The results are the following:

1. The rotation of the tail at $\delta e=0^o$ produces relatively small changes in yaw moment; It can be seen in Figure 69 that these values are of order 10^{-3}.

2. When alpha is negative as the rotation becomes more positive the Cn produced is more positive and when the rotation is more negative the Cn produced is more negative too.

3. When alpha is positive as the rotation becomes more positive the Cn produces is more negative and when the rotation is more negative the Cn produced is more positive.

4. Points 2 and 3 are important to consider because this data is evidence for the cross control phenomena that consists of the following: the yaw moment produced for a same angle of rotation, when $\delta e=0^o$ will produce an opposite effect on the UAV, depending in the angle of attack of the aircraft. In other words, in a traditional piloted aircraft with an elevator, rudder and ailerons, to execute a turn to the left, the pilot would need to push the stick control to the left; however for this tail configuration, the same user would have to think: is the airplane with positive or negative angle of attack? If positive, he would push the stick control to the right in order to have an increment of C_n in the left direction, and if the angle of attack is negative, he would push the stick control to the left in order to have a increment of C_n in the left direction. An important observation is that this phenomena occurs when for $\delta e=0^o$, because as the data presented describes, once elevator deflection is applied in the tail the dependence in the angle of attack is only in the magnitude of the resultant force rather than in the direction.

On the other hand, it is important to remember that essentially what is desirable is for the rotation of the tail is to change the direction of the UAV and this can be made by using a rolling moment, a yaw moment or a combination of both. Therefore, it is necessary to also consider the rolling moment produced by the tail and to compare it with the yaw moment and see the final effect. This analysis is made in the roll control analysis section.

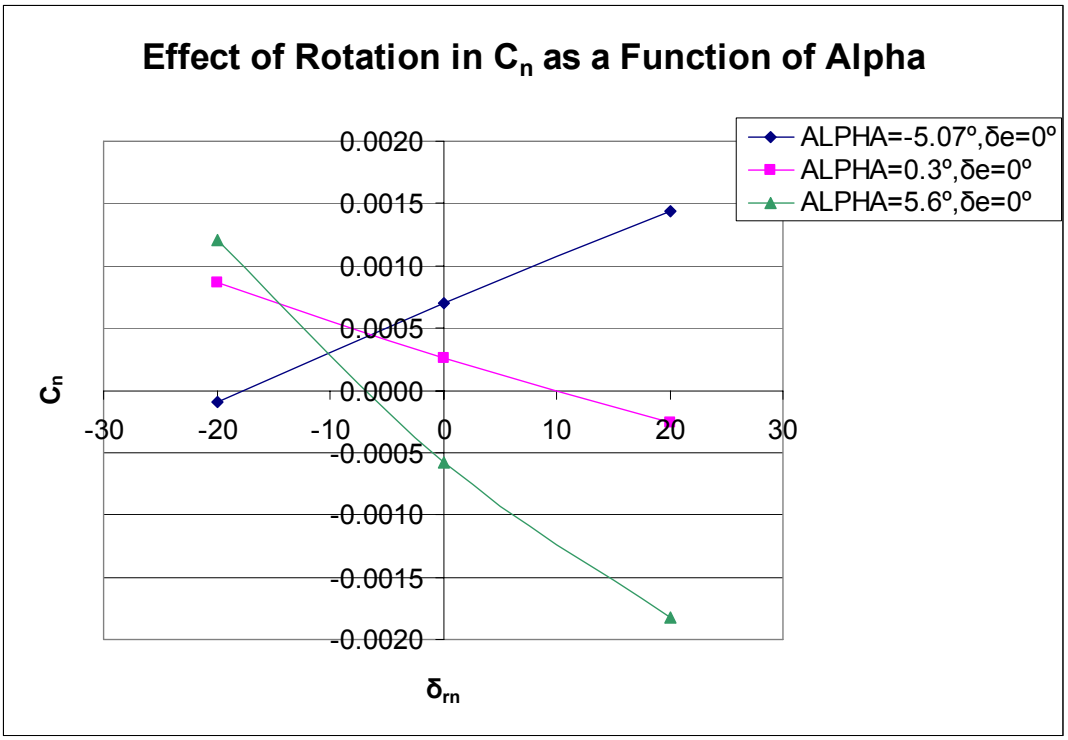

Figure 69. Production of the Yaw Moment (C_n) at Different Tail Rotations

Figure 70, Figure 71, Figure 72 and Figure 73 show the Cn produced not only as a function of rotation but also as a function of elevator deflection. The results are the following:

1. At positive elevator deflections of the tail, its effectiveness is bigger than at negative elevator deflections. This phenomenon is clearly seen in Figure 70 and in Table 12 where considering angle of attack 3.6º the change in Cn is more than 114% larger for positive elevator deflection compared with the change in Cn for negative elevator deflection. In a few words, the tail is more effective for changing the yaw of the UAV when it is deflected at positive elevator deflections.

2. At zero elevator deflection the sign in the direction of the moment produced by the rotation of the tail depends on the angle of attack as it is shown in Figure 71; moreover, once elevator deflection is applied, the value of the moment produced is function of the angle of attack of the UAV, because the angle of attack of the tail is function of the angle of attack of the wing.

3. Figure 72 shows that at negative elevator deflections, a positive rotation of the tail produces positive values of Cn and a negative rotation of the tail produces negative values of Cn. This means that the forces acting on the tail at negative values of δe is a consequence of the higher pressure on the upper surface of the tail.

4. Figure 73 shows that with positive deflections of the tail, positive values of δrn produce negative values of Cn, moreover, once again, notice that the values of Cn produced with δe positives are bigger compared with those obtained with δe negatives. This means that the forces acting on the tail for positive values of δe is a consequence of the higher pressure on the lower surface of the tail.

Table 12. Effects of the Elevator Deflection in the Rate of Change in Cn as a Consequence of the Rotation of the Tail for Angle of Attack of 3.6º.

ELEVATOR DEFLECTION (δe)	CHANGE IN Cn AS A FUNCTION OF ROTATION OF THE TAIL (δrn)
δe=0º	-0.0000719 per degree
δe=8º	-0.000396 per degree
δe=-9º	0.000185 per degree

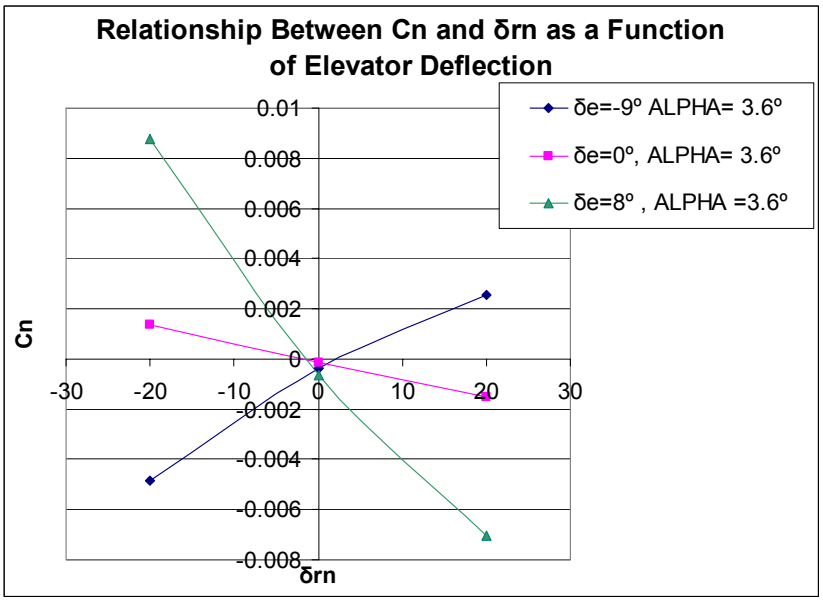

Figure 70. Effects of Simultaneous Elevator Deflection and Rotation of the Tail on Cn

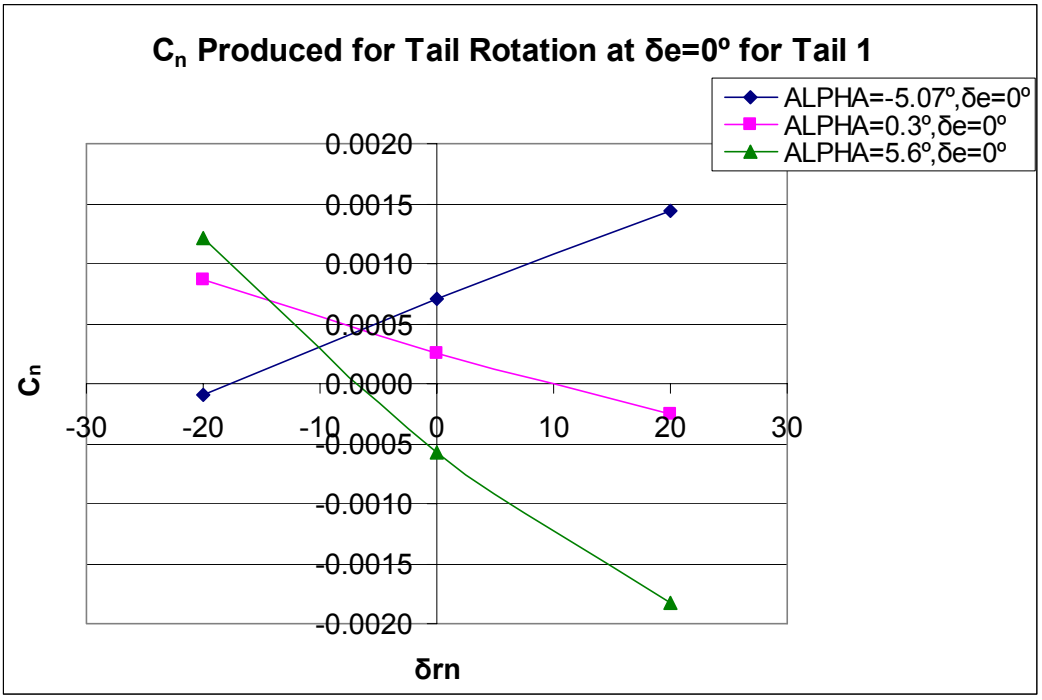

Figure 71. Cn Produced for Tail Rotation at δe=0º

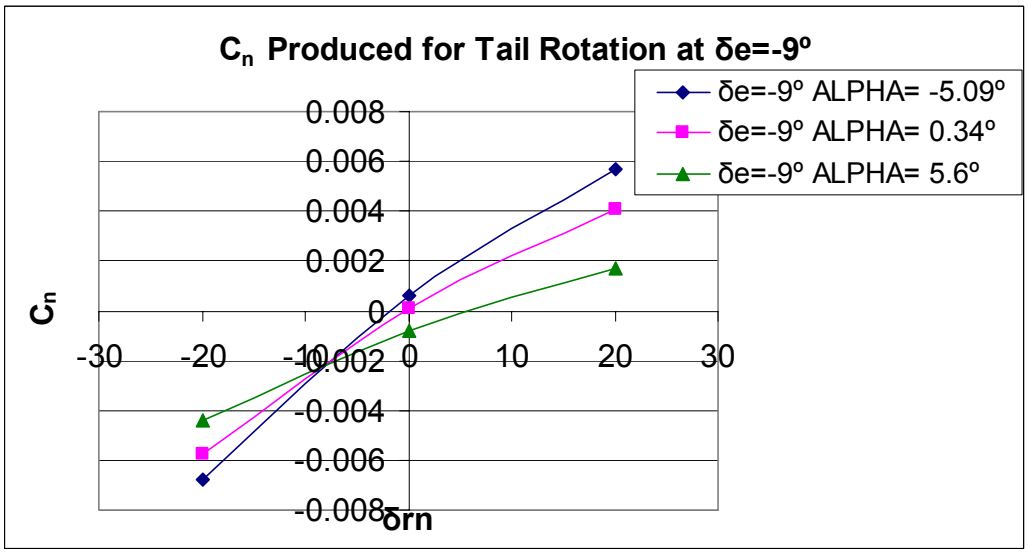

Figure 72. Cn Produced for Tail Rotation at δe=-9º

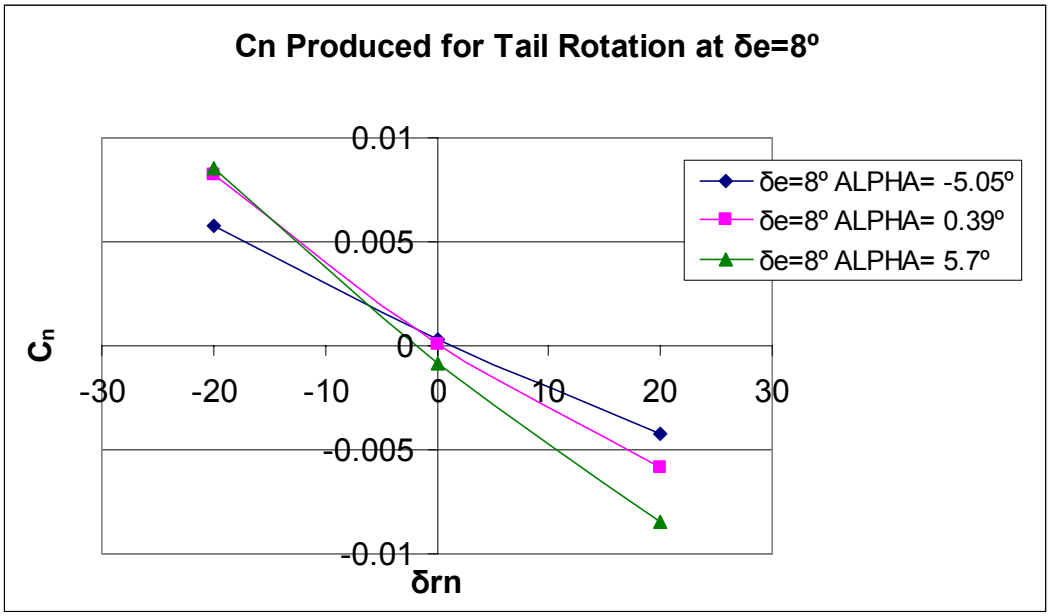

Figure 73. Cn Produced for Tail Rotation at δe=8º

b. Change in Coefficient of Side Force at Different Tail Rotations

Figure 74, Figure 75, and Figure 76 show the production of side force with the following results:

1. As was expected from the prior analysis, it can be seen that the rotation of the tail produce small changes in the side force, specifically at negative angles of attack.

2. The same opposite effect already mentioned in the prior point is present in the production of the side force.

3. As was expected, the effectiveness of the tail for producing the side force is larger when an elevator deflection of the tail is applied; moreover, at these elevator deflections the slope of the curve indicates that the change in the direction of the side force produced is more successful.

4. Notice in the three figures that with δrn =0º the UAV by itself has a negative side force and that this negative side force is smaller as the angle of attack becomes more negative. This can be the results of asymmetric characteristics of the UAV, as well as the fact that the side slip angle (Beta) used during the test was not exactly zero. Refer to the limitations of

experimental effort for additional information related with this kind of errors.

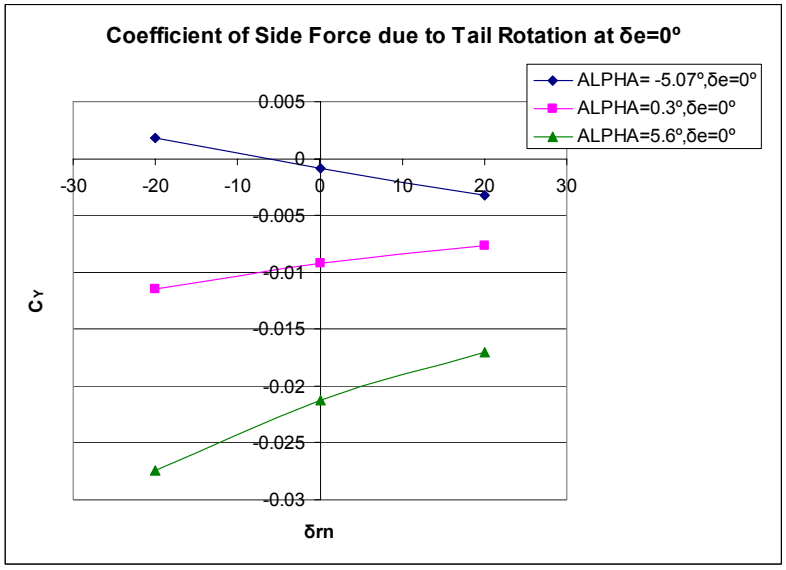

Figure 74. Coefficient of Side Force Production with Different Tail Rotations at δe=0º

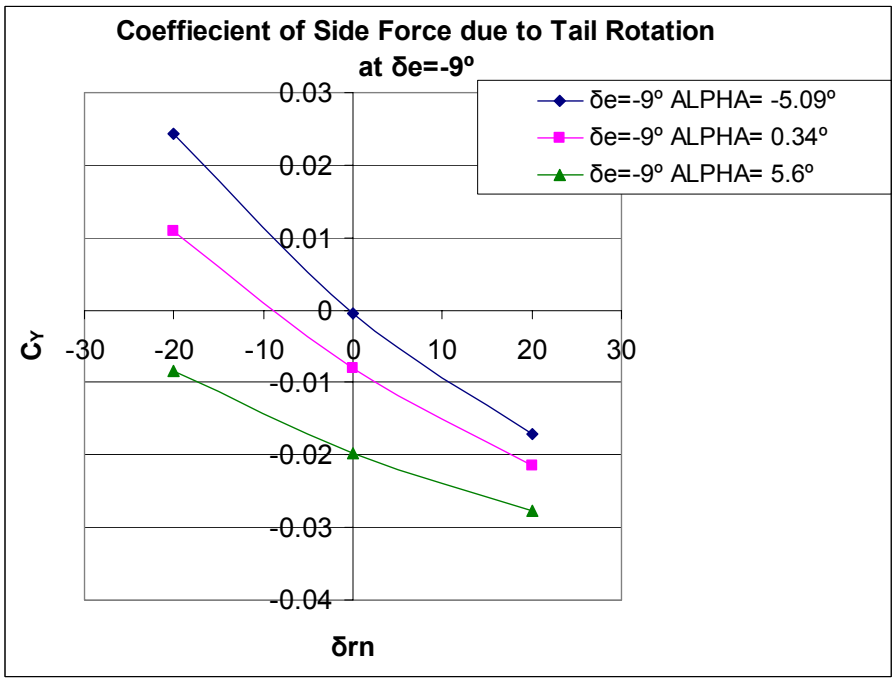

Figure 75. Coefficient of Side Force Production with Different Tail Rotations at δe=-9º

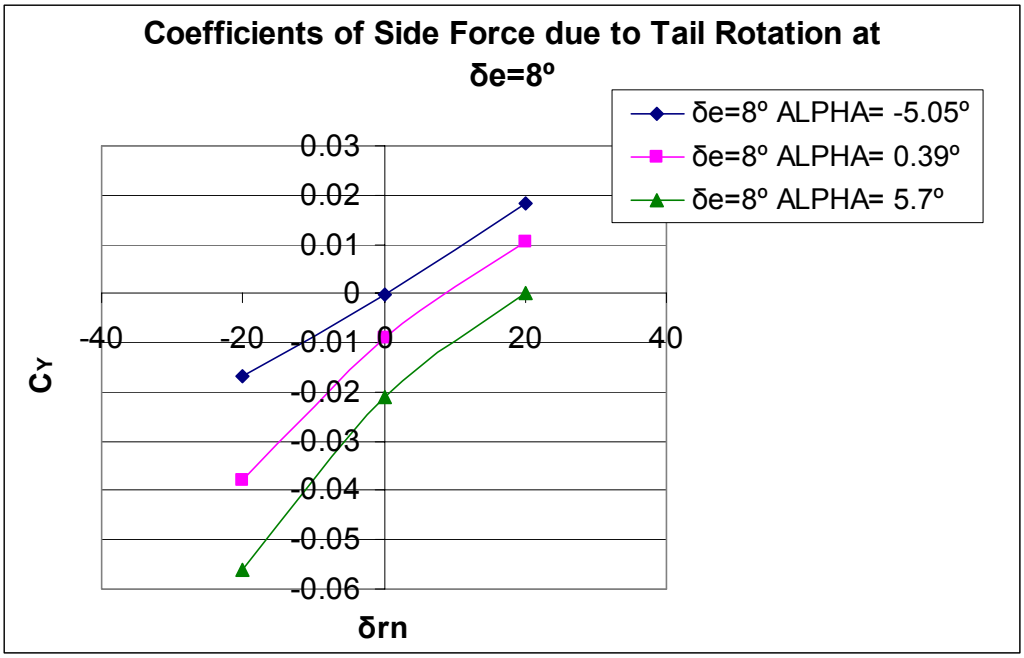

Figure 76. Coefficient of Side Force Production with Different Tail Rotations at δe=8º

c. Analysis of the Drag Produced at Different Tail Rotations.

Figure 77 gives a complete view of the relationship between drag, side force, tail rotation and angle of attack for δe=0º. It is important to consider that the drag shown is not only a function of tail rotation, but of angle of attack too. The following results were obtained:

1. Negative tail rotations produce bigger side force with the same amount of increment of drag if it they are compared with positive tail rotations.

2. As it was expected, the bigger angle of attack the bigger drag; however it is important to notice the curve of zero tail rotation: it has a negative side force for most of the angles of attack. The cause of this is maybe the irregularities in the fabrication of the UAV, as well as the tail (that is not exactly at the center line).

3. As was stated in a prior point, it can be seen in Figure 77 that there is a tendency of the UAV to have a negative side force under most of the tested conditions.

4. It is important to consider that this data presented for elevator deflection of the tail equals zero, therefore the values of the side force produced are small.

Figure 78, Figure 79 and Figure 80 show the C_D produced by the rotation of the tail at different δe and angles of attack. The results are the following:

1. The major contribution to the drag is the angle of attack instead of the elevator deflection of the tail, as was expected.

2. Positive angles of attack produce increase C_D and negative angles of attack decreased it. Since lift has the same behavior, it is deduced that this increase in the C_D is because of increasing the induced drag.

3. Figure 79 shows that the C_D produced by negative deflection of the tail is almost the same that the one produced by δe=0.

4. At zero elevator deflection as well at negative elevator deflections of the tail the curves have almost zero slope. This fact indicates that rotation almost does not increase the drag for these conditions. However, as can be seen in Figure 80, the drag produced by the rotation of the tail with positive elevator deflections, has a larger slope change at positive angles of attack. Notice, however, that increasing the drag using positive deflections is relatively low if we consider, for example that C_D at Alpha 0.3º with δe=0º and δrn=0º is 0.08 and for Alpha 0.39º with δe=8º and δrn=20º is 0.084 which represent only an increment of 4.7%.

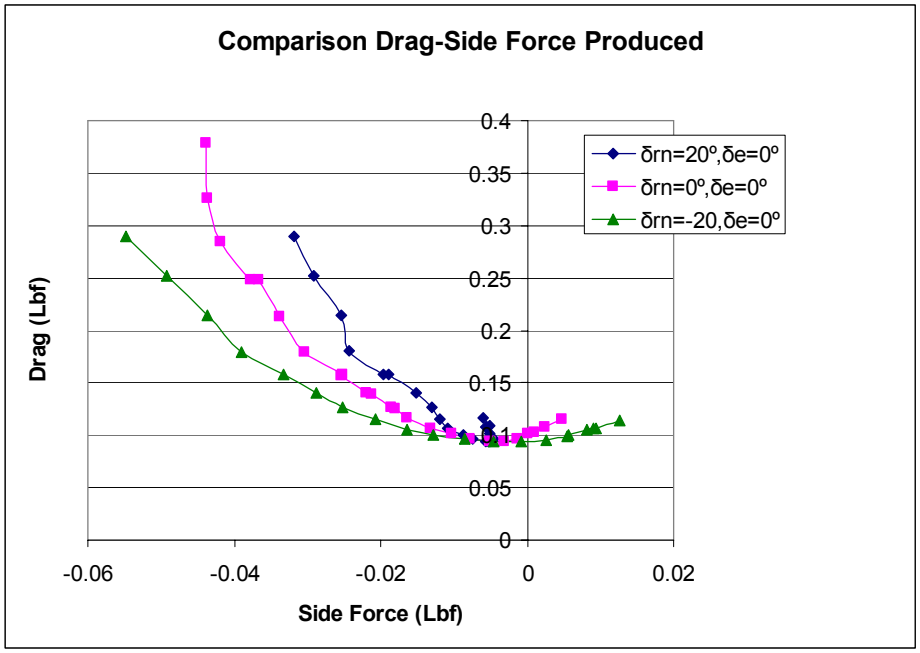

Figure 77. Comparison Drag-Side Force Produced at Different Tail Rotations

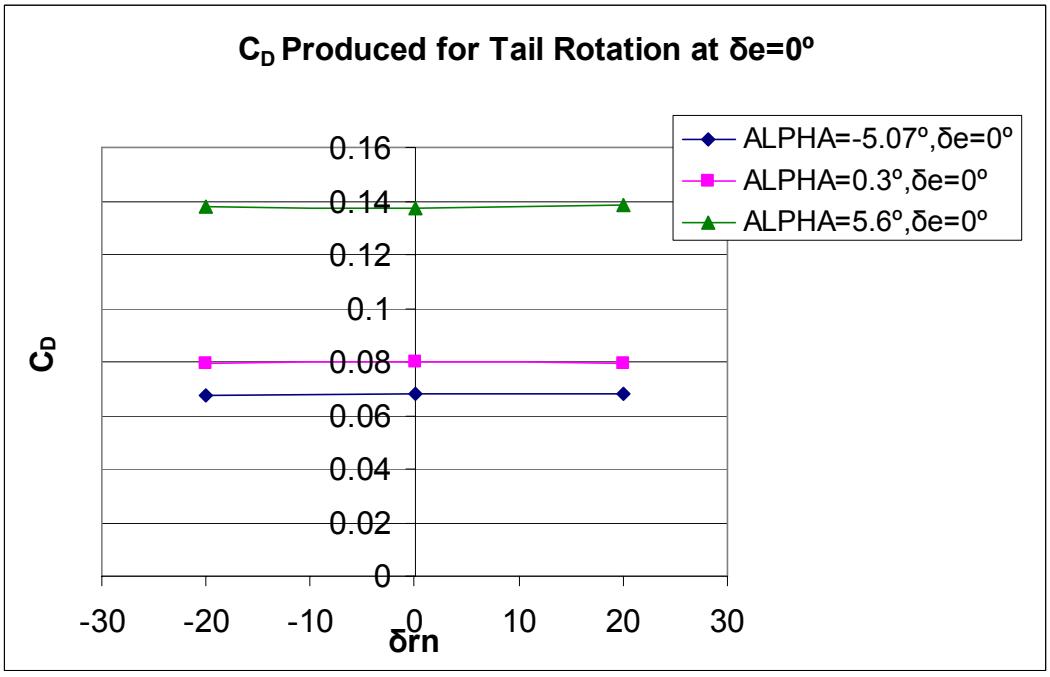

Figure 78. C_D Produced by the Rotation of the Tail at δe=0º

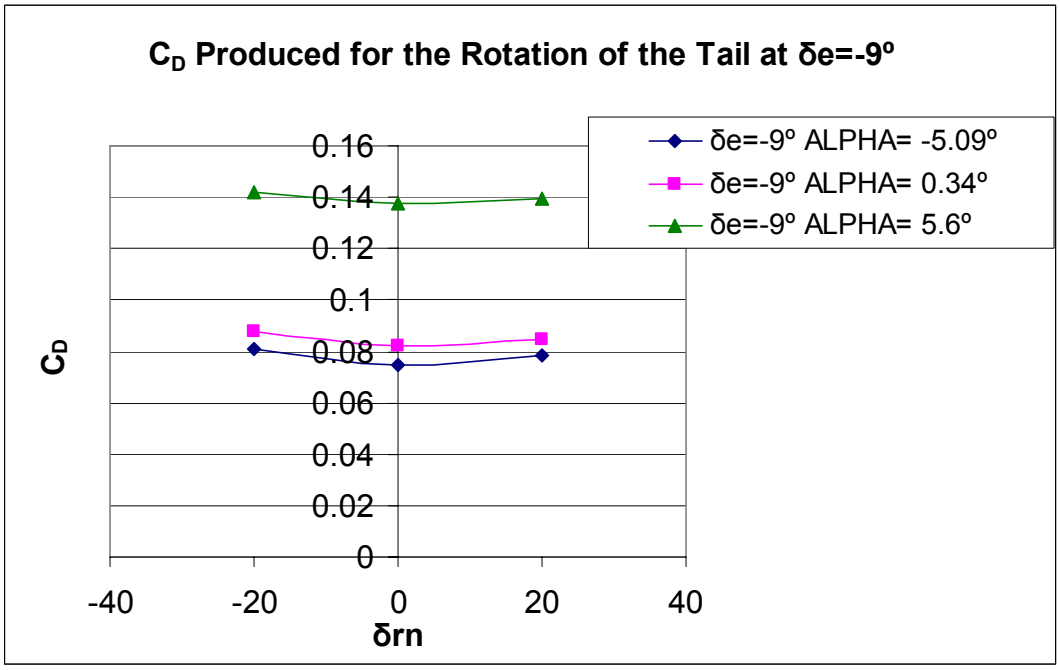

Figure 79. C_D Produced for the Rotation of the Tail at δe=-9º

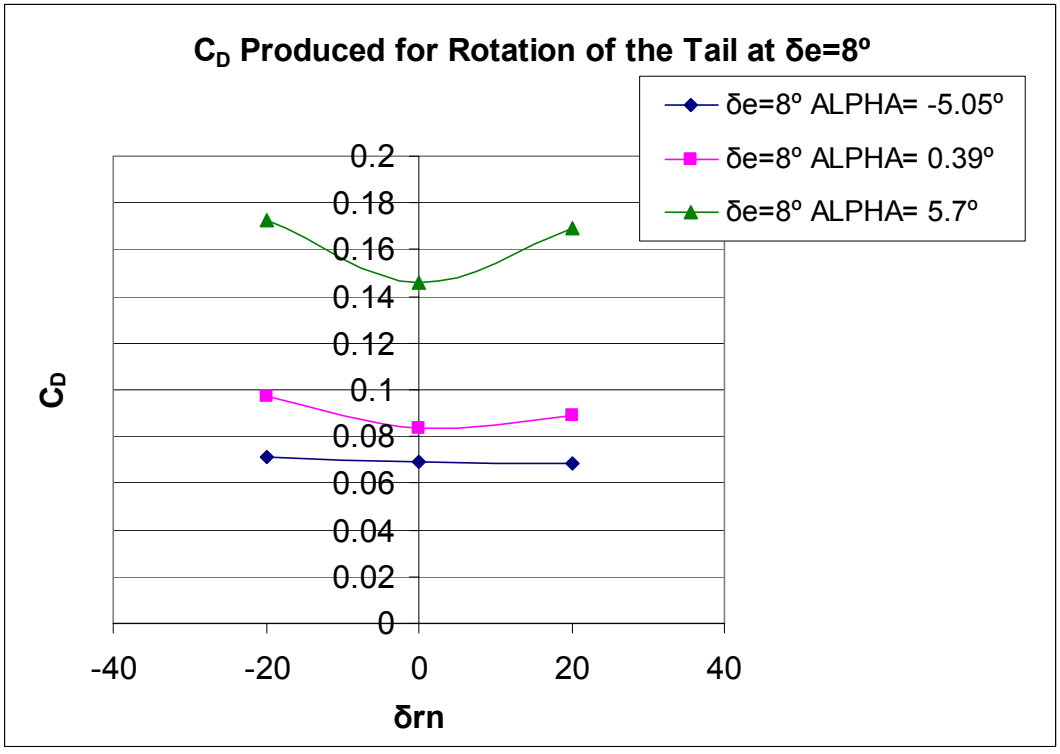

Figure 80. C_D Produced for the Rotation of the Tail at δe=8º

d. Analysis of the Effects on the Pitch Moment Coefficient Due to the Activation of Simultaneous Elevator Deflection and Rotation of the Tail.

In the previous analysis it was stated that the effectiveness of the tail in rotation is better when the elevator is applied. This brings the question: How does the elevator deflection affect Cm? In order to answer this question, Figure 81, Figure 82 and Figure 83 are presented. These compare Cm produced at different rotations as a function of δe and alpha. The results are the following:

1. The slope of the curves for δe=0º are almost flat that indicates that the value of Cm is more a function of alpha and δe rather than a function of δrn.

2. The slope of the curves for δe=8º and δe=-9º are somewhat larger indicating that indicates that rotation of the tail using deflections of it affects directly the Cm produced, though not to the level which the elevator effects it. This phenomenon is larger when alpha is positive.

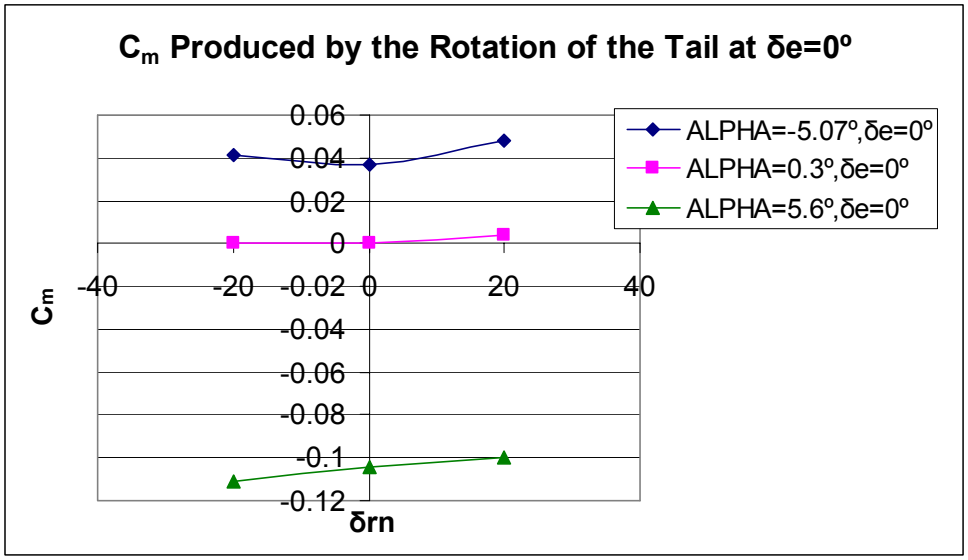

Figure 81. Cm Produced by the Rotation of the Tail at δe=0º

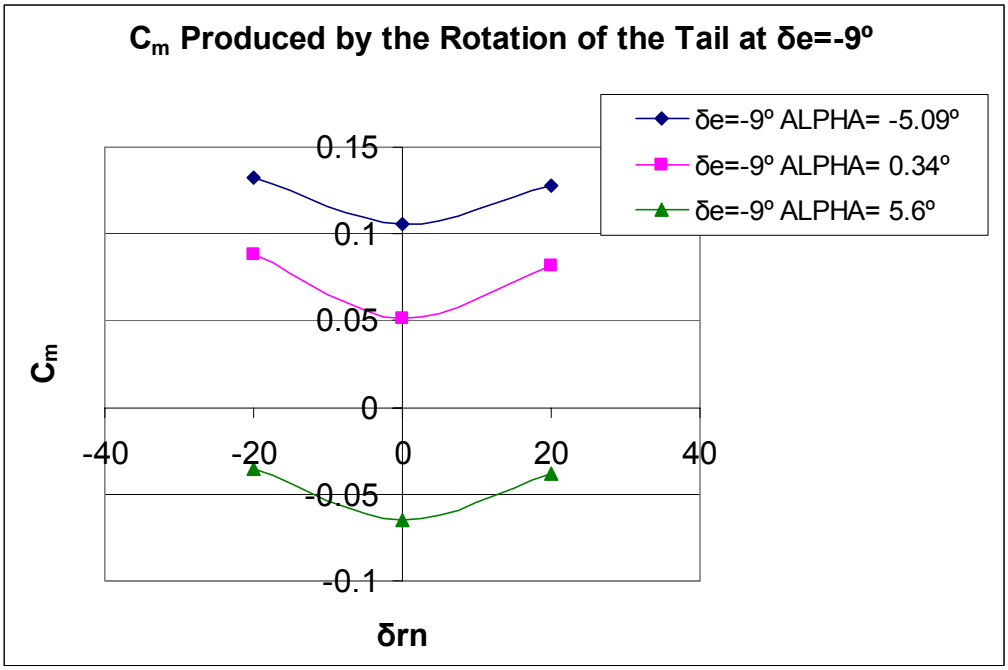

Figure 82. Cm Produced by the Rotation of the Tail at δe=-9º

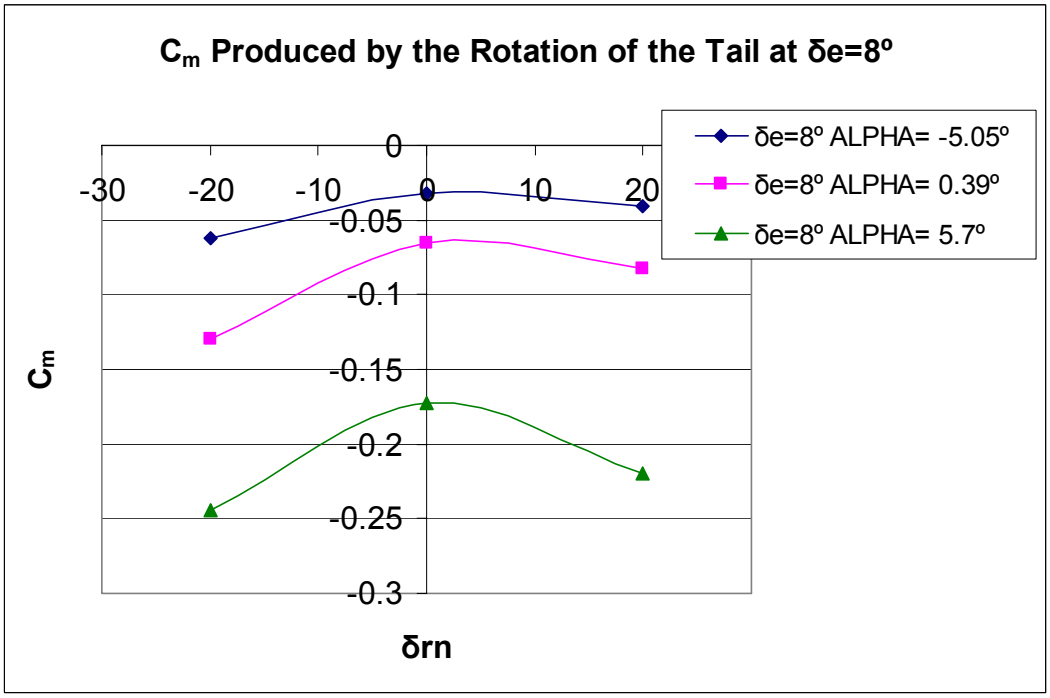

Figure 83. Cm Produced by the Rotation of the Tail at δe=8º

4.1.5. Roll Stability for Tail 1

As was stated in Chapter II, this type of stability will allow the UAV to return to its equilibrium condition when it is subjected to a wing level disturbance.

In order to check the directional stability of the UAV, Figure 84 was generated from the wind tunnel tests already mentioned in Table 11 by (alpha = 4°).

Since in order to have static roll stability it is necessary that the condition of $\frac{\partial C_l}{\partial \beta}$<0 is present, it can be seen in Figure 84 that the UAV with tail 1 does have roll stability for the conditions tested, because $\frac{\partial C_l}{\partial \beta}$=-0.0018.

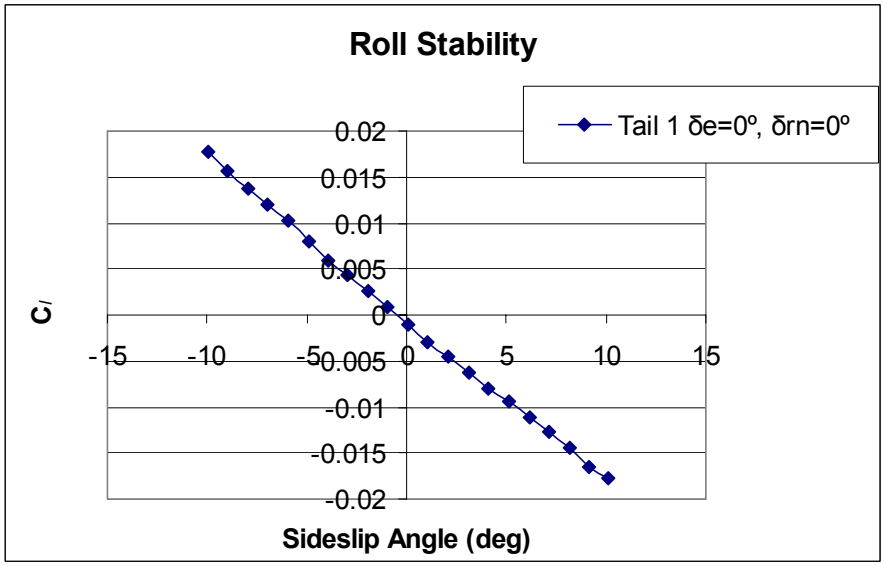

Figure 84. Roll Stability

4.1.6. Roll Control for Tail 1

In order to test the effectiveness of the different tails in the directional control, the first following analyses were made, by considering "pure roll control", in other words, using only rotation (δr) with zero elevator deflection tail (δe = 0º), after that, the second analysis was made using elevator deflection in the tail of 8º, 0º and -9º, in combination with δrn from -20º to 20º:

a. Production of the roll moment at different tail rotations

b. Analysis of the effects on the roll moment coefficient of the simultaneous elevator deflection and rotation of the tail.

c. Relationship between yaw moment and roll moment coefficients

a. Production of the Roll Moment at Different Tail Rotations

Figure 85 shows the effects in the change in C_l by using δe=0º and values of δrn =-30º and 32º. It can be seen that rotation of the tail with no elevator deflection produces almost no increase in the roll moment coefficient. Figure 87 shows the relationship between the roll moment coefficient and the tail rotation at different angle of attack values. The results are the following:

1. Once again, at δe=0º, the effects of tail rotation in the roll moment coefficients are small, its values are of order 10^{-3}.

2. At almost zero angle of attack (0.3º) the UAV has, with no deflection nor rotation of the tail a positive roll moment coefficient of 0.00025, moreover, if under these conditions the angle of attack is increased to 5.6 º the roll moment change to -0.000426 and if it is changed to -5.07º the roll moment change to 0.00168. On the other hand, under these conditions, the contribution to the roll moment coefficient by δrn when δe=0º is almost negligible and does not change the sign of the coefficient, in other words, to rotate in the positive direction of the tail or to do it in the negative direction does not produce roll moment of different sign. This means that

at zero elevator deflection of the tail the main contribution of the roll moment is the angle of attack, rather than the rotation of the tail, even if these values are so small.

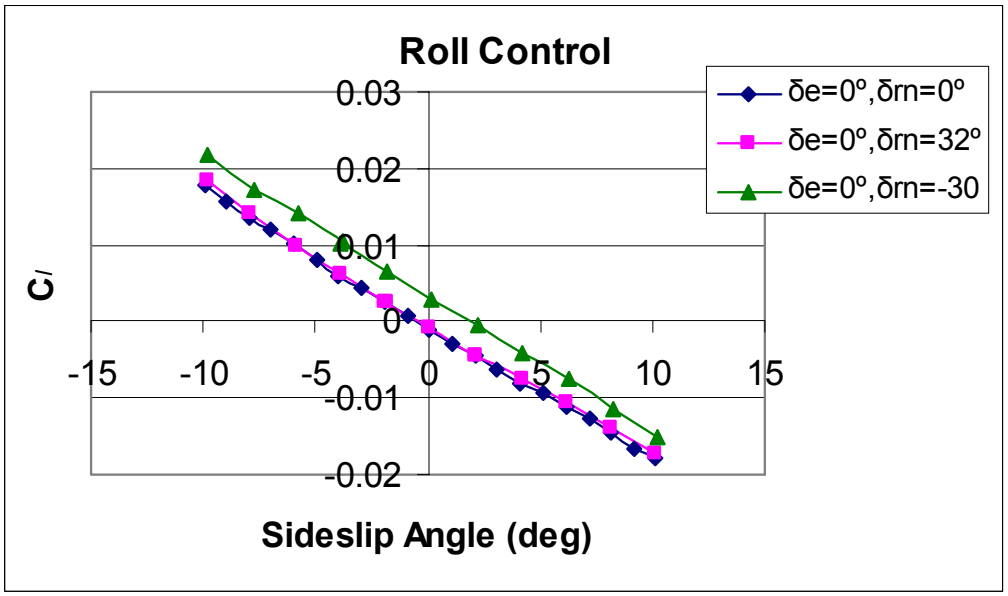

Figure 85. Roll control

b. Analysis of the Effects on the Roll Moment Coefficient of the Simultaneous Elevator Deflection and Rotation of the Tail.

Figure 86, Figure 88 and Figure 89 show the effects on the Roll moment coefficient for the combination of rotation and elevator deflection of the tail. The results are the following:

1. The tail has a very small effect on the roll moment coefficient compared to a traditional aileron system.

2. Figure 86 shows the same phenomena explain the prior point: that at zero elevator deflection of the tail increasing in the positive side the rotation of the tail decreases the value of C_l in the positive direction. On the other hand, by keeping this elevator deflection of the tail (zero) and changing the direction of rotation of the tail it should be expected to obtain negatives values of C_l, but instead of that it obtains, once again, an increase in the values of C_l, but with a larger value. In an ideal situation it

is expected to obtain a line with a constant slope in order that when the rotation of the tail is increased in one direction, values of C_l were obtained with the same sign and when the tail were increasing its rotation in the opposite direction, values of C_l were obtained with this new sign. This situation does not occur with tail 1 because independently of the direction of the rotation of the tail, with zero degrees of elevator deflection most of the values of C_l are negative.

3. It can be seen Figure 88 that with δrn=-9º the part of the curve that is in the negative side of the rotation became more horizontal when positive alphas are used and with alpha almost zero (0.34º) the curvature it is almost flat, consequently, it can be seen that the UAV with tail 1 still using negative elevator deflections has a poor roll effectiveness due to the phenomena mentioned in the prior point.

4. Figure 89 illustrates the effectiveness of the tail by using 8º of elevator deflection, it can be seen that as alpha increases the effectiveness increases, too. For instance, at angle of attack 5.7º and δe=8º the moment produced are as it was desired: with zero degrees of δrn the roll moment is close to zero: -0.0025116, using δrn=20º produces a roll moment of -0.0028853 and using δrn=-20º a roll moment of 0.00084745 is produced. In a few words, this is what it was expected: positive rotations of the tail produce negative roll and negative rotations of the tail produce positive roll moments.

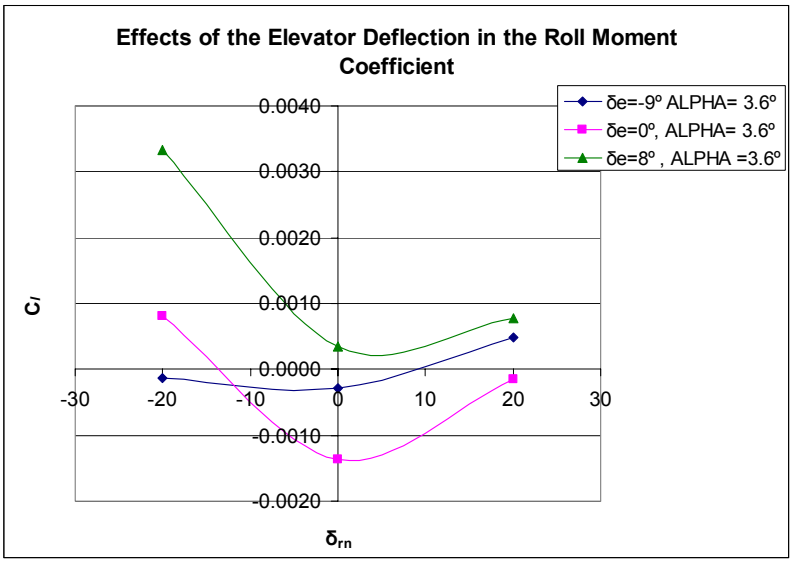

Figure 86. Effects on the Roll Moment Coefficient of the Simultaneous Elevator deflection and Rotation of the Tail.

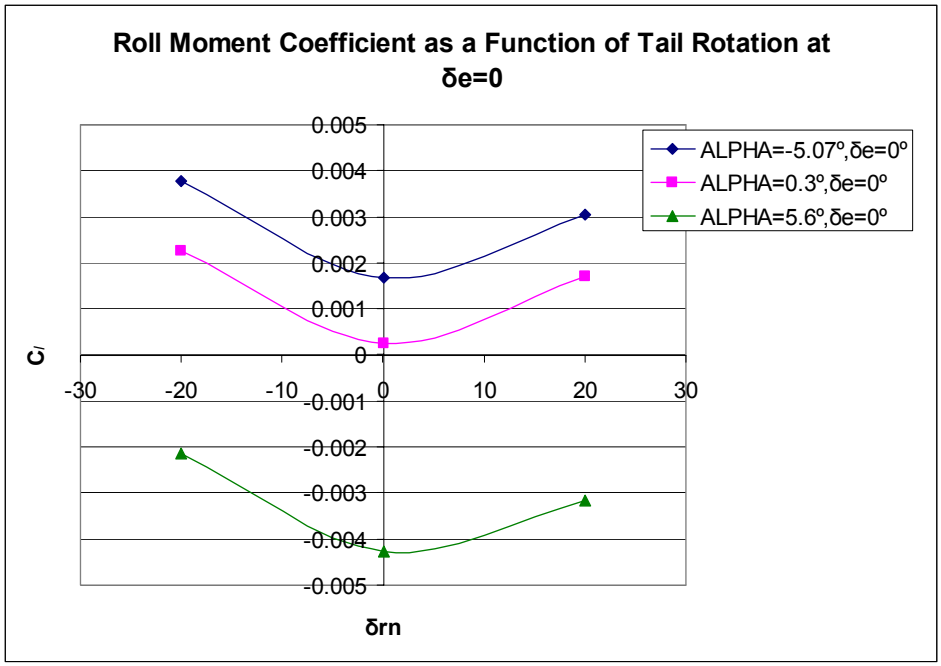

Figure 87. Roll moment Coefficient as a Function of Tail Rotation for δe=0°

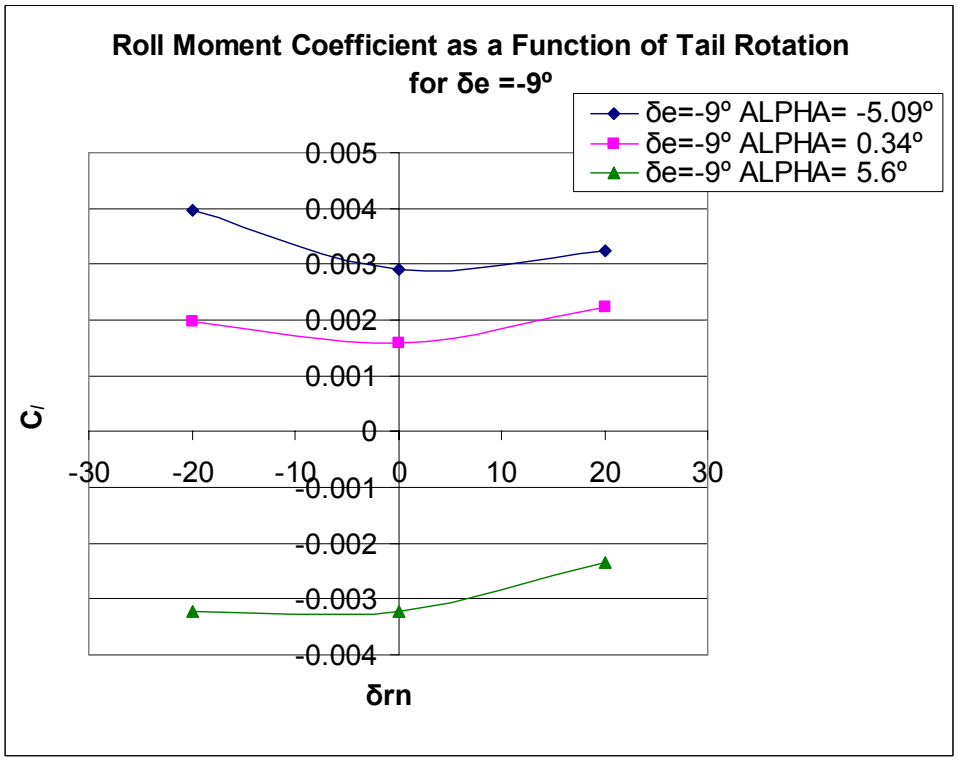

Figure 88. Roll Moment Coefficient as a Function of Tail Rotation for δe=-9°

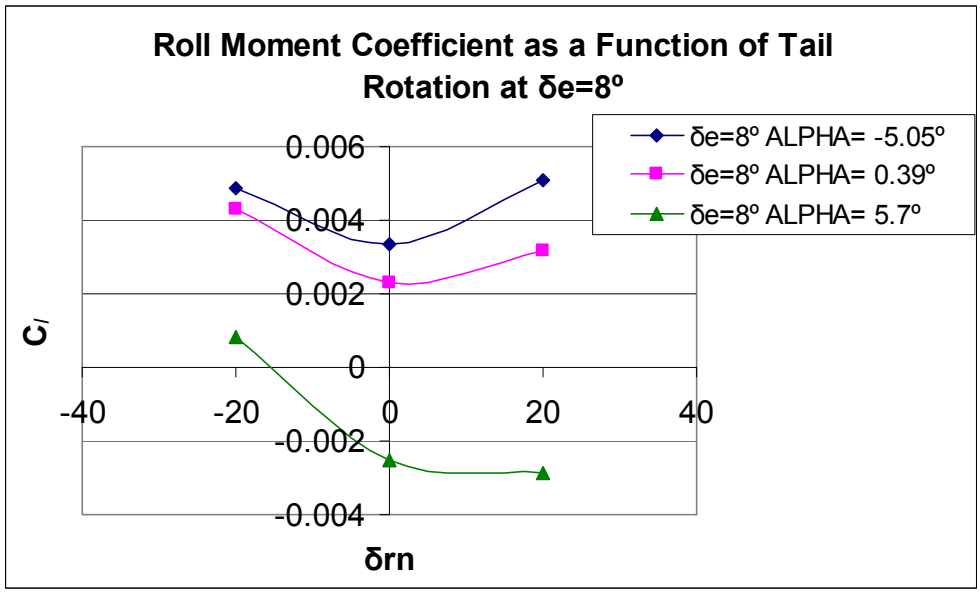

Figure 89. Roll Moment Coefficient as a Function of Tail Rotation for δe=8º

b. Relationship Between Yaw Moment and Roll Moment Coefficients

For tail1, it would be ideal that when the tail is rotated in a determined direction the roll and yaw moment produced were of the same sign. In this section analysis was made in order to determine the relationship between these two moment coefficients.

Figure 90, Figure 91 and Figure 92 set the relationship between C_l and Cn. Notice that these plots can be divided into four quadrants: the first quadrant (upper left) present the condition of positive values of C_l and negative values of Cn, the second quadrant (upper right) present the condition of positive values of C_l and positive values of Cn, the third quadrant (lower right) present the condition of negative values of C_l and positive values of Cn. The fourth quadrant (lower left) present the condition of negative values of C_l and negative values of Cn; therefore, the best results were obtained when data is present only in the second and fourth quadrant, since the yaw and the roll produced by

the tail is of the same sign. Under such a condition, the yaw is said to be favorable. In addition it would be ideal to find the point at zero rotation at the center of the axes were rotation and elevator deflection moments are zero; however, the results are different.

Figure 90 confirms the results already explained in prior sections. At zero elevator deflection, the tail rotation provides a very small increment in yaw and roll; besides that, roll and yaw moment with different sign are present with angles of attack -5.07º, 0.3º and 5.7º when rotation of the tail is positive, in the first two cases and when rotation is negative as in the third case. Once again, notice that angle of attack plays an important role in the determination of the sign of the roll and moment coefficients.

Figure 91 shows the results obtained using δe=-9º. It can be seen that the three curves presented in the plot have opposite sign combinations of yaw and roll coefficients, moreover, notice that for alpha 0.34º and -5.09º it is possible to obtain positive and negative values of Cn but only positive values of C_l. On the other hand, with alpha at 5.6º it is possible to obtain positive and negative values of Cn but only negative values of C_l.

Figure 92 illustrates the cases for δe=8º. It can be seen that once again at alpha 0.39º and -5.05º, due to the inherent positive roll moment in the UAV, it is not possible to obtain negative roll moment under these conditions, then in case of the positive rotation of the tail opposite roll moment is present. The only case that is closer to what is desired is the condition of alpha 5.7º because: first, the point of zero rotation of the tail is close to the zero value of roll and pitch moments, second, there is no opposite sign of yaw-roll combination, third, under these conditions the increment in both coefficients are bigger than the ones obtained for under the conditions; and fourth the effect of the moment

produced are what are expected. Positive rotation of the tail produce negative values of C_l and Cn and negative rotations produce positive values of these coefficients.

To summarize this section, the combination of roll and yaw of tail 1 is more desirable when this vehicle has a positive alpha and positive elevator deflection of the tail. The data indicates that this effectiveness is directly proportional to δe. It is expected, however that the maximum limit for the elevator deflection of the tail is 90º and the angle of attack is limited by the stall. Furthermore, it is important to remember that these are not the only factors that it is necessary to consider for improving the characteristics of the tail because size of the flap and tail volume ratio play an indispensable roll in the design of any flight control (Nelson, 1998:63).

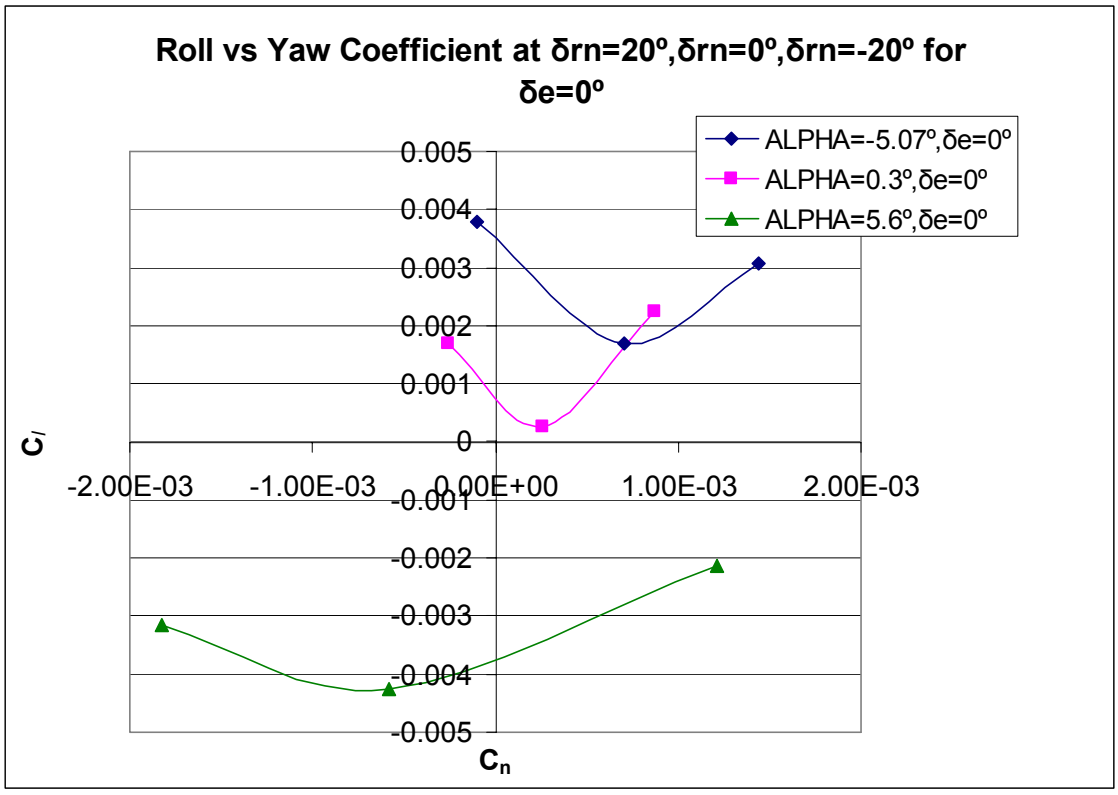

Figure 90. Roll Versus Yaw for δe=0º

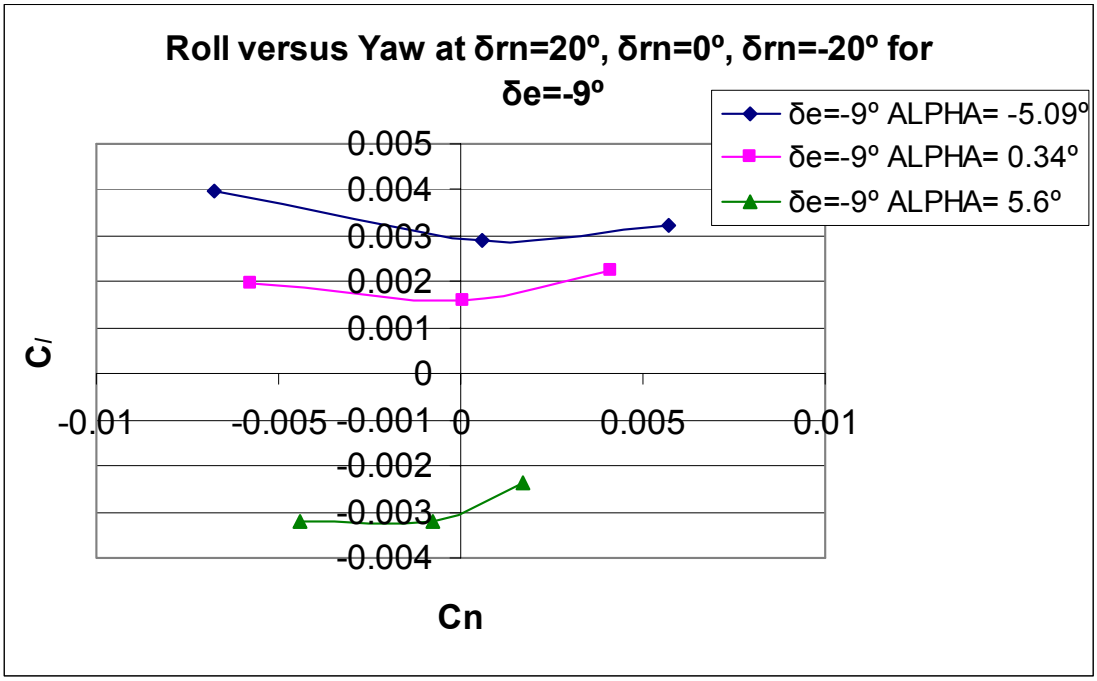

Figure 91. Roll Versus Yaw for δe=-9º

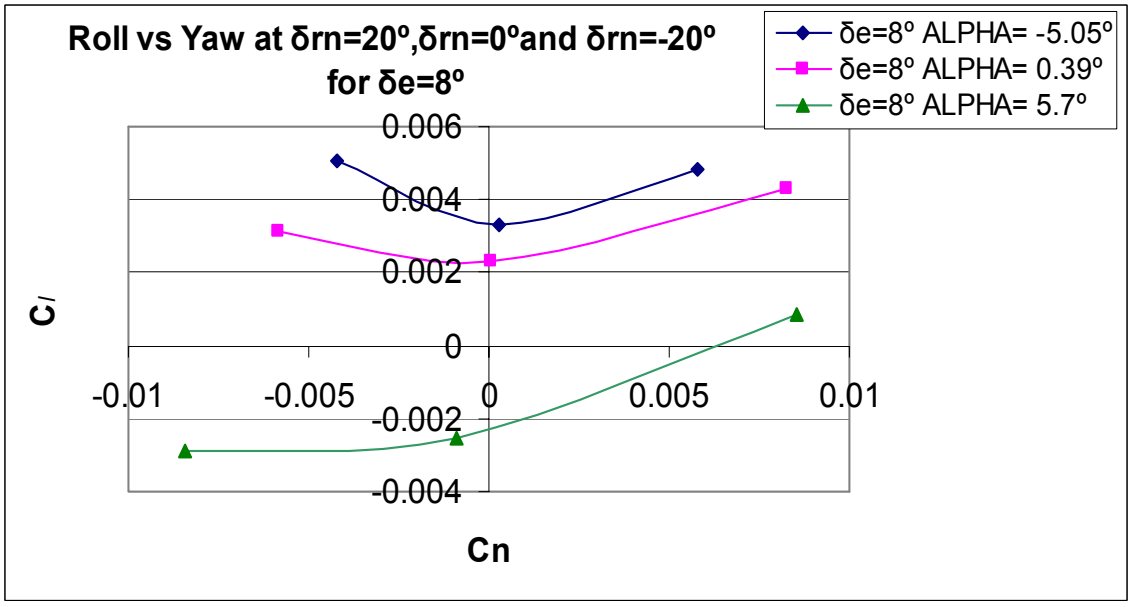

Figure 92. Roll Versus Yaw for δe=8º

4.2. Parametric Analysis of the Tail 1 Control Using Two Degrees of Freedom

In order to improve understanding the general behavior of the UAV using tail 1 under different combinations of rotation and elevator deflection, a wind tunnel tests was done by using the conditions mentioned in Table 10. These results and analysis are presented in contour and surface plots for C_L, C_S, $C_{D,}$ C_m, C_n and $C_{l..}$ Notably, the aircraft angle of attack was held constant at 4º, furthermore, β=0º for all the cases presented here. As in the results given in previous sections the moment coefficients were determined about the C.G. of the aircraft as tested. Note that this location may be altered through battery placement, and this issue is discussed in Section 4.4.

4.2.1. Coefficient of Lift (C_L)

In accordance with the data presented in Figure 93 and Figure 94 the coefficient of lift (C_L) has the following behavior:

1. The lift produced is a function of the elevator deflection of the tail.
2. As was expected, by using positive elevator deflection of the tail the coefficient of lift increases, due to the increment in the curvature of the entire UAV and due to the increase of lift in the tail.
3. As was expected, by using negative elevator deflection of the tail the coefficient of lift decreases, due to the effect of a spoiler action that the tail does when it is deflected upwards and due to the decrease of lift in the tail.
4. The rotation of the tail effects the lift production very little, especially between rotations less than +/-20º.

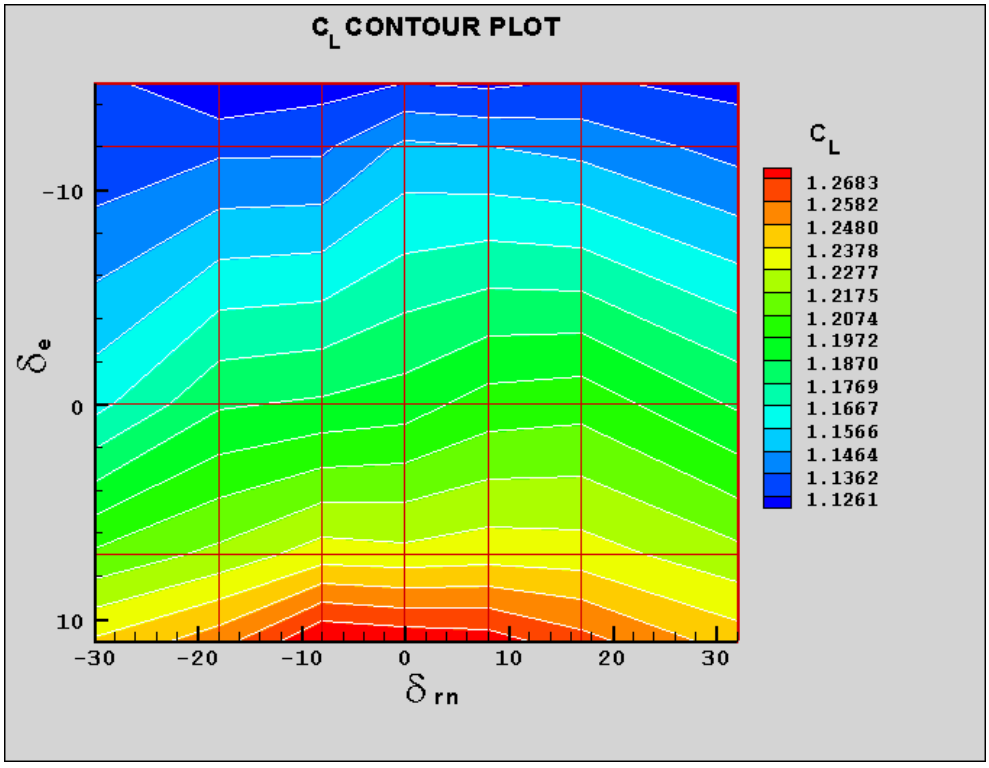

Figure 93. C_L Contour Plot

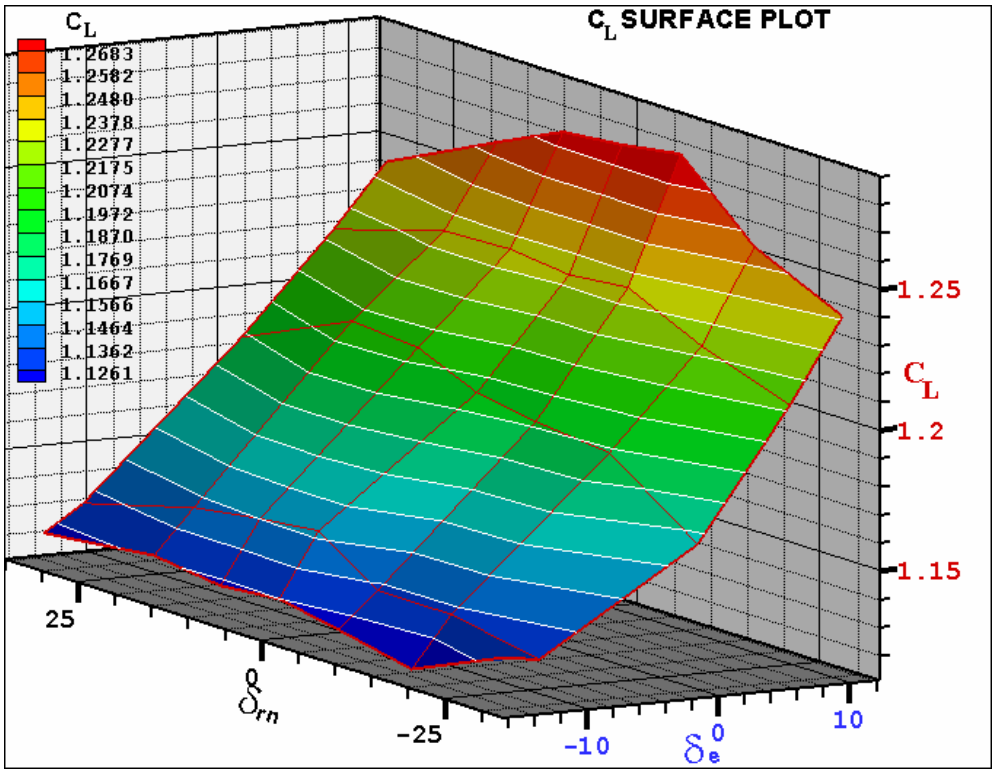

Figure 94. C_L Surface Plot

4.2.2. Coefficient of Drag (C_D)

In accordance with the data presented in and Figure 95 and Figure 96, the coefficient of drag (C_D) has the following behavior:

1. The drag produced is a function of the elevator deflection of the tail.

2. As was expected, by using positive elevator deflection of the tail the coefficient of drag increases, due to the increment in the area that is presented by the tail to the wind stream conditions and due to the increasing of the lift and a consequence the increasing of the induced drag.

3. As was expected, by using negative elevator deflection of the tail the coefficient of drag increases, too, but different from the case of the positive elevator deflections, the increment of drag is smaller due to an apparent parasitic drag. In other words, because the lift is decreasing then, the total increase in drag must be due to parasite drag.

4. The rotation of the tail affects the drag production very little, with the effect increasing as the rotation exceeds +/- 20º.

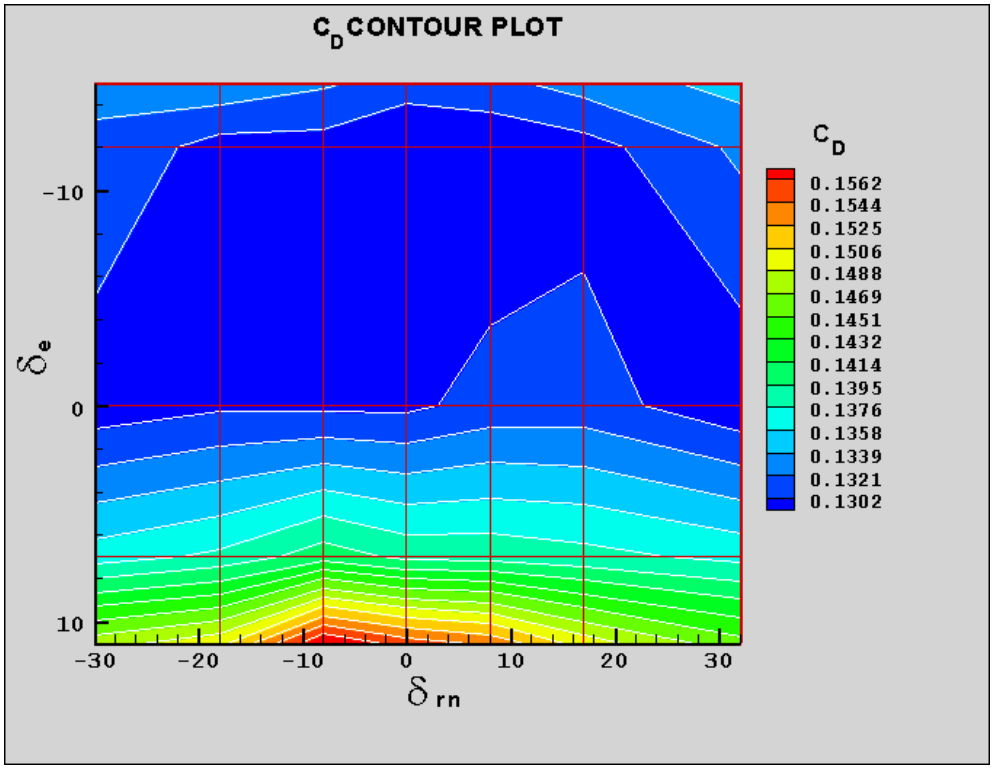

Figure 95. C_D Contour Plot

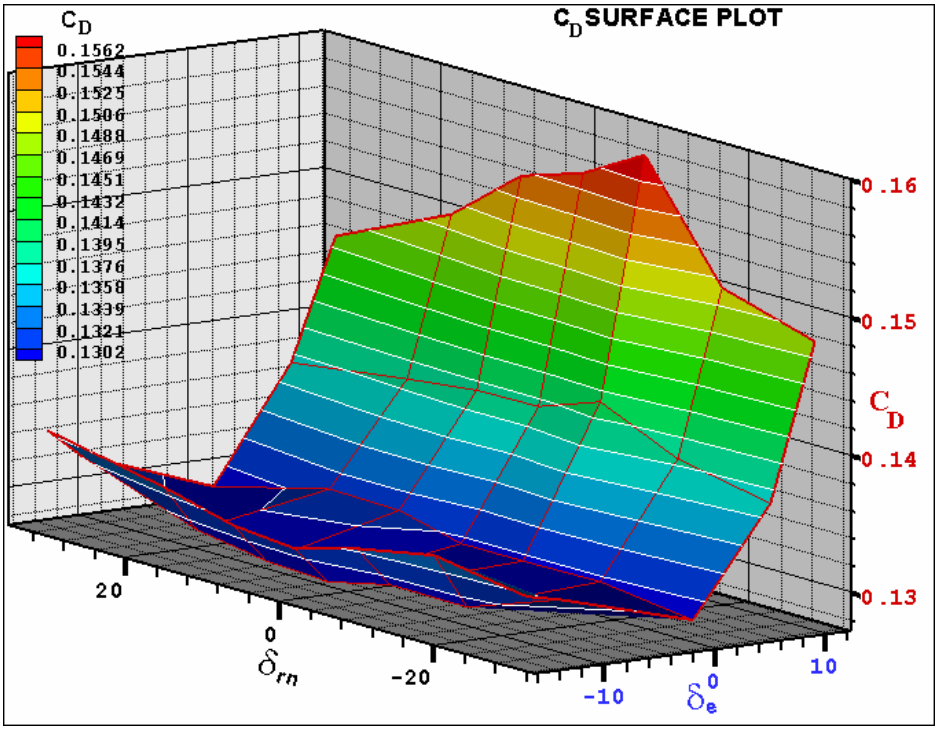

Figure 96. C_D Surface Plot

4.2.3. Coefficient of Side Force (C_S)

In accordance with the data presented in Figure 97 and Figure 98, the coefficient of side force (C_S) has the following behavior:

1. The side force produced is a function of the combinations of elevator deflection and rotation of the tail. It can be seen in the figures that in the areas where only rotation or elevator deflection alone is used, the increment in side force is not considerable; rather, the highest absolute values are located in the corners of the plots where the combination of δe and δrn are applied simultaneously.

2. It can be seen that the figures illustrate the phenomena already discuss in prior sections: the sign of the side force coefficient produced when the tail is rotated, changes as function of the elevator deflection; moreover, at zero elevator deflection and rotation the value of this side force is not zero, instead of that, there exists a constant negative side force that tends to zero when at zero elevator deflection, positive rotation of the tail is applied.

3. Larger absolute values of coefficient of side force are obtained for positive elevator deflection than for negative ones.

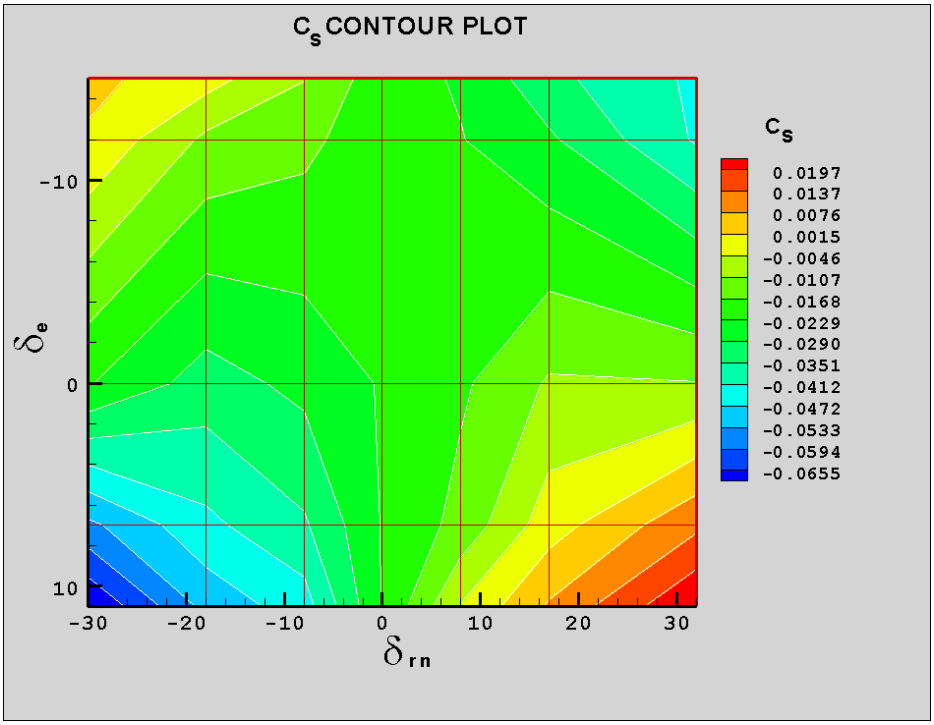

Figure 97. C_S Contour Plot

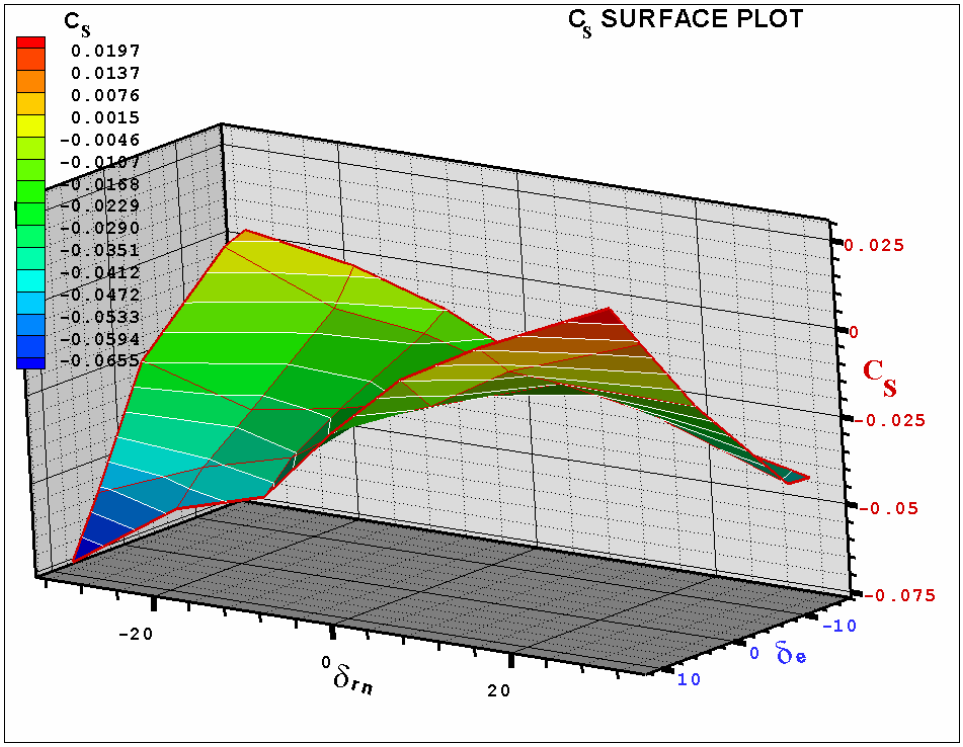

Figure 98. Cs Surface Plot

4.2.4. Pitch Moment Coefficient (C_m)

In accordance with the data presented in Figure 99 and Figure 100 the pitch moment coefficient (Cm) has the following behavior:

1. The pitch moment produced is primarily a function of the elevator deflection rather than rotation of the tail.

2. As was expected, by using positive elevator deflection of the tail the pitch moment coefficient increases in the negative direction, due to the increment in the lift in the tail.

3. As was expected, by using negative elevator deflection of the tail the pitch moment coefficient increases in the positive direction, due to the decreasing of lift in the tail when it is deflected upwards.

4. The rotation of the tail affects the pitch moment coefficient production by a relatively small amount compared to the elevator change between $-20^{o} \leq \delta rn \leq +20^{o}$.

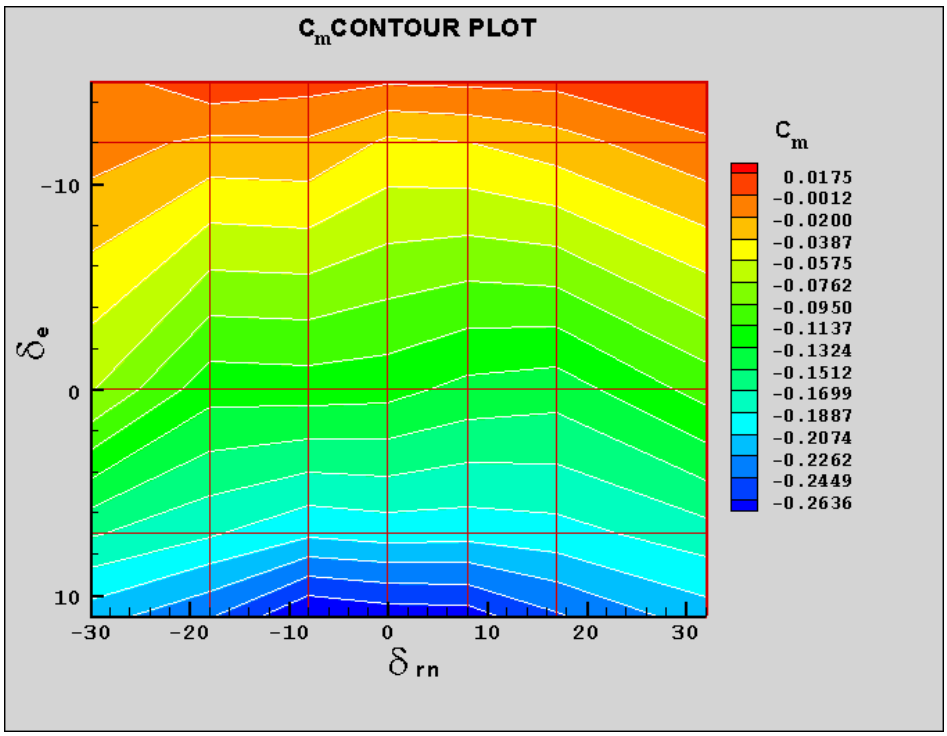

Figure 99. C_m Contour Plot

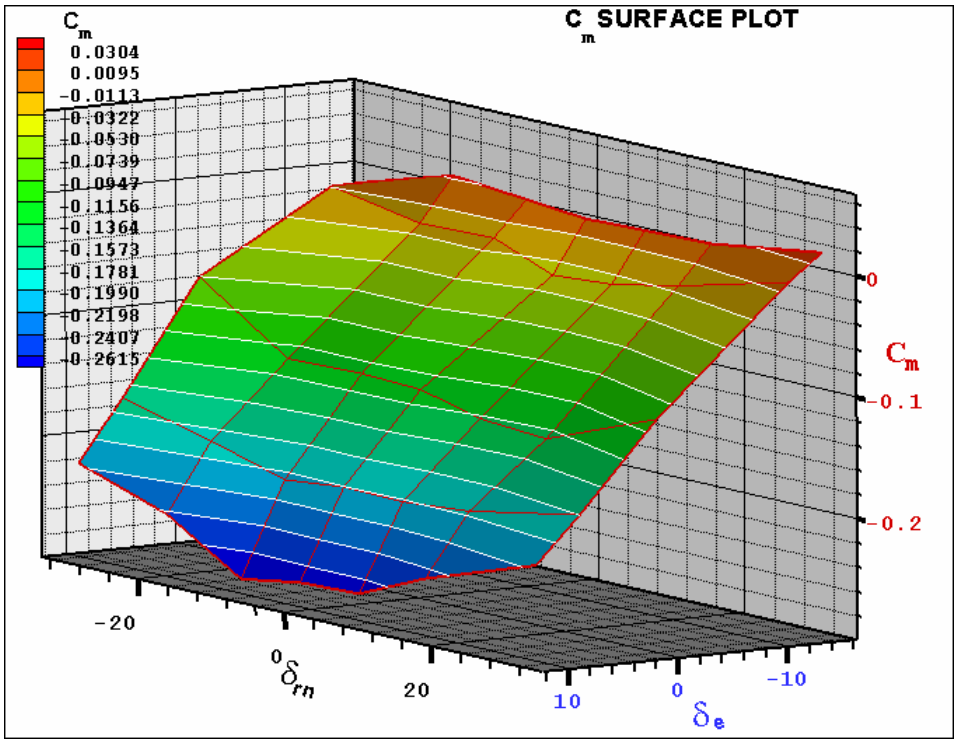

Figure 100. Cm Surface Plot

4.2.5. Yaw Moment Coefficient (C_n)

In accordance with the data presented in Figure 101 and Figure 102, the coefficient of yaw moment coefficient (C_n) has the following behavior:

1. The yaw moment coefficient produced is a function of the combinations of elevator deflection and rotation of the tail. It can be seen in the figures that in the areas where only rotation or elevator deflection alone is used the increment in yaw moment coefficient is not considerable; rather, the highest values are presented at the corners of the plots where the combination of δe and δrn are used simultaneously. The largest range of values obtained in these tests (-0.013 to +0.013) compares to the values of $\pm$ 0.02 for a typical rudder (Barlow, Rae and Pope; 1999:527), indicate that the rudder control could be poor, though these are not quite as large, the values obtained are of the same order of magnitude, suggesting that for δe=9º, yaw control could be executed by rotating the tail.

2. Using positive elevator deflection of the tail in combination with rotation, produces larger absolute values of yaw moment coefficient in comparison with the ones obtained using negative elevator deflections of the tail, this indicated that in order to execute a turn, a positive elevator deflection is preferable.

3. For a given rotation, the sign of the yaw moment coefficient and therefore the turning direction, can change with elevator deflection, δe. This result is consistent with higher pressures acting on the windward side of the tail. Note that at zero elevator deflection and rotation the value of this yaw moment is not zero, instead of that, there exists a constant yaw moment of -0.00028 that tends to zero when at zero elevator deflection, negative rotation of the tail is applied.

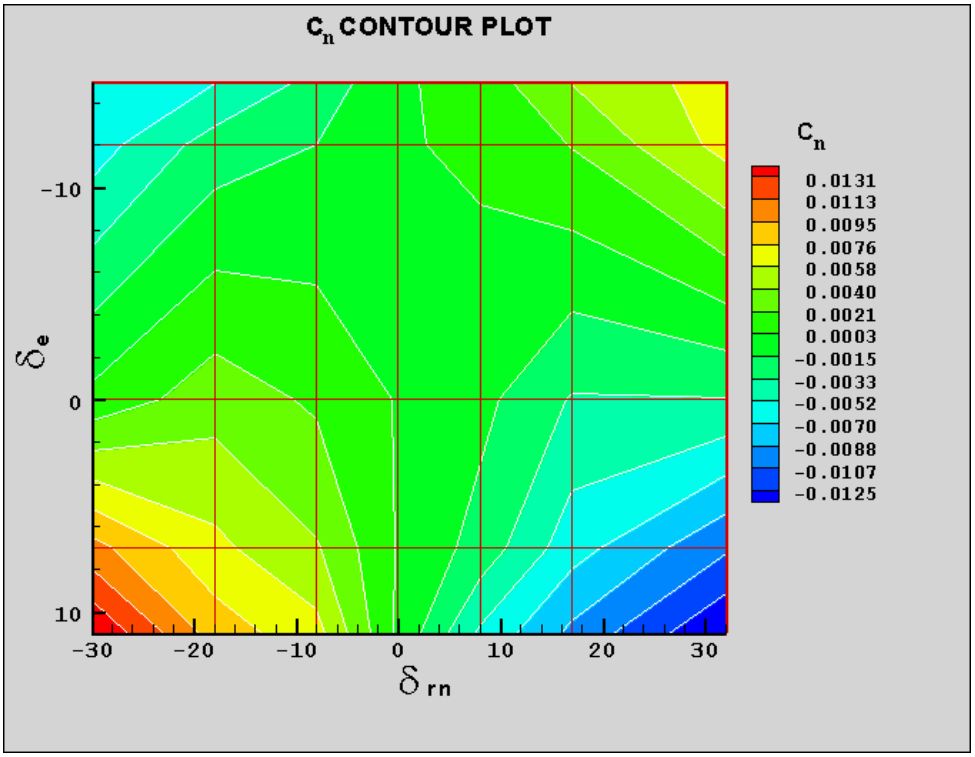

Figure 101. Cn Contour Plot

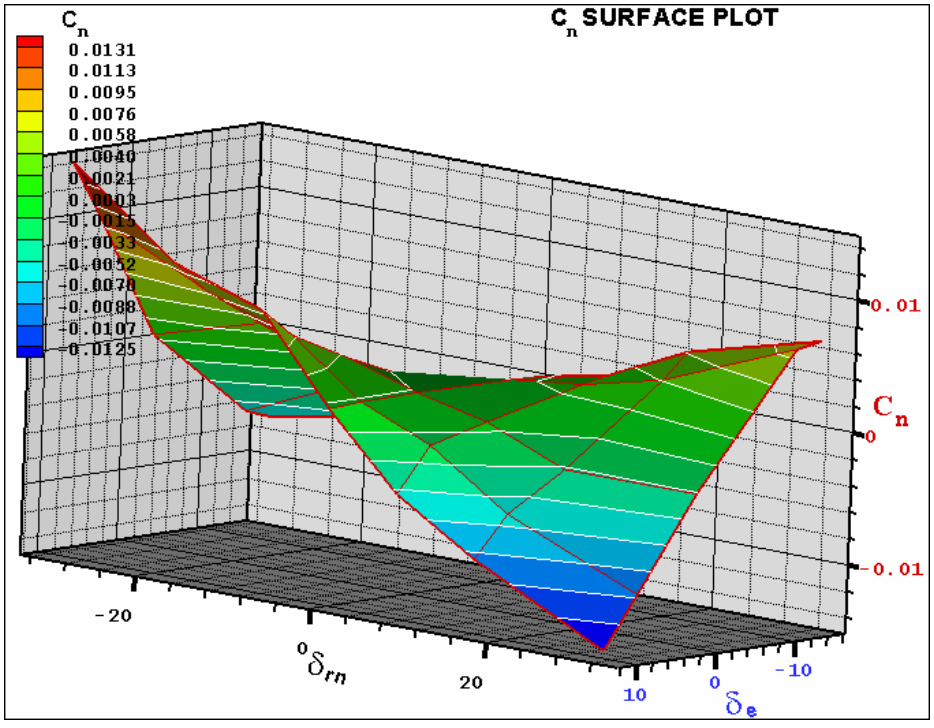

Figure 102. Cn Surface Plot

4.2.6. Roll Moment Coefficient (C_l)

In accordance with the data presented in Figure 103 and Figure 104, the roll moment coefficient (C_l) has the following behavior:

1. The roll moment coefficient produced is a function of the combinations of elevator deflection and rotation of the tail. It can be seen in the figures that in the areas where only rotation or elevator deflection alone is used the increment in yaw moment coefficient is not considerable; rather, the highest values are presented at the corners of the plots where the combination of δe and δrn are used simultaneously. By comparison, typical roll moment coefficients produced by ailerons are in the range of $\pm$ 0.02 (Barlow, Rae and Pope; 1999:500) which are approximately 5 times the largest value measured for this rotary tail. Thus the tail would appear to produce poor roll control.

2. As was expected, due to the increment in the area that is presented by the tail to the wind stream conditions by using positive elevator deflection of the tail in combination with rotation, larger values of roll moment coefficient are obtained in comparison with the ones obtained using negative elevator deflections of the tail.

3. As in the yaw moment, for a given rotation the sign of the roll moment coefficient, and therefore the turning direction can change with elevator deflection, δe. At zero elevator deflection and rotation the value of this roll moment is not zero, for the conditions tested. Instead, there exists a roll moment coefficient of 0.001363 that tends to zero when at zero elevator deflection, positive rotation of the tail is applied.

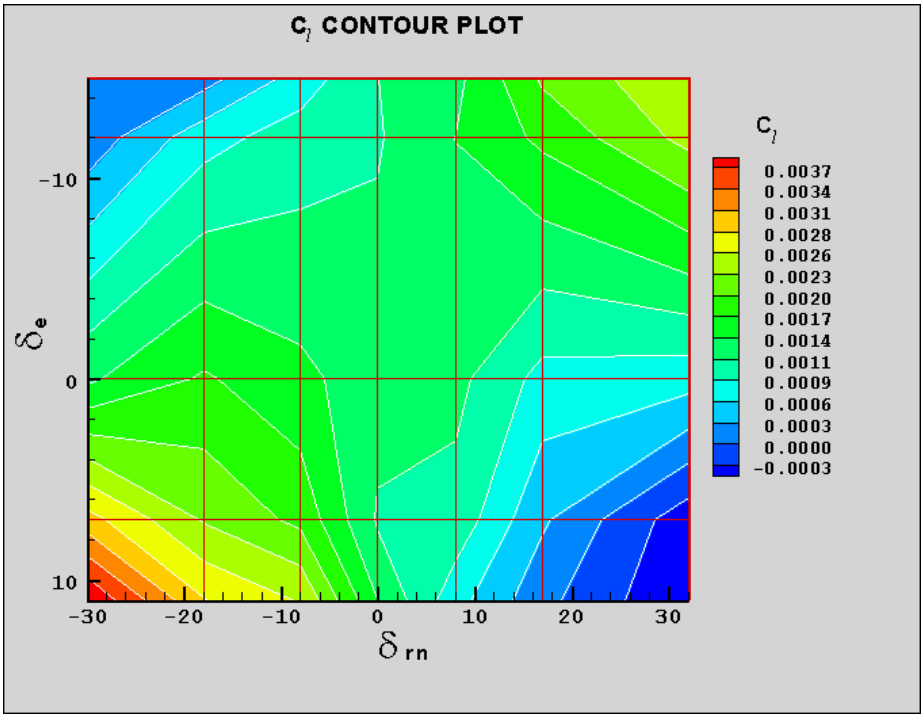

Figure 103. C_l Contour Plot

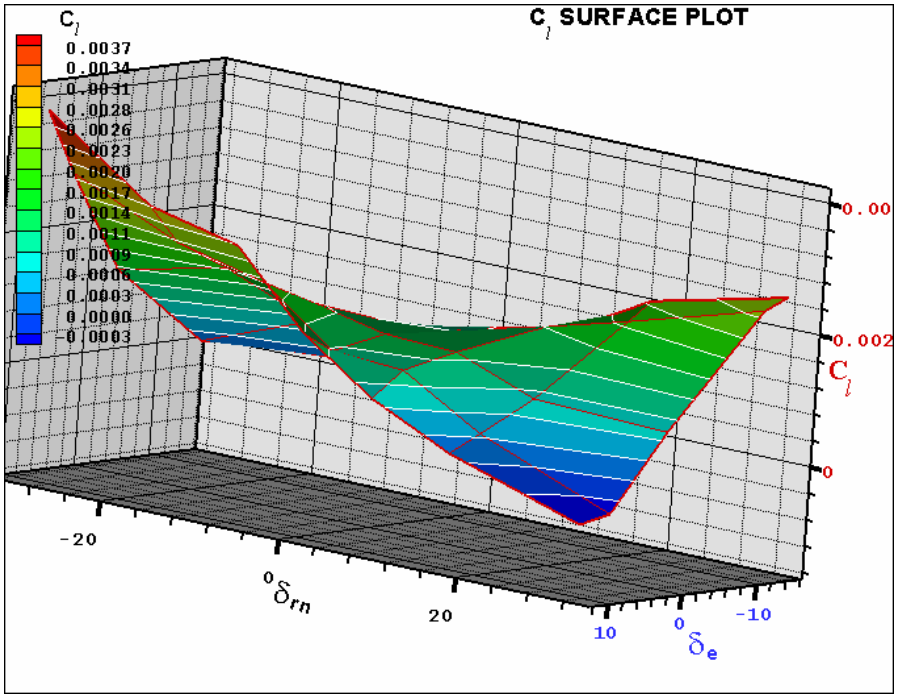

Figure 104. C_l Surface Plot

4.3. Results for Tail 2.

Since by using tail 1 a better understanding of the function of a rotary tail was obtained, and because it was shown that under the correct combination of rotation and elevator deflection of the tail as well angle of attack, and a control about the three axes can be done, tail 2 was built in order to provide yaw stability to the UAV. Recall from the static stability point of view tail 1 provided only longitudinal and roll stability. Tail 2 represents a departure from the bird tail geometry in that two vertical fins were added to the outer portions of the tail. Note that with an additional modification, one would still be able to fold this tail over the fuselage.

The results on this section are presented in the following form; in addition, the test made using tail 2 and their conditions are presented in Table 13 and Table 14:

a. Longitudinal static stability for tail 2

b. Longitudinal control for tail 2

c. Directional stability for tail 2

d. Directional control for tail 2

e. Roll stability for tail 2

f. Roll control for tail 2

Table 13. Alpha Runs for Tail 2

ALPHA RUNS FOR TAIL 2 CONDITIONS: α= -8º to 10º β=0º SPEED= 30 MPH							
DATE	***DESCRIPTION***	***WEIGHT (Grams)***	***TEMP. (ºF)***	***PRES. (mm Hg)***	X_{CM}	Y_{CM}	Z_{CM}
10/26/2004	δe=0º, δrn=0º	415	71.75	29.24	0.71"	0	-1.31
10/26/2004	δe=-9º, δrn=0º	415	72.5	29.11	0.71"	0	-1.31
10/27/2004	δe=8º, δrn=0º	415	71.9	29.05	0.71"	0	-1.31
10/27/2004	δe=0º, δrn=20º	415	72.4	29.06	0.71"	0	-1.31
10/27/2004	δe=-9º, δrn=20º	415	72.4	29.06	0.71"	0.05	-1.31
10/27/2004	δe=-9º, δrn=-20º	415	72.3	29.06	0.71"	-0.05	-1.31
10/27/2004	δe=0º, δrn=-20º	415	72.6	29.07	0.71"	0	-1.31
10/27/2004	δe=8º, δrn=-20º	415	72.7	29.07	0.71"	0	-1.31
10/27/2004	δe=8º, δrn=20º	415	72.7	29.07	0.71"	0	-1.31

Table 14. Beta Runs for Tail 2

BETA RUNS FOR TAIL 2 CONDITIONS: β=-10º to 10º SPEED= 30 MPH							
DATE	***DESCRIPTION***	***WEIGHT (Grams)***	***TEMP. (ºF)***	***PRES. (mm Hg)***	X_{CM}	Y_{CM}	Z_{CM}
10/26/2004	α=4º,δe=0º, δrn=0º	415	73	29.14	0.71"	0	-1.31
10/26/2004	α=0º,δe=0º, δrn=0º	415	72.8	29.14	0.71"	0	-1.31

4.3.1. Longitudinal Static Stability for Tail 2

Figure 105 shows the comparison of the static stability of the UAV under the three conditions: No tail, tail 1 and tail 2. It can be seen that even if tail 2 still has a negative slope on the curve : the average $\frac{\partial Cm}{\partial \alpha}$ = -0.01, the main contribution to the longitudinal stability is because of the change in the center of gravity of the MAV, since tail 2 has a weight of 20 grams and the weight of tail 1 is 10 grams. Note that the battery placement could be used to alter the slope of Cm versus α. This phenomenon can be reconfirmed by the data presented in Figure 106, Figure 107 and Figure 108.In these last two figures it can be seen that the contribution to the total lift of the UAV from tail 2 is bigger than from tail 1. However this contribution is still small, for example for 4.6º of angle of attack the lift coefficient for no tail was 1.15, with tail 1 was 1.17 and for tail 2 was 1.24 that represent an increment only of 1.73 % 7.82 %, respectively.

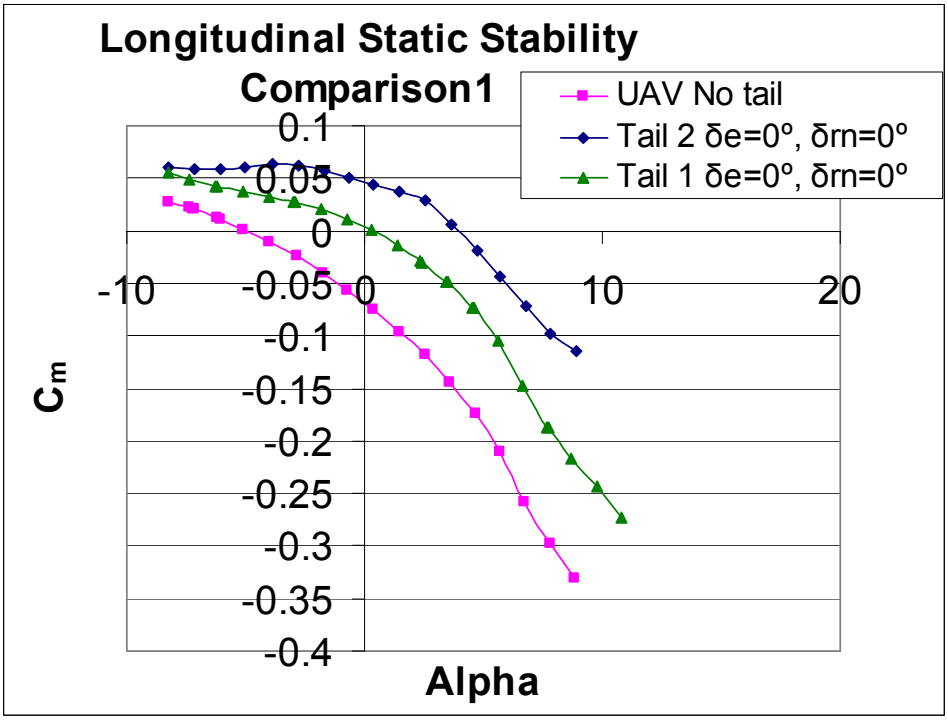

Figure 105. Longitudinal Static Stability Comparison 1 for Tail 2

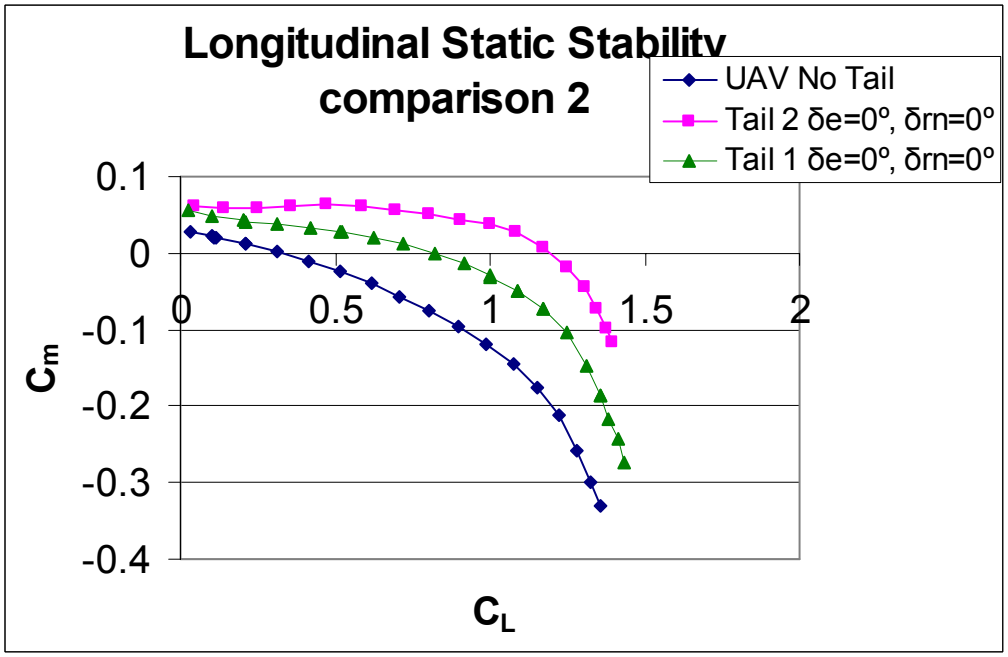

Figure 106. Longitudinal Static Stability Comparison 2 for Tail 2

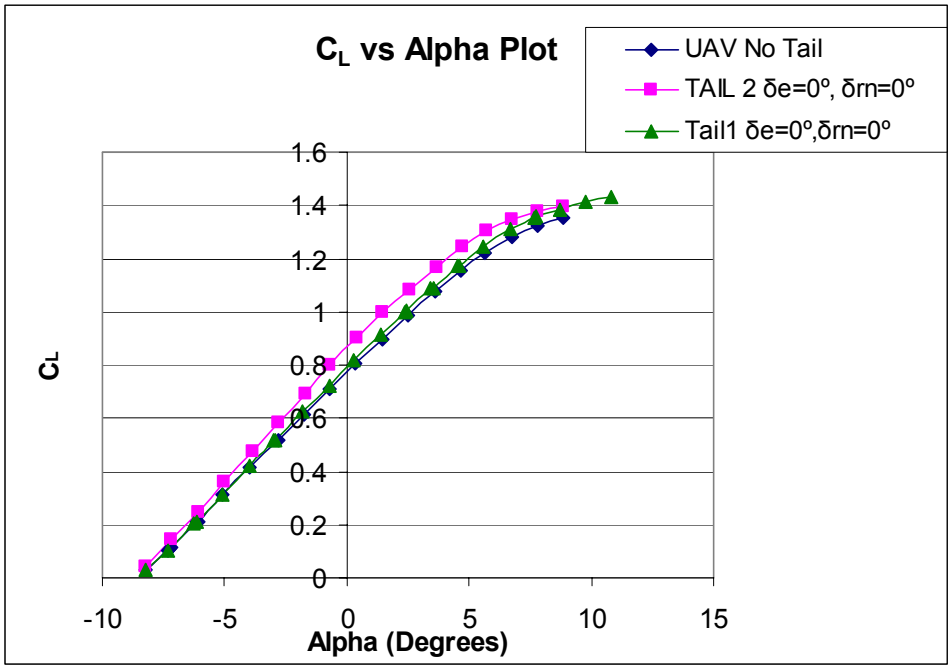

Figure 107. CL vs. Alpha Comparison for Tail 2

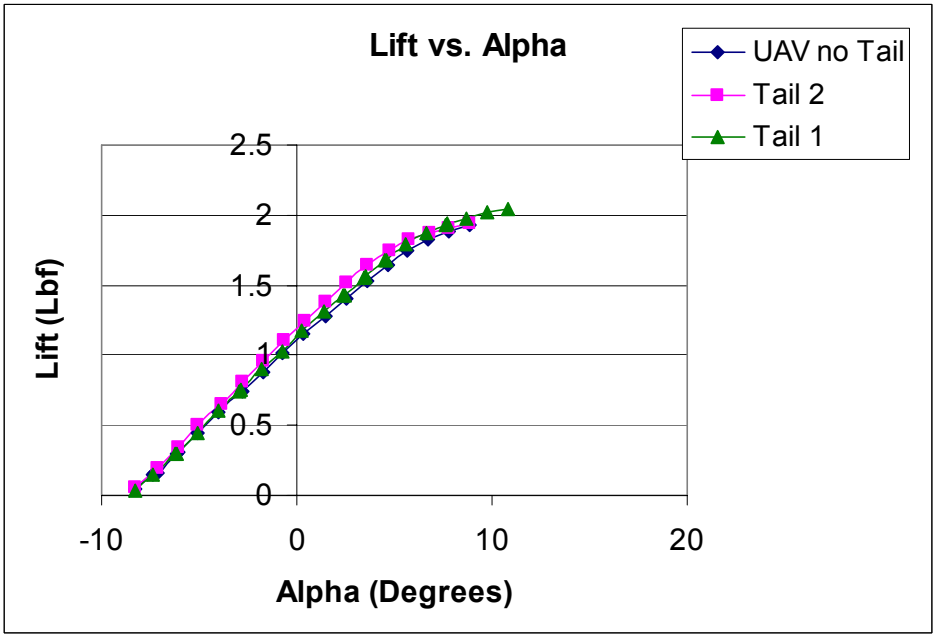

Figure 108. Lift versus Alpha Comparison for Tail 2

4.3.2. Longitudinal Control for Tail 2

In order to test the effectiveness of tail 2 in the longitudinal control, the following analyses were made by considering " pure longitudinal control", in other words, using only elevator deflection (δe) with zero tail rotation (δrn = 0º):

a. Production of the pitch moment at different elevator deflections

b. Change in coefficient of lift at different elevator deflections

a. Production of the Pitch Moment at Different Elevator Deflections

Figure 109 and Figure 110 show the longitudinal control for tail 2. It can be seen that the effectiveness of tail 2 is similar to the one obtained by using tail 1 (Figure 62), however an important difference must be considered: since the center of gravity was moved backward the negative pitch moment that the UAV has at zero elevator deflection of the tail became less negative, and now with this tail the same negative elevator deflection of the tail produce a more positive pitch moment. Additionally for the same positive deflection of the tail the results are less negative coefficients of pitch. For example: at 0.34º angle of attack using -9º of elevator deflection the pitch moment produced by tail 1 was 0.051571 and with tail 2 was 0.12272. That represents an increase of 137.96 %. On the other hand, by using δe=8º the pitch moment produced by tail 1 was -0.064914 and with tail 2 was -0.05097.

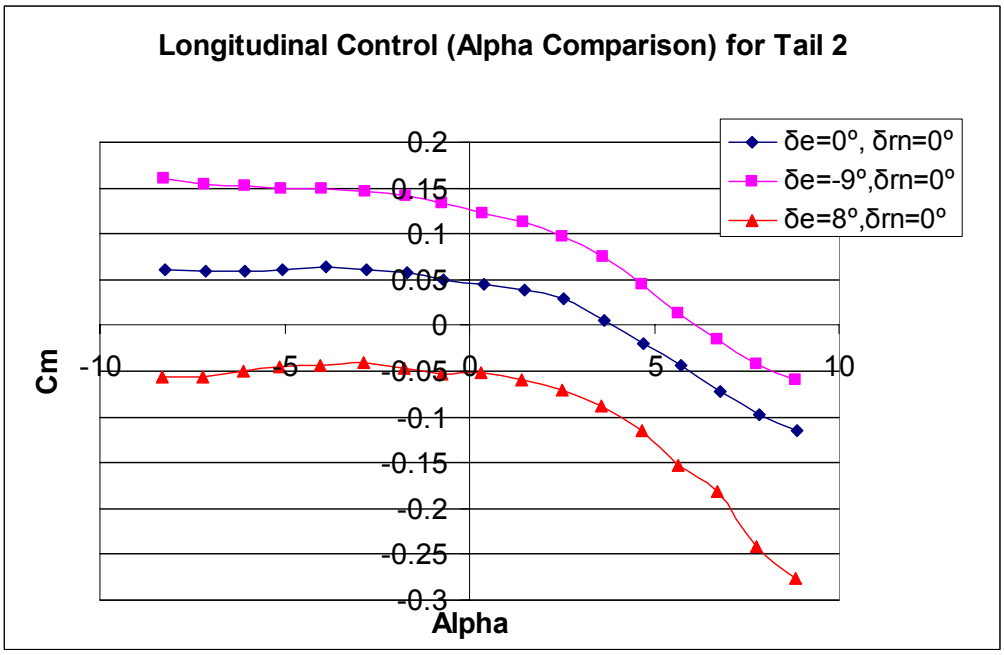

Figure 109. Longitudinal Control 1 for Tail 2

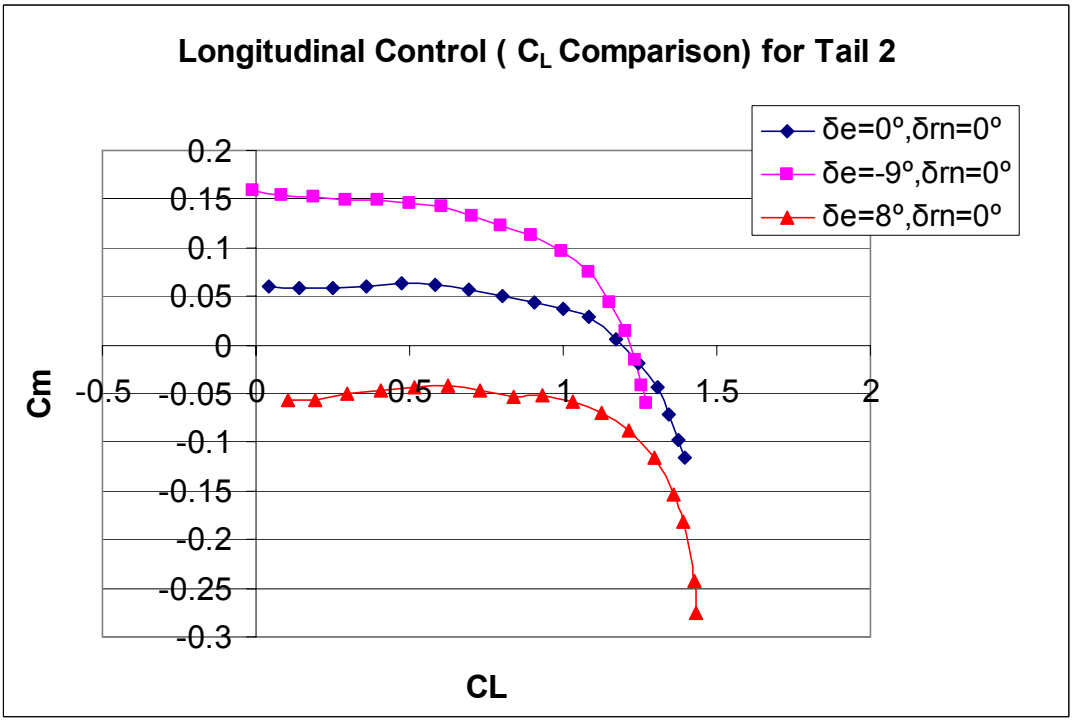

Figure 110. Longitudinal Control 2 for Tail 2

b. Change in Coefficient of Lift at Different Elevator Deflections for Tail 2

As it can be seen in Figure 111, the contribution to the coefficient of lift due to the elevator deflection is similar to the contribution of tail 1, with the exception that, as it was expected the values of this coefficient for tail 2 are more positive than the ones obtained by tail 1.

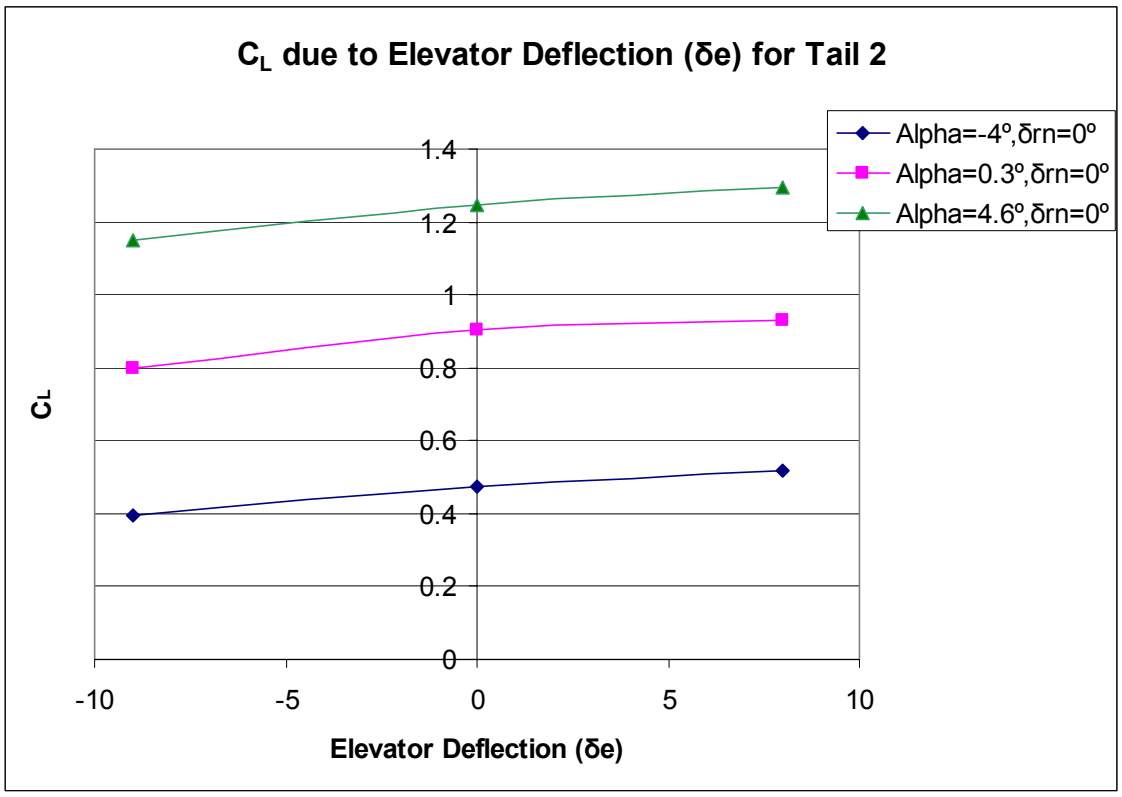

Figure 111. Coefficient of Lift at Different Elevator Deflections for Tail 2

4.3.3. Directional Stability for Tail 2

Figure 112 shows the directional static stability for tail 2 and its comparison with tail 1. It can be seen that the two vertical stabilizers included in the tail 2 configuration provide to the UAV the yaw stability desired, because the curve produced has positive

slope, $\frac{\partial Cn}{\partial \beta} = 0.0007$. This is the most important result obtained from the test conducted with tail 2.

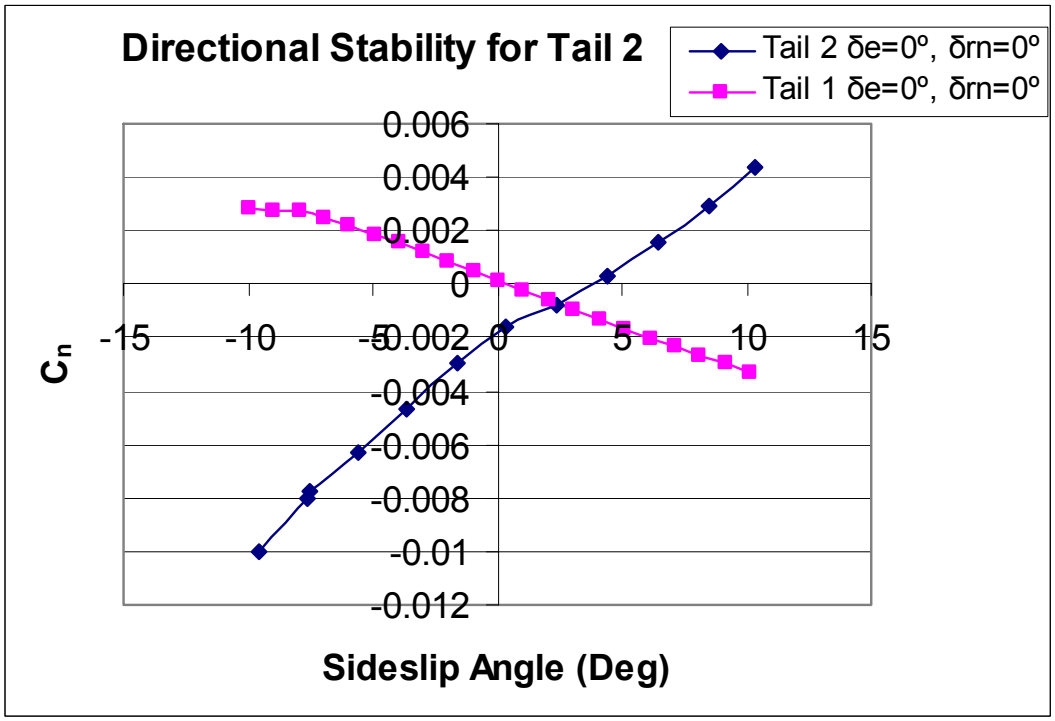

Figure 112. Directional Stability Comparison for Tail 2

4.3.4. Directional Control for Tail 2

The directional control obtained by using tail 2 are presented in Figure 113, Figure 114 and Figure 115 where the coefficient of yaw moment was plotted versus the rotation of the tail at different elevator deflections and angles of attack. Taking note that the values of yaw moment coefficient are approximately an order of magnitude smaller in range than those shown in Figure 112, these data reconfirms the results obtained for tail 1. At zero elevator deflection of the tail the coefficient of yaw moment is extremely small and the effectiveness of the tail as a device for production of this moment is improved as

the tail is deflected. The main difference between the data presented for tail 1 and 2 is that for elevator deflection -9º the direction of the yaw produced is in the opposite direction of the one obtained with tail 1 but with small values. This phenomenon is partly consequence of the movement of the center of gravity in the Y axes for the rotation of tail 2. Comparing Figure 115 to Figure 101, one may observe that the range of Cn as δrn varies while δe=8º is similar in nature though the range for tail 2 is slightly larger.

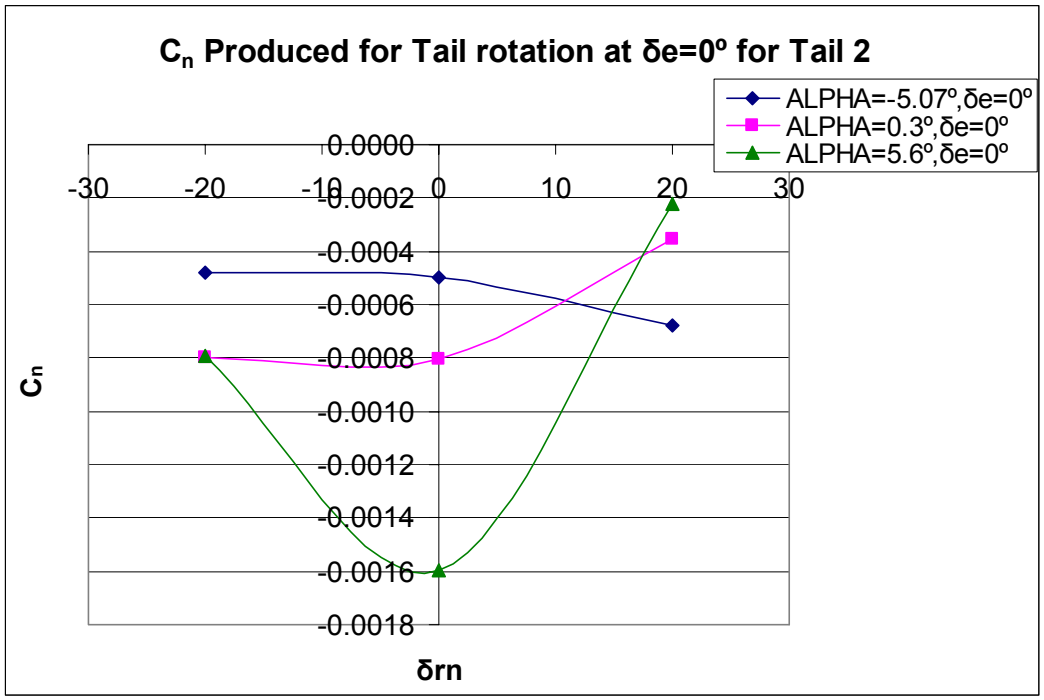

Figure 113. Cn Produced at δe=0º for Tail 2

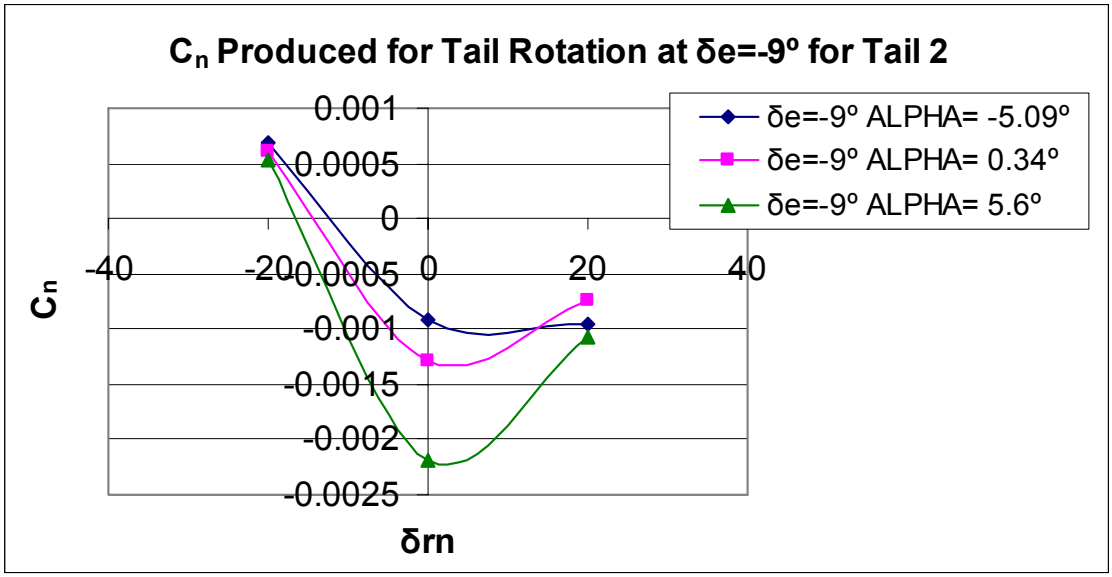

Figure 114. Cn Produced at δe=-9º for Tail 2

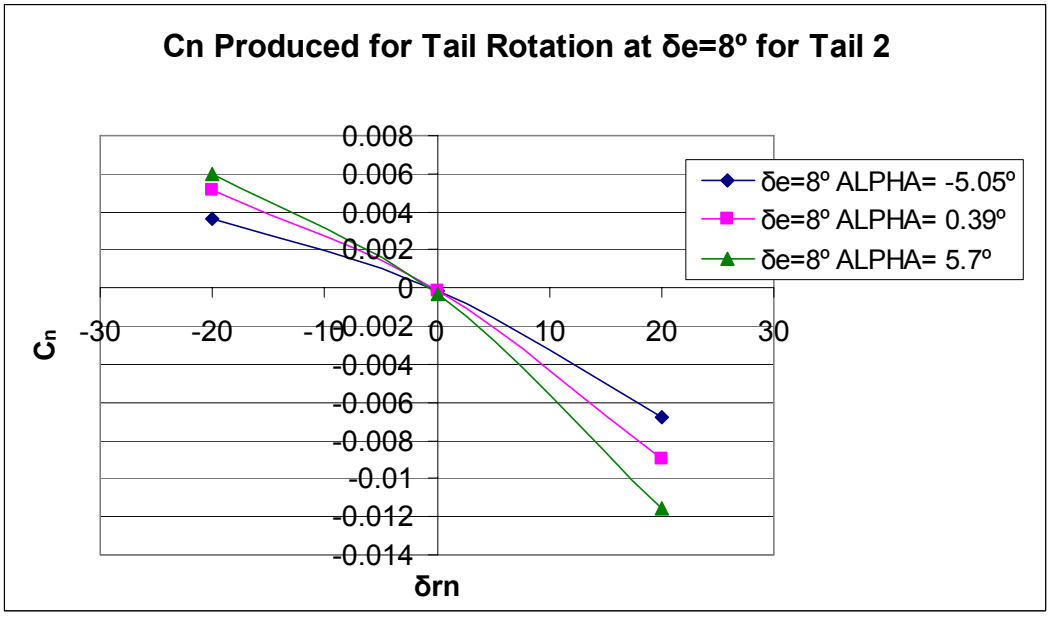

Figure 115. Cn Produced at δe=8º For Tail 2

4.3.5. Roll Stability for Tail 2

Figure 116 shows the roll static stability provided by tail 2 and its comparison with the one provided by tail 1. It can be seen that both tails provide the same stability to the UAV, because both curves have a negative slope: $\frac{\partial C_l}{\partial \beta} = -0.0018$. The only difference is that both curves are shifted, the one of tail 1 towards the negative side of C_l and the one of tail 2 towards the positive side.

This data confirms the expectation that the vertical fin in the tail has a small contribution in the roll stability because the main contributor is the wing dihedral (Dittrich; 1966: VIII-30).

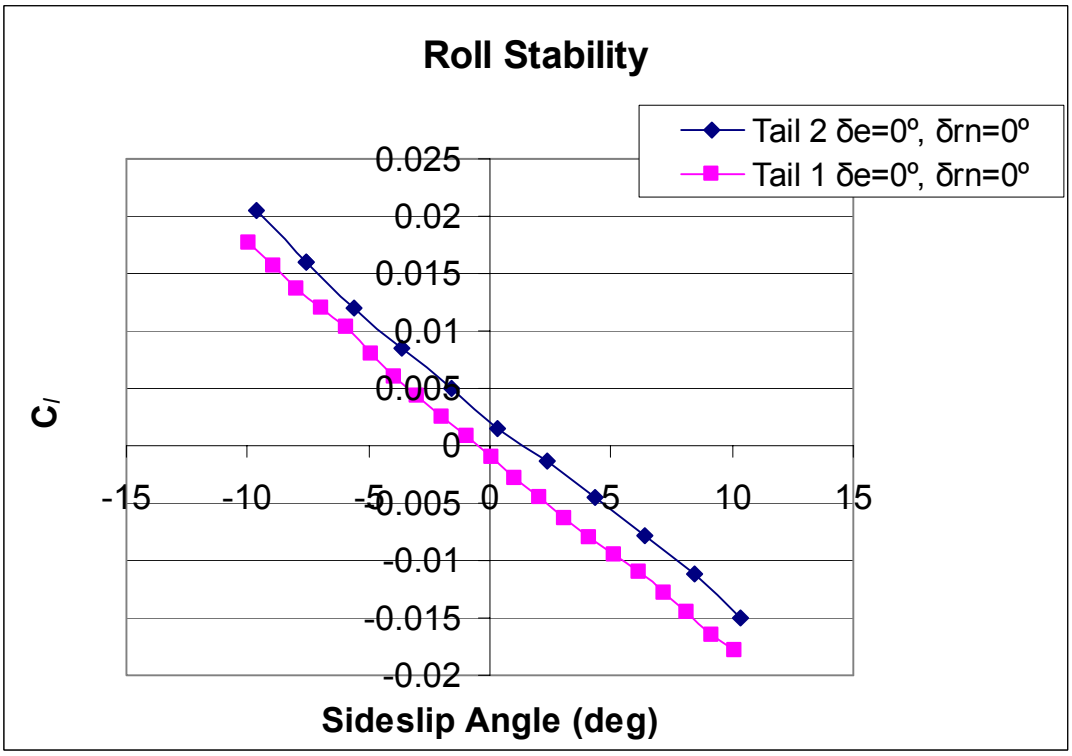

Figure 116. Roll Stability Comparison for Tail 2

4.3.6. Roll Control for Tail 2

Figure 117, Figure 118 and Figure 119 show the effect of the rotation of tail 2 as a roll control device. The results are similar to those obtained for tail 1, because in for elevator deflection zero and 8º the production of roll moment is small of order 10^{-3} and the effectiveness of the tail increases with the use of elevator deflection. However, the main difference in both tails is that for elevator deflection -9º the roll moment is more efficient since the values are of order 10^{-2}. Another difference with the results obtained from tail 1 is that the at elevator deflection zero the plot of tail 2 has a tendency to increases the roll in the positive direction, and once the tail has elevator deflection either in the positive or negative direction, tail 2 has a tendency of increasing the roll moment in the negative direction, compared with the results obtained for tail 1.

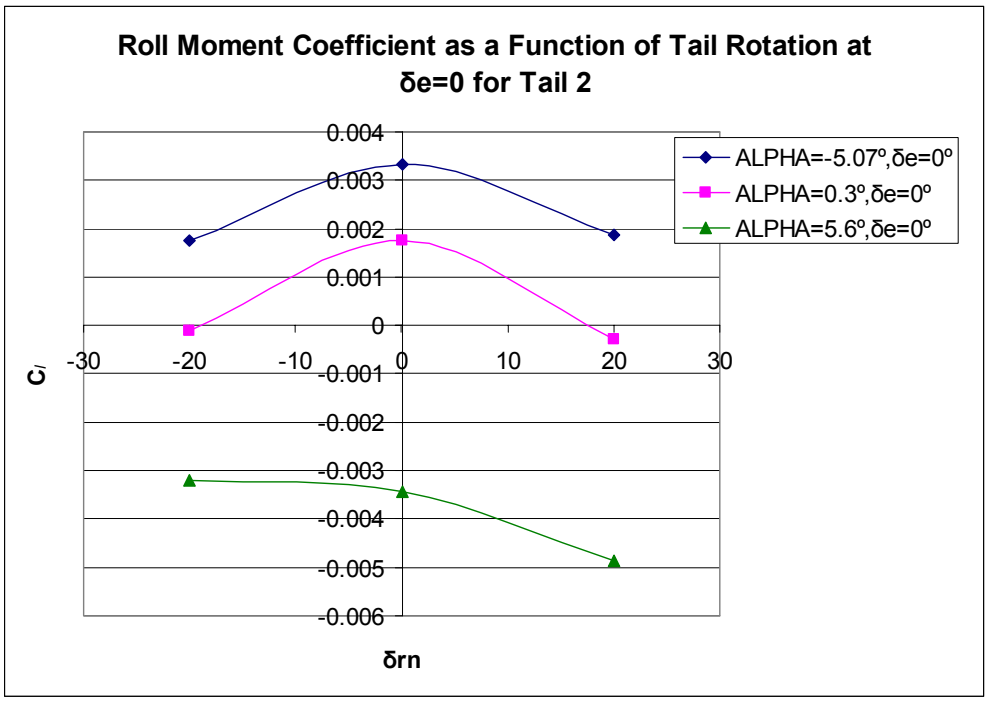

Figure 117. Roll Moment Coefficient Produced by Tail 2 at δe=0º

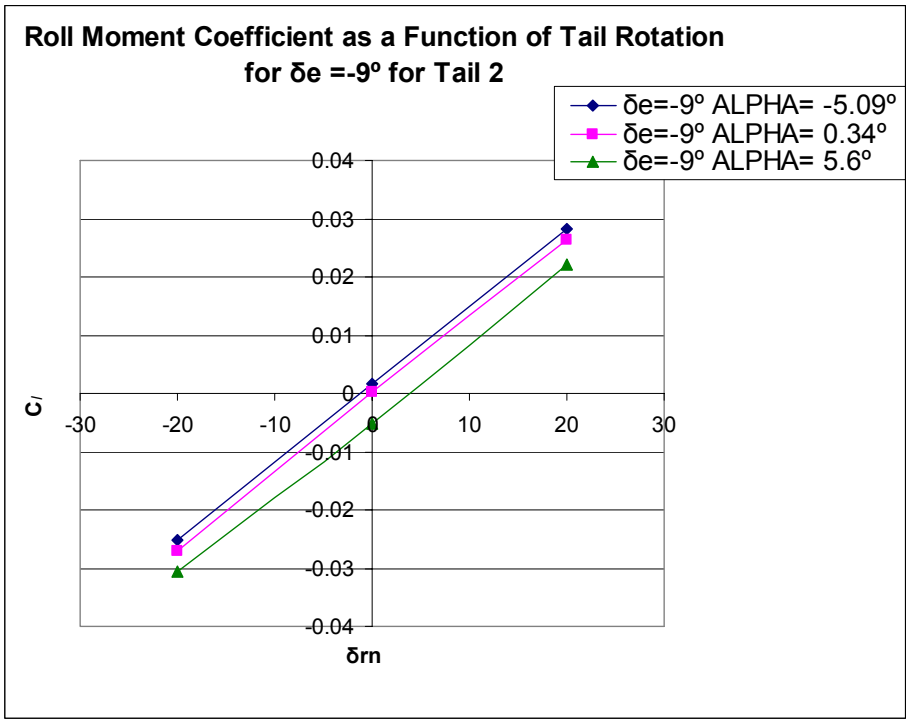

Figure 118. Roll Moment Coefficient Produced by Tail 2 at δe=-9º

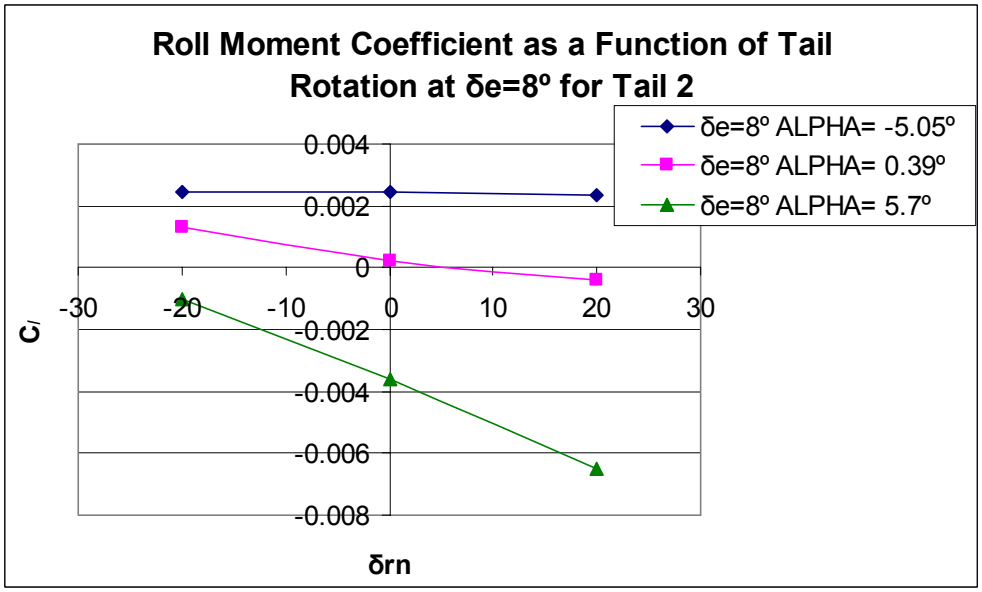

Figure 119. Roll Moment Coefficient Produced by Tail 2 at δe=8º

4.4. Movement of the Center of Gravity

Because the two tails have different weights and since the battery position may be controlled by the user, the philosophy governing the data presentation was that C.G. be represented by the actual center of gravity for the UAV as tested; however, it is very important to consider how the center of gravity position could influence the moment coefficients and an analysis is given here. This movement of the center of gravity was done along the longitudinal axes; therefore, the main characteristic that is affected due to these changes is the longitudinal static stability.

Figure 120, Figure 121, Figure 122, Figure 123, Figure 124 and Figure 125 show the longitudinal static stability for the three configurations of the UAV : no tail, tail 1 ($\delta e=0^{o}$, $\delta rn=0^{o}$) and tail 2 ($\delta e=0^{o}$, $\delta rn=0^{o}$). For obtaining the data of these figures the center of gravity was moved from 2" to 0.2 ahead of the center of the balance. It can be seen that in all cases the slope of the curves was becoming more positive as the center of gravity moves backwards; moreover this data shows clearly that the rotary tail has little contribution to the static longitudinal stability because the main factor that determines the value of this stability is the position of the center of gravity; in other words, the difference between the position of the neutral point as well the stick fixed static margin of each of the configurations is almost negligible because the influence of the rotary tail is small.

From the mentioned figures, the neutral point was obtained by interpolating between the curves in order to obtain the position where, in accordance with the definition of neutral point, the slope of the curve is zero, in other words, the position of the center of gravity where the UAV becomes longitudinally neutral stable. Table 15

shows these stick fixed neutral point positions. Moreover, since during the development of this experimental thesis, four different position of the center of gravity were used, Table 16 shows the value of the stick fixed static margin for each case, this stick fixed static margin was obtained, in accordance with its definition, as a difference between the neutral point and the position of the center of gravity (Nelson; 1998:70):

$$\textbf{Stick fixed static margin} = \frac{X_{NP}}{\bar{c}} - \frac{Xcg}{\bar{c}} \qquad \textbf{(70)}$$

In accordance with the data shown in Table 16, the no tail and tail configurations have a big value if they are compared with the tail 2 configuration, where position of the center of gravity seems to be so close to the stick fixed neutral point. However for most aircraft it is desirable to have a stick fixed static margin of approximately 5% of the mean chord (Nelson; 1998:70). This means that, 6% of the stick fixed static margin that tail 2 has is fine.

Table 15. Stick Fixed Neutral Point for the Three Configurations

Configuration	Xcm (Inches)	X_{NP} (Inches)	$\frac{X_{NP}}{\bar{c}}$
No Tail	0.630	1.267	0.305
Tail 1	0.490	1.407	0.339
Tail2	0.452	1.445	0.348

Table 16. Stick Fixed Static Margin for the Positions of the Center of Gravity Used

Configuration	$\frac{X_{NP}}{\bar{c}}$	Xcm (Inches)	Xcg (Inches)	Stick Fixed Static Margin
No Tail	0.305	1.46”	0.4375	0.199
Tail 1	0.339	1.0225”	0.875	0.128
Tail 1	0.339	0.96”	0.9375	0.113
Tail2	0.348	0.71”	1.1875	0.062

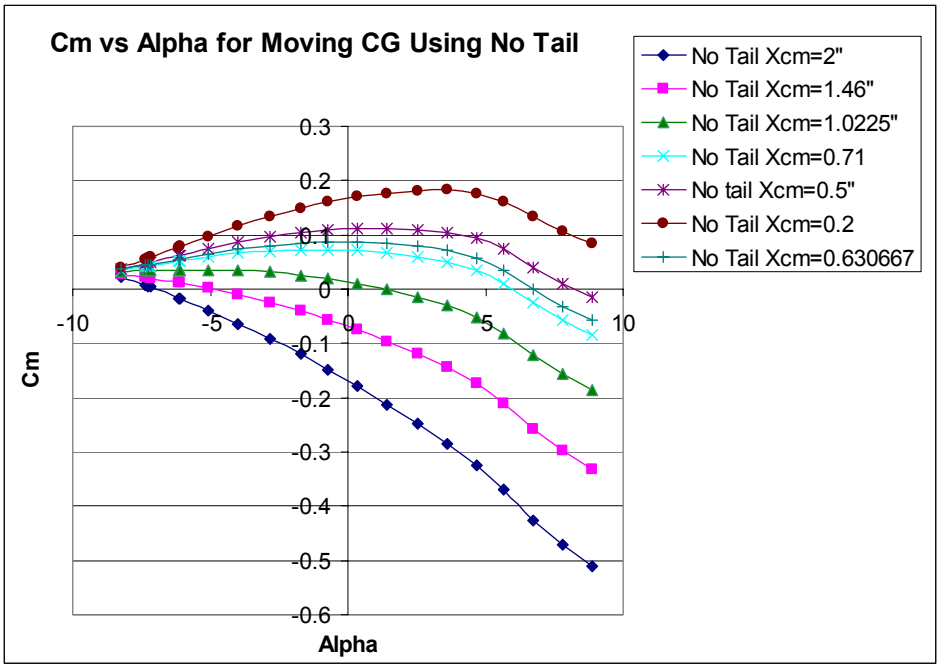

Figure 120. Cm_{α} Due to the Movement of the Center of Gravity on the UAV with No Tail

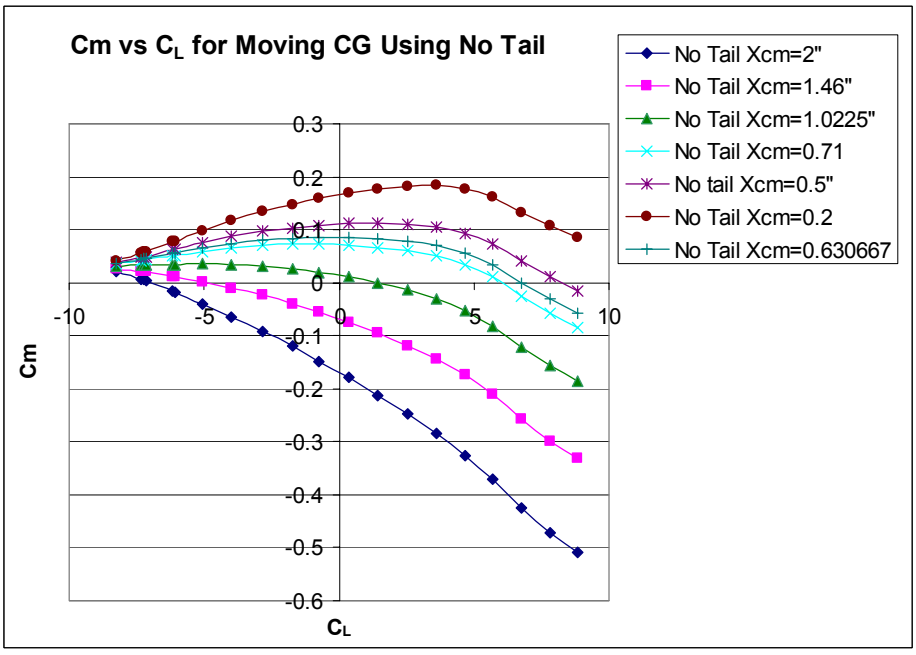

Figure 121. Cm Vs C_L Due to the Movement of the Center of Gravity on the UAV with No Tail

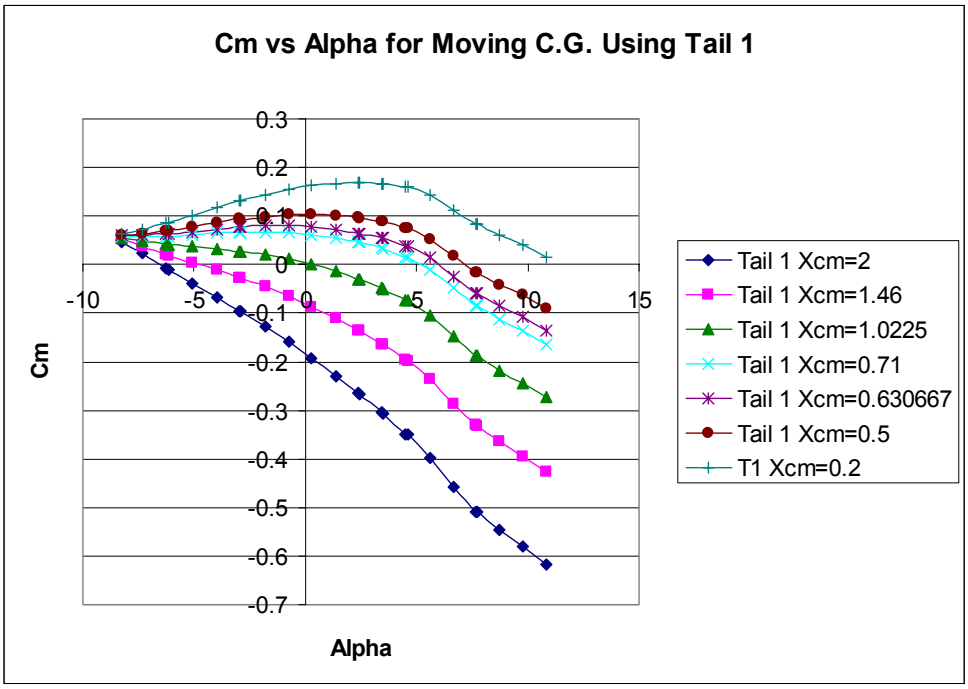

Figure 122. Cm_{α} Due to the Movement of the Center of Gravity on the UAV Using Tail 1

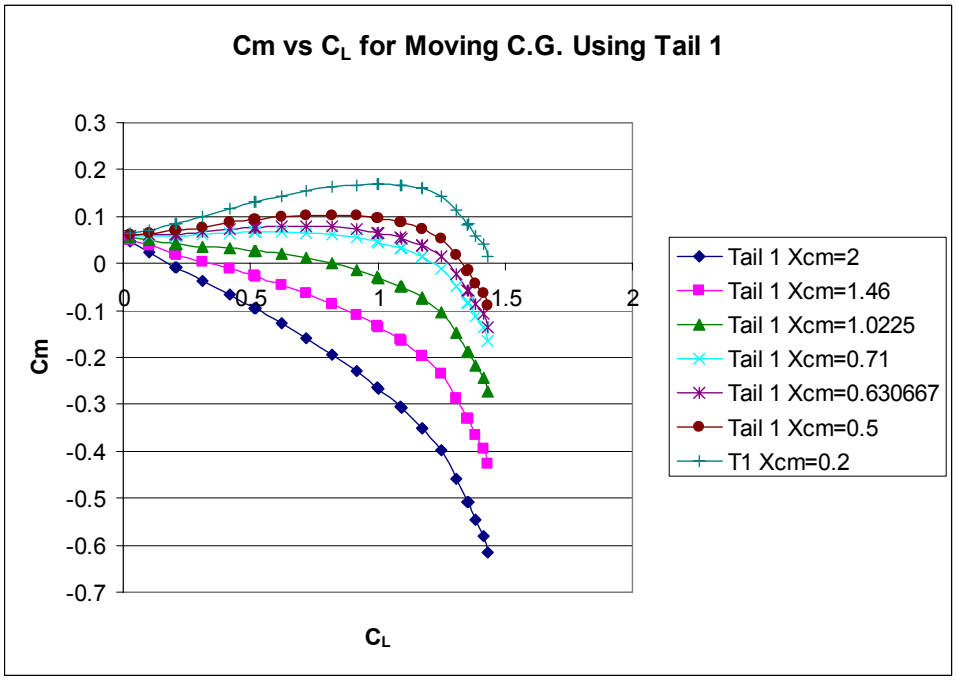

Figure 123. Cm Vs C_L Due to the Movement of the Center of Gravity on the UAV Using Tail 1

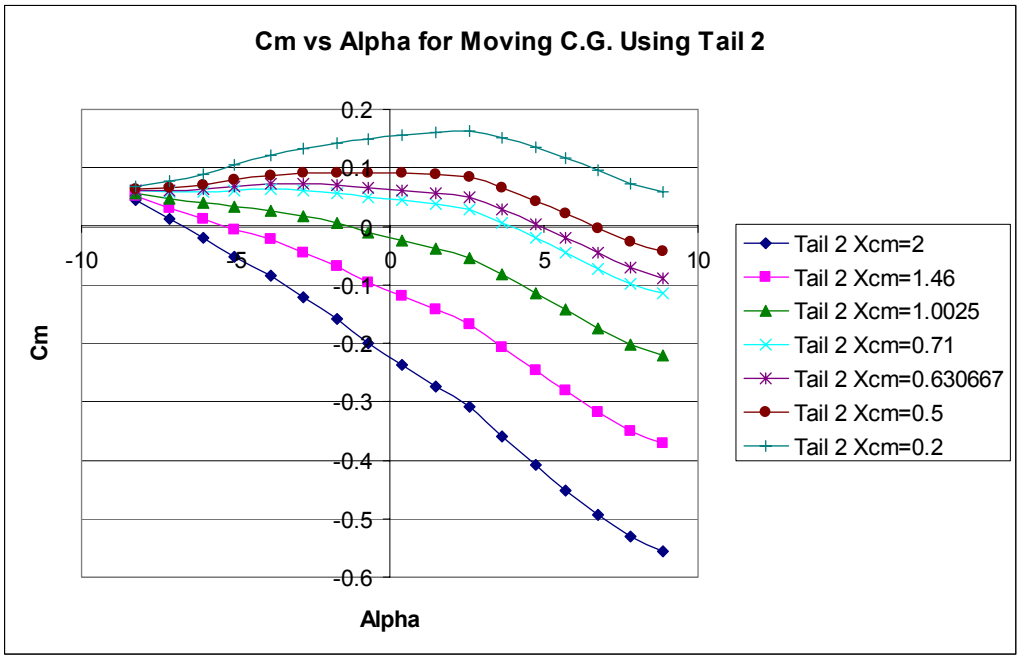

Figure 124. Cm_{α} Due to the Movement of the Center of Gravity on the UAV using Tail 2

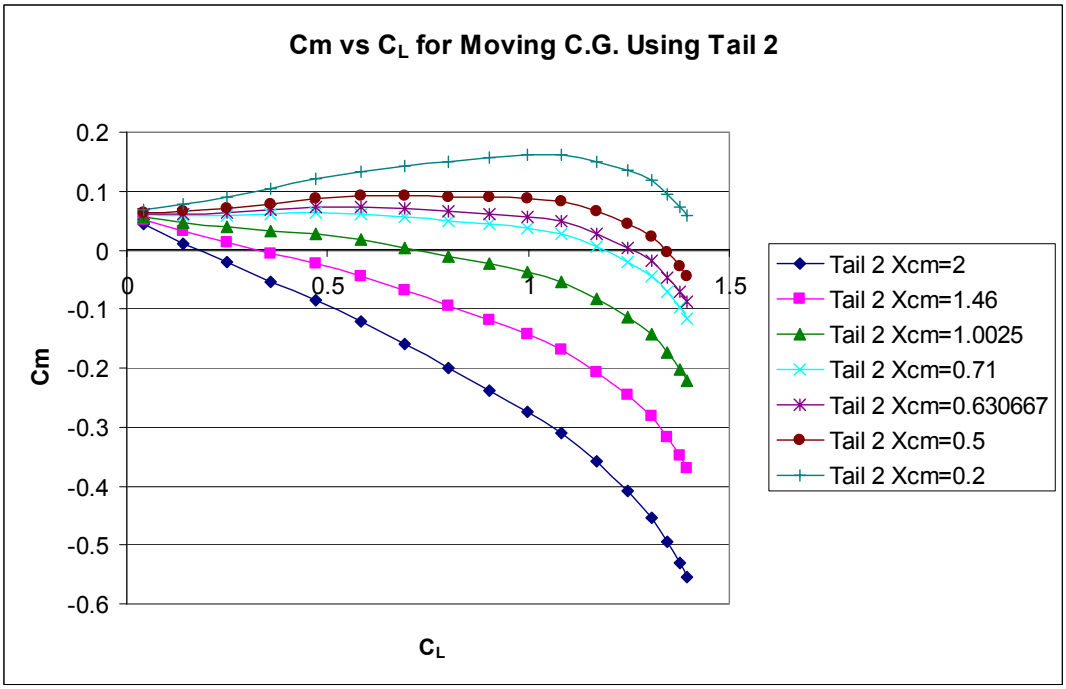

Figure 125. Cm Vs C_L Due to the Movement of the Center of Gravity on the UAV using Tail 2.

4.5. Limitations of Experimental Effort

The data presented and analyzed for this thesis was obtained with some inherent errors that are mentioned in this section.

Since the raw data has some small variation values on order of the balance precision, the data has errors due to the accuracy of the balance, in accordance with the following parameters: the AFIT-1 balance manufactured by Modern Machine & Tool Co., that is the balance used to collect the forces and moments acting on the UAV, has a resolution of 0.12% in the calculation of the normal force, since the maximum load capacity for this force is 10 lb_f, the balance has the capability of measuring normal load variations as small as 0.012 lb_f. The maximum load capacity for the axial forces is 5 lb_f, and the accuracy for this force is 0.04 %, then, the balance has the capability of measuring load axial variations as small as 0.002lb_f. The maximum load capacity for the side forces is 5 lb_f, and the accuracy for this force is 0.07 %, then, the balance has the capability of measuring load axial variations as small as 0.0035lb_f. The maximum load capacity for the pitch moment is 10 in-lb_f, and the accuracy for this moment is 0.05 %, then, the balance has the capability of measuring load pitch moment variations as small as 0.005 in-lb_f. The maximum load capacity for the roll moment is 4 in-lb_f, and the accuracy for this moment is 0.11 %, then, the balance has the capability of measuring load roll moment variations as small as 0.0044 in-lb_f. The maximum load capacity for the yaw moment is 5 in-lb_f, and the accuracy for this moment is 0.07 %, then, the balance has the capability of measuring load pitch moment variations as small as 0.0035 in-lb_f.

The fabrication and installation of the system that control the tails is not longitudinally symmetric; therefore, the forces and moments produced have induced errors. This asymmetric characteristic is shown in Figure 126.

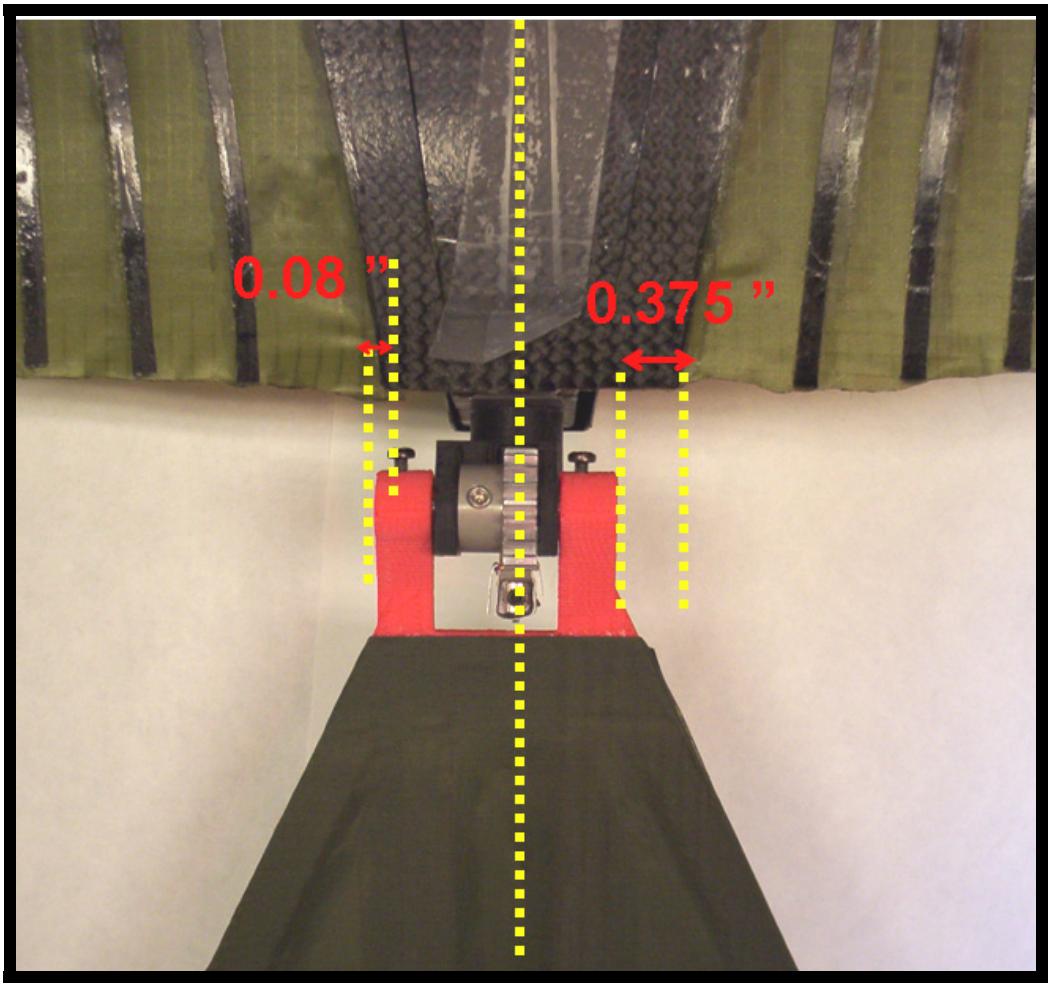

Figure 126. Asymmetric Characteristics of the Tails

Another source of error was the fact that in the β runs, it is desirable to have zero side slip angle; however, this angle had different values such as 0.555º, 0.085º, 0.34º, 0.127º and 0.255º as can be seen in the data tables presented in Appendix B.

The data presented in this thesis was obtained by using a model ‘similar’ to the original UAV, in other words, there are differences in sizes, geometry and weights with

respect to the UAV used in the battlefield. In addition, error in the production as well the fact that the model used was equipped with a mounting block simulating the camera of the real UAV, where the internal balance was installed, increases the sources of differences between the model tested and the actual UAV used in the battlefield.

During the development of the thesis the deflection of the tail in rotation and elevator deflection was done by using the radio control equipment and by acting the control by using the actuators inside the model, moreover, the amount of deflection was checked by using a digital inclinometer, however, after the wind tunnel runs it was noted that the deflection was reduced due to the action of the dynamic pressure. Some of these angle reductions had values of 1 or 2 degrees; in order to avoid these variations, during the test of tail 2 the sticks of the controller were actuated; as a consequence it is estimated that the δe and δrn angles given in the data presented can have a variation of $\pm$ 2º.

There were errors produced by the quantization of the analog to digital converter 16 bit data acquisition card due the fact that this card has an error of $10Volts/2^{16} = 0.000152588$ (DeLuca;2004:131).

An induced mathematical error was introduced, since the test tares were calculated by fitting a 4^{TH} degree polynomial.

Since the electric energy used to move the tail was taken from the battery, the reduction in the amperage from this energy source as the time was go on, introduced error reflected in the decrement of the angles of deflection and rotation of the tail.

V. Conclusions and Recommendations

5.1. Conclusions

The goal of this experimental study was to determine the general behavior and the aerodynamic characteristics that rotary tails provide to a specific UAV. Its effects on the static stability and control effectiveness were characterized for two tail designs.

In the production of lift, a rotary tail works in the same manner as a conventional tail in that the main contributor to the lift production is the elevator deflection. The results indicate that as the tail is deflected in the positive direction the lift of the whole aircraft is incremented and as it is deflected in the negative direction the total lift is decreased. The rotation of the tail has little effect on the production of lift at angles of rotation of 20º or less; however, as this rotation is increased the effect was larger and as a consequence the production of lift is smaller for the tails tested.

In the drag production, the main contributor for a rotary tail is the elevator deflection; however, positive elevator deflections produce more drag than negative elevator deflections due to increased induced drag. The rotation of the tail has little effect in the production of drag at angles of rotation of 20º or less.

In the production of side force, the largest forces were obtained by using a combination of rotation and elevator deflection. One prominent characteristic of the production of this force in a rotary tail is that there is a control reversal effect when the tail keeps the rotation angle and changes the elevator deflection from the positive sign to the negative or vice versa. In a other words, the magnitude of the side force depends on the magnitude of the deflection and elevator deflection of the tail and moving either past

its zero setting (while holding the other constant) can change the direction of the side force.

In the production of pitch moment coefficient (Cm), as control device, for moderate rotation angles the main contributor is the deflection of the tail. In this sense the rotary tail works in the same manner than a conventional tail: positive elevator deflection of the tail produce negative pitch values and negative elevator deflections produce positive pitch moment. It was found that the elevator deflection range of both tails tested was sufficient to longitudinally trim the aircraft through an alpha range of -5° to +5°, at a minimum. The level of longitudinal static stability was affected by the placement of the center of gravity more than it was by the tail style.

In the production of yaw moment coefficient (Cn), the best results are obtained by using a combination of rotation and elevator deflection. One unique and potentially challenging characteristic of the production of a yaw moment for a rotary tail is that there is a control reversal effect due to the same phenomena that affects the side force production: when the tail keeps the rotation angle and changes the elevator deflection from the positive sign to the negative or vice versa. In other words, as a control device the magnitude of the yaw moment depends on the magnitude of the deflection and elevator deflection of the tail and the sign of this coefficient produced when the tail is rotated is function of elevator deflection. On the other hand, as a stabilizer device, a rotary tail with no vertical fins like tail 1 does not provide static directional stability, however, it was found that it was possible to obtain positive values of $\frac{\partial Cn}{\partial \beta}$ for a rotary tail if vertical stabilizers are used, as in the case of tail 2.

In the production of roll moment coefficient (C_l) by a rotary tail as a control device, the contribution is similar to the one obtained in side force and yaw moment coefficient: the best results are obtained by using a combination of rotation and elevator deflection; however the values of this moment coefficient are so small as an indication of the little contribution to the tail. Once again, an important characteristic of the production of this coefficient in a rotary tail is that the control reverse effect mentioned in the cases of the side force and yaw moment, in other words, as a control device the magnitude of the roll moment depends on the magnitude of the deflection and elevator deflection of the tail and the sign of this coefficient produced when the tail is rotated is function of elevator deflection. On the other hand, as a stabilizer device, rotary tails do not have a substantial contribution to the static roll stability, since the main contributor to $\frac{\partial C_l}{\partial \beta}$ is the wing dihedral. It should be noted that the weight of the tail could be another consideration in controlling the aircraft, but a thorough investigation of this effect was beyond the scope of the current work.

Another important phenomenon presented in the production of side force, roll moment and yaw moment is that when the elevator deflection is zero the sign of the force or moment produced is function also of the angle of attack. However this situation disappears when elevator deflection is applied and the angle of attack will influence the amount of moment produced because the angle of attack of the tail is function of the angle of attack of the UAV.

Table 17 shows the stability derivatives obtained for the two tails compared to the original UAV design and to what are described as generic value that are the data of a

general aviation airplane NAVION (Nelson; 1998:400). Figure 127 shows that the longitudinal static stability obtained with both tails is less than the one that the original UAV had. However, compared with the generic value, the level of longitudinal stability obtained are similar. Moreover, one important point to remember is that this level of stability was obtained via center of gravity placement, and therefore it can be increased if necessary. Figure 128 shows the comparison of the directional stability obtained and it can be seen that only the tail with vertical stabilizer is stable in yaw and its level of stability is just 10% less than the one of the original UAV and 43 % smaller than the generic one, however, this level of stability can be increased by augmenting the area of the vertical stabilizers of tail 2. Figure 129 shows the comparison of the roll stability obtained. It can be seen that by using the rotary tail the roll stability increases by approximately 40 % from the one of the original UAV. However, if it is necessary to change this value, it can be done by changing the sweep and dihedral angle of the wing. These data prove that a UAV can be stabilized by a rotary tail.

Table 17. Compendium of Static Stability Derivatives

Derivative	Tail 1	Tail 2	Original UAV	Generic Value
$\frac{\partial Cm}{\partial \alpha}$ *	-0.0166	-0.01	-0.0466	-0.0119
$\frac{\partial Cn}{\partial \beta}$	-0.0003	0.0007	0.00078	0.00123
$\frac{\partial Cl}{\partial \beta}$	-0.0018	-0.0017	-0.00076	-0.00129

*Controllable via CG placement.

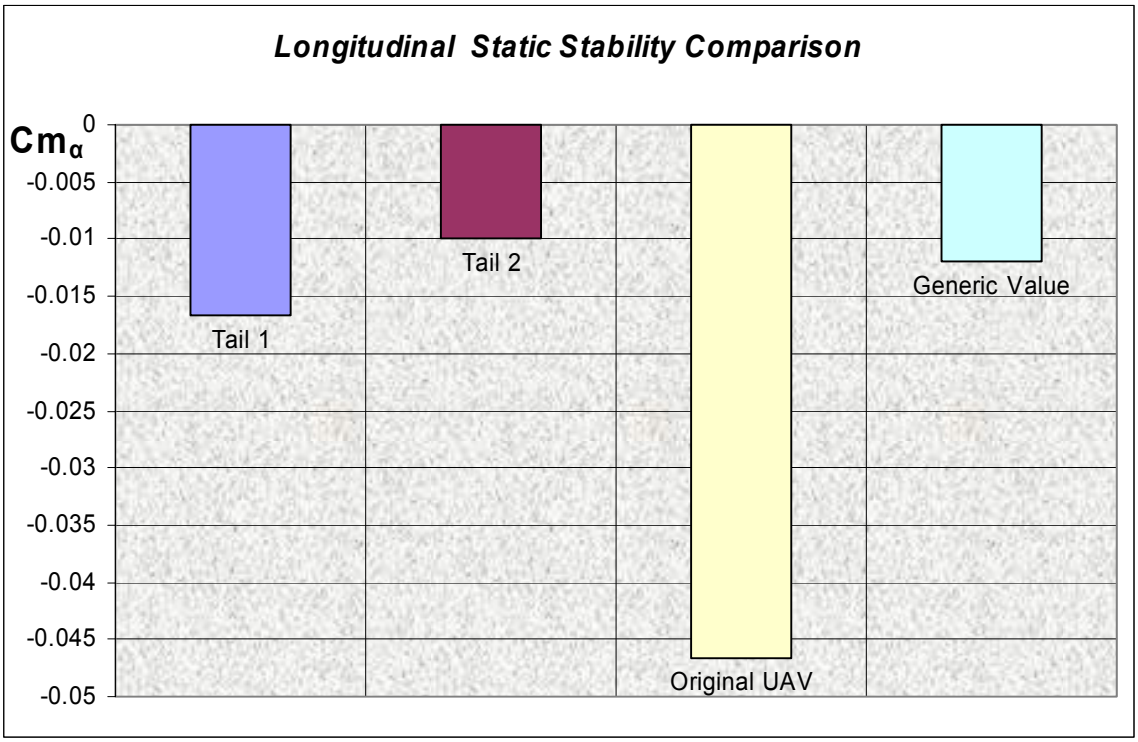

Figure 127. Longitudinal Static Stability Comparison

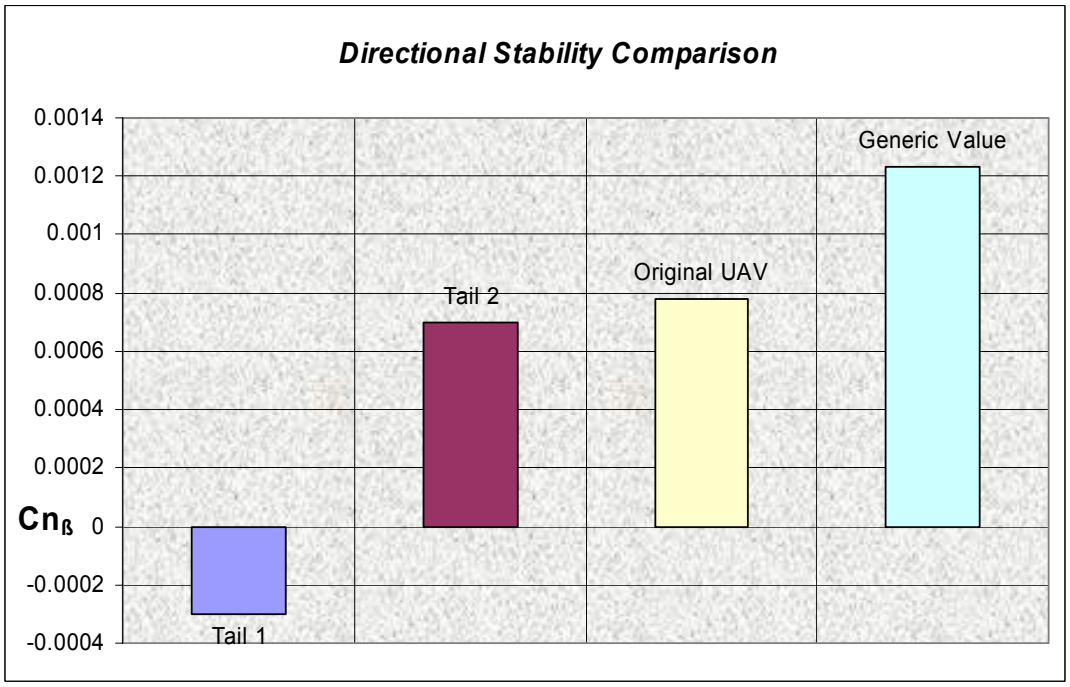

Figure 128. Directional Stability Comparison

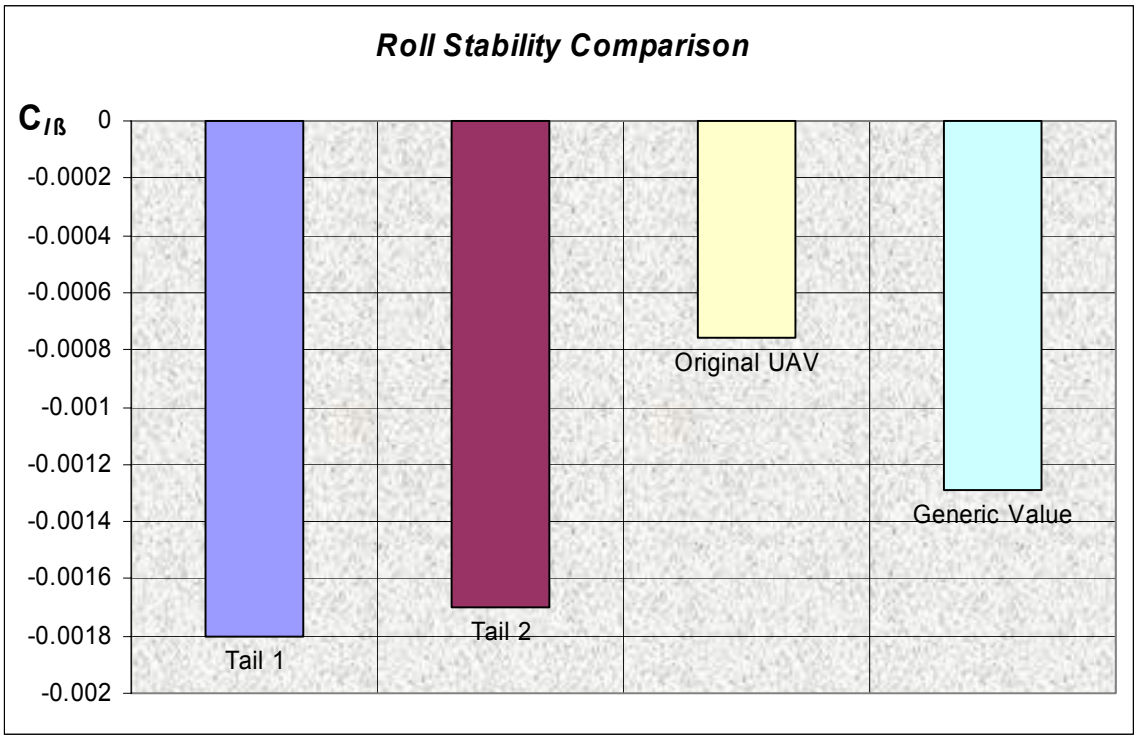

Figure 129. Roll Stability Comparison

Table 18 presents the values of the derivative of the moment coefficients with respect to deflection and rotation angles of the tails. Figure 130 shows the comparison of the elevator control effectiveness, it can be seen that tail 1 has 40% less effectiveness of the original UAV configuration and tail 2 has only 9% less. Figure 131 and Figure 132 show the control effectiveness comparison on the roll and yaw respectively. The generic values of these figures were obtained by using ailerons for roll control and conventional rudder for yaw control. In these two figures notice that negative elevator deflection of the tail produces a derivative of opposite sign than the one obtained with positive elevator deflection and the one presented for the original configuration and generic values, this is consequence of the control reverse effect mentioned that appears when the tail keeps the rotation angle and changes the elevator deflection from the positive sign to negative or

vice verse. However this is not a problem if the tail works in elevator deflection of only one sign. It can be seen in Figure 131 that with the exception of rotation of tail 2 with negative deflection of the tail which has a roll control effectiveness of approximately 60 % of that shown as a generic value, all other cases, including the original configuration of the UAV have poor control in roll. In other words, tail 1 with δe=-9º has 0.3 % of the generic value, tail 1 with δe =8º has 1.2 % of the generic value, tail 2 with δe=8º has 1.8% and the original configuration has only 9%. On the other hand, Figure 132 shows that the yaw control effectiveness is better than the one obtained from roll because tail 1 with δe=-9º has 34 % of the original configuration and 20% of the generic value. Tail 1 with δe=8º has 49 % of the yaw control of the original configuration and 30 % of the generic value; tail 2 with δe=-9º has 5% of the original UAV and only 2.6 % of the generic value, tail 2 with δe=8 º has 48 % of the original configuration and 29 % of the generic value. Finally the original configuration has only 58 % of the control of the generic value. It is important to remember that even if these values appear to be small compared with the generic values, it is expected that the UAV can be controlled, especially by using directional control because the generic values shown were taken from a general aviation airplane that has to obey FAA regulations such as enough rudder control for spin recovery (Raymer;1999:83); nevertheless, it is expected that by increasing the area of the tail, increasing its elevator deflection or increasing the horizontal tail volume coefficient more control can be achieved in the pitch, yaw and roll. These data prove that a UAV can be controlled by using a rotary tail.

Table 18. Compendium of Control Effectiveness Derivatives

Derivative	Tail 1	Tail 2	Original UAV	Generic Value
$\frac{\partial Cm}{\partial \delta e}$	-0.0068	-0.0102	-0.0111	-0.0161
$\frac{\partial C_l}{\partial \delta rn}$	For δe=-9 0.0000068 For δe=8 -0.000029	For δe=-9 0.001337 For δe=8 -0.000042	-0.00022	$(\frac{\partial C_l}{\partial \delta_a})$ -0.00233
$\frac{\partial Cn}{\partial \delta rn}$	For δe=-9 0.00025 For δe=8 -0.00036	For δe=-9 -0.000033 For δe=8 -0.00035	-0.00073	$(\frac{\partial Cn}{\partial \delta r})$ -0.00126

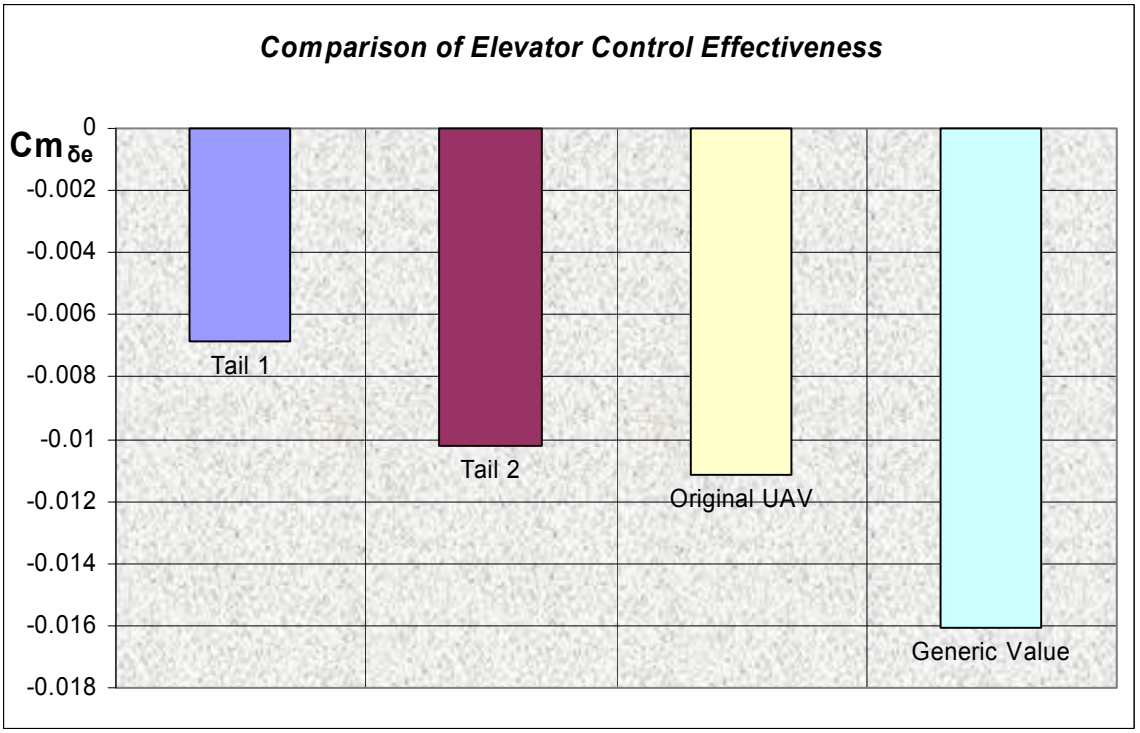

Figure 130. Comparison of Elevator Control Effectiveness

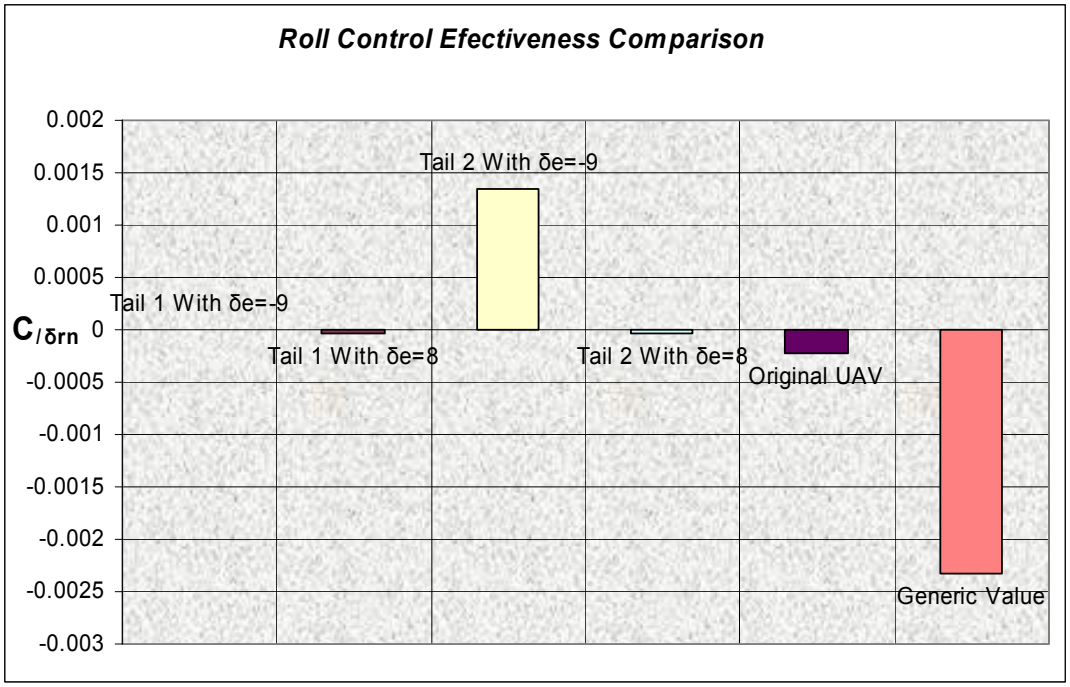

Figure 131. Roll Control Effectiveness Comparison

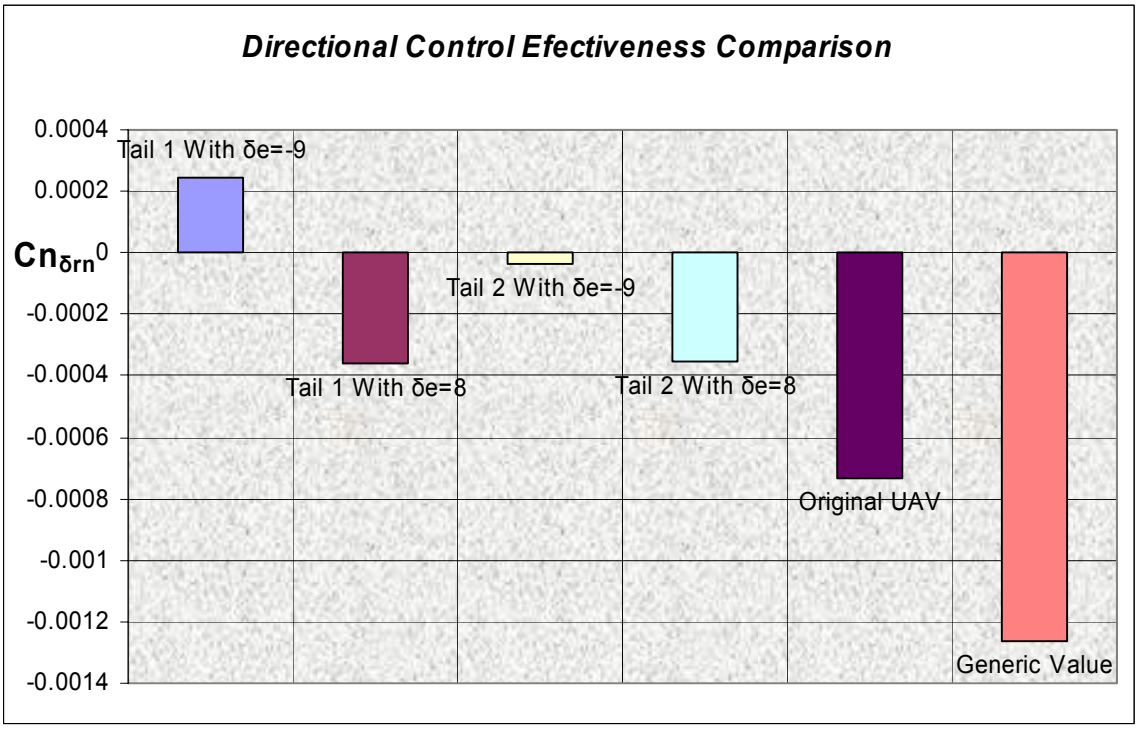

Figure 132. Directional Control Effectiveness Comparison

To summarize, these wind tunnel tests strongly suggest that it is feasible to use a rotary tail in a UAV, yet maintain a stable and controllable vehicle. The magnitude in the longitudinal stability should be selected by placing the center of gravity ahead of the neutral point in accordance with the stability desirable. The yaw stability can be adjusted by changing the area of the vertical stabilizers as in the conventional tail configurations. The roll stability was satisfactory for the rotary tail and can be adjusted by changing the wing dihedral, wing sweep and position of the wing on the fuselage.

The level of control desired can be achieved by changing the area of the tail, tail volume coefficient and deflection angle; moreover, in order to avoid the change in the sign of the yaw and roll moment as a consequence of change the elevator deflection of the tail, the UAV should have the capability of changing its pitch moment from negative values to positive values by moving in elevator deflection of the tail with values of δe of the same sign. This can be achieved by locating the center of gravity in such as position that provides a constant positive pitch moment that for trimming the UAV for zero and positive pitch moment values will be necessary to keep under all conditions a negative deflection of the tail. This condition will avoid the change in the direction of the roll and moment coefficient obtained when $\delta e=0^{o}$.

5.2. Recommendations

The objective of this experimental study was to determine the general behavior and the aerodynamic characteristics that rotary tails provide to the UAV and its effects on the static stability and control effectiveness; this objective was effectively reached; however, in order to improve the understanding of this new tail concept and evaluate the

possibility its implementation on the actual UAV, the following recommendations can be defined as future projects:

1. To do experimental wind tunnel investigation by using 10 MPH and 20 MPH, because this thesis was done by limiting the wind velocity to 30 MPH.

2. To explore the characteristics of the UAV obtained by using other tail configurations, considering the possibility of increasing the area of the tail in order to have more control effectiveness and changing the angle of attack of the tail when the deflection is zero.

3. To do experimental wind tunnel investigation by using power runs configurations.

4. To do an analysis of the electric energy consumption increasing due the increment of the demand of power as a consequence of the augmentation of the hinge moment, and to develop a trade study of the advantages or disadvantages of saving room versus the increment of weight or decrement of autonomy of the UAV with this new tail configuration.

5. Change the actuators in the model used in order to have more accurate deflections.

6. To build the tail and the components of the system developed for controlled with carbon fiber, because the tails tested are relatively heavier because of the plastic material that are made of.

7. Since the investigation was limited to small elevator deflection, in part due to the wind tunnel fixture, to explore the aerodynamic characteristics of the UAV obtained with a larger range of this angle as well of rotation.

8. A flow visualization will provide a better illustration of the behavior of this new tail configuration.

9. To develop analytical models of the rotary tail.

Appendix A: Approximate Data for Comparison of Tail Volume Coefficient Between Birds and Airplanes.

Table 19. Horizontal Tail Volume Coefficient of Some Type of Airplanes (Raymer; 1999:125)

TYPE	HORIZONTAL TAIL VOLUME COEFFICIENT
JET FIGHTER	0.4
SAILPLANE	0.5
HOMEBUILT	0.5
AGRICULTURAL	0.5
GENERAL AVIATION-SINGLE ENGINE	0.7
FLYING BOAT	0.7
JET TRAINER	0.7
GENERAL AVIATION-TWIN ENGINE	0.8
TWIN TURBOPROP	0.9
MILITARY CARGO/BOMBER	1
JET TRANSPORT	1

Table 20. Approximate Aerodynamic Data of Some Birds

BIRD	WING AREA (M^2)	TAIL AREA (M^2)	WING MEAN CHORD (M)	TAIL MOMENT ARM(M)	HORIZONTAL TAIL VOLUME COEFFICIENT
STORK	0.296831853	0.01	0.31	0.285	0.030972243
SWAN	0.238	0.012	0.28	0.4	0.072028812
PIGEON	0.0695	0.005	0.1	0.13	0.09352518
MALLARD	0.055	0.0055	0.14	0.17	0.121428571
EAGLE	0.3356	0.0333	0.34	0.43	0.12549078
ALBATROSS	0.305	0.0225	0.25	0.47	0.138688525
LAPWING	0.0322	0.0035	0.13	0.17	0.142140468
TERN	0.036	0.003	0.11	0.2	0.151515152
BLACKBIRD	0.0137	0.0018	0.09	0.11	0.160583942
SWIFT	0.00675	0.0006	0.04	0.08	0.177777778
SPARRO	0.00665	0.0009	0.05	0.07	0.189473684
BUZZARD	0.108	0.014	0.19	0.28	0.191033138
GULL	0.0741	0.0085	0.14	0.25	0.204839021
CROW	0.0578	0.0126	0.17	0.2	0.256462447
MAGPIE	0.0372	0.0096	0.16	0.17	0.274193548
GOSHAWK	0.108	0.0232	0.2	0.28	0.300740741
GANNET	0.1053	0.0168	0.15	0.3	0.319088319
SPARROWHAWK	0.0376	0.01	0.12	0.18	0.39893617
KESTREL	0.021	0.008	0.08	0.14	0.6666667

Appendix B: Data Tables

No Tail

Table 21. No Tail Data

ALPHA(α) [Degrees]	BETA(β) [Degrees]	MACH #	Re	Dynamic pressure (qc) [lbf/ft^2]	U∞ [mph]	C_L	C_D	C_S	$C_{l\,eg}$	C_{meg}	C_{neg}	Drag (D) [lbf]	Side Force(S) [lbf]	Lift(L) [lbf]
-8.2468	0.255	0.0393	1.33E+05	2.2037	30.323	0.032117	0.076981	0.001707	0.001974	0.027533	0.000726	0.11014	0.002442	0.045957
-7.3459	0.255	0.039292	1.33E+05	2.2028	30.317	0.10207	0.072621	0.001249	0.002046	0.021831	0.000648	0.10376	0.001786	0.146
-7.2552	0.255	0.039284	1.33E+05	2.2019	30.311	0.11043	0.072143	0.001083	0.002108	0.021182	0.000647	0.10301	0.001549	0.15789
-7.1661	0.255	0.039272	1.33E+05	2.2006	30.302	0.11513	0.071894	0.001311	0.002101	0.020605	0.000665	0.10259	0.001873	0.16451
-6.1681	0.255	0.039302	1.33E+05	2.2039	30.325	0.21016	0.068581	0.00032	0.002057	0.011863	0.000566	0.097659	0.000457	0.30077
-6.0802	0.255	0.039299	1.33E+05	2.2036	30.322	0.21236	0.067847	0.00016	0.002158	0.01168	0.00059	0.096582	0.000228	0.30385
-5.0797	0.255	0.039296	1.33E+05	2.2033	30.321	0.31073	0.065739	-0.00031	0.002327	0.001714	0.000534	0.092989	-0.00044	0.44456
-3.9912	0.255	0.039314	1.33E+05	2.2053	30.334	0.41358	0.064823	-0.00175	0.002249	-0.00984	0.000479	0.090935	-0.00251	0.59223
-2.8138	0.255	0.039324	1.33E+05	2.2064	30.342	0.51875	0.065412	-0.0031	0.001984	-0.02406	0.000457	0.090743	-0.00444	0.74322
-1.7282	0.255	0.039322	1.33E+05	2.2062	30.341	0.61498	0.067419	-0.00479	0.001757	-0.03964	0.000394	0.092406	-0.00686	0.88102
-0.72927	0.255	0.039313	1.33E+05	2.2051	30.333	0.70995	0.070813	-0.0068	0.001369	-0.05618	0.000336	0.095829	-0.00974	1.0166
0.35525	0.255	0.039295	1.33E+05	2.2032	30.319	0.80391	0.076195	-0.00884	0.000948	-0.07459	0.000275	0.10187	-0.01265	1.1501
1.4389	0.255	0.039302	1.33E+05	2.2039	30.325	0.89584	0.083843	-0.01054	0.000524	-0.09562	0.00017	0.11113	-0.01508	1.282
2.523	0.255	0.039271	1.33E+05	2.2004	30.301	0.98664	0.092384	-0.01236	-9.24E-05	-0.11851	7.39E-05	0.12127	-0.01766	1.4097
3.6048	0.255	0.039241	1.33E+05	2.1972	30.278	1.0745	0.10316	-0.01423	-0.00067	-0.14404	-0.00011	0.13447	-0.0203	1.5329
4.6841	0.255	0.039259	1.33E+05	2.1992	30.292	1.1543	0.11695	-0.01662	-0.00185	-0.17462	-0.00039	0.15233	-0.02374	1.6484
5.6704	0.255	0.039224	1.33E+05	2.1952	30.264	1.2228	0.13292	-0.01974	-0.00367	-0.21082	-0.00054	0.17303	-0.02814	1.743
6.7403	0.255	0.039197	1.33E+05	2.1922	30.244	1.2816	0.15807	-0.02144	-0.00444	-0.258	-0.00063	0.20698	-0.03052	1.8243
7.8025	0.255	0.039203	1.33E+05	2.1928	30.248	1.3251	0.18475	-0.02355	-0.00597	-0.29821	-0.00066	0.24379	-0.03353	1.8867
8.8599	0.255	0.039151	1.33E+05	2.187	30.208	1.3552	0.21167	-0.02723	-0.00856	-0.33135	-0.00063	0.28049	-0.03867	1.9245

Tail 1 Alpha Sweeps

Table 22. Tail 1 δe=0º, δrn=0º

ALPHA(α) [Degrees]	BETA(β) [Degrees]	MACH #	Re	Dynamic pressure (qc) [lbf/ft^2]	U∞ [mph]	C_L	C_D	C_Y	$C_{l\,eg}$	C_{meg}	C_{neg}	Drag (D) [lbf]	Side Force(S) [lbf]	Lift(L) [lbf]
-8.249	0.255	0.039297	1.34E+05	2.2087	30.323	0.027247	0.080409	0.003363	0.001985	0.055422	0.000853	0.11531	0.004823	0.039077
-7.347	0.255	0.039348	1.34E+05	2.2145	30.364	0.099611	0.075338	0.00166	0.002063	0.049666	0.000794	0.10823	0.002387	0.14324
-6.2568	0.255	0.039355	1.34E+05	2.2153	30.368	0.20631	0.07144	0.00073	0.001946	0.042221	0.000774	0.10229	0.00105	0.29677
-6.1688	0.255	0.039367	1.34E+05	2.2166	30.378	0.20865	0.07061	8.76E-05	0.001801	0.041996	0.000757	0.10115	0.000126	0.30031
-5.0787	0.255	0.039341	1.34E+05	2.2137	30.358	0.31298	0.067999	-0.00088	0.001682	0.036896	0.000702	0.096659	-0.00126	0.44989
-3.9881	0.255	0.039338	1.34E+05	2.2134	30.356	0.42076	0.06698	-0.00213	0.001786	0.032987	0.000657	0.094305	-0.00306	0.60474
-2.9884	0.255	0.039373	1.34E+05	2.2173	30.382	0.51731	0.067781	-0.00354	0.001267	0.027901	0.000572	0.094617	-0.0051	0.74479
-2.9005	0.255	0.039376	1.34E+05	2.2176	30.385	0.51943	0.06759	-0.00344	0.001297	0.027598	0.000564	0.094333	-0.00495	0.74797
-1.8114	0.255	0.039337	1.34E+05	2.2132	30.355	0.62369	0.070428	-0.00546	0.000774	0.020185	0.000444	0.096903	-0.00785	0.89633
-0.72459	0.255	0.039286	1.33E+05	2.2075	30.315	0.72055	0.074612	-0.00718	0.000744	0.011474	0.000362	0.10121	-0.01029	1.0329
0.27532	0.255	0.039254	1.33E+05	2.2039	30.29	0.8199	0.080013	-0.00923	0.000248	0.000332	0.000259	0.10708	-0.01321	1.1733
1.3615	0.255	0.03923	1.33E+05	2.2013	30.272	0.91538	0.087626	-0.01144	-0.0002	-0.01407	0.000136	0.11601	-0.01636	1.3084
2.3542	0.255	0.039229	1.33E+05	2.2011	30.271	0.99842	0.095801	-0.01265	-0.0005	-0.02932	4.06E-05	0.12594	-0.01808	1.427
2.443	0.255	0.039222	1.33E+05	2.2003	30.266	1.0024	0.096511	-0.01299	-0.00066	-0.03035	2.38E-05	0.12682	-0.01856	1.4323
3.4382	0.255	0.039226	1.33E+05	2.2007	30.269	1.089	0.10681	-0.01491	-0.00137	-0.04834	-0.00016	0.13957	-0.02131	1.5562
3.5254	0.255	0.039243	1.33E+05	2.2027	30.282	1.0917	0.1071	-0.01542	-0.00137	-0.04904	-0.00015	0.14004	-0.02206	1.5614
4.5185	0.255	0.039239	1.33E+05	2.2022	30.279	1.1734	0.1203	-0.01769	-0.00266	-0.07327	-0.00044	0.15684	-0.0253	1.678
4.606	0.255	0.03925	1.33E+05	2.2035	30.288	1.1744	0.12099	-0.01763	-0.0025	-0.07394	-0.00044	0.15789	-0.02523	1.6803
5.5946	0.255	0.039262	1.33E+05	2.2048	30.297	1.2481	0.13721	-0.02129	-0.00426	-0.10425	-0.00058	0.17924	-0.03047	1.7869
6.6661	0.255	0.039245	1.33E+05	2.2029	30.284	1.3105	0.16206	-0.02359	-0.00524	-0.14769	-0.00059	0.21287	-0.03375	1.8746
7.6413	0.255	0.039225	1.33E+05	2.2007	30.268	1.3538	0.18764	-0.02561	-0.0065	-0.18718	-0.00068	0.24794	-0.0366	1.9346
7.7299	0.255	0.039218	1.33E+05	2.1998	30.263	1.3575	0.18845	-0.02648	-0.0069	-0.18729	-0.00058	0.24889	-0.03782	1.9391
8.6987	0.255	0.039221	1.33E+05	2.2002	30.265	1.3843	0.21364	-0.02927	-0.00896	-0.21754	-0.00065	0.28412	-0.04182	1.9777
9.7549	0.255	0.03922	1.33E+05	2.2001	30.265	1.4142	0.24326	-0.03061	-0.01125	-0.2432	-0.00079	0.32549	-0.04372	2.0204
10.806	0.255	0.039235	1.33E+05	2.2018	30.276	1.4307	0.28098	-0.03071	-0.01351	-0.27372	-0.00133	0.37915	-0.04391	2.0454

Table 23. Tail 1 δe=0º, δrn=20º

ALPHA(α) [Degrees]	BETA(β) [Degrees]	MACH #	Re	Dynamic pressure (qc) [lbf/ft^2]	U∞ [mph]	C_L	C_D	C_Y	$C_{l\,cg}$	C_{mcg}	C_{ncg}	Drag (D) [lbf]	Side Force(S) [lbf]	Lift(L) [lbf]
-8.2486	0.255	0.039259	1.33E+05	2.1991	30.291	0.027983	0.081258	-0.00415	0.003001	0.061932	0.002532	0.11602	-0.00593	0.039959
-7.3467	0.255	0.039293	1.33E+05	2.203	30.318	0.10021	0.07619	-0.00363	0.003408	0.057604	0.002254	0.10888	-0.00519	0.14335
-7.257	0.255	0.039296	1.33E+05	2.2032	30.32	0.10644	0.075599	-0.00393	0.00319	0.057714	0.002199	0.10803	-0.00563	0.15228
-6.167	0.255	0.0393	1.33E+05	2.2038	30.324	0.21279	0.071392	-0.00361	0.002973	0.052157	0.001769	0.10166	-0.00516	0.30451
-5.0783	0.255	0.039309	1.33E+05	2.2047	30.33	0.31392	0.068188	-0.00323	0.00306	0.047785	0.00144	0.09653	-0.00462	0.44942
-3.9882	0.255	0.039302	1.33E+05	2.2039	30.325	0.42051	0.067326	-0.0037	0.003122	0.042916	0.00111	0.094398	-0.0053	0.60178
-2.9876	0.255	0.039297	1.33E+05	2.2034	30.321	0.51904	0.067994	-0.00353	0.002677	0.036491	0.000753	0.094311	-0.00505	0.74262
-2.8093	0.255	0.039292	1.33E+05	2.2028	30.317	0.52889	0.068086	-0.004	0.002711	0.035661	0.000754	0.094302	-0.00573	0.75651
-1.7218	0.255	0.039298	1.33E+05	2.2035	30.322	0.62962	0.070282	-0.00516	0.002344	0.027173	0.000411	0.096188	-0.00739	0.90089
-0.72286	0.255	0.039303	1.33E+05	2.2041	30.326	0.72445	0.074116	-0.00607	0.002181	0.017033	7.65E-05	0.10028	-0.00868	1.0368
0.36262	0.255	0.039273	1.33E+05	2.2007	30.302	0.82058	0.079478	-0.00765	0.001691	0.00417	-0.00026	0.10615	-0.01093	1.1726
1.4476	0.255	0.039242	1.33E+05	2.1972	30.279	0.91556	0.087265	-0.0084	0.001217	-0.01223	-0.00069	0.11528	-0.01198	1.3063
2.5337	0.255	0.039245	1.33E+05	2.1976	30.281	1.0109	0.096488	-0.00913	0.000709	-0.03073	-0.00111	0.12644	-0.01303	1.4426
3.6145	0.255	0.039266	1.33E+05	2.1999	30.297	1.0964	0.10731	-0.01063	-0.00015	-0.05069	-0.00153	0.14005	-0.01519	1.5662
4.6062	0.255	0.039273	1.33E+05	2.2007	30.302	1.1749	0.12118	-0.01328	-0.00128	-0.07061	-0.00168	0.15796	-0.01897	1.6789
4.6934	0.255	0.039264	1.33E+05	2.1997	30.296	1.1754	0.12126	-0.0138	-0.00147	-0.07128	-0.0017	0.15799	-0.01972	1.6789
5.68	0.255	0.039267	1.33E+05	2.2001	30.298	1.2446	0.13841	-0.01704	-0.00315	-0.09967	-0.00183	0.18066	-0.02434	1.778
6.7504	0.255	0.03924	1.33E+05	2.1971	30.277	1.3044	0.16381	-0.01778	-0.00427	-0.14767	-0.00233	0.21498	-0.02537	1.861
7.8128	0.255	0.039247	1.33E+05	2.1978	30.282	1.3482	0.19038	-0.02044	-0.00602	-0.1827	-0.00234	0.25168	-0.02917	1.9241
8.8694	0.255	0.039226	1.33E+05	2.1954	30.266	1.3768	0.21767	-0.0223	-0.00849	-0.21743	-0.00268	0.28947	-0.03179	1.9627

Table 24. Tail 1 δe=0º, δrn=-20º

ALPHA(α) [Degrees]	BETA(β) [Degrees]	MACH #	Re	Dynamic pressure (qc) [lbf/ft^2]	U∞ [mph]	C_L	C_D	C_Y	$C_{l\,cg}$	C_{mcg}	C_{ncg}	Drag (D) [lbf]	Side Force(S) [lbf]	Lift(L) [lbf]
-8.2479	0.255	0.039233	1.33E+05	2.2	30.274	0.029614	0.079857	0.008821	0.003605	0.05757	-0.00131	0.11407	0.012601	0.042305
-7.3447	0.255	0.039278	1.33E+05	2.2051	30.309	0.10472	0.074631	0.006581	0.003572	0.052399	-0.00093	0.10674	0.009423	0.14995
-7.2544	0.255	0.039279	1.33E+05	2.2052	30.31	0.11215	0.074218	0.006319	0.00354	0.051791	-0.0009	0.10614	0.009048	0.16059
-7.1648	0.255	0.039253	1.33E+05	2.2023	30.29	0.11804	0.073578	0.005711	0.00348	0.051939	-0.00089	0.10506	0.008167	0.1688
-6.1656	0.255	0.039269	1.33E+05	2.2041	30.303	0.21592	0.070291	0.003986	0.003575	0.046076	-0.00048	0.10009	0.005704	0.30903
-6.078	0.255	0.039275	1.33E+05	2.2048	30.307	0.21726	0.069548	0.003793	0.003648	0.045673	-0.00046	0.099046	0.00543	0.31104
-5.0772	0.255	0.039282	1.33E+05	2.2055	30.312	0.31634	0.067599	0.00185	0.003776	0.041188	-9.88E-05	0.095706	0.002649	0.45305
-3.9878	0.255	0.039309	1.33E+05	2.2086	30.333	0.4214	0.066943	-0.00053	0.0035	0.036766	0.000163	0.094042	-0.00077	0.60434
-2.809	0.255	0.039294	1.33E+05	2.2069	30.321	0.52957	0.067509	-0.00319	0.003044	0.030069	0.000377	0.093642	-0.00457	0.75888
-1.7214	0.255	0.039237	1.33E+05	2.2005	30.277	0.63054	0.070416	-0.00601	0.002682	0.021928	0.000524	0.096233	-0.00859	0.90094
-0.72232	0.255	0.039246	1.33E+05	2.2015	30.284	0.72568	0.074001	-0.00894	0.002422	0.012543	0.000666	0.099978	-0.01278	1.0374
0.36179	0.255	0.039236	1.33E+05	2.2004	30.277	0.81871	0.079272	-0.01151	0.002245	0.000239	0.000869	0.10588	-0.01644	1.1698
1.4473	0.255	0.039167	1.33E+05	2.1926	30.223	0.915	0.087394	-0.01449	0.001784	-0.01533	0.001067	0.11524	-0.02064	1.3027
2.5326	0.255	0.039204	1.33E+05	2.1968	30.252	1.0083	0.096629	-0.01763	0.001346	-0.03417	0.001328	0.12665	-0.02514	1.4382
3.6148	0.255	0.039186	1.33E+05	2.1947	30.238	1.097	0.10748	-0.02017	0.000815	-0.05352	0.001348	0.13994	-0.02874	1.5634
4.6943	0.255	0.039178	1.33E+05	2.1939	30.232	1.1775	0.12116	-0.02335	-0.00053	-0.07742	0.001143	0.15737	-0.03327	1.6774
5.6818	0.255	0.039184	1.33E+05	2.1945	30.237	1.2488	0.13802	-0.02739	-0.00213	-0.11086	0.001209	0.17954	-0.03903	1.7795
6.7537	0.255	0.039174	1.33E+05	2.1934	30.229	1.3118	0.16394	-0.03063	-0.00272	-0.15929	0.001574	0.21459	-0.04363	1.8683
7.8171	0.255	0.039187	1.33E+05	2.1949	30.239	1.3581	0.19092	-0.03456	-0.00395	-0.20244	0.001978	0.25183	-0.04925	1.9355
8.8749	0.255	0.039183	1.33E+05	2.1945	30.236	1.3892	0.21783	-0.03846	-0.00636	-0.23739	0.002102	0.28919	-0.0548	1.9795

Table 25. Tail 1 δe=8º, δrn=0º

ALPHA(α) [Degrees]	BETA(β) [Degrees]	MACH #	Re	Dynamic pressure (qc) [lbf/ft^2]	U∞ [mph]	C_L	C_D	C_Y	$C_{l\,cg}$	C_{mcg}	C_{ncg}	Drag (D) [lbf]	Side Force(S) [lbf]	Lift(L) [lbf]
-8.2302	0.255	0.039174	1.33E+05	2.1897	30.226	0.069774	0.078521	0.002962	0.003419	-0.01511	0.00033	0.11159	0.004211	0.099207
-7.3287	0.255	0.039211	1.33E+05	2.1938	30.255	0.14104	0.074494	0.001751	0.003781	-0.0193	0.000409	0.1059	0.002494	0.20092
-7.2387	0.255	0.039224	1.33E+05	2.1952	30.265	0.14778	0.074148	0.001649	0.003629	-0.02009	0.00041	0.10545	0.002351	0.21066
-6.1496	0.255	0.039231	1.33E+05	2.196	30.27	0.25206	0.071127	0.000838	0.003537	-0.02708	0.000352	0.10072	0.001195	0.35942
-5.0573	0.255	0.039178	1.33E+05	2.1901	30.229	0.36139	0.069501	-0.00036	0.003334	-0.03251	0.000282	0.097407	-0.00052	0.51394
-3.9691	0.255	0.039194	1.33E+05	2.1918	30.241	0.46363	0.069318	-0.00176	0.003532	-0.03589	0.000332	0.096296	-0.0025	0.65985
-2.7896	0.255	0.03926	1.33E+05	2.1992	30.292	0.5734	0.070907	-0.00356	0.003106	-0.04411	0.000282	0.097637	-0.00508	0.81882
-1.7038	0.255	0.039238	1.33E+05	2.1968	30.275	0.67038	0.07357	-0.00552	0.002899	-0.04811	0.00023	0.1	-0.00787	0.95626
-0.70432	0.255	0.039209	1.33E+05	2.1936	30.253	0.76641	0.077715	-0.00726	0.002548	-0.05485	0.000102	0.10424	-0.01034	1.0916
0.38096	0.255	0.039217	1.33E+05	2.1944	30.259	0.8621	0.083777	-0.00903	0.002312	-0.06491	3.94E-05	0.11121	-0.01287	1.2284
1.4652	0.255	0.039217	1.33E+05	2.1944	30.259	0.95549	0.092145	-0.01103	0.001604	-0.08123	-0.00018	0.12126	-0.01572	1.3615
2.5506	0.255	0.039225	1.33E+05	2.1953	30.265	1.0491	0.10228	-0.01266	0.001058	-0.10008	-0.00041	0.1337	-0.01805	1.4954
3.6314	0.255	0.039226	1.33E+05	2.1955	30.266	1.1347	0.11411	-0.01445	0.000351	-0.11859	-0.00065	0.14853	-0.02061	1.6177
4.6231	0.255	0.039215	1.33E+05	2.1942	30.258	1.2131	0.12733	-0.01778	-0.00088	-0.13661	-0.00074	0.16525	-0.02533	1.7284
5.6983	0.255	0.039208	1.33E+05	2.1934	30.252	1.2861	0.14603	-0.02113	-0.00251	-0.17215	-0.00088	0.18981	-0.0301	1.8317
6.7682	0.255	0.039233	1.33E+05	2.1962	30.271	1.3447	0.17233	-0.02277	-0.00341	-0.21967	-0.00107	0.22587	-0.03247	1.9176
7.8313	0.255	0.039191	1.33E+05	2.1915	30.239	1.3901	0.1993	-0.02563	-0.00515	-0.25224	-0.00106	0.2624	-0.03647	1.9782
8.8912	0.255	0.039179	1.33E+05	2.1902	30.23	1.4261	0.22863	-0.02884	-0.0074	-0.29433	-0.0011	0.30284	-0.04101	2.0281

Table 26. Tail 1 δe=8º, δrn=20º

ALPHA(α) [Degrees]	BETA(β) [Degrees]	MACH #	Re	Dynamic pressure (qc) [lbf/ft^2]	U∞ [mph]	C_L	C_D	C_Y	$C_{l\,cg}$	C_{mcg}	C_{ncg}	Drag (D) [lbf]	Side Force(S) [lbf]	Lift(L) [lbf]
-8.2279	0.085	0.039183	1.35E+05	2.2233	30.236	0.074855	0.077368	0.018884	0.005413	-0.03481	-0.00339	0.11163	0.027262	0.10806
-7.3253	0.085	0.039562	1.36E+05	2.2665	30.528	0.14867	0.072822	0.018515	0.005251	-0.03569	-0.00353	0.10692	0.027249	0.2188
-7.2362	0.085	0.039754	1.37E+05	2.2885	30.676	0.15341	0.071244	0.018266	0.005274	-0.03557	-0.00353	0.1056	0.027144	0.22797
-6.0579	0.085	0.039729	1.37E+05	2.2857	30.657	0.26275	0.068965	0.01815	0.004775	-0.03888	-0.004	0.10157	0.026938	0.38996
-5.0546	0.085	0.039693	1.37E+05	2.2816	30.63	0.3674	0.06819	0.018322	0.005083	-0.04067	-0.00423	0.099484	0.027145	0.54432
-3.9641	0.085	0.039718	1.37E+05	2.2844	30.648	0.47495	0.069119	0.01786	0.00497	-0.04448	-0.0046	0.099946	0.026492	0.70451
-2.7834	0.085	0.039696	1.37E+05	2.2819	30.632	0.58738	0.071791	0.017023	0.004526	-0.05551	-0.00523	0.10243	0.025224	0.87035
-1.6941	0.085	0.039682	1.36E+05	2.2803	30.621	0.69218	0.075839	0.015314	0.004133	-0.06353	-0.00552	0.10682	0.022675	1.0249
-0.69308	0.085	0.039711	1.37E+05	2.2836	30.643	0.79185	0.08173	0.013037	0.00354	-0.07149	-0.00572	0.11402	0.019331	1.1742
0.39237	0.085	0.039715	1.37E+05	2.2841	30.647	0.88792	0.089071	0.010595	0.003162	-0.08253	-0.00586	0.12309	0.015714	1.3169
1.4802	0.085	0.039697	1.37E+05	2.2821	30.633	0.98933	0.099004	0.008521	0.002515	-0.09916	-0.00621	0.13552	0.012627	1.466
2.5673	0.085	0.039691	1.37E+05	2.2814	30.628	1.0869	0.11048	0.006327	0.001577	-0.11679	-0.00659	0.15017	0.009373	1.6101
3.6495	0.085	0.039726	1.37E+05	2.2853	30.655	1.1757	0.12472	0.004648	0.000781	-0.14116	-0.00705	0.16927	0.006898	1.7446
4.733	0.085	0.039689	1.37E+05	2.2811	30.626	1.2649	0.145	0.003482	-0.00067	-0.17879	-0.00794	0.1965	0.005157	1.8736
5.721	0.085	0.039666	1.36E+05	2.2785	30.609	1.3373	0.16903	1.31E-05	-0.00289	-0.21935	-0.00845	0.22967	1.95E-05	1.9785
6.7884	0.085	0.039667	1.36E+05	2.2786	30.609	1.3904	0.19607	-0.00284	-0.00485	-0.25935	-0.00889	0.26804	-0.00421	2.0572
7.8487	0.085	0.039672	1.36E+05	2.2792	30.614	1.4296	0.22576	-0.00552	-0.00656	-0.29491	-0.00902	0.3108	-0.00817	2.1158
8.9025	0.085	0.039704	1.37E+05	2.2828	30.638	1.4516	0.25294	-0.00739	-0.00787	-0.31378	-0.00884	0.35084	-0.01095	2.1517
9.9535	0.085	0.039669	1.36E+05	2.2788	30.611	1.4698	0.28748	-0.00838	-0.01022	-0.33959	-0.009	0.40074	-0.0124	2.1749
10.91	0.085	0.039602	1.36E+05	2.2711	30.559	1.4682	0.32923	-0.00997	-0.01084	-0.3869	-0.00908	0.46099	-0.0147	2.1651

Table 27. Tail 1 δe=8º, δrn=-20º

ALPHA(α) [Degrees]	BETA(β) [Degrees]	MACH #	Re	Dynamic pressure (qc) [lbf/ft^2]	U∞ [mph]	C_L	C_D	C_Y	$C_{l\,cg}$	C_{mcg}	C_{ncg}	Drag (D) [lbf]	Side Force(S) [lbf]	Lift(L) [lbf]
-8.2306	0.085	0.039638	1.36E+05	2.2745	30.616	0.068815	0.076879	-0.00717	0.004921	-0.0435	0.004191	0.11349	-0.01059	0.10163
-7.3269	0.085	0.039618	1.36E+05	2.2721	30.6	0.14509	0.07383	-0.01006	0.004887	-0.04823	0.004638	0.10869	-0.01484	0.21407
-7.2366	0.085	0.039633	1.36E+05	2.2738	30.611	0.15248	0.073275	-0.01021	0.004816	-0.0489	0.004744	0.10793	-0.01508	0.22513
-6.0582	0.085	0.039684	1.36E+05	2.2798	30.651	0.26202	0.071771	-0.01386	0.004788	-0.0562	0.005385	0.10546	-0.02052	0.38788
-5.0551	0.085	0.039706	1.36E+05	2.2823	30.668	0.36641	0.071489	-0.01671	0.004858	-0.06248	0.005776	0.10441	-0.02477	0.54301
-3.965	0.085	0.039684	1.36E+05	2.2798	30.651	0.4729	0.072535	-0.01886	0.005128	-0.06594	0.00609	0.10482	-0.02792	0.70004
-2.7848	0.085	0.039676	1.36E+05	2.2788	30.645	0.58423	0.075443	-0.02329	0.00497	-0.07583	0.006583	0.10774	-0.03446	0.86448
-1.6914	0.085	0.03967	1.36E+05	2.2781	30.64	0.69824	0.082894	-0.03025	0.004817	-0.10375	0.007729	0.11706	-0.04474	1.0329
-0.68849	0.085	0.03966	1.36E+05	2.277	30.632	0.80224	0.089431	-0.03407	0.004553	-0.11554	0.007994	0.12489	-0.05037	1.1861
0.39787	0.085	0.039706	1.36E+05	2.2822	30.668	0.90035	0.097205	-0.03792	0.00432	-0.12972	0.008243	0.13479	-0.0562	1.3343
1.4834	0.085	0.039719	1.36E+05	2.2838	30.678	0.99652	0.10725	-0.04163	0.004073	-0.14613	0.008523	0.14768	-0.06174	1.4778
2.5724	0.085	0.039682	1.36E+05	2.2795	30.65	1.0985	0.11961	-0.04565	0.003666	-0.16629	0.008769	0.16328	-0.06757	1.626
3.6551	0.085	0.039673	1.36E+05	2.2785	30.643	1.1882	0.13362	-0.04861	0.003329	-0.18887	0.008787	0.18158	-0.07192	1.758
4.7355	0.085	0.039692	1.36E+05	2.2807	30.657	1.2707	0.15101	-0.05172	0.002177	-0.21262	0.008572	0.20519	-0.07659	1.8818
5.7213	0.085	0.039688	1.36E+05	2.2802	30.654	1.3381	0.1727	-0.05615	0.000847	-0.24454	0.008523	0.23526	-0.08314	1.9813
6.7928	0.085	0.03963	1.36E+05	2.2735	30.609	1.4004	0.20243	-0.06322	5.98E-05	-0.29407	0.009505	0.27652	-0.09333	2.0674
7.8535	0.085	0.039689	1.36E+05	2.2803	30.655	1.4403	0.23358	-0.06677	-0.00065	-0.33644	0.009805	0.32216	-0.09887	2.1326
8.9063	0.085	0.039812	1.37E+05	2.2944	30.75	1.4603	0.26179	-0.06773	-0.00158	-0.36249	0.009735	0.36553	-0.10091	2.1757

Table 28. Tail 1 δe=-9º, δrn=0º

ALPHA(α) [Degrees]	BETA(β) [Degrees]	MACH #	Re	Dynamic pressure (qc) [lbf/ft^2]	U∞ [mph]	C_L	C_D	C_Y	$C_{l\,cg}$	C_{mcg}	C_{ncg}	Drag (D) [lbf]	Side Force(S) [lbf]	Lift(L) [lbf]
-8.2688	0.255	0.039286	1.33E+05	2.2075	30.315	-0.01765	0.092627	0.003365	0.003253	0.13628	0.00079	0.13277	0.004824	-0.02529
-7.3655	0.255	0.039314	1.34E+05	2.2107	30.337	0.057629	0.085236	0.001338	0.002793	0.12703	0.000705	0.12232	0.00192	0.082725
-6.2755	0.255	0.0393	1.34E+05	2.2091	30.326	0.16402	0.079683	0.000489	0.002752	0.11518	0.000639	0.114	0.000702	0.23528
-6.1869	0.255	0.039311	1.34E+05	2.2103	30.334	0.16767	0.078991	0.000308	0.002764	0.11493	0.000618	0.11306	0.000442	0.24064
-5.0967	0.255	0.03933	1.34E+05	2.2125	30.35	0.27216	0.074704	-0.0005	0.002902	0.10558	0.000596	0.1065	-0.00072	0.391
-4.0071	0.255	0.039336	1.34E+05	2.2131	30.354	0.37779	0.072988	-0.00128	0.00302	0.098194	0.000505	0.10331	-0.00185	0.5429
-2.9146	0.255	0.039337	1.34E+05	2.2133	30.355	0.48749	0.073499	-0.00263	0.002798	0.089217	0.000426	0.103	-0.00379	0.70062
-2.8276	0.255	0.039326	1.34E+05	2.2121	30.347	0.4875	0.072828	-0.00259	0.002638	0.088846	0.000411	0.10198	-0.00372	0.70023
-1.7391	0.255	0.039327	1.34E+05	2.2121	30.347	0.59034	0.074445	-0.00433	0.002188	0.07764	0.000262	0.10307	-0.00623	0.84799
-0.73944	0.255	0.039319	1.34E+05	2.2112	30.341	0.68694	0.077908	-0.00607	0.002033	0.066074	0.000174	0.10664	-0.00871	0.98632
0.34489	0.255	0.039334	1.34E+05	2.2128	30.352	0.78046	0.082203	-0.00804	0.001582	0.051571	7.98E-05	0.11137	-0.01156	1.1214
1.4303	0.255	0.039303	1.34E+05	2.2094	30.329	0.87639	0.089355	-0.01001	0.001132	0.033645	-5.65E-05	0.1197	-0.01436	1.2573
2.5184	0.255	0.039234	1.33E+05	2.2017	30.275	0.97614	0.097735	-0.01192	0.000489	0.012977	-0.00019	0.12922	-0.01704	1.3955
3.6018	0.255	0.039206	1.33E+05	2.1985	30.253	1.0676	0.10829	-0.01404	-0.00029	-0.00963	-0.00039	0.14205	-0.02005	1.524
4.5945	0.255	0.039229	1.33E+05	2.2011	30.271	1.1484	0.12084	-0.0166	-0.00145	-0.03532	-0.00065	0.15817	-0.02373	1.6414
5.669	0.255	0.039215	1.33E+05	2.1995	30.26	1.2198	0.13729	-0.01979	-0.00323	-0.06487	-0.00077	0.17969	-0.02827	1.7422
6.7416	0.255	0.039209	1.33E+05	2.1989	30.256	1.2843	0.16303	-0.02163	-0.00398	-0.1145	-0.00083	0.21462	-0.03089	1.8338
7.8027	0.255	0.039239	1.33E+05	2.2023	30.279	1.3254	0.1888	-0.0243	-0.00573	-0.15084	-0.00087	0.25061	-0.03475	1.8953
8.8601	0.255	0.039233	1.33E+05	2.2015	30.274	1.3558	0.21608	-0.02742	-0.00822	-0.18553	-0.00088	0.28863	-0.0392	1.9381

Table 29. Tail 1 δe=-9º, δrn=20º

ALPHA(α) [Degrees]	BETA(β) [Degrees]	MACH #	Re	Dynamic pressure (qc) [lbf/ft^2]	U∞ [mph]	C_L	C_D	C_Y	$C_{l\,cg}$	C_{mcg}	C_{ncg}	Drag (D) [lbf]	Side Force(S) [lbf]	Lift(L) [lbf]
-8.268	0.255	0.039296	1.33E+05	2.2056	30.323	-0.01587	0.094725	-0.01844	0.002818	0.14896	0.006968	0.13566	-0.02641	-0.02273
-7.3637	0.255	0.039316	1.33E+05	2.2078	30.338	0.061869	0.08789	-0.0186	0.002623	0.14126	0.006547	0.12596	-0.02666	0.088697
-7.2733	0.255	0.039352	1.34E+05	2.2119	30.366	0.069419	0.087393	-0.01863	0.002527	0.14012	0.006492	0.12546	-0.02675	0.099703
-6.1835	0.255	0.03937	1.34E+05	2.2139	30.38	0.17537	0.08184	-0.0177	0.002669	0.13232	0.006001	0.11731	-0.02544	0.2521
-5.0946	0.255	0.039354	1.34E+05	2.212	30.367	0.2769	0.078331	-0.01719	0.003249	0.12768	0.005705	0.11166	-0.02469	0.39773
-4.0058	0.255	0.039347	1.33E+05	2.2113	30.362	0.38066	0.076305	-0.01768	0.003082	0.12209	0.005389	0.10796	-0.02538	0.54658
-2.8267	0.255	0.039342	1.33E+05	2.2107	30.358	0.48958	0.076319	-0.0185	0.002826	0.11492	0.005112	0.1069	-0.02656	0.70279
-1.7407	0.255	0.039334	1.33E+05	2.2098	30.352	0.58685	0.077624	-0.01914	0.002767	0.10644	0.004809	0.10757	-0.02746	0.84208
-0.74155	0.255	0.039344	1.33E+05	2.211	30.36	0.68215	0.080472	-0.02008	0.002508	0.095645	0.00444	0.11038	-0.02882	0.97934
0.34325	0.255	0.039323	1.33E+05	2.2086	30.344	0.77675	0.084669	-0.0215	0.002236	0.081909	0.004108	0.11475	-0.03083	1.1139
1.4294	0.255	0.039264	1.33E+05	2.202	30.299	0.87435	0.091337	-0.02244	0.001739	0.06439	0.003624	0.12217	-0.03209	1.2502
2.5163	0.255	0.039252	1.33E+05	2.2007	30.289	0.97159	0.099424	-0.02324	0.001	0.044108	0.003108	0.13167	-0.03321	1.3884
3.597	0.255	0.039278	1.33E+05	2.2036	30.309	1.0569	0.10921	-0.02369	0.000493	0.021199	0.002535	0.14395	-0.0339	1.5122
4.6774	0.255	0.039253	1.33E+05	2.2007	30.29	1.1392	0.12289	-0.02546	-0.00065	-0.00487	0.002058	0.16131	-0.03638	1.6279
5.6648	0.255	0.039239	1.33E+05	2.1992	30.279	1.2102	0.1396	-0.02772	-0.00235	-0.03837	0.00168	0.18322	-0.03959	1.7282
6.7345	0.255	0.039272	1.33E+05	2.2029	30.305	1.2684	0.16389	-0.02767	-0.00326	-0.08761	0.001127	0.21669	-0.03958	1.8143
7.7998	0.255	0.039258	1.33E+05	2.2013	30.294	1.3189	0.19022	-0.02888	-0.00522	-0.13089	0.00051	0.25272	-0.04127	1.8853
8.8562	0.255	0.039237	1.33E+05	2.1989	30.277	1.347	0.21737	-0.03149	-0.00759	-0.16606	0.000238	0.29038	-0.04496	1.9233

Table 30. Tail 1 δe=-9º, δrn=-20º

ALPHA(α) [Degrees]	BETA(β) [Degrees]	MACH #	Re	Dynamic pressure (qc) [lbf/ft^2]	U∞ [mph]	C_L	C_D	C_Y	$C_{l\,cg}$	C_{mcg}	C_{ncg}	Drag (D) [lbf]	Side Force(S) [lbf]	Lift(L) [lbf]
-8.2665	0.255	0.039297	1.33E+05	2.2072	30.324	-0.01248	0.095153	0.031047	0.004393	0.15004	-0.00766	0.13638	0.044498	-0.01789
-7.3627	0.255	0.039306	1.33E+05	2.2082	30.331	0.064133	0.089964	0.02854	0.004191	0.14416	-0.00734	0.12895	0.040923	0.091961
-7.2724	0.255	0.039304	1.33E+05	2.208	30.329	0.071527	0.088945	0.02804	0.004211	0.14279	-0.00727	0.12747	0.040203	0.10255
-6.1836	0.255	0.039298	1.33E+05	2.2074	30.325	0.17519	0.084498	0.026543	0.00423	0.13732	-0.00697	0.12077	0.038045	0.2511
-5.0932	0.255	0.039296	1.33E+05	2.2071	30.323	0.28016	0.080713	0.02441	0.003961	0.13221	-0.00676	0.11481	0.034983	0.40151
-4.0048	0.255	0.0393	1.33E+05	2.2076	30.326	0.383	0.078788	0.022364	0.003856	0.12739	-0.00655	0.11132	0.032057	0.54901
-2.8266	0.255	0.039306	1.33E+05	2.2082	30.33	0.48965	0.078933	0.02001	0.003341	0.12045	-0.00638	0.11053	0.028692	0.70209
-1.7395	0.255	0.039335	1.34E+05	2.2115	30.353	0.58943	0.080228	0.016745	0.00284	0.11114	-0.00617	0.11136	0.024046	0.84643
-0.74069	0.255	0.03933	1.34E+05	2.211	30.35	0.68412	0.083438	0.014103	0.002439	0.101	-0.00601	0.11461	0.020248	0.98217
0.34343	0.255	0.039315	1.33E+05	2.2092	30.338	0.77717	0.088009	0.010975	0.001965	0.088109	-0.00577	0.11957	0.015744	1.1149
1.4279	0.255	0.039322	1.33E+05	2.21	30.343	0.8711	0.093932	0.007654	0.001296	0.071647	-0.00551	0.1264	0.010983	1.2501
2.5134	0.255	0.039291	1.33E+05	2.2065	30.319	0.96487	0.10228	0.004222	0.00063	0.051858	-0.00518	0.13626	0.006049	1.3824
3.5958	0.255	0.039264	1.33E+05	2.2035	30.298	1.0541	0.11193	0.000432	-0.00013	0.028593	-0.00485	0.14789	0.000618	1.5082
4.6767	0.255	0.03922	1.33E+05	2.1986	30.265	1.1375	0.12563	-0.00367	-0.0014	-0.0007	-0.00465	0.16511	-0.00523	1.624
5.664	0.255	0.039214	1.33E+05	2.1979	30.26	1.2084	0.14191	-0.00832	-0.00321	-0.03561	-0.00438	0.18645	-0.01188	1.7246
6.7321	0.255	0.039233	1.33E+05	2.2	30.274	1.2629	0.16577	-0.01141	-0.00375	-0.08074	-0.00409	0.21924	-0.01629	1.8041
7.7977	0.255	0.039218	1.33E+05	2.1984	30.263	1.3142	0.19232	-0.01696	-0.00531	-0.12813	-0.00325	0.25552	-0.02421	1.8759
8.8532	0.255	0.039192	1.33E+05	2.1954	30.242	1.34	0.21759	-0.02252	-0.00777	-0.1651	-0.00258	0.29045	-0.03211	1.9102

Tail 1 Beta Sweeps

Table 31. Tail 1 Beta Sweep δe=0º, δrn=0º

ALPHA(α) [Degrees]	BETA(β) [Degrees]	MACH #	Re	Dynamic pressure (qc) [lbf/ft^2]	U∞ [mph]	C_L	C_D	C_Y	$C_{l\,cg}$	C_{mcg}	C_{ncg}	Drag (D) [lbf]	Side Force(S) [lbf]	Lift(L) [lbf]
4.6867	10.106	0.039672	1.36E+05	2.2784	30.628	1.1601	0.14711	-0.07332	-0.01778	-0.08456	-0.0033	0.20228	-0.10847	1.7163
4.6936	9.172	0.039653	1.36E+05	2.2761	30.613	1.1759	0.14584	-0.0695	-0.01654	-0.09969	-0.00293	0.19979	-0.10272	1.7379
4.696	8.153	0.039656	1.36E+05	2.2765	30.615	1.1812	0.14321	-0.06386	-0.01444	-0.10184	-0.00265	0.1958	-0.0944	1.7461
4.6991	7.176	0.03964	1.36E+05	2.2747	30.603	1.1883	0.14155	-0.0592	-0.01277	-0.10214	-0.00237	0.19299	-0.08744	1.7551
4.6993	6.157	0.039654	1.36E+05	2.2763	30.613	1.1886	0.13886	-0.05418	-0.01105	-0.1021	-0.00201	0.18914	-0.08009	1.7569
4.7012	5.138	0.039689	1.36E+05	2.2803	30.641	1.193	0.13646	-0.0493	-0.00947	-0.10367	-0.00167	0.18581	-0.073	1.7664
4.7052	4.119	0.039713	1.36E+05	2.2831	30.659	1.202	0.13445	-0.0445	-0.00797	-0.11158	-0.0013	0.18281	-0.06597	1.782
4.7054	3.1	0.039707	1.36E+05	2.2824	30.655	1.2025	0.13124	-0.03923	-0.0063	-0.10937	-0.00099	0.17798	-0.05815	1.7823
4.7058	2.081	0.039668	1.36E+05	2.2779	30.624	1.2034	0.13051	-0.03372	-0.00455	-0.10897	-0.00063	0.17652	-0.04988	1.7799
4.7046	1.062	0.03971	1.36E+05	2.2827	30.657	1.2008	0.12996	-0.02854	-0.00292	-0.10848	-0.00021	0.17615	-0.04231	1.7798
4.7006	0.042	0.039737	1.37E+05	2.2859	30.678	1.1917	0.12943	-0.02256	-0.00104	-0.10812	0.000136	0.17585	-0.03348	1.7689
4.6992	-0.934	0.039693	1.36E+05	2.2807	30.643	1.1884	0.13081	-0.01704	0.000861	-0.11104	0.000462	0.1776	-0.02523	1.76
4.6953	-1.953	0.039676	1.36E+05	2.2788	30.63	1.1797	0.13315	-0.01146	0.002528	-0.11358	0.000842	0.18114	-0.01696	1.7456
4.691	-2.972	0.03968	1.36E+05	2.2792	30.633	1.1699	0.13534	-0.00552	0.004366	-0.11126	0.001196	0.18468	-0.00817	1.7315
4.6881	-3.949	0.03966	1.36E+05	2.277	30.618	1.1633	0.13702	9.60E-05	0.005946	-0.11036	0.001536	0.18716	0.000142	1.7201
4.6867	-4.926	0.039623	1.36E+05	2.2728	30.59	1.1602	0.13843	0.006486	0.007923	-0.10857	0.001853	0.18897	0.009572	1.7123
4.687	-5.945	0.039584	1.36E+05	2.2682	30.559	1.1608	0.14064	0.012668	0.010331	-0.12271	0.002183	0.19184	0.018658	1.7097
4.683	-6.964	0.039601	1.36E+05	2.2703	30.573	1.1517	0.14285	0.018767	0.012056	-0.12308	0.002441	0.1955	0.027666	1.6978
4.6759	-7.941	0.039623	1.36E+05	2.2727	30.589	1.1357	0.1449	0.024689	0.013663	-0.11905	0.002714	0.19916	0.036434	1.676
4.6726	-8.96	0.039591	1.36E+05	2.2691	30.565	1.1283	0.14751	0.031571	0.015703	-0.11466	0.002714	0.20287	0.046517	1.6625
4.6671	-9.936	0.039587	1.36E+05	2.2686	30.562	1.1159	0.14933	0.038619	0.01771	-0.09956	0.002818	0.20583	0.056889	1.6438

Table 32. Tail 1 Beta Sweep δe=0º, δrn=32º

ALPHA(α) [Degrees]	BETA(β) [Degrees]	MACH #	Re	Dynamic pressure (qc) [lbf/ft^2]	U∞ [mph]	C_L	C_D	C_Y	$C_{l\,cg}$	C_{mcg}	C_{ncg}	Drag (D) [lbf]	Side Force(S) [lbf]	Lift(L) [lbf]
4.6833	10.149	0.039765	1.37E+05	2.2892	30.694	1.1524	0.14605	-0.06938	-0.01719	-0.07801	-0.00444	0.20187	-0.10313	1.7131
4.6892	8.195	0.039794	1.37E+05	2.2926	30.716	1.1659	0.14177	-0.05742	-0.0138	-0.08701	-0.00457	0.19544	-0.08548	1.7356
4.6947	6.2	0.039808	1.37E+05	2.2941	30.727	1.1784	0.13742	-0.04621	-0.01065	-0.09335	-0.00448	0.18875	-0.06883	1.7554
4.6994	4.161	0.039781	1.37E+05	2.2911	30.706	1.189	0.13286	-0.03412	-0.0076	-0.0945	-0.00442	0.18143	-0.05077	1.7689
4.6998	2.166	0.039788	1.37E+05	2.2919	30.711	1.1898	0.1291	-0.02125	-0.00437	-0.09582	-0.00418	0.17587	-0.03162	1.7706
4.6997	2.123	0.039768	1.37E+05	2.2896	30.696	1.1896	0.12927	-0.02195	-0.00434	-0.09538	-0.00413	0.17596	-0.03263	1.7686
4.6958	0.085	0.039752	1.37E+05	2.2877	30.683	1.1808	0.12903	-0.0114	-0.0009	-0.0995	-0.00319	0.1757	-0.01693	1.7541
4.691	-1.911	0.039739	1.37E+05	2.2863	30.674	1.1699	0.13268	0.000105	0.002661	-0.10874	-0.00277	0.1813	0.000156	1.7369
4.6935	-1.868	0.039725	1.37E+05	2.2846	30.662	1.1757	0.13431	0.000371	0.002511	-0.11166	-0.00279	0.18344	0.000551	1.7441
4.6851	-3.907	0.03973	1.37E+05	2.2851	30.666	1.1565	0.13692	0.011909	0.006211	-0.11489	-0.00234	0.18786	0.017671	1.716
4.6865	-5.86	0.039704	1.36E+05	2.2823	30.647	1.1599	0.14193	0.032284	0.009857	-0.14508	-0.00453	0.19495	0.047844	1.7189
4.6793	-7.898	0.039683	1.36E+05	2.2798	30.63	1.1434	0.14732	0.046949	0.01411	-0.14406	-0.0046	0.20316	0.069501	1.6927
4.6715	-9.851	0.039667	1.36E+05	2.278	30.618	1.1258	0.15281	0.059394	0.018465	-0.13233	-0.00436	0.21158	0.087855	1.6653

Table 33. Tail 1 Beta Sweep δe=0º, δrn=-30

ALPHA(α) [Degrees]	BETA(β) [Degrees]	MACH #	Re	Dynamic pressure (qc) [lbf/ft^2]	U∞ [mph]	C_L	C_D	C_Y	$C_{l\,cg}$	C_{mcg}	C_{ncg}	Drag (D) [lbf]	Side Force(S) [lbf]	Lift(L) [lbf]
4.6984	10.234	0.039671	1.36E+05	2.2775	30.621	1.1867	0.15349	-0.09381	-0.01522	-0.13514	0.003062	0.21093	-0.13874	1.7549
4.7018	8.28	0.03968	1.36E+05	2.2786	30.628	1.1943	0.14819	-0.08344	-0.01159	-0.13271	0.003176	0.20298	-0.12345	1.767
4.7037	6.242	0.039701	1.36E+05	2.281	30.644	1.1987	0.14299	-0.07103	-0.00756	-0.12941	0.003239	0.19537	-0.10521	1.7754
4.7045	4.204	0.039745	1.37E+05	2.2859	30.678	1.2004	0.13743	-0.05947	-0.00402	-0.11929	0.003357	0.18751	-0.08827	1.7818
4.7032	2.208	0.039722	1.37E+05	2.2834	30.661	1.1976	0.13265	-0.04848	-0.00058	-0.11294	0.003893	0.18028	-0.07187	1.7757
4.7017	0.127	0.039658	1.36E+05	2.276	30.611	1.1943	0.13241	-0.03775	0.002786	-0.11582	0.004614	0.17943	-0.0558	1.765
4.6979	-1.826	0.039625	1.36E+05	2.2721	30.585	1.1856	0.13631	-0.0269	0.00656	-0.12303	0.005367	0.18512	-0.03969	1.7492
4.6937	-3.864	0.039638	1.36E+05	2.2737	30.595	1.176	0.13949	-0.01991	0.010297	-0.13496	0.006812	0.19019	-0.02939	1.7362
4.6941	-3.822	0.039681	1.36E+05	2.2786	30.629	1.177	0.14059	-0.01771	0.010502	-0.13411	0.006818	0.19222	-0.02621	1.7414
4.6783	-5.775	0.040039	1.38E+05	2.3199	30.905	1.1411	0.13982	-0.00438	0.01406	-0.12864	0.00688	0.1955	-0.0066	1.719
4.6611	-7.771	0.040282	1.38E+05	2.3481	31.092	1.1024	0.14153	0.008913	0.01731	-0.11979	0.006852	0.20151	0.01359	1.6808
4.661	-9.809	0.039904	1.37E+05	2.3044	30.801	1.1021	0.14856	0.024423	0.021655	-0.10651	0.006651	0.20828	0.036545	1.6491

Tail 1 Matrix

Table 34. Tail 1 Matrix δrn=32º

	ALPHA(α) [Degrees]	BETA(β) [Degrees]	MACH #	Re	Dynamic pressure(qc) [lbf/ft^2]	U∞ [mph]	C_L	C_D	C_Y	$C_{l\,cg}$	C_{mcg}	C_{ncg}	Drag (D) [lbf]	Side Force(S) [lbf]	Lift(L) [lbf]
δe=11°	4.7232	0.212	0.039814	1.37E+05	2.2947	30.688	1.2428	0.14581	0.02583	-0.00055	-0.21587	-0.01432	0.1995	0.038487	1.8518
δe=7°	4.7134	0.212	0.0398	1.37E+05	2.2931	30.677	1.2207	0.13705	0.012465	-0.00044	-0.17798	-0.01043	0.18696	0.018561	1.8176
δe=0°	4.6979	0.212	0.039707	1.37E+05	2.2824	30.605	1.1856	0.12883	-0.01052	0.000699	-0.10575	-0.00344	0.17486	-0.01559	1.7571
δe=M12°	4.6743	0.212	0.039632	1.36E+05	2.2738	30.548	1.1322	0.13243	-0.04182	0.002364	-0.00412	0.006428	0.18092	-0.06175	1.6717
δe=M15°	4.6702	0.212	0.039623	1.36E+05	2.2728	30.541	1.123	0.13457	-0.04231	0.002522	0.017501	0.006746	0.18424	-0.06243	1.6573

Table 35. Tail 1 Matrix δrn=17º

	ALPHA(α) [Degrees]	BETA(β) [Degrees]	MACH #	Re	Dynamic pressure (qc) [lbf/ft^2]	U∞ [mph]	C_L	C_D	C_Y	$C_{l\,cg}$	C_{mcg}	C_{ncg}	Drag (D) [lbf]	Side Force(S) [lbf]	Lift(L) [lbf]
δe=11°	4.7317	0.212	0.039793	1.37E+05	2.2923	30.672	1.2621	0.14979	0.008421	0.00010203	-0.24753	-0.00929	0.20468	0.012535	1.8786
δe=7°	4.7186	0.212	0.039803	1.37E+05	2.2934	30.679	1.2325	0.13826	-0.00128	0.00034233	-0.1957	-0.00624	0.18844	-0.00191	1.8354
δe=0°	4.7059	0.212	0.039763	1.37E+05	2.2889	30.649	1.2037	0.13103	-0.01005	0.00076851	-0.14269	-0.00349	0.17814	-0.01493	1.7889
δe=M12°	4.6791	0.212	0.039654	1.37E+05	2.2763	30.565	1.143	0.12941	-0.02792	0.0017702	-0.027917	0.002216	0.17639	-0.04127	1.6894
δe=M15°	4.6722	0.212	0.039628	1.36E+05	2.2733	30.545	1.1274	0.13286	-0.0334	0.0020361	0.003955	0.004064	0.18164	-0.04931	1.6642

Table 36. Tail 1 Matrix δrn=8º

	ALPHA(α) [Degrees]	BETA(β) [Degrees]	MACH #	Re	Dynamic pressure (qc) [lbf/ft^2]	U∞ [mph]	C_L	C_D	C_Y	$C_{l\,cg}$	C_{mcg}	C_{ncg}	Drag (D) [lbf]	Side Force(S) [lbf]	Lift(L) [lbf]
δe=11°	4.7366	0.212	0.039834	1.37E+05	2.297	30.703	1.2732	0.15402	-0.00428	0.000678	-0.27237	-0.0055	0.21107	-0.00638	1.8991
δe=7°	4.719	0.212	0.039819	1.37E+05	2.2953	30.692	1.2334	0.13887	-0.01486	0.001048	-0.20038	-0.00216	0.18948	-0.02215	1.8382
δe=0°	4.705	0.212	0.039731	1.37E+05	2.2851	30.624	1.2017	0.13091	-0.01779	0.001221	-0.13847	-0.00103	0.17772	-0.02639	1.7831
δe=M12°	4.6806	0.212	0.039654	1.37E+05	2.2763	30.565	1.1465	0.12858	-0.02263	0.001431	-0.03906	0.000727	0.17507	-0.03345	1.6946
δe=M15°	4.6708	0.212	0.039636	1.36E+05	2.2743	30.551	1.1241	0.1315	-0.0235	0.001345	0.002595	0.001132	0.1798	-0.03471	1.6601

Table 37. Tail 1 Matrix δrn=0º

	ALPHA(α) [Degrees]	BETA(β) [Degrees]	MACH #	Re	Dynamic pressure (qc) [lbf/ft^2]	U∞ [mph]	C_L	C_D	C_Y	$C_{l\,cg}$	C_{mcg}	C_{ncg}	Drag (D) [lbf]	Side Force(S) [lbf]	Lift(L) [lbf]
δe=11º	4.7375	0.212	0.039862	1.37E+05	2.3002	30.725	1.2752	0.15549	-0.02257	0.001426	-0.27428	-4.66E-05	0.2135	-0.03371	1.9047
δe=7º	4.718	0.212	0.039847	1.37E+05	2.2985	30.713	1.2309	0.13896	-0.02254	0.001111	-0.19927	0.000113	0.18995	-0.03364	1.8372
δe=0º	4.7009	0.212	0.039715	1.37E+05	2.2833	30.612	1.1923	0.12977	-0.02234	0.001263	-0.12557	0.000186	0.17614	-0.03312	1.7677
δe=M12º	4.6816	0.212	0.039662	1.37E+05	2.2773	30.571	1.1488	0.12833	-0.02113	0.00112	-0.0425	9.73E-05	0.17471	-0.03124	1.6987
δe=M15º	4.6716	0.212	0.039613	1.36E+05	2.2716	30.533	1.126	0.13108	-0.02057	0.001144	0.001084	4.48E-05	0.17893	-0.03034	1.6609

Table 38. Tail 1 Matrix δrn=-8º

	ALPHA(α) [Degrees]	BETA(β) [Degrees]	MACH #	Re	Dynamic pressure (qc) [lbf/ft^2]	U∞ [mph]	C_L	C_D	C_Y	$C_{l\,cg}$	C_{mcg}	C_{ncg}	Drag (D) [lbf]	Side Force(S) [lbf]	Lift(L) [lbf]
δe=11º	4.739	0.212	0.039836	1.37E+05	2.2973	30.705	1.2785	0.15809	-0.04406	0.002535	-0.28239	0.006426	0.21702	-0.06573	1.9071
δe=7º	4.7189	0.212	0.039811	1.37E+05	2.2943	30.686	1.233	0.14058	-0.0359	0.001915	-0.20434	0.004131	0.19198	-0.05349	1.837
δe=0º	4.6992	0.212	0.039702	1.37E+05	2.2818	30.602	1.1886	0.12978	-0.02728	0.001499	-0.12345	0.001831	0.17615	-0.04041	1.7611
δe=M12º	4.6752	0.212	0.039654	1.37E+05	2.2763	30.565	1.1342	0.12939	-0.01511	0.000996	-0.02281	-0.00152	0.17658	-0.02233	1.6764
δe=M15º	4.6697	0.212	0.039625	1.36E+05	2.273	30.543	1.1217	0.13235	-0.01049	0.000697	0.005889	-0.00277	0.18102	-0.01549	1.6555

Table 39. Tail 1 Matrix δrn=-18º

	ALPHA(α) [Degrees]	BETA(β) [Degrees]	MACH #	Re	Dynamic pressure(qc) [lbf/ft^2]	U∞ [mph]	C_L	C_D	C_Y	$C_{l\,cg}$	C_{mcg}	C_{ncg}	Drag (D) [lbf]	Side Force(S) [lbf]	Lift(L) [lbf]
δe=11º	4.7281	0.212	0.039839	1.37E+05	2.2976	30.707	1.2538	0.15002	-0.0515	0.002848	-0.24288	0.008685	0.20573	-0.07683	1.8706
δe=7º	4.7133	0.212	0.039831	1.37E+05	2.2967	30.701	1.2204	0.13802	-0.04267	0.002239	-0.18617	0.006266	0.18871	-0.06364	1.82
δe=0º	4.698	0.212	0.039774	1.37E+05	2.2901	30.658	1.1858	0.12987	-0.03174	0.001743	-0.12507	0.003175	0.17699	-0.0472	1.7634
δe=M12º	4.6751	0.212	0.039679	1.37E+05	2.2792	30.584	1.1339	0.12936	-0.01198	0.000757	-0.02469	-0.00249	0.17678	-0.01773	1.6781
δe=M15º	4.6671	0.212	0.039647	1.36E+05	2.2755	30.56	1.1159	0.13346	-0.00225	0.000178	0.011777	-0.00528	0.18302	-0.00333	1.6488

Table 40. Tail Matrix δrn=-30º

	ALPHA(α) [Degrees]	BETA(β) [Degrees]	MACH #	Re	Dynamic pressure (qc) [lbf/ft^2]	U∞ [mph]	C_L	C_D	C_Y	$C_{l\,cg}$	C_{mcg}	C_{ncg}	Drag (D) [lbf]	Side Force(S) [lbf]	Lift(L) [lbf]
δe=11º	4.7215	0.212	0.039794	1.37E+05	2.2924	30.673	1.239	0.14804	-0.0716	0.003962	-0.21733	0.014943	0.20274	-0.10658	1.8443
δe=7º	4.7084	0.212	0.039808	1.37E+05	2.294	30.684	1.2093	0.1367	-0.05479	0.002946	-0.16736	0.010074	0.18684	-0.08161	1.8013
δe=0º	4.688	0.212	0.039666	1.37E+05	2.2777	30.574	1.1632	0.12899	-0.02248	0.001377	-0.07406	0.000795	0.17534	-0.03324	1.7203
δe=M12º	4.6724	0.212	0.039659	1.37E+05	2.2768	30.568	1.1279	0.13181	0.000679	0.000117	-0.01077	-0.00605	0.18037	0.001004	1.6675
δe=M15º	4.6732	0.212	0.03963	1.36E+05	2.2736	30.547	1.1297	0.13237	0.003139	7.76E-05	-0.01035	-0.00676	0.18089	0.004634	1.6677

Table 41. Coefficients of Lift For Tail 1 Matrix

C_L						
		δe				
		11°	7°	0°	-12°	-15°
δrn	32°	1.2428	1.2207	1.1856	1.1322	1.123
	17°	1.2621	1.2325	1.2037	1.143	1.1274
	8°	1.2732	1.2334	1.2017	1.1465	1.1241
	0°	1.2752	1.2309	1.1923	1.1488	1.126
	-8°	1.2785	1.233	1.1886	1.1342	1.1217
	-18°	1.2538	1.2204	1.1858	1.1339	1.1159
	-30°	1.239	1.2093	1.1632	1.1279	1.1297

Table 42. Coefficients of Drag For Tail 1 Matrix

C_D						
		δe				
		11°	7°	0°	-12°	-15°
δrn	32°	0.14581	0.13705	0.12883	0.13243	0.13457
	17°	0.14979	0.13826	0.13103	0.12941	0.13286
	8°	0.15402	0.13887	0.13091	0.12858	0.1315
	0°	0.15549	0.13896	0.12977	0.12833	0.13108
	-8°	0.15809	0.14058	0.12978	0.12939	0.13235
	-18°	0.15002	0.13802	0.12987	0.12936	0.13346
	-30°	0.14804	0.1367	0.12899	0.13181	0.13237

Table 43. Coefficients of Side Force For Tail 1Matrix

C_Y						
		δe				
		11°	7°	0°	-12°	-15°
δrn	32°	0.02583	0.012465	-0.01052	-0.04182	-0.04231
	17°	0.008421	-0.00128	-0.01005	-0.02792	-0.0334
	8°	-0.00428	-0.01486	-0.01779	-0.02263	-0.0235
	0°	-0.02257	-0.02254	-0.02234	-0.02113	-0.02057
	-8°	-0.04406	-0.0359	-0.02728	-0.01511	-0.01049
	-18°	-0.0515	-0.04267	-0.03174	-0.01198	-0.00225
	-30°	-0.0716	-0.05479	-0.02248	0.000679	0.003139

Table 44. Coefficients of Roll Moment For Tail 1Matrix

C_ℓ						
		δe				
		11°	7°	0°	-12°	-15°
δrn	32°	-0.00055	-0.00044	0.000699	0.002364	0.002522
	17°	0.000102	0.000342	0.000769	0.00177	0.002036
	8°	0.000678	0.001048	0.001221	0.001431	0.001345
	0°	0.001426	0.001111	0.001263	0.00112	0.001144
	-8°	0.002535	0.001915	0.001499	0.000996	0.000697
	-18°	0.002848	0.002239	0.001743	0.000757	0.000178
	-30°	0.003962	0.002946	0.001377	0.000117	7.76E-05

Table 45. Coefficients of Pitch Moment For Tail 1Matrix

C_m						
		δe				
		11°	7°	0°	-12°	-15°
δrn	32°	-0.21587	-0.17798	-0.10575	-0.00412	0.017501
	17°	-0.24753	-0.1957	-0.14269	-0.02792	0.003955
	8°	-0.27237	-0.20038	-0.13847	-0.03906	0.002595
	0°	-0.27428	-0.19927	-0.12557	-0.0425	0.001084
	-8°	-0.28239	-0.20434	-0.12345	-0.02281	0.005889
	-18°	-0.24288	-0.18617	-0.12507	-0.02469	0.011777
	-30°	-0.21733	-0.16736	-0.07406	-0.01077	-0.01035

Table 46. Coefficients of Yaw Moment For Tail 1Matrix

C_n						
		δe				
		11°	7°	0°	-12°	-15°
δrn	32°	-0.01432	-0.01043	-0.00344	0.006428	0.006746
	17°	-0.00929	-0.00624	-0.00349	0.002216	0.004064
	8°	-0.0055	-0.00216	-0.00103	0.000727	0.001132
	0°	-4.66E-05	0.000113	0.000186	9.73E-05	4.48E-05
	-8°	0.006426	0.004131	0.001831	-0.00152	-0.00277
	-18°	0.008685	0.006266	0.003175	-0.00249	-0.00528
	-30°	0.014943	0.010074	0.000795	-0.00605	-0.00676

Tail 2 Alpha Sweeps

Table 47. Tail 2 δe=0º, δrn=0º

ALPHA(α) [Degrees]	BETA(β) [Degrees]	MACH #	Re	Dynamic pressure(qc) [lbf/ft^2]	U∞ [mph]	C_L	C_D	C_S	C_{l_cg}	C_{mcg}	C_{ncg}	Drag (D) [lbf]	Side Force(S) [lbf]	Lift(L) [lbf]
-8.2417	0.34	0.038518	1.33E+05	2.1478	29.674	0.043625	0.078555	0.010821	0.002979	0.060908	-0.00091	0.10953	0.015091	0.06084
-7.1545	0.34	0.038451	1.32E+05	2.1403	29.622	0.14153	0.072757	0.0083	0.003001	0.058434	-0.00075	0.1009	0.011534	0.19669
-6.0643	0.34	0.038406	1.32E+05	2.1353	29.588	0.24835	0.069173	0.006492	0.003288	0.058657	-0.00055	0.09525	0.009002	0.34434
-5.0583	0.34	0.038378	1.32E+05	2.1322	29.566	0.35903	0.068496	0.004278	0.003334	0.060516	-0.0005	0.093457	0.005923	0.49708
-3.8783	0.34	0.038369	1.32E+05	2.1311	29.559	0.47221	0.068536	0.001369	0.002951	0.063158	-0.00049	0.092462	0.001894	0.65345
-2.7851	0.34	0.038382	1.32E+05	2.1326	29.569	0.58368	0.070479	-0.00208	0.002545	0.061528	-0.00055	0.093959	-0.00287	0.80826
-1.6936	0.34	0.038416	1.32E+05	2.1363	29.595	0.69327	0.074099	-0.00504	0.002348	0.057148	-0.00065	0.09765	-0.00698	0.96171
-0.68964	0.34	0.038379	1.32E+05	2.1322	29.566	0.79964	0.080476	-0.00805	0.002135	0.050036	-0.00065	0.10459	-0.01114	1.1071
0.39959	0.34	0.038327	1.32E+05	2.1265	29.527	0.90426	0.088971	-0.01089	0.001745	0.04457	-0.00081	0.11415	-0.01503	1.2486
1.484	0.34	0.038409	1.32E+05	2.1357	29.59	0.99801	0.098373	-0.014	0.001202	0.037861	-0.00094	0.12577	-0.01942	1.384
2.5658	0.34	0.038552	1.33E+05	2.1516	29.7	1.0834	0.1096	-0.01692	0.000626	0.028448	-0.00104	0.14047	-0.02364	1.5137
3.647	0.34	0.038615	1.33E+05	2.1585	29.748	1.1699	0.12453	-0.02109	-0.00016	0.006103	-0.00096	0.15974	-0.02955	1.6398
4.7251	0.34	0.038597	1.33E+05	2.1566	29.735	1.2471	0.14382	-0.02485	-0.00169	-0.01953	-0.00123	0.1846	-0.03479	1.7464
5.7074	0.34	0.038548	1.33E+05	2.1511	29.697	1.3067	0.16648	-0.02831	-0.00343	-0.04402	-0.00159	0.21414	-0.03955	1.8251
6.7684	0.34	0.038466	1.32E+05	2.142	29.634	1.3451	0.19403	-0.03001	-0.00453	-0.07171	-0.00202	0.25047	-0.04173	1.8709
7.8249	0.34	0.038426	1.32E+05	2.1375	29.603	1.3756	0.22287	-0.03309	-0.00651	-0.09772	-0.002	0.28907	-0.04593	1.9093
8.8774	0.34	0.038431	1.32E+05	2.1381	29.607	1.3949	0.25349	-0.0332	-0.00673	-0.11525	-0.00179	0.3311	-0.04609	1.9366

Table 48. Tail 2 δe=0º, δrn=20º

ALPHA(α) [Degrees]	BETA(β) [Degrees]	MACH #	Re	Dynamic pressure (qc) [lbf/ft^2]	U∞ [mph]	C_L	C_D	C_S	C_{l_cg}	C_{mcg}	C_{ncg}	Drag (D) [lbf]	Side Force(S) [lbf]	Lift(L) [lbf]
-8.3322	0.085	0.038131	1.30E+05	2.0918	29.394	0.035694	0.081572	0.003794	0.002803	0.060661	-0.0009	0.11079	0.005154	0.048483
-7.2458	0.085	0.038123	1.30E+05	2.0909	29.387	0.13172	0.075911	0.001269	0.002498	0.060506	-0.00079	0.10289	0.001722	0.17884
-6.2444	0.085	0.038126	1.30E+05	2.0913	29.39	0.23454	0.071958	0.002541	0.002352	0.059692	-0.00078	0.097139	0.003451	0.31849
-6.1547	0.085	0.038147	1.30E+05	2.0936	29.406	0.2405	0.072163	-5.87E-05	0.002246	0.059548	-0.00071	0.097497	-7.99E-05	0.32696
-5.1497	0.085	0.038175	1.31E+05	2.0967	29.428	0.34911	0.070754	-0.00201	0.00186	0.061148	-0.00068	0.095049	-0.00273	0.4753
-4.0564	0.085	0.038151	1.31E+05	2.094	29.409	0.46308	0.071425	-0.00383	0.001282	0.062813	-0.00077	0.094871	-0.00521	0.62967
-2.8762	0.085	0.038121	1.30E+05	2.0907	29.386	0.57423	0.073314	-0.00683	0.000941	0.065484	-0.00068	0.096077	-0.00927	0.77956
-1.7865	0.085	0.038081	1.30E+05	2.0864	29.355	0.67992	0.076916	-0.01049	0.00053	0.06895	-0.00045	0.099373	-0.01421	0.92113
-0.78221	0.085	0.03804	1.30E+05	2.0819	29.323	0.78703	0.08323	-0.01317	0.000122	0.062513	-0.00046	0.10606	-0.0178	1.0639
0.30503	0.085	0.038055	1.30E+05	2.0835	29.335	0.88714	0.09076	-0.01601	-0.0003	0.054903	-0.00035	0.11458	-0.02166	1.2002
1.3937	0.085	0.038109	1.30E+05	2.0895	29.377	0.98824	0.099995	-0.01866	-0.00098	0.044734	-0.00039	0.12545	-0.02532	1.3408
2.4798	0.085	0.038125	1.30E+05	2.0912	29.389	1.0858	0.11134	-0.0219	-0.00174	0.033122	-0.00034	0.13884	-0.02974	1.4745
3.5647	0.085	0.038099	1.30E+05	2.0883	29.369	1.1806	0.12617	-0.02555	-0.00236	0.015216	-0.00025	0.15651	-0.03464	1.6009
4.6478	0.085	0.03808	1.30E+05	2.0863	29.354	1.2691	0.14607	-0.0293	-0.00381	-0.01396	-0.00027	0.18105	-0.0397	1.7193
5.6329	0.085	0.038076	1.30E+05	2.0858	29.351	1.3349	0.1703	-0.0325	-0.00485	-0.05483	-0.00022	0.21204	-0.04402	1.8079
6.6949	0.085	0.038095	1.30E+05	2.0879	29.366	1.3757	0.19749	-0.03669	-0.00651	-0.08553	0.000254	0.24797	-0.04974	1.8652
7.7518	0.085	0.038073	1.30E+05	2.0855	29.349	1.407	0.22688	-0.03993	-0.0086	-0.11964	0.000554	0.28657	-0.05408	1.9053
8.8059	0.085	0.038071	1.30E+05	2.0853	29.348	1.4299	0.25743	-0.04013	-0.01055	-0.14775	0.000513	0.32723	-0.05434	1.9362

Table 49. Tail 2 δe=0º, δrn=-20º

ALPHA(α) [Degrees]	BETA(β) [Degrees]	MACH #	Re	Dynamic pressure (qc) [lbf/ft^2]	U∞ [mph]	C_L	C_D	C_S	$C_{l\,cg}$	C_{mcg}	C_{ncg}	Drag (D) [lbf]	Side Force(S) [lbf]	Lift(L) [lbf]
-8.3316	0.127	0.039658	1.36E+05	2.2635	30.576	0.037097	0.075855	0.003728	0.001747	0.061628	-0.00065	0.11147	0.005479	0.054523
-7.2483	0.127	0.039604	1.36E+05	2.2574	30.535	0.12595	0.070631	0.001476	0.001717	0.061223	-0.00064	0.10335	0.002163	0.18463
-6.1591	0.127	0.039383	1.35E+05	2.2323	30.365	0.23061	0.068066	-0.00066	0.001845	0.061743	-0.00054	0.098066	-0.00096	0.33426
-5.1552	0.127	0.039309	1.34E+05	2.2239	30.308	0.33669	0.067619	-0.00325	0.001761	0.063096	-0.00048	0.096384	-0.0047	0.4862
-4.0649	0.127	0.039334	1.35E+05	2.2267	30.327	0.44366	0.068029	-0.00572	0.001308	0.065203	-0.00051	0.096168	-0.00827	0.64148
-2.8875	0.127	0.039314	1.35E+05	2.2244	30.311	0.54886	0.069504	-0.00804	0.000838	0.06595	-0.00064	0.097036	-0.01161	0.79278
-1.8001	0.127	0.039308	1.34E+05	2.2237	30.306	0.64935	0.073542	-0.01067	0.000573	0.062384	-0.00073	0.10149	-0.0154	0.93762
-0.79876	0.127	0.03929	1.34E+05	2.2218	30.293	0.74957	0.079435	-0.01391	0.000273	0.055835	-0.00065	0.10835	-0.02007	1.0814
0.28509	0.127	0.039353	1.35E+05	2.2288	30.341	0.84203	0.086437	-0.0164	-0.00011	0.04823	-0.0008	0.11718	-0.02373	1.2186
1.3701	0.127	0.039372	1.35E+05	2.231	30.356	0.93476	0.095379	-0.01927	-0.00074	0.039382	-0.00085	0.12841	-0.02792	1.3542
2.454	0.127	0.039327	1.35E+05	2.2259	30.321	1.0273	0.10614	-0.02236	-0.00117	0.027939	-0.00093	0.14164	-0.03231	1.4849
3.5334	0.127	0.039375	1.35E+05	2.2313	30.358	1.1098	0.11994	-0.02517	-0.00163	0.01022	-0.00097	0.16002	-0.03647	1.6079
4.6134	0.127	0.039437	1.35E+05	2.2383	30.406	1.1911	0.13752	-0.0304	-0.00252	-0.02748	-0.00051	0.18398	-0.04418	1.7312
5.5956	0.127	0.039414	1.35E+05	2.2358	30.388	1.2504	0.16056	-0.03253	-0.00319	-0.06303	-0.00079	0.2156	-0.04723	1.8153
6.66	0.127	0.039402	1.35E+05	2.2344	30.379	1.2966	0.18704	-0.03521	-0.00436	-0.10271	-0.00097	0.25257	-0.05109	1.8812
7.715	0.127	0.039513	1.35E+05	2.247	30.465	1.3237	0.21312	-0.03809	-0.00528	-0.13766	-0.00086	0.29123	-0.05557	1.9314
8.768	0.127	0.039574	1.35E+05	2.254	30.512	1.3441	0.24161	-0.04293	-0.00675	-0.17046	0.000228	0.33322	-0.06283	1.9672

Table 50. Tail 2 δe=8º, δrn=0º

ALPHA(α) [Degrees]	BETA(β) [Degrees]	MACH #	Re	Dynamic pressure (qc) [lbf/ft^2]	U∞ [mph]	C_L	C_D	C_S	$C_{l\,cg}$	C_{mcg}	C_{ncg}	Drag (D) [lbf]	Side Force(S) [lbf]	Lift(L) [lbf]
-8.3028	0.085	0.038713	1.32E+05	2.1555	29.829	0.10222	0.077563	0.001886	0.002881	-0.056	-0.00034	0.10845	0.00264	0.14307
-7.2185	0.085	0.038991	1.33E+05	2.1865	30.043	0.19349	0.07292	-0.00069	0.002841	-0.05583	-0.00027	0.10312	-0.00098	0.27472
-6.1296	0.085	0.038842	1.33E+05	2.1698	29.928	0.29736	0.071266	-0.0024	0.002717	-0.0505	-0.00016	0.099451	-0.00338	0.41896
-5.1244	0.085	0.038729	1.33E+05	2.1573	29.841	0.40631	0.072295	-0.00516	0.002427	-0.04604	-0.00014	0.099488	-0.00722	0.56917
-4.0323	0.085	0.038728	1.33E+05	2.1571	29.84	0.51762	0.073782	-0.00709	0.001868	-0.04318	-0.00025	0.10045	-0.00994	0.72504
-2.8536	0.085	0.038685	1.32E+05	2.1523	29.806	0.62537	0.0766	-0.00985	0.001567	-0.04124	-0.0002	0.10284	-0.01376	0.874
-1.7637	0.085	0.038641	1.32E+05	2.1475	29.773	0.73166	0.081595	-0.01284	0.001073	-0.04678	-0.00018	0.10802	-0.0179	1.0203
-0.76035	0.085	0.038617	1.32E+05	2.1448	29.755	0.8365	0.08919	-0.01582	0.000881	-0.05302	-0.00015	0.1167	-0.02203	1.165
0.32456	0.085	0.038629	1.32E+05	2.1461	29.764	0.93134	0.09608	-0.01883	0.000238	-0.05097	-0.00015	0.12457	-0.02625	1.2979
1.4119	0.085	0.038651	1.32E+05	2.1485	29.78	1.0294	0.10665	-0.0217	-0.00031	-0.05889	-0.00019	0.13738	-0.03028	1.4362
2.497	0.085	0.03864	1.32E+05	2.1473	29.772	1.1247	0.11891	-0.02481	-0.00086	-0.07055	-0.00022	0.15219	-0.03459	1.5683
3.5795	0.085	0.03863	1.32E+05	2.1462	29.764	1.214	0.13382	-0.02812	-0.00163	-0.08735	-0.00026	0.17066	-0.03919	1.6919
4.6599	0.085	0.03864	1.32E+05	2.1474	29.772	1.2963	0.1533	-0.03226	-0.00281	-0.11554	-0.00013	0.19568	-0.04498	1.8076
5.6433	0.085	0.038659	1.32E+05	2.1494	29.787	1.3585	0.17783	-0.03496	-0.00359	-0.15313	-0.00027	0.22833	-0.04879	1.8961
6.7024	0.085	0.038791	1.33E+05	2.1641	29.888	1.3926	0.20339	-0.03749	-0.00475	-0.18162	-0.00034	0.2648	-0.05268	1.9569
7.7598	0.085	0.039039	1.34E+05	2.1919	30.079	1.4251	0.23639	-0.03986	-0.00565	-0.2418	-0.00035	0.31415	-0.05674	2.0283
8.8077	0.085	0.039359	1.35E+05	2.2279	30.326	1.4339	0.26637	-0.04351	-0.00825	-0.27592	0.000417	0.36242	-0.06294	2.0745

Table 51. Tail 2 δe=8º, δrn=20º

ALPHA(α) [Degrees]	BETA(β) [Degrees]	MACH #	Re	Dynamic pressure (qc) [lbf/ft^2]	U∞ [mph]	C_L	C_D	C_S	$C_{l\,cg}$	C_{mcg}	C_{ncg}	Drag (D) [lbf]	Side Force(S) [lbf]	Lift(L) [lbf]
-8.3143	0.085	0.038115	1.30E+05	2.0908	29.39	0.076303	0.083789	0.027001	0.003574	-0.03014	-0.00682	0.11369	0.036658	0.10359
-7.23	0.085	0.038079	1.30E+05	2.0869	29.362	0.16754	0.079118	0.02402	0.003278	-0.02386	-0.00642	0.10692	0.03255	0.22704
-6.2266	0.085	0.038074	1.30E+05	2.0863	29.358	0.27469	0.076911	0.022481	0.002901	-0.02216	-0.00642	0.10341	0.030456	0.37214
-5.1344	0.085	0.038119	1.30E+05	2.0912	29.393	0.38384	0.075727	0.022092	0.002351	-0.01893	-0.00677	0.10129	0.029999	0.52122
-4.0407	0.085	0.038134	1.30E+05	2.0929	29.404	0.49858	0.077216	0.021452	0.001958	-0.01965	-0.00722	0.10233	0.029153	0.67757
-2.8573	0.085	0.038126	1.30E+05	2.092	29.398	0.61721	0.081003	0.022658	0.001341	-0.02835	-0.00832	0.10605	0.03078	0.83844
-1.7667	0.085	0.038113	1.30E+05	2.0906	29.388	0.72473	0.085417	0.019404	0.000765	-0.02991	-0.00837	0.11046	0.026341	0.98384
-0.76331	0.085	0.038118	1.30E+05	2.0912	29.392	0.82981	0.091565	0.015801	0.000201	-0.03135	-0.00823	0.11712	0.021455	1.1268
0.32639	0.085	0.038142	1.30E+05	2.0938	29.411	0.93548	0.10131	0.015811	-0.0004	-0.04616	-0.00896	0.12857	0.021497	1.2719
1.4155	0.085	0.038164	1.31E+05	2.0962	29.427	1.0376	0.11284	0.014301	-0.00124	-0.05906	-0.00942	0.14229	0.019466	1.4124
2.5053	0.085	0.038163	1.31E+05	2.0961	29.427	1.1434	0.1276	0.01465	-0.00223	-0.07959	-0.01048	0.15995	0.01994	1.5563
3.5896	0.085	0.038154	1.31E+05	2.0951	29.419	1.2369	0.14217	0.009183	-0.00309	-0.09244	-0.00992	0.17736	0.012492	1.6827
4.6728	0.085	0.03816	1.31E+05	2.0957	29.424	1.3256	0.16433	0.008873	-0.00475	-0.1289	-0.01116	0.20518	0.012074	1.8039
5.6599	0.085	0.038163	1.31E+05	2.0961	29.427	1.396	0.19058	0.006552	-0.0065	-0.16794	-0.01154	0.23893	0.008918	1.9001
6.7244	0.085	0.038145	1.30E+05	2.0941	29.412	1.4425	0.21943	0.000822	-0.0082	-0.20197	-0.01071	0.27655	0.001117	1.9614
7.7831	0.085	0.038122	1.30E+05	2.0916	29.395	1.4778	0.25051	-0.00389	-0.01054	-0.23614	-0.01011	0.31735	-0.00529	2.0071
8.8406	0.085	0.038108	1.30E+05	2.09	29.384	1.5085	0.28511	-0.00336	-0.01371	-0.27046	-0.01074	0.36311	-0.00455	2.0473

Table 52. Tail 2 δe=8º, δrn=-20º

ALPHA(α) [Degrees]	BETA(β) [Degrees]	MACH #	Re	Dynamic pressure (qc) [lbf/ft^2]	U∞ [mph]	C_L	C_D	C_S	$C_{l\,cg}$	C_{mcg}	C_{ncg}	Drag (D) [lbf]	Side Force(S) [lbf]	Lift(L) [lbf]
-8.3168	0.085	0.040678	1.39E+05	2.3815	31.366	0.070612	0.073736	-0.01103	0.002265	-0.01629	0.002776	0.11397	-0.01706	0.10919
-7.2364	0.085	0.040674	1.39E+05	2.381	31.363	0.15298	0.069645	-0.01302	0.002186	-0.01263	0.002665	0.1074	-0.02013	0.23652
-6.1486	0.085	0.040508	1.39E+05	2.3616	31.235	0.2544	0.068587	-0.01721	0.002447	-0.01609	0.003285	0.10441	-0.02639	0.39012
-5.1478	0.085	0.040497	1.39E+05	2.3603	31.226	0.35357	0.068475	-0.02062	0.002472	-0.01724	0.003641	0.10347	-0.0316	0.54189
-4.0584	0.085	0.040496	1.39E+05	2.3602	31.226	0.45853	0.07173	-0.02576	0.002253	-0.02285	0.00441	0.10745	-0.03947	0.70273
-2.8807	0.085	0.040411	1.38E+05	2.3502	31.16	0.56425	0.07491	-0.03018	0.002065	-0.02822	0.004919	0.11057	-0.04606	0.8611
-1.7945	0.085	0.040377	1.38E+05	2.3464	31.134	0.66197	0.079266	-0.03362	0.001863	-0.0325	0.005127	0.11562	-0.05123	1.0086
-0.79578	0.085	0.040407	1.38E+05	2.3498	31.157	0.75632	0.08546	-0.03731	0.001494	-0.03801	0.005348	0.12367	-0.05693	1.154
0.28408	0.085	0.040493	1.39E+05	2.3598	31.223	0.83974	0.09181	-0.03916	0.00129	-0.04013	0.005181	0.13235	-0.06	1.2868
1.3657	0.085	0.040675	1.39E+05	2.3811	31.364	0.92478	0.10086	-0.04304	0.000958	-0.05179	0.005512	0.14574	-0.06655	1.4298
2.4418	0.085	0.040894	1.40E+05	2.4068	31.532	0.99971	0.11085	-0.04624	0.000653	-0.06221	0.005626	0.16119	-0.07226	1.5624
3.5183	0.085	0.040998	1.40E+05	2.419	31.612	1.0756	0.12357	-0.04954	0.000166	-0.07685	0.005632	0.18008	-0.07782	1.6895
4.5961	0.085	0.040993	1.40E+05	2.4185	31.609	1.1521	0.14123	-0.05378	-0.00063	-0.10112	0.005762	0.20572	-0.08446	1.8094
5.5798	0.085	0.040911	1.40E+05	2.4089	31.546	1.2147	0.16426	-0.05779	-0.00101	-0.13742	0.005945	0.23913	-0.09039	1.9
6.6454	0.085	0.040919	1.40E+05	2.4098	31.552	1.2637	0.19184	-0.06219	-0.00166	-0.17667	0.006378	0.28091	-0.09731	1.9774
7.6997	0.085	0.040958	1.40E+05	2.4144	31.582	1.2893	0.21928	-0.06509	-0.00266	-0.20916	0.006451	0.32368	-0.10205	2.0213
8.752	0.085	0.040959	1.40E+05	2.4145	31.583	1.3081	0.24582	-0.06634	-0.00462	-0.23076	0.006276	0.36471	-0.10402	2.0509

Table 53. Tail 2 δe=-9º, δrn=0º

ALPHA(α) [Degrees]	BETA(β) [Degrees]	MACH #	Re	Dynamic pressure (qc) [lbf/ft^2]	U∞ [mph]	C_L	C_D	C_S	$C_{l\,cg}$	C_{mcg}	C_{ncg}	Drag (D) [lbf]	Side Force(S) [lbf]	Lift(L) [lbf]
-8.2662	0.552	0.03996	1.37E+05	2.3012	30.806	-0.01176	0.088126	0.011242	0.0015	0.15967	-0.00081	0.13168	0.016799	-0.01758
-7.1804	0.552	0.039712	1.36E+05	2.2729	30.616	0.082815	0.081025	0.009546	0.001521	0.15439	-0.00082	0.1195	0.014088	0.12222
-6.091	0.552	0.039614	1.36E+05	2.2617	30.54	0.18777	0.076114	0.008072	0.001652	0.1519	-0.00086	0.11138	0.011855	0.27576
-5.0889	0.552	0.03977	1.36E+05	2.2794	30.66	0.28991	0.073513	0.006173	0.001618	0.14944	-0.00093	0.10785	0.009137	0.42911
-3.9985	0.552	0.039768	1.36E+05	2.2793	30.659	0.39709	0.072774	0.003348	0.001306	0.1497	-0.00096	0.10591	0.004955	0.58769
-2.8216	0.552	0.039785	1.36E+05	2.2811	30.671	0.501	0.073128	0.000597	0.00119	0.14654	-0.001	0.10545	0.000884	0.7421
-1.7339	0.552	0.039815	1.36E+05	2.2847	30.695	0.60223	0.075497	-0.00248	0.000796	0.1421	-0.00107	0.10785	-0.00369	0.89343
-0.7331	0.552	0.039826	1.36E+05	2.2859	30.703	0.70128	0.080197	-0.00514	0.000622	0.13293	-0.00114	0.11341	-0.00763	1.0409
0.35278	0.552	0.039773	1.36E+05	2.2798	30.662	0.79832	0.087194	-0.00766	0.000218	0.12272	-0.00128	0.1218	-0.01135	1.1818
1.4392	0.552	0.039663	1.36E+05	2.2672	30.578	0.89659	0.096038	-0.01036	-0.00012	0.1129	-0.00137	0.13226	-0.01524	1.32
2.526	0.552	0.039562	1.36E+05	2.2557	30.5	0.99338	0.10703	-0.0132	-0.00074	0.096824	-0.00144	0.14563	-0.01933	1.455
3.6091	0.552	0.039541	1.35E+05	2.2533	30.484	1.0841	0.12145	-0.01646	-0.0016	0.074497	-0.00156	0.16444	-0.02409	1.5862
4.6826	0.552	0.039595	1.36E+05	2.2594	30.525	1.151	0.14005	-0.0196	-0.00331	0.04418	-0.00187	0.19048	-0.02875	1.6886
5.661	0.552	0.039629	1.36E+05	2.2634	30.551	1.2016	0.16081	-0.02251	-0.00519	0.013496	-0.00219	0.21997	-0.03309	1.766
6.7198	0.552	0.039631	1.36E+05	2.2635	30.552	1.2352	0.18424	-0.02413	-0.00626	-0.01487	-0.00243	0.25351	-0.03547	1.8154
7.7712	0.552	0.039619	1.36E+05	2.2622	30.544	1.2542	0.20925	-0.02643	-0.00794	-0.04196	-0.00227	0.28956	-0.03883	1.8424
8.8224	0.552	0.039767	1.36E+05	2.2791	30.658	1.2704	0.23655	-0.0268	-0.00786	-0.05995	-0.00184	0.33165	-0.03966	1.88

Table 54. Tail 2 δe=-9º, δrn=20º

ALPHA(α) [Degrees]	BETA(β) [Degrees]	MACH #	Re	Dynamic pressure (qc) [lbf/ft^2]	U∞ [mph]	C_L	C_D	C_S	$C_{l\,cg}$	C_{mcg}	C_{ncg}	Drag (D) [lbf]	Side Force(S) [lbf]	Lift(L) [lbf]
-8.3527	0.085	0.039435	1.35E+05	2.2374	30.399	-0.01067	0.087056	-0.0096	0.028861	0.14576	-0.00079	0.12647	-0.01395	-0.0155
-7.2685	0.085	0.039522	1.35E+05	2.2472	30.466	0.080347	0.079931	-0.0117	0.028521	0.14339	-0.00086	0.11656	-0.01707	0.11724
-6.1805	0.085	0.039522	1.35E+05	2.2473	30.466	0.18214	0.075479	-0.01254	0.028487	0.14462	-0.00083	0.10977	-0.0183	0.26579
-5.1774	0.085	0.039526	1.35E+05	2.2477	30.469	0.28641	0.073406	-0.01413	0.028259	0.14427	-0.00095	0.10621	-0.02063	0.41801
-4.0881	0.085	0.039573	1.35E+05	2.2531	30.505	0.39119	0.072627	-0.01599	0.027812	0.14475	-0.00093	0.10453	-0.0234	0.57231
-2.9118	0.085	0.039653	1.36E+05	2.2622	30.567	0.49368	0.072828	-0.0186	0.027224	0.14182	-0.00085	0.10422	-0.02732	0.72517
-1.8251	0.085	0.03968	1.36E+05	2.2653	30.588	0.59263	0.07505	-0.02131	0.026774	0.13733	-0.00077	0.10641	-0.03135	0.87173
-0.82249	0.085	0.039527	1.35E+05	2.2479	30.47	0.69587	0.080817	-0.02437	0.026664	0.13169	-0.00062	0.11251	-0.03557	1.0157
0.26509	0.085	0.039318	1.35E+05	2.2241	30.308	0.79675	0.087758	-0.02685	0.026398	0.12382	-0.00074	0.11967	-0.03878	1.1507
1.3546	0.085	0.039215	1.34E+05	2.2124	30.229	0.89984	0.09645	-0.02929	0.025959	0.11273	-0.00086	0.12959	-0.04208	1.2927
2.4382	0.085	0.039243	1.34E+05	2.2156	30.251	0.9917	0.10647	-0.03142	0.025441	0.098156	-0.00099	0.14226	-0.0452	1.4267
3.5207	0.085	0.039278	1.34E+05	2.2196	30.278	1.0811	0.11964	-0.03396	0.024654	0.078133	-0.00111	0.15945	-0.04894	1.5582
4.5982	0.085	0.039324	1.35E+05	2.2248	30.313	1.1569	0.13669	-0.03713	0.023387	0.048695	-0.00117	0.18255	-0.05364	1.6713
5.5747	0.085	0.03956	1.35E+05	2.2516	30.495	1.2032	0.15674	-0.039	0.022208	0.010362	-0.00108	0.21284	-0.05702	1.7592
6.6032	0.085	0.040851	1.40E+05	2.401	31.491	1.168	0.17026	-0.03811	0.019533	-0.02209	-0.00092	0.24904	-0.05941	1.821
7.6226	0.085	0.042218	1.44E+05	2.5643	32.544	1.1148	0.18121	-0.03832	0.01672	-0.04899	-0.00062	0.28576	-0.06381	1.8563
8.6597	0.085	0.042816	1.46E+05	2.6375	33.005	1.0991	0.19888	-0.03886	0.014662	-0.06742	-0.00021	0.32465	-0.06655	1.8823

Table 55. Tail 2 δe=-9, δrn=-20º

ALPHA(α) [Degrees]	BETA(β) [Degrees]	MACH #	Re	Dynamic pressure (qc) [lbf/ft^2]	U∞ [mph]	C_L	C_D	C_S	$C_{l\,cg}$	C_{mcg}	C_{ncg}	Drag (D) [lbf]	Side Force(S) [lbf]	Lift(L) [lbf]
-8.3468	0.085	0.039169	1.34E+05	2.2073	30.191	0.0028	0.084972	0.012913	-0.02509	0.12022	0.001007	0.12179	0.018508	0.004014
-7.2625	0.085	0.039208	1.34E+05	2.2116	30.221	0.093833	0.078632	0.010509	-0.02511	0.11938	0.000968	0.11283	0.015092	0.13475
-6.1738	0.085	0.03923	1.34E+05	2.2142	30.238	0.19725	0.074119	0.009718	-0.02513	0.11889	0.000709	0.10614	0.013973	0.2836
-5.17	0.085	0.039198	1.34E+05	2.2106	30.214	0.30316	0.072847	0.007681	-0.02517	0.11902	0.00069	0.10355	0.011025	0.43516
-4.0792	0.085	0.039125	1.34E+05	2.2023	30.157	0.41142	0.073158	0.005426	-0.02554	0.12095	0.000652	0.10275	0.00776	0.58835
-2.9003	0.085	0.039124	1.34E+05	2.2022	30.156	0.51968	0.073866	0.002756	-0.02612	0.11949	0.000591	0.10265	0.003941	0.74313
-1.8134	0.085	0.039158	1.34E+05	2.2061	30.183	0.61925	0.077119	-0.00036	-0.02644	0.11565	0.000522	0.10624	-0.00052	0.88708
-0.81276	0.085	0.039203	1.34E+05	2.2111	30.217	0.71789	0.082044	-0.00329	-0.02679	0.10823	0.000543	0.11209	-0.00473	1.0307
0.27261	0.085	0.039207	1.34E+05	2.2115	30.22	0.81377	0.088562	-0.00617	-0.02711	0.099817	0.000605	0.11985	-0.00886	1.1686
1.3599	0.085	0.039208	1.34E+05	2.2117	30.221	0.91166	0.096982	-0.00945	-0.02765	0.088866	0.000647	0.13008	-0.01358	1.3093
2.4435	0.085	0.039216	1.34E+05	2.2126	30.227	1.0036	0.10761	-0.0127	-0.02817	0.074911	0.000719	0.14345	-0.01824	1.4418
3.5255	0.085	0.039217	1.34E+05	2.2127	30.228	1.0919	0.12106	-0.01616	-0.02879	0.05558	0.000807	0.16072	-0.02322	1.5688
4.6034	0.085	0.039334	1.35E+05	2.2259	30.318	1.1686	0.13807	-0.02008	-0.02994	0.026188	0.00086	0.18434	-0.02902	1.689
5.5819	0.085	0.039386	1.35E+05	2.2318	30.358	1.2196	0.15975	-0.02152	-0.03051	-0.01072	0.000529	0.21489	-0.03118	1.7675
6.6177	0.085	0.040457	1.38E+05	2.3548	31.183	1.2009	0.17545	-0.02173	-0.03001	-0.04391	0.000397	0.25126	-0.03322	1.8363
7.628	0.085	0.042181	1.44E+05	2.5598	32.512	1.127	0.18363	-0.02224	-0.02884	-0.07101	0.000428	0.28894	-0.03697	1.8732
8.6468	0.085	0.04349	1.49E+05	2.7211	33.522	1.0699	0.19381	-0.02351	-0.02898	-0.07786	0.001119	0.32685	-0.04154	1.8905

Tail 2 Beta Sweeps

Table 56. Tail 2 Beta Sweep Alpha =4º, δe=0º, δrn=0º

ALPHA(α) [Degrees]	BETA(β) [Degrees]	MACH #	Re	Dynamic pressure (qc) [lbf/ft^2]	U∞ [mph]	C_L	C_D	C_S	$C_{l\,cg}$	C_{mcg}	C_{ncg}	Drag (D) [lbf]	Side Force(S) [lbf]	Lift(L) [lbf]
4.7255	10.361	0.038443	1.32E+05	2.132	29.651	1.248	0.17012	-0.09645	-0.01493	-0.0796	0.004417	0.21889	-0.13352	1.7277
4.734	8.45	0.038307	1.31E+05	2.117	29.546	1.2673	0.165	-0.08185	-0.01118	-0.0809	0.002902	0.20979	-0.11252	1.7422
4.742	6.412	0.03824	1.31E+05	2.1096	29.494	1.2854	0.16059	-0.06767	-0.00783	-0.08328	0.001569	0.20253	-0.09269	1.7608
4.7443	4.374	0.038231	1.31E+05	2.1086	29.487	1.2906	0.15477	-0.05292	-0.00443	-0.07895	0.000315	0.19433	-0.07246	1.767
4.7435	2.335	0.03824	1.31E+05	2.1096	29.494	1.2888	0.14871	-0.03838	-0.00131	-0.07103	-0.00077	0.18616	-0.05258	1.7655
4.7383	0.297	0.038248	1.31E+05	2.1105	29.501	1.2771	0.1474	-0.0245	0.001555	-0.0737	-0.0016	0.18477	-0.03357	1.7501
4.7322	-1.614	0.038241	1.31E+05	2.1098	29.495	1.2631	0.15136	-0.00792	0.005017	-0.07317	-0.00299	0.1905	-0.01085	1.7304
4.7267	-3.609	0.038205	1.31E+05	2.1057	29.467	1.2507	0.15502	0.009446	0.008525	-0.07087	-0.00466	0.19547	0.012916	1.7101
4.7181	-5.605	0.038149	1.31E+05	2.0996	29.424	1.2314	0.15951	0.027495	0.012018	-0.07283	-0.00634	0.20153	0.037485	1.6788
4.7102	-7.558	0.038116	1.31E+05	2.096	29.399	1.2133	0.16424	0.04564	0.015999	-0.06944	-0.00773	0.20808	0.062116	1.6513
4.7102	-7.601	0.038094	1.31E+05	2.0936	29.382	1.2133	0.16512	0.045147	0.015931	-0.06851	-0.00803	0.20903	0.061375	1.6494
4.705	-9.597	0.038039	1.30E+05	2.0875	29.34	1.2017	0.16906	0.065	0.020556	-0.04967	-0.01002	0.21407	0.088108	1.629

Appendix C: Matlab® Code Used

```
%*****************************************************************
%**********        Lt. Gebbie & Capt Anthony DeLuca    **********************
%* Adapted for the Balance AFIT 1 and rotary tails by Lt. Rivera Parga %***********
%**********    Calculation of Lift, Drag, Moments      **********************
%**********    FLEX WING, Prop OFF, ALPHA SWEEPS       *****************

%This Code will transfer measured Forces and Moments on the AFIT 1 balance to Wind
%(earth) centered frame of reference by correcting for tare effects, balance
%interactions, and wind tunnel irregularities, then gives a file with all the
%corrected data

clear;
clc;
close all;
format long
%#########################################################################
%                       INPUT DECK
%FIRST FILL THE FOLLOWING INFORMATION

Masskg=0.415;                           % Mass of the UAV in KGS
T_room = mean([72.3]) + 459.67;         %deg R  **Changed for each day of testing*
P_barro = mean([29.06]) * 0.4911541; %Psi  ****Changed for each day of testing****

%Offset distances from the Mounting Block to the Model C.G. (inches)
Y_cmb =  -(0.05);                        %inches
X_cmb = 0.71;                            %inches
Z_cmb = -1.31;                           %inches

% Requeried for the Solid body blockage corrections due to wing and fuselage

 Body_Volume = ((9.42962435*(2/16))+(.2497)+ (0.9375)+...
         (3.5*((2.75+1.35)/2)*((1.95+1.32)/2))...
         +(5.25*3.0*((1.95+1.45)/2))) / 12^3;
%(ft^3): Tail+vertical stabilizers (Tail 2)+ Connector+Prop-to-Wing+Wing Front-to-
Wing Back

% Requeried for the Pitching Moment Correction
l_t =  9/12;                            % ft = length from tail MAC to aircraft CG
Span_t =(4+(6/16)) / 12;                % ft = horizontal span
Tail_Area = (9.42962435) / 144;    % ft^2 =  horizontal tail area

% BEFORE CONTINUING IT IS NECCESARY TO CHANGE THE NAME:
% INPUT DATA FILE AND INPUT DATA TARE FILE
```

```
% THE OUTPUT DATA FILE

%#########################################################################
%I. Polynomial Curve fit of Chord Dimensions to Spanwise length to get an
%    Equation defining thet Chord anywhere along the span.
%#########################################################################

Span_Location = [0 2.62 (2.62*2) (2.62*3) (2.62*4)]; %in
Chord_Dist = [1/2 59/16 5 89/16 6]; %in

c1 = polyfit(Span_Location,Chord_Dist,2);
Chord1 = polyval(c1,Span_Location);

c2 = polyfit(Span_Location,Chord_Dist,3);
Chord2 = polyval(c2,Span_Location);

c3 = polyfit(Span_Location,Chord_Dist,4);
Chord3 = polyval(c3,Span_Location);

 figure(1)
plot(Span_Location,Chord_Dist,'x',Span_Location,Chord1,'- .',Span_Location,Chord2,'o-
.',Span_Location,Chord3,'*-');

%4th order chord equation as a function of the span (b) or C(y) integrated
%from  0 to b/2 to calculate 1/2 of the wing area.

chord_eqn = inline('-0.00044213367831*b.^4+0.01737585355753*b.^3-
0.25190354097469*b.^2+1.76526717557252*b+0.50');
Wing_Area = (2 * quad(chord_eqn,0,4*2.62)) / 144;                    %ft^2

%#########################################################################
%II.   Room Conditions and Model Specifics :
%       UNITS are in Ft, Sec, lbm, Psf, Rankine, fps
%#########################################################################

Mass = (Masskg * 1000) * 0.0022046;                %lbm (flex MAV with batteries)
Gas_Const = 1716;                                  %ft-lbf/Slug-R
Density = (P_barro * 144)/(1716 * T_room);         %lbm/ft^3 or lbf-s^2/ft^4
Root_Chord = 6 * (1/12);                           %ft
Span = 24 / 12;                                    %ft
Aspect_Ratio = Span^2 / Wing_Area;
Viscosity = .372e-6;                               %slug/ft-s
Speed_of_Sound = sqrt(1.4 * T_room * Gas_Const);    %fps

%#########################################################################
```

```
%III.     Solid body blockage corrections due to wing and fuselage
%#########################################################################

K_1 = 0.9;
K_3 = 0.93;
delta = 0.1125;
Tau_1 = 0.83125;
X_Section = (31/12)*(44/12);                              %ft^2
Wing_Volume = Wing_Area * (.006/12);                      %ft^3
Epsilon_sb_w = (K_1*Tau_1*Wing_Volume) / X_Section^(3/2);
Epsilon_sb_b = (K_3*Tau_1*Body_Volume) / X_Section^(3/2);
Epsilon_tot = Epsilon_sb_w + Epsilon_sb_b;

%#########################################################################
% III.  Load the static tare data for the alpha sweep w/o the wind,
%       separate each force from the file, and fit a 4th order poly
%       as an x-y plot (AoA vs.Force) for each of the 6 force sensors.
%#########################################################################

load TARET2.txt  % Raw data file to be read in.
FILE=TARET2(:,1:9);
j=1;
k=1;
L=length(FILE);

for i=1:L
   if i~=L
      i2=i+1;
      C=FILE(i2,1);
   else if i==L
      C=50;
   end
   end
   A(j,:)=FILE(i,:);
   B=FILE(i,1);
   if B==C;
      j=j+1;
   else if B~=C;
      for m=1:9;
         AA(k,m)=mean(A(:,m));
      end
      j=1;
      k=k+1;
      clear A
   end
```

```
   end
end

tare=[AA];
%_____________________________________End of inserted code
[row,col] = size(tare);

for k = 1:row;

theta_tare(k,:,:)   = tare(k,1).* (pi/180);
NF_tare(k,:,:)      = tare(k,4);
PM_tare(k,:,:)      = tare(k,5);
SF_tare(k,:,:)      = tare(k,7);
YM_tare(k,:,:)      = tare(k,8);
AF_tare(k,:,:)      = tare(k,6);
RM_tare(k,:,:)      = tare(k,9);

end

NF_poly = polyfit(theta_tare,NF_tare,4);
PM_poly = polyfit(theta_tare,PM_tare,4);
SF_poly = polyfit(theta_tare,SF_tare,4);
YM_poly = polyfit(theta_tare,YM_tare,4);
AF_poly  = polyfit(theta_tare,AF_tare,4);
RM_poly  = polyfit(theta_tare,RM_tare,4);

%##########################################################################
%IV. Load the specific test run files,
%##########################################################################

clear ('AA','B','C','L')
load T2DEM9DRNM20.txt;              % Raw data file to be read in.
FILE=T2DEM9DRNM20(:,1:9);
j=1;
k=1;
L=length(FILE);

for i=1:L;
   if i~=L;
      i2=i+1;
      C=FILE(i2,1);
   else if i==L;
      C=50;
   end
   end
```

```
    A(j,:)=FILE(i,:);
    B=FILE(i,1);
    if B==C;
       j=j+1;
    else if B~=C;
       for m=1:9;
          AA(k,m)=mean(A(:,m));
       end
       j=1;
       k=k+1;
       clear A
    end
    end
end

sample_data=[AA];
%_____________________________________End of inserted code
[row2,col2] = size(sample_data);

for i = 1:row2;

%Angles of the model during test runs (Roll, Pitch {AoA}, Yaw {Beta}):

phi               = 0;
theta(i,:)        = sample_data(i,1) .* (pi/180);              %radians
si(i,:)           = sample_data(i,2) .* (pi/180);              %radians
Wind_Speed(i,:)   = sample_data(i,3) .* (5280/3600);      %fps

%Flight Parameters (Re#, Ma#, Dynamic Pressure):

q = (.5 * Density) .* Wind_Speed.^2;                    %lbf/ft^2
q_Corrected = q .* (1 + Epsilon_tot)^2;                 %lbf/ft^2
Wind_Speed_Corrected = Wind_Speed .* (1 + Epsilon_tot);   %fps
Mach_Number = Wind_Speed_Corrected ./ Speed_of_Sound;     %NonDimensional
Reynolds_Number = ((Density * Root_Chord) .* Wind_Speed_Corrected) ./ Viscosity;
%NonDimensional
Flight_Parameters = [Mach_Number Reynolds_Number q_Corrected];

%individual forces and moments for each sensor:
NF_test(i,:,:)     = sample_data(i,4);
PM_test(i,:,:)     = sample_data(i,5);
SF_test(i,:,:)     = sample_data(i,7);
YM_test(i,:,:)     = sample_data(i,8);
AF_test(i,:,:)     = sample_data(i,6);
RM_test(i,:,:)     = sample_data(i,9);
```

```
%#########################################################################
%V.   Subtract the effect of the static
%      weight with the tare polynomials above
%#########################################################################

%Evaluating the actual test theta angle (AoA) in the tare polynomial to
%determine the tare values for the angles tested in each run.

NF_eval = polyval(NF_poly,theta);
PM_eval = polyval(PM_poly,theta);
SF_eval = polyval(SF_poly,theta);
YM_eval = polyval(YM_poly,theta);
AF_eval  = polyval(AF_poly,theta);
RM_eval  = polyval(RM_poly,theta);

%The Time-Averaged (raw) forces and momentums NF,AF,SF,PM,YM AND RM
measured in the wind
%tunnel (body axis) with the tare effect of the weight subtracted off.

NF_resolved = NF_test - (NF_eval);
PM_resolved = PM_test - (PM_eval);
SF_resolved = SF_test - (SF_eval);
YM_resolved = YM_test - (YM_eval);
AF_resolved  = AF_test -  (AF_eval);
RM_resolved  = RM_test -  (RM_eval);


Forces_minus_tare = [NF_resolved, AF_resolved, PM_resolved, RM_resolved,
YM_resolved, SF_resolved]';

%#########################################################################
%VI. CORRECT FORCES AND MOMENTS FOR BALANCE INTERATIONS (body
axis)
%#########################################################################

%USING THE REDUCTION EQUATIONS
%LET US SET A MAXIMUN NUMBER OF INTERATIONS (FOR AVOIDING AN
INFINIT LOOP)
MAXIT=100;
%SET THE LIMIT FOR THE DIFFERENCE BETWEEN INTERATIONS(CRITERIA
FOR FINISH THE INTERATIONS)
LIMIT=  10E-14;

%MATCHING EACH NAME WITH  THE DATA
```

```
MNF=NF_resolved(i);
MAF=AF_resolved(i);
MPM=PM_resolved(i);
MRM=RM_resolved(i);
MYM=YM_resolved(i);
MSF=SF_resolved(i);

%INPUT OF THE CONSTANTS VALUES FROM THE MATRIX FOR
SENSITIVITIES AND INTERATIONS
K=[0  -1.3567E-03  -3.8021E-03  -4.2814E-03  -1.6966E-03   1.7567E-03  ...
   5.3167E-05  -1.3867E-04  -5.5629E-05  3.5181E-05  1.0601E-05  -2.5271E-04...
   5.6693E-05  -1.9537E-04   1.7908E-05  -3.6606E-05  -4.9934E-05  4.1205E-05...
   2.5648E-05  -1.9289E-05  8.9661E-05  -1.9594E-05  -4.9859E-04  -1.1599E-03...
   5.7163E-05  8.9798E-05  -7.8591E-05  9.3187E-03  0  -3.8421E-03  3.5740E-03...
   9.7714E-05  -2.7776E-03  -1.3552E-04  5.1538E-04  2.2082E-04  -1.2706E-05...
  -2.3637E-05  1.3686E-05  1.1085E-04  -3.6557E-06  4.9876E-06  8.1085E-06...
   3.7381E-05  1.2791E-04  -9.4527E-06  -2.3083E-06  -1.2046E-06  7.8161E-04...
   -1.1997E-03  -3.0560E-05  -6.6202E-05  3.7227E-04  -2.1469E-04  4.8386E-03...
   -3.7387E-03  0  -1.8479E-02  3.9077E-03  9.9165E-04  -1.4825E-05  -1.4830E-06...
   6.0845E-05  8.0667E-05  1.8547E-05  -5.0212E-05  1.0539E-04  -2.2676E-04...
   4.3793E-05  -1.0456E-05  -8.1186E-06  -2.1653E-05  -3.3070E-05  1.7280E-05...
   -7.4509E-05  -3.4399E-05  -8.2999E-04  -6.7962E-04  4.0521E-05  -5.1604E-05...
   9.1132E-06  -5.7360E-03  -2.2213E-04  9.9131E-04  0  -9.5790E-03  6.7114E-03...
   3.6824E-05  1.0056E-04  -3.7105E-05  -9.0295E-05  -7.4580E-05  1.4814E-04...
   7.2634E-05  -8.4778E-06  6.3486E-05  5.6328E-05  -1.3617E-04  2.2196E-05...
   1.3606E-05  -3.6689E-05  8.3283E-05  1.1865E-04  1.8544E-05  -1.9831E-05...
   1.7894E-05  -6.8164E-05  -7.0892E-05  1.2378E-03  1.6961E-03  -6.5102E-03...
   -9.3202E-03  0  5.1349E-03  1.3612E-05  -1.3175E-04  7.2442E-06  5.6705E-04...
   -1.4723E-05  -4.8656E-05  -1.4282E-04  5.9711E-05  5.9046E-05  -3.6490E-04...
   7.4881E-05  5.4601E-06  1.0129E-03  -1.3867E-04  8.1617E-05  6.6053E-05...
   -1.3417E-05  9.0025E-05  -4.5362E-05  -4.4672E-06  9.5087E-05  -3.4077E-02...
   7.9142E-04  1.6667E-03  -6.6512E-03  8.1538E-03 0  -1.4185E-05  7.3209E-05...
   -2.5849E-05  1.2325E-03  -4.1696E-05  4.6266E-05  8.6146E-05  2.1436E-05...
   5.0874E-05  -3.2738E-04  2.2218E-04  8.6478E-06  7.3395E-04  -4.1453E-05...
   3.5719E-05  2.5313E-05  1.5182E-04  3.6007E-05  -2.8844E-05  8.9741E-05...
  -7.3257E-05];

%COMPUTE THE UNCORRECTED FORCES AND MOMENTS BY
%CONSIDERING THAT THE PRIME SENSITIVITY CONSTANTS ARE ALREADY
APLIED:

NF1=MNF;
AF1=MAF;
PM1=MPM;
RM1=MRM;
```

```
YM1=MYM;
SF1=MSF;

%FOR THE FIRST INTERACTION LET US INIZIALICE THE VALUES OF FORCES
AND
%MOMENTS WITH THE VALUES OF THE UNCORRECTED FORCES AND
MOMENTS

NF(1)=NF1;
AF(1)=AF1;
PM(1)=PM1;
RM(1)=RM1;
YM(1)=YM1;
SF(1)=SF1;

%DOING THE INTERACTION EQUATIONS:

for n=2:MAXIT;

NF(n)=NF1-((K(2)*AF(n-1))+(K(3)*PM(n-1))+(K(4)*RM(n-1))+(K(5)*YM(n-
1))+(K(6)*SF(n-1))+(K(7)*NF(n-1)^2)+...
      (K(8)*(NF(n-1)*AF(n-1)))+(K(9)*(NF(n-1)*PM(n-1)))+(K(10)*(NF(n-1)*RM(n-
1)))+(K(11)*(NF(n-1)*YM(n-1)))+...
      (K(12)*(NF(n-1)*SF(n-1)))+(K(13)*(AF(n-1)^2))+(K(14)*(AF(n-1)*PM(n-
1)))+(K(15)*(AF(n-1)*RM(n-1)))+...
      (K(16)*(AF(n-1)*YM(n-1)))+(K(17)*(AF(n-1)*SF(n-1)))+(K(18)*(PM(n-
1)^2))+(K(19)*(PM(n-1)*RM(n-1)))+...
      (K(20)*(PM(n-1)*YM(n-1)))+(K(21)*(PM(n-1)*SF(n-1)))+(K(22)*(RM(n-
1)^2))+(K(23)*(RM(n-1)*YM(n-1)))+...
      (K(24)*(RM(n-1)*SF(n-1)))+(K(25)*(YM(n-1)^2))+(K(26)*(YM(n-1)*SF(n-
1)))+(K(27)*(SF(n-1)^2)));

AF(n)=AF1-((K(28)*NF(n-1))+(K(30)*PM(n-1))+(K(31)*RM(n-1))+(K(32)*YM(n-
1))+(K(33)*SF(n-1))+(K(34)*NF(n-1)^2)+...
      (K(35)*(NF(n-1)*AF(n-1)))+(K(36)*(NF(n-1)*PM(n-1)))+(K(37)*(NF(n-
1)*RM(n-1)))+(K(38)*(NF(n-1)*YM(n-1)))+...
      (K(39)*(NF(n-1)*SF(n-1)))+(K(40)*(AF(n-1)^2))+(K(41)*(AF(n-1)*PM(n-
1)))+(K(42)*(AF(n-1)*RM(n-1)))+...
      (K(43)*(AF(n-1)*YM(n-1)))+(K(44)*(AF(n-1)*SF(n-1)))+(K(45)*(PM(n-
1)^2))+(K(46)*(PM(n-1)*RM(n-1)))+...
      (K(47)*(PM(n-1)*YM(n-1)))+(K(48)*(PM(n-1)*SF(n-1)))+(K(49)*(RM(n-
1)^2))+(K(50)*(RM(n-1)*YM(n-1)))+...
      (K(51)*(RM(n-1)*SF(n-1)))+(K(52)*(YM(n-1)^2))+(K(53)*(YM(n-1)*SF(n-
1)))+(K(54)*(SF(n-1)^2)));
```

```
PM(n)=PM1-((K(55)*NF(n-1))+(K(56)*AF(n-1))+(K(58)*RM(n-1))+(K(59)*YM(n-
1))+(K(60)*SF(n-1))+(K(61)*NF(n-1)^2)+...
      (K(62)*(NF(n-1)*AF(n-1)))+(K(63)*(NF(n-1)*PM(n-1)))+(K(64)*(NF(n-
1)*RM(n-1)))+(K(65)*(NF(n-1)*YM(n-1)))+...
      (K(66)*(NF(n-1)*SF(n-1)))+(K(67)*(AF(n-1)^2))+(K(68)*(AF(n-1)*PM(n-
1)))+(K(69)*(AF(n-1)*RM(n-1)))+...
      (K(70)*(AF(n-1)*YM(n-1)))+(K(71)*(AF(n-1)*SF(n-1)))+(K(72)*(PM(n-
1)^2))+(K(73)*(PM(n-1)*RM(n-1)))+...
      (K(74)*(PM(n-1)*YM(n-1)))+(K(75)*(PM(n-1)*SF(n-1)))+(K(76)*(RM(n-
1)^2))+(K(77)*(RM(n-1)*YM(n-1)))+...
      (K(78)*(RM(n-1)*SF(n-1)))+(K(79)*(YM(n-1)^2))+(K(80)*(YM(n-1)*SF(n-
1)))+(K(81)*(SF(n-1)^2)));

RM(n)=RM1-((K(82)*NF(n-1))+(K(83)*AF(n-1))+(K(84)*PM(n-1))+(K(86)*YM(n-
1))+(K(87)*SF(n-1))+(K(88)*NF(n-1)^2)+...
      (K(89)*(NF(n-1)*AF(n-1)))+(K(90)*(NF(n-1)*PM(n-1)))+(K(91)*(NF(n-
1)*RM(n-1)))+(K(92)*(NF(n-1)*YM(n-1)))+...
      (K(93)*(NF(n-1)*SF(n-1)))+(K(94)*(AF(n-1)^2))+(K(95)*(AF(n-1)*PM(n-
1)))+(K(96)*(AF(n-1)*RM(n-1)))+...
      (K(97)*(AF(n-1)*YM(n-1)))+(K(98)*(AF(n-1)*SF(n-1)))+(K(99)*(PM(n-
1)^2))+(K(100)*(PM(n-1)*RM(n-1)))+...
      (K(101)*(PM(n-1)*YM(n-1)))+(K(102)*(PM(n-1)*SF(n-1)))+(K(103)*(RM(n-
1)^2))+(K(104)*(RM(n-1)*YM(n-1)))+...
      (K(105)*(RM(n-1)*SF(n-1)))+(K(106)*(YM(n-1)^2))+(K(107)*(YM(n-1)*SF(n-
1)))+(K(108)*(SF(n-1)^2)));

YM(n)=YM1-((K(109)*NF(n-1))+(K(110)*AF(n-1))+(K(111)*PM(n-
1))+(K(112)*RM(n-1))+(K(114)*SF(n-1))+(K(115)*NF(n-1)^2)+...
      (K(116)*(NF(n-1)*AF(n-1)))+(K(117)*(NF(n-1)*PM(n-1)))+(K(118)*(NF(n-
1)*RM(n-1)))+(K(119)*(NF(n-1)*YM(n-1)))+...
      (K(120)*(NF(n-1)*SF(n-1)))+(K(121)*(AF(n-1)^2))+(K(122)*(AF(n-1)*PM(n-
1)))+(K(123)*(AF(n-1)*RM(n-1)))+...
      (K(124)*(AF(n-1)*YM(n-1)))+(K(125)*(AF(n-1)*SF(n-1)))+(K(126)*(PM(n-
1)^2))+(K(127)*(PM(n-1)*RM(n-1)))+...
      (K(128)*(PM(n-1)*YM(n-1)))+(K(129)*(PM(n-1)*SF(n-1)))+(K(130)*(RM(n-
1)^2))+(K(131)*(RM(n-1)*YM(n-1)))+...
      (K(132)*(RM(n-1)*SF(n-1)))+(K(133)*(YM(n-1)^2))+(K(134)*(YM(n-1)*SF(n-
1)))+(K(135)*(SF(n-1)^2)));

SF(n)=SF1-((K(136)*NF(n-1))+(K(137)*AF(n-1))+(K(138)*PM(n-1))+(K(139)*RM(n-
1))+(K(140)*YM(n-1))+(K(142)*NF(n-1)^2)+...
      (K(143)*(NF(n-1)*AF(n-1)))+(K(144)*(NF(n-1)*PM(n-1)))+(K(145)*(NF(n-
1)*RM(n-1)))+(K(146)*(NF(n-1)*YM(n-1)))+...
      (K(147)*(NF(n-1)*SF(n-1)))+(K(148)*(AF(n-1)^2))+(K(149)*(AF(n-1)*PM(n-
1)))+(K(150)*(AF(n-1)*RM(n-1)))+...
```

```
    (K(151)*(AF(n-1)*YM(n-1)))+(K(152)*(AF(n-1)*SF(n-1)))+(K(153)*(PM(n-
1)^2))+(K(154)*(PM(n-1)*RM(n-1)))+...
    (K(155)*(PM(n-1)*YM(n-1)))+(K(156)*(PM(n-1)*SF(n-1)))+(K(157)*(RM(n-
1)^2))+(K(158)*(RM(n-1)*YM(n-1)))+...
    (K(159)*(RM(n-1)*SF(n-1)))+(K(160)*(YM(n-1)^2))+(K(161)*(YM(n-1)*SF(n-
1)))+(K(162)*(SF(n-1)^2)));

% SET THE LIMIT FOR THE DIFFERENCE BETWEEN INTERATIONS(CRITERIA
FOR FINISH THE INTERATIONS)

DIFFNF(n)=abs(NF(n)-NF(n-1));
DIFFAF(n)=abs(AF(n)-AF(n-1));
DIFFPM(n)=abs(PM(n)-PM(n-1));
DIFFRM(n)=abs(RM(n)-RM(n-1));
DIFFYM(n)=abs(YM(n)-YM(n-1));
DIFFSF(n)=abs(SF(n)-SF(n-1));

if DIFFNF(n)&DIFFAF(n)&DIFFPM(n)&DIFFRM(n)&DIFFYM(n)&DIFFSF(n) <
LIMIT
break
end
end

disp('THE FINAL VALUES ARE (NF,AF,PM,RM,YM,SF):')
Corrected_Data(:,i)= [NF(n);AF(n);PM(n);RM(n);YM(n);SF(n)];

disp('THE FINAL DIFFERENCE BETWEEN INTERATIONS ARE(FOR
NF,AF,PM,RM,YM,SF) :')
FINAL_DIFFERENCE=[DIFFNF(n),DIFFAF(n),DIFFPM(n),DIFFRM(n),DIFFYM(n),
DIFFSF(n)]

disp('THE NUMBER OF INTERATIONS USED WAS:')
%#########################################################################
%VII. Calculation of the Axial, Side, & Normal Forces from the corrected balance
%      forces in the Body Axis reference frame
%#########################################################################

Forces_b(:,i) = [Corrected_Data(2,i); Corrected_Data(6,i); Corrected_Data(1,i)];

%Calculation of the Drag, Side, & Lift Forces in the Wind Axis reference frame

Forces_w = [Forces_b(1,:).*cos(theta').*cos(si')+Forces_b(2,:).*sin(si')+Forces_b(3,:).
            *sin(theta').*cos(si'); -Forces_b(1,:).*sin(si').*cos(theta')+
            Forces_b(2,:).*cos(si') -Forces_b(3,:).*sin(theta').*sin(si');
           -Forces_b(1,:).*sin(theta')+Forces_b(3,:).*cos(theta')];
```

```
%First entry is the moments calculated by the balance or direct calculation
%in the Body Reference Frame.  Balance measures Roll (l), Yaw is about the
%z-axis (n), and Pitch is about the y-axis (m).  Distances from strain
%gages to C.G. are in INCHES.  Moments are in-lbf

m = Corrected_Data(3,i);
n = Corrected_Data(5,i);
l = Corrected_Data(4,i);

Moments_b(:,i) = [l; m; n];

%Second entry is the conversion from the "Balance Centeric" moments to the
%Wind Reference monments with respect to the Balance Center (bc)

Moments_w_bc =      [Moments_b(1,:).*cos(theta').*cos(si')-Moments_b(2,:).
                    *sin(si')+Moments_b(3,:).*sin(theta').*cos(si');
                    Moments_b(1,:).*sin(si').*cos(theta')+Moments_b(2,:).*cos(si')+
                    Moments_b(3,:).*sin(theta').*sin(si');
                   -Moments_b(1,:).*sin(theta')+Moments_b(3,:).*cos(theta')];

%Finally, the balance centered moments are converted to moments about the
%Model's Center of Mass (cm) or Center of Gravity (CG)

cgdist=sqrt((X_cmb)^2+(Z_cmb)^2); %Obtaining the direct distance between the
                                    center of the balance and the center of mass
w=atan(-Z_cmb/X_cmb);  %Obtaining the angle between cgdist and the x axes at zero
                         angle of attack

X_cm(i,:)= cos(theta(i,:)+w)*cos(si(i,:))*(cgdist);
Y_cm(i,:) = Y_cmb + X_cm(i,:)*tan(si(i,:));
Z_cm(i,:)= -sin(theta(i,:)+w)*(cgdist);


Moments_w_cg_u =   [Moments_w_bc(1,:) + Z_cm(i,:)*Forces_w(2,:) + Forces_w(3,:)*
                    Y_cm;
                    Moments_w_bc(2,:) - Forces_w(3,:)* X_cm(i,:) + Forces_w(1,:)*
                    Z_cm(i,:);
                    Moments_w_bc(3,:) - Forces_w(1,:)* Y_cm - Forces_w(2,:)*
                    X_cm(i,:)];

%#########################################################################
 %VIII. Calculation of the actual Lift and Drag no dimensional Coefficients, uncorrected
for tunnel effects, (Cl  and Cd)
%#########################################################################
```

```
C_D_u = Forces_w(1,:) ./ (q_Corrected' .* Wing_Area);
C_Y_u = Forces_w(2,:) ./ (q_Corrected' .* Wing_Area);
C_L_u = Forces_w(3,:) ./ (q_Corrected' .* Wing_Area);
Coefficients = [C_L_u; C_D_u; C_Y_u]';
 Ave_Cl = mean(Coefficients(:,1));
 Ave_Cd = mean(Coefficients(:,2));

end
%#########################################################################
%IX          Drag Coefficient Correction
%#########################################################################

C_D_o = min(Coefficients(:,2));
C_L_u_sqrd = Coefficients(:,1).^2;
Delta_C_D_w = ((delta * Wing_Area) / X_Section) .* C_L_u_sqrd;
C_D_Corrected = C_D_u' + Delta_C_D_w;

%#########################################################################
%X.  Angle of Attack due to upwash Correction
%#########################################################################

alpha = sample_data(:,1);
Delta_alpha_w = ((delta * Wing_Area) / X_Section) .* (57.3 * C_L_u);
alpha_Corrected = alpha + Delta_alpha_w';

%#########################################################################
%XI.  Pitching Moment Correction
%#########################################################################

tau2 = 0.65;
c_bar = (mean([6, 5+9/16, 5, 3+11/16, 0.5])) / 12;          % ft = Mean Chord of wing
V_bar = (Tail_Area * l_t) / (Wing_Area * c_bar);            %  Horizontal tail volume ratio
eta_t = 1.0;
epsilon_o = 0;
i_t = pi/4;                                                  % radians
i_w = 0;
Aspect_Ratio_t = Span_t^2 / Tail_Area;
D_epslion_D_alpha = ((2 .* C_L_u) ./ (pi* Aspect_Ratio))';
epsilon = epsilon_o + (D_epslion_D_alpha .* alpha_Corrected );
alpha_t = alpha_Corrected - i_w - epsilon + i_t;
C_L_alpha_t = ((0.1* Aspect_Ratio) / (Aspect_Ratio_t +2)) * 0.8;
D_Cm_cg_t_D_alpha_t = -C_L_alpha_t* V_bar * eta_t;
Delta_C_m_cg_t =     ((D_Cm_cg_t_D_alpha_t) * (delta*tau2) * (Wing_Area /
                     X_Section) .* (C_L_u * 57.3))';
```

```
Cl_w_cg =   Moments_w_cg_u(1,:) ./ (q_Corrected' .* (Wing_Area * Span*12));
Cm_w_cg_u = Moments_w_cg_u(2,:) ./ (q_Corrected' .* (Wing_Area * c_bar*12));
Cn_w_cg =   Moments_w_cg_u(3,:) ./ (q_Corrected' .* (Wing_Area * Span*12));
Cm_w_cg_corrected = Cm_w_cg_u - Delta_C_m_cg_t';
Corrected_Moment_Coefficients = [Cl_w_cg' Cm_w_cg_corrected' Cn_w_cg'];

%OBTAINING THE MOMENTS COEFFICIENTS CORRECTED ABOUT THE
CENTER OF THE
%BALANCE

Cl_w_bc =   Moments_w_bc(1,:) ./ (q_Corrected' .* (Wing_Area * Span*12));
Cm_w_bc_u = Moments_w_bc(2,:) ./ (q_Corrected' .* (Wing_Area * c_bar*12));
Cn_w_bc =   Moments_w_bc(3,:) ./ (q_Corrected' .* (Wing_Area * Span*12));
Cm_w_bc_corrected = Cm_w_bc_u - Delta_C_m_cg_t';
Corrected_Moment_Coefficients_bc = [Cl_w_bc' Cm_w_bc_corrected' Cn_w_bc'];

%##########################################################################
%XII. OUTPUT VARIABLES FORMATING
%##########################################################################

fprintf ('alpha_c  Yaw Data(Beta)  M#         Re#         q_c         Uoo         C_L
         C_D_c   C_S \r   Cl_cg_w      Cm_cg_c_w    Cn_cg_w       Drag   Sideforce
         Lift  Cl_bc_w     Cm_bc_c_w    Cn_bc_w '  );
TOTAL_DATA=      [alpha_Corrected, sample_data(:,2)*(-1), Flight_Parameters,
                  (Wind_Speed_Corrected .* (3600/5280)), C_L_u',
                  C_D_Corrected,C_Y_u',Corrected_Moment_Coefficients,
                  Forces_w',Corrected_Moment_Coefficients_bc]

% LET US SAVE TOTAL DATA IN A EXTERNAL FILE
dlmwrite('test TOTAL DATA T2 DE M9 DRN M20',TOTAL_DATA,'\t')
```

Appendix D: Iteration Data for the Balance AFIT-1

This appendix presents the notation, data reduction equations and the values for the constants used for the iteration process of the balance AFIT-1, already explained in section **3.3. Data Processing**". The information presented was received from Modern Machine &Tool Co, Inc that is the manufacturer of the Balance.

Table 57. Notation of the Constants used for the AFIT -1 Balance

6 X 27 INTERACTION COEFFICIENT MATRIX

INTERACTION TERM	COMPONENT					
	NF	AF	PM	RM	YM	SF
KNF	K1 (A)	K28	K55	K82	K109	K136
KAF	K2	K29 (A)	K56	K83	K110	K137
KPM	K3 (B)	K30	K57 (A)	K84	K111	K138
KRM	K4	K31	K58	K85 (A)	K112	K139
KYM	K5	K32	K59	K86	K113 (A)	K140
KSF	K6	K33	K60	K87	K114	K141(A)
KNF^2	K7	K34	K61	K88	K115	K142
K(NF x AF)	K8	K35	K62	K89	K116	K143
K(NF x PM)	K9	K36	K63	K90	K117	K144
K(NF x RM)	K10	K37 (C)	K64	K91	K118	K145
K(NF x YM)	K11	K38	K65	K92	K119	K146
K(NF x SF)	K12	K39	K66	K93	K120	K147
KAF^2	K13	K40	K67	K94	K121	K148
K(AF x PM)	K14	K41	K68	K95	K122	K149
K(AF x RM)	K15	K42	K69	K96	K123	K150
K(AF x YM)	K16	K43	K70	K97	K124	K151
K(AF x SF)	K17	K44	K71	K98	K125	K152
KPM^2	K18	K45	K72	K99(D)	K126	K153
K(PM x RM)	K19	K46	K73	K100	K127	K154
K(PM x YM)	K20	K47	K74	K101	K128	K155
K(PM x SF)	K21	K48	K75	K102	K129	K156
KRM^2	K22	K49	K76	K103	K130	K157
K(RM x YM)	K23	K50	K77	K104	K131	K158
K(RM x SF)	K24	K51	K78	K105	K132	K159
KYM^2	K25	K52	K79	K106	K133	K160
K(YM x SF)	K26	K53	K80	K107	K134	K161
KSF^2	K27	K54	K81	K108	K135	K162

Table 58. Values of the Constants Used for the AFIT -1 Balance

Full Scale Output and Sensitivity						
COMPONENT	NF	AF	PM	RM	YM	SF
FS LOAD (lb or in-lb)	10	5	10	4	5	5
FS OUTPUT (μV/5V)	5,637	5,637	6,715	6,344	5,530	5,576
Sens (lb/μV/5V or in-lb/μV/5V)	1.7739E-03	8.8706E-04	1.4892E-03	6.3049E-04	9.0418E-04	8.9666E-04
Interactions						
COMPONENT	NF	AF	PM	RM	YM	SF
NF	0	9.3187E-03	4.8386E-03	-5.7360E-03	1.2378E-03	-3.4077E-02
AF	-1.3567E-03	0	-3.7387E-03	-2.2213E-04	1.6961E-03	7.9142E-04
PM	-3.8021E-03	-3.8421E-03	0	9.9131E-04	-6.5102E-03	1.6667E-03
RM	-4.2814E-03	3.5740E-03	-1.8479E-02	0	-9.3202E-03	-6.6512E-03
YM	-1.6966E-03	9.7714E-05	3.9077E-03	-9.5790E-03	0	8.1538E-03
SF	1.7567E-03	-2.7776E-03	9.9165E-04	6.7114E-03	5.1349E-03	0
NF^2	5.3167E-05	-1.3552E-04	-1.4825E-05	3.6824E-05	1.3612E-05	-1.4185E-05
NF x AF	-1.3867E-04	5.1538E-04	-1.4830E-06	1.0056E-04	-1.3175E-04	7.3209E-05
NF x PM	-5.5629E-05	2.2082E-04	6.0845E-05	-3.7105E-05	7.2442E-06	-2.5849E-05
NF x RM	3.5181E-05	-1.2706E-05	8.0667E-05	-9.0295E-05	5.6705E-04	1.2325E-03
NF x YM	1.0601E-05	-2.3637E-05	1.8547E-05	-7.4580E-05	-1.4723E-05	-4.1696E-05
NF x SF	-2.5271E-04	1.3686E-05	-5.0212E-05	1.4814E-04	-4.8656E-05	4.6266E-05
AF^2	5.6693E-05	1.1085E-04	1.0539E-04	7.2634E-05	-1.4282E-04	8.6146E-05
AF x PM	-1.9537E-04	-3.6557E-06	-2.2676E-04	-8.4778E-06	5.9711E-05	2.1436E-05
AF x RM	1.7908E-05	4.9876E-06	4.3793E-05	6.3486E-05	5.9046E-05	5.0874E-05
AF x YM	-3.6606E-05	8.1085E-06	-1.0456E-05	5.6328E-05	-3.6490E-04	-3.2738E-04
AF x SF	-4.9934E-05	3.7381E-05	-8.1186E-06	-1.3617E-04	7.4881E-05	2.2218E-04
PM^2	4.1205E-05	1.2791E-04	-2.1653E-05	2.2196E-05	5.4601E-06	8.6478E-06
PM x RM	2.5648E-05	-9.4527E-06	-3.3070E-05	1.3606E-05	1.0129E-03	7.3395E-04
PM x YM	-1.9289E-05	-2.3083E-06	1.7280E-05	-3.6689E-05	-1.3867E-04	-4.1453E-05
PM x SF	8.9661E-05	-1.2046E-06	-7.4509E-05	8.3283E-05	8.1617E-05	3.5719E-05
RM^2	-1.9594E-05	7.8161E-04	-3.4399E-05	1.1865E-04	6.6053E-05	2.5313E-05
RM x YM	-4.9859E-04	-1.1997E-03	-8.2999E-04	1.8544E-05	-1.3417E-05	1.5182E-04
RM x SF	-1.1599E-03	-3.0560E-05	-6.7962E-04	-1.9831E-05	9.0025E-05	3.6007E-05
YM^2	5.7163E-05	-6.6202E-05	4.0521E-05	1.7894E-05	-4.5362E-05	-2.8844E-05
YM x SF	8.9798E-05	3.7227E-04	-5.1604E-05	-6.8164E-05	-4.4672E-06	8.9741E-05
SF^2	-7.8591E-05	-2.1469E-04	9.1132E-06	-7.0892E-05	9.5087E-05	-7.3257E-05

Table 59. Data Reduction Equations for the AFIT-1 Balance

DATA REDUCTION EQUATIONS

NF, AF, PM, RM, YM, & SF = FORCES AND MOMENTS ACTING ON THE MODEL (lb. or in-lb.)

MNF = OUTPUT OF NF CHANNEL (mV)
MAF = OUTPUT OF AF CHANNEL (mV)
MPM = OUTPUT OF PM CHANNEL (mV)
MRM = OUTPUT OF RM CHANNEL (mV)
MYM = OUTPUT OF YM CHANNEL (mV)
MSF = OUTPUT OF SF CHANNEL (mV)

NF = K_{1X}MNF - [Σ (Interactions on NF)]

$$NF = K_{1X}MNF - [K_{2X}AF + K_{3X}PM + K_{4X}RM + K_{5X}YM + K_{6X}SF + K_{7X}NF^2 + K_{8X}(NFxAF) + K_{9X}(NFxPM) + K_{10X}(NFxRM) + K_{11X}(NFxYM) + K_{12X}(NFxSF) + K_{13X}AF^2 + K_{14X}(AFxPM) + K_{15X}(AFxRM) + K_{16X}(AFxYM) + K_{17X}(AFxSF) + K_{18X}PM^2 + K_{19X}(PMxRM) + K_{20X}(PMxYM) + K_{21X}(PMxSF) + K_{22X}RM^2 + K_{23X}(RMxYM) + K_{24X}(RMxSF) + K_{25X}YM^2 + K_{26X}(YMxSF) + K_{27X}SF^2] \quad \textbf{EQUATION -1}$$

$$AF = K_{29X}MAF - [K_{28X}NF + K_{30X}PM + K_{31X}RM + K_{32X}YM + K_{33X}SF + K_{34X}NF^2 + K_{35X}(NFxAF) + K_{36X}(NFxPM) + K_{37X}(NFxRM) + K_{38X}(NFxYM) + K_{39X}(NFxSF) + K_{40X}AF^2 + K_{41X}(AFxPM) + K_{42X}(AFxRM) + K_{43X}(AFxYM) + K_{44X}(AFxSF) + K_{45X}PM^2 + K_{46X}(PMxRM) + K_{47X}(PMxYM) + K_{48X}(PMxSF) + K_{49X}RM^2 + K_{50X}(RMxYM) + K_{51X}(RMxSF) + K_{52X}YM^2 + K_{53X}(YMxSF) + K_{54X}SF^2] \quad \textbf{EQUATION -2}$$

$$PM = K_{57X}MPM - [K_{55X}NF + K_{56X}AF + K_{58X}RM + K_{59X}YM + K_{60X}SF + K_{61X}NF^2 + K_{62X}(NFxAF) + K_{63X}(NFxPM) + K_{64X}(NFxRM) + K_{65X}(NFxYM) + K_{66X}(NFxSF) + K_{67X}AF^2 + K_{68X}(AFxPM) + K_{69X}(AFxRM) + K_{70X}(AFxYM) + K_{71X}(AFxSF) + K_{72X}PM^2 + K_{73X}(PMxRM) + K_{74X}(PMxYM) + K_{75X}(PMxSF) + K_{76X}RM^2 + K_{77X}(RMxYM) + K_{78X}(RMxSF) + K_{79X}YM^2 + K_{80X}(YMxSF) + K_{81X}SF^2] \quad \textbf{EQUATION -3}$$

$$RM = K_{85X}MRM - [K_{82X}NF + K_{83X}AF + K_{84X}PM + K_{86X}YM + K_{87X}SF + K_{88X}NF^2 + K_{89X}(NFxAF) + K_{90X}(NFxPM) + K_{91X}(NFxRM) + K_{92X}(NFxYM) + K_{93X}(NFxSF) + K_{94X}AF^2 + K_{95X}(AFxPM) + K_{96X}(AFxRM) + K_{97X}(AFxYM) + K_{98X}(AFxSF) + K_{99X}PM^2 + K_{100X}(PMxRM) + K_{101X}(PMxYM) + K_{102X}(PMxSF) + K_{103X}RM^2 + K_{104X}(RMxYM) + K_{105X}(RMxSF) + K_{106X}YM^2 + K_{107X}(YMxSF) + K_{108X}SF^2] \quad \textbf{EQUATION -4}$$

$$YM = K_{113X}MYM - [K_{109X}NF + K_{110X}AF + K_{111X}PM + K_{112X}RM + K_{114X}SF + K_{115X}NF^2 + K_{116X}(NFxAF) + K_{117X}(NFxPM) + K_{118X}(NFxRM) + K_{119X}(NFxYM) + K_{120X}(NFxSF) + K_{121X}AF^2 + K_{122X}(AFxPM) + K_{123X}(AFxRM) + K_{124X}(AFxYM) + K_{125X}(AFxSF) + K_{126X}PM^2 + K_{127X}(PMxRM) + K_{128X}(PMxYM) + K_{129X}(PMxSF) + K_{130X}RM^2 + K_{131X}(RMxYM) + K_{132X}(RMxSF) + K_{133X}YM^2 + K_{134X}(YMxSF) + K_{135X}SF^2] \quad \textbf{EQUATION -5}$$

$$SF = K_{141X}MSF - [K_{136X}NF + K_{137X}AF + K_{138X}PM + K_{139X}RM + K_{140X}YM + K_{142X}NF^2 + K_{143X}(NFxAF) + K_{144X}(NFxPM) + K_{145X}(NFxRM) + K_{146X}(NFxYM) + K_{147X}(NFxSF) + K_{148X}AF^2 + K_{149X}(AFxPM) + K_{150X}(AFxRM) + K_{151X}(AFxYM) + K_{152X}(AFxSF) + K_{153X}PM^2 + K_{154X}(PMxRM) + K_{155X}(PMxYM) + K_{156X}(PMxSF) + K_{157X}RM^2 + K_{158X}(RMxYM) + K_{159X}(RMxSF) + K_{160X}YM^2 + K_{161X}(YMxSF) + K_{162X}SF^2] \quad \textbf{EQUATION -6}$$

Bibliography

AAI, Corp. Online! Shadow TUAV. Maryland, USA 5 November 2004 http://www.shadowtuav.com/index.html

Aerovirоment. Online! *Unmaned Aerial Vehicles*.Monrovia CA. 5 November 2004 http://www.aerovironment.com/area-aircraft/unmanned.html

Airbus. Airbus 4U Online Magazine. Toulouse, France 20 October 2004 http://www.airbus.com/airbus4u/photo_album.html

A d-el-Hak, Mohamed. "Micro-Air-Vehicles: Can They be Controlled Better?". *Journal of Aircraft* Vol.38,No.3, May-June 2001.

Barlow, Jewel B;Rae, William H; and Pope, Alan. *Low-Speed Wind Tunnel Testing* (3rd Edition).New York: John Wiley and Sons, 1999.

DeLuca,Anthony M., Captain, USAF. *Experimental Investigation into the Aerodynamic Performance of both Rigid and Flexible Wing Structured Micro-Air-Vehicles*. Air Force Institute of Technology, Wright-Patterson Air Force Base, Ohio. March 2004.

Desktop Aeronautics. Online! "Tailless Aircraft".Stanford, CA. 19 November 2004 http://www.desktopaero.com/applieadero/configuration/tailless.

Dittrich, Mark S. Performance, Stability and Control Vol.II. Aero 456. United States Air Force Academy, Department of Aeronautics. Colorado Springs CO. 1966

Etlein, B. *Dynamics of Flight: Stability and Control*, New York: John Wiley and Sons, 1982.

Horton-Smith, Clifford. *The Flight of Birds*. H.F & G. Witherby,Ltd. London, 1938

Huayiu, Sun Dong and Zhou Zhaoying. "Micro Air Vehicle: Configuration, Analysis, Fabrication, and Test". *IEEE/ASME Transactions on Mechatronics,* Vol.9, No. 1, March 2004.

Jones, Kevin D., Bradshaw Chris J and Papadopoulos Jason."Improved Preformance and Control of Flapping-Wing Propelled Micro Air Vehicles. *42nd Aerospace Sciences Meeting & Exhibit*, AIAA paper 2002-0399. Reno NV, Jauary 5-8, 2004.

Johnson Harold S. and Hayes Williams C. "Wind Tunnel Investigation of the Effect of Various Dorsal-Fin and Vertical-Tail Configurations on the Directional Stability of Streamlined Body at Transonic Speeds". *Research Memorandum National Advisory Committee for Aeronautics*. Washington, D.C., April 1953

Johnson, Don. Online! "Eagle Photos collection". Bethalto, IL. 10 June 2004 http://www.riverbend2000.com/eaglephotos

Kennon,Matthew T. and Grasmeyer,Joel M.. "Development of the Black Widow and Microbat MAVs and a Vision of the Future of MAV Design".*AIAA/ICAS International Air and Space Symposium and Exposition: The Next 100Y*. Dayton, Ohio. 14-17 July 2003.

Keuthe, Arnold, M. and Chuen-Yen Chow. *Foundations of Aerodynamics-Bases of Aerodynamics Design* (5th Edition). New York:John Wiley and Sons, 1998.

Nash William. Online! "Tail Unit With Rotatable Tailplane".*United States Patent number 5,096,143.* Alexandria, VA. Mar 17 1992. 17 November 2004 http://www.uspto.gov/patft/index.html.

Nelson, Robert, C. *Flight Stability and Automatic Control* (2nd Edition). Boston: McGraw Hill Press, 1998.

Nickel, Karl and Wohlfahrt, Michael. *Tailless Aircraft in Theory and Practice*. AIAA Education Series.American Institute of Aeronautics and Astronautics; London, Englan: E. Arnold, 1994.

Military.com. On line! *Desert Hawk up: New Small Unmanned Aerial Vehicles*. 5 November 2004. http://www.military.com/soldiertech.html.

Modern Machine & Tool, Co; Inc. *Report of Calibration for Balance AFIT-1*. Newport News, VA. January 2004

Patel Naresh. "Data Reduction Equations For Multicomponent Strain-Gages Balances". Modern Machine & Tool, Co; Inc. Newport News, VA. 2004

Penn State. Online! *Stress, Strain and Strain Gages*. Pennsylvania State University 23 November 2004 http://www.me.psu.edu/me82/Learning/Strain/strain.html

Raymer,Daniel P. *Aircraft Design: A Conceptual Approach* (Third Edition).AIAA Education Series,Reston, Virginia.1999.

Rayner, Jeremy M.V. "Form and Function in Avian Flight", *Current Ornithology,* Vol. 5 1988

Ribaud Yves & Dessories Olivier. Microprpulsion Microcombustion. On line! 5 November 2004. http://www.onera.fr/conferences/micropropulsion.html

Silver Fox. Online!. *Unmanned Vehicle Systems.* Tucson, AZ. 5 November 2004. http://www.acrtucson.com/UAV/silverfox.html

Sparta Inc. On line! *Dragon Eye UAV*. San Diego, CA. 5 Nov 2004. http://www.coposites.sparta.com/uav.html

Stevens, Brian L.and Lewis, Frank L. *Aircraft Control and Simulation*.(2nd Edition) New Jersey: John Wiley and Sons, 1999.

Storer, John H.The *Flight of Birds Analyzed Through Slow-Motion Photography*. Cranbrook Institute of Science.Bloomfield Hills, Mich., c1948

Tennekes Henk. *The Simple Science of Flight*.Mtt Press. London, England, 1977

Waszak, Martin R. and Jenkins Luther N. "Stability and Control Properties of an Aeroelastic Fixed Wing Micro Aerial Vehicle". *AIAA Atmospheric Flight Mechanics Conference*. AIAA Paper 2001-4005. Montreal, Canada. 6-9 August 2001.

White, Frank, M. *Fluid Mechanics* (2nd Edition). New York: McGraw-Hill Press, 1996

Wood, Richard M."A Discussion of Aerodynamic Control Effectors (ACEs) for Unmanned Air Vehicles (UAV)". *AIAA's 1st Technical Conference and Workshop on Unmanned Aerospace Vehicles*. AIAA Paper 2002-3494.Portsmounth, Virginia, May 2002.

Vita

Lieutenant Jose R. Rivera Parga was born in Aguascalientes, Mexico. He entered as a cadet in 1987 to the Mexican Navy Academy where graduated in 1992 with a Bachelor of Aero naval Science degree.

Upon graduation he received several assignments in different naval squadrons of the Mexican navy such as La Paz, B.C.S, Campeche, Camp.; Veracruz, Ver; Ensenada B.C. and Mexico City, where he was working as a pilot.

In December 2002 he entered the School of Engineering and Management, Air Force Institute of Technology, Wright Patterson AFB, OH.

REPORT DOCUMENTATION PAGE

Form Approved
OMB No. 074-0188

1. REPORT DATE *(DD-MM-YYYY)*	**2. REPORT TYPE**	**3. DATES COVERED** *(From – To)*
09-12-2004	**Master's Thesis**	Jan 2003 – Dec 2004

4. TITLE AND SUBTITLE
Wind Tunnel Investigation of the Static Stability and Control Effectiveness of a Rotary Tail in a Portable UAV

5a. CONTRACT NUMBER

5b. GRANT NUMBER

5c. PROGRAM ELEMENT NUMBER

6. AUTHOR(S)

Rivera Parga, Jose R., Lieutenant, Mexican Navy

5d. PROJECT NUMBER

5e. TASK NUMBER

5f. WORK UNIT NUMBER

7. PERFORMING ORGANIZATION NAMES(S) AND ADDRESS(S)

Air Force Institute of Technology
Graduate School of Engineering and Management (AFIT/EN)
2950 Hobson Way
WPAFB OH 45433-7765

8. PERFORMING ORGANIZATION REPORT NUMBER
AFIT/GAE/ENY/04-D02

9. SPONSORING/MONITORING AGENCY NAME(S) AND ADDRESS(ES)
Air Force Research Lab / MNAV
Attn: Lt. Kirk Koleft (for Maj. John Anttonen)
1865 4th Street
Eglin AFB, FL 32542 DSN: 872-8876 ext. 3335

10. SPONSOR/MONITOR'S ACRONYM(S)

11. SPONSOR/MONITOR'S REPORT NUMBER(S)

12. DISTRIBUTION/AVAILABILITY STATEMENT
APPROVED FOR PUBLIC RELEASE; DISTRIBUTION UNLIMITED

13. SUPPLEMENTARY NOTES

14. ABSTRACT

The Air Force Research Lab, Munitions Directorate, Flight Vehicles Integration Branch (AFRL/MNAV) developed a man-portable, carbon-fiber matrix UAV with a flexible rectangular wing of 24" span and 6" chord, 18.2" length. There is a need for the development of smaller and lighter UAV's to perform certain missions. The objective of this experimental study was to determine the behavior and the aerodynamic characteristics of rotary tails. The bird-inspired rotary tail mechanism studied enabled control of two degrees of freedom and was configured to provide elevator deflection and rotation. Its effects on the static stability and control effectiveness were measured using the Air Force Institute of Technology (AFIT) low speed wind tunnel. The yaw moment provided by each rotary tail was found to be on the same order of magnitude as a typical rudder, and in that respect it offers promise as an effective flight control scheme. However, it was also found that the side force, and consequently the yaw moment, generated by the two tail controls (elevator deflection and rotation) were strongly coupled, which could lead to challenging aircraft control issues. A benefit is that the configurations used in this thesis would reduce the storage length by 48%.

15. SUBJECT TERMS
Rotary Tails, Wind Tunnel Tests, Air Force Research, UAV, Static Stability, Portable UAV, Control Effectiveness, Biologically-Inspired Flight Controls

16. SECURITY CLASSIFICATION OF:			**17. LIMITATION OF ABSTRACT**	**18. NUMBER OF PAGES**	**19a. NAME OF RESPONSIBLE PERSON**
REPORT	**ABSTRACT**	**c. THIS PAGE**			Dr. Mark F. Reeder
U	**U**	**U**	**UU**	229	**19b. TELEPHONE NUMBER** *(Include area code)* (937) 255-3636, ext 4530; e-mail: Mark.Reeder@afit.edu

Standard Form 298 (Rev: 8-98)
Prescribed by ANSI Std. Z39-18